FERMILAB-PUB-08-495-E

Review of Top Quark Properties Measurements at the Tevatron

Marc-André Pleier
Physikalisches Institut, Universität Bonn
Nussallee 12, 53115 Bonn, Germany

October 12, 2008

Abstract

This review summarises the top quark physics program pursued at Fermilab's Tevatron proton-antiproton collider, operating at a centre of mass energy of 1.96 TeV, and its two collider detectors CDF and D0. More than a decade after the discovery of the top quark at the Tevatron, it remains the only place to produce top quarks and study them directly until the Large Hadron Collider at CERN starts operation.

The Tevatron's increased luminosity and centre of mass energy offer the possibility to scrutinise the properties of the heaviest fundamental particle known to date by performing new measurements that were not feasible before, like the first evidence for electroweak production of top quarks and the resulting direct constraints on the involved couplings. In addition, the precision of prior measurements has been improved to an unprecedented level, illustrated for example by the measurement of the top quark mass with a relative precision of 0.7%, marking the most precisely measured quark mass to date and allowing the prediction of the mass of the Higgs boson that still remains to be discovered. The various measurements of top quark properties provide stringent tests on the predictions performed in the framework of the Standard Model of elementary particle physics.

Contents

1 Introduction

The existence of a third and most massive generation of fundamental fermions was unveiled first in 1975 with the discovery of the τ lepton at SLAC-LBL [1]. In 1977, the discovery of the bottom quark [2] at Fermilab extended the knowledge of a third generation into the quark sector and immediately raised the question of the existence of the top quark as the weak isospin partner of the bottom quark.

The Standard Model of elementary particle physics both required the existence of the top quark to remain self consistent and via electroweak precision measurements allowed increasingly precise predictions of properties like its mass. The top quark's large mass prevented its discovery for almost two decades and by 1994 was indirectly constrained to be $178 \pm 11\ ^{+18}_{-19}$ GeV/c^2 [3]. After mounting experimental evidence [4–9] the top quark was finally discovered in 1995 at Fermilab by the CDF and D0 collaborations [10, 11] in the mass range predicted by the Standard Model, demonstrating its predictive power and completing the Standard Model quark sector.

By now, the mass of the top quark has been measured to be 172.4 ± 1.2 GeV/c^2 [12], marking the most precisely measured quark mass and the most massive fundamental particle known to date. Consequently, the lifetime of the top quark of approximately $5{\cdot}10^{-25}$ s is extremely short so it decays before hadronising. This makes it the only quark to not form any bound states,

allowing the study of a bare quark with its properties like spin undisturbed by hadronisation.

The measurement of top quark pair production allows one to probe our understanding of the strong interaction by testing the predictions from perturbative QCD calculations, while the decay of top quarks and the single top quark production allow for the study of the electroweak interaction. Measuring further properties of the top quark such as its electric charge, W boson helicity in its decay, branching fraction $\mathcal{B}(t \to Wb)$, etc., and comparing them with Standard Model predictions is a very powerful tool in searching for "new" physics beyond the Standard Model framework.

The top quark can also be used to constrain the mass range of the last undiscovered particle in the Standard Model, the Higgs boson, since their masses and the mass of the W boson are linked via radiative corrections. The Higgs boson is a manifestation of the Higgs mechanism implemented in the Standard Model providing the necessary breaking of the electroweak symmetry to which the top quark seems to be intimately connected due to its large mass.

Because of its fairly recent discovery, the top quark's properties have not yet been explored with the same scrutiny as the lighter quarks. However, in the ongoing data taking at Fermilab's Tevatron proton-antiproton collider, an integrated luminosity of more than four fb^{-1} has been recorded by each of the collider experiments CDF and D0, corresponding to an increase of about a factor seventy compared to the data available for the discovery of the top quark. These datasets allow to refine previously performed measurements with unprecedented precision such that some start to become limited by systematic uncertainties rather than statistical ones. In addition, measurements that were never performed before become feasible like the first evidence for electroweak production of single top quarks and consequently a first direct measurement of the CKM matrix element $|V_{tb}|$ recently published by D0 [13, 14].

This article is intended to give an overview of the current status of the top quark physics program pursued at the Tevatron without suffering from the space limitations of previous articles by the author [15–17]. Results available until the LHC startup in September 2008 are included, utilising datasets of up to 2.8 fb^{-1}. Some former reviews of top quark physics including the current Tevatron data taking are given in [18–22]. The outline of this article is as follows: In the second chapter, a brief introduction to the Standard Model is given with emphasis on the special role of the top quark. Chapter 3 describes production and decay modes for top quarks in the Standard Model framework. Chapter 4 outlines the experimental setup used for the measurements described in the following sections. Chapter 5 presents studies

of the production of top quarks including the cross section measurements which form the basis for all further measurements of top quark characteristics. Chapter 6 elaborates on the different results for top quark decay properties, followed by measurements of fundamental top quark attributes like its charge or mass in Chapter 7. The final Chapter 8 gives a brief summary of the achievements so far.

2 The Standard Model and the Top Quark

2.1 A Brief Standard Model Overview

The Standard Model of elementary particle physics describes so far very successfully the interactions of the known fundamental constituents of matter which are spin $J = \frac{1}{2}$ fermions via the exchange of spin $J = 1$ gauge bosons.

fermion type	electric charge [e]	generation		
		1.	2.	3.
quarks	$+\frac{2}{3}$	up (u) 1.5 - 3.3 MeV/c^2	charm (c) $1.27\ ^{+0.07}_{-0.11}$ GeV/c^2	top (t) 172.4 ± 1.2 GeV/c^2
	$-\frac{1}{3}$	down (d) 3.5 - 6.0 MeV/c^2	strange (s) $104\ ^{+26}_{-34}$ MeV/c^2	bottom (b) $4.20\ ^{+0.17}_{-0.07}$ GeV/c^2
leptons	0	ν_e < 2 eV/c^2 (95% C.L.)	ν_μ < 0.19 MeV/c^2 (90% C.L.)	ν_τ < 18.2 MeV/c^2 (95% C.L.)
	-1	e 0.511 MeV/c^2	μ 105.658 MeV/c^2	τ 1777 MeV/c^2

Table 1: The known fundamental fermions and their masses [12, 23].

As shown in Table 1, both quarks and leptons occur in pairs differing by one unit in electric charge e that are replicated thrice in three generations which show a strong hierarchy in mass. The fermion masses span at least 11 orders of magnitude, with the top quark being by far the heaviest fundamental particle which may thus provide further insights into the process of mass generation. The origin of this breaking of the flavour symmetry and consequent mass hierarchy is still not understood but can be accommodated in the Standard Model as shown below.

The forces among the fundamental fermions are mediated by the exchange of the gauge bosons of the corresponding quantised gauge fields as listed

interaction type	couples to	affected particles	exchange boson	mass [GeV/c^2]	charge [e]	spin
strong	colour charge	quarks, gluons	gluon (g)	0	0	1
weak	weak charge	quarks, $W^{\pm}$, leptons, Z^0	W^+, W^- Z^0	80.4 91.2	+1, -1 0	1 1
electro-magnetic	electric charge	electrically charged	photon (γ)	0	0	1
gravitation	mass, energy	all	graviton (unobserved)	0	0	2

Table 2: The known fundamental interactions and their properties [23]. Gravitation is shown separately as it is not included in the Standard Model of elementary particle physics.

in Table 2. The gravitational force is not included in the framework of the Standard Model and will not be considered further in this article as its strength is small compared to that of the other interactions amongst the fundamental fermions at the energy scales considered in this article.

The Standard Model is a quantum field theory based on the local gauge symmetries $SU(3)_{QCD} \times SU(2)_L \times U(1)_Y$.

The theory of the strong interaction coupling to the three different colour charges ("red", "green" and "blue") carried by the quarks and the eight massless gauge bosons (gluons) themselves is called Quantum Chromo Dynamics (QCD) and is based on the gauge group $SU(3)_{QCD}$ [24–29]. This symmetry is exact, and the gluons carry both a colour and an anti-colour charge. At increasingly short distances (or large relative momenta) the interaction gets arbitrarily weak (asymptotic freedom), allowing for perturbative treatment. Via the strong interaction, quarks form bound colour-singlet states called hadrons, consisting of either a quark and an antiquark (Mesons) or three quarks respectively antiquarks (Baryons). The fact that only colour-neutral states and no free quarks are observed is referred to as the confinement of quarks in hadrons. Since due to its large mass the top quark decays faster than the typical hadronisation time of QCD ($\Gamma_{top} \gg \Lambda_{QCD}$), it is the only quark to not form any bound states and hence its decay offers the unique possibility to study the properties of a bare quark.

The theory of the electroweak interactions developed by Glashow [30], Salam [31] and Weinberg [32] is based on the $SU(2)_L \times U(1)_Y$ gauge group of the weak left-handed isospin T and hypercharge Y. Since the weak $(V-A)$

interaction only couples to left-handed particles, the fermion fields Ψ are split up into left-handed and right-handed fields $\Psi_{L,R} = \frac{1}{2}(1 \mp \gamma_5)\Psi$ that are arranged in weak isospin $T = \frac{1}{2}$ doublets and $T = 0$ singlets:

$$\begin{pmatrix} u \\ d \end{pmatrix}_L \quad \begin{pmatrix} c \\ s \end{pmatrix}_L \quad \begin{pmatrix} t \\ b \end{pmatrix}_L \qquad \begin{matrix} u_R & c_R & t_R \\ d_R & s_R & b_R \end{matrix}$$

$$\begin{pmatrix} \nu_e \\ e \end{pmatrix}_L \quad \begin{pmatrix} \nu_\mu \\ \mu \end{pmatrix}_L \quad \begin{pmatrix} \nu_\tau \\ \tau \end{pmatrix}_L \qquad \begin{matrix} \nu_{eR} & \nu_{\mu R} & \nu_{\tau R} \\ e_R & \mu_R & \tau_R \end{matrix}$$

In the doublets, neutrinos and the up-type quarks (u, c, t) have the weak isospin $T_3 = +\frac{1}{2}$ while the charged leptons and down-type quarks (d, s, b) carry the weak isospin $T_3 = -\frac{1}{2}$. The weak hypercharge Y is then defined via electric charge and weak isospin to be $Y = 2Q - 2T_3$. Consequently, members within a doublet carry the same hypercharge: $Y = -1$ for leptons and $Y = \frac{1}{3}$ for quarks, as implied by the product of the two symmetry groups.

The $SU(2)_L \times U(1)_Y$ gauge group does not allow to accommodate mass terms for the gauge bosons or fermions without violating the gauge invariance. A minimal way to incorporate these observed masses is to implement spontaneous electroweak symmetry breaking (EWSB) at energies around the mass scale of the W and Z boson, often referred to as the "Higgs mechanism"[33–38], by introducing an SU(2) doublet of complex scalar fields $\Phi = (\Phi^+, \Phi^0)^T$. When the neutral component obtains a non-zero vacuum expectation value $v/\sqrt{2} \neq 0$, the $SU(2)_L \times U(1)_Y$ symmetry is broken to $U(1)_{QED}$, giving mass to the three electroweak gauge bosons $W^\pm, Z^0$ while keeping the photon massless and hence leaving the electromagnetic symmetry $U(1)_{QED}$ unbroken. From the remaining degree of freedom of the scalar doublet, we obtain an additional scalar particle, the Higgs boson.

The Higgs mechanism also allows one to introduce fermion masses by Yukawa couplings to the scalar field and its conjugate, given by $m_f = \lambda_f v/\sqrt{2}$, hence introducing a Yukawa coupling constant λ_f for each massive fermion in the Standard Model. With its Yukawa coupling close to unity, the top quark seems to play a special role in the mass generation process.

The mixing of the mass (flavour) eigenstates into the weak charged current eigenstates for quarks is described by the Cabibbo-Kobayashi-Maskawa (CKM) matrix [39, 40]. By convention, this is done by a 3 x 3 unitary matrix V_{CKM} which operates on the negatively charged flavour states d, s and b.

$$\begin{pmatrix} d' \\ s' \\ b' \end{pmatrix}_L = \begin{pmatrix} V_{ud} & V_{us} & V_{ub} \\ V_{cd} & V_{cs} & V_{cb} \\ V_{td} & V_{ts} & V_{tb} \end{pmatrix} \begin{pmatrix} d \\ s \\ b \end{pmatrix}_L \equiv \mathbf{V_{CKM}} \begin{pmatrix} d \\ s \\ b \end{pmatrix}_L$$

This complex matrix could have 18 independent parameters. However, to conserve the number of states, this matrix has to be unitary which means that only nine free parameters remain. An additional five out of the nine can be absorbed as phases in the quark wave functions. This results in four independent parameters in total – three real Euler angles and one complex phase, implementing CP violation in the Standard Model. Since the CKM matrix is not diagonal, charged current weak interactions can infer transitions between the quark generations ("generation mixing") with the coupling strengths of the $W^{\pm}$ boson to the physical up and down type quarks given by the matrix elements.

Due to the experimental evidence [41–47], neutrinos also have to be considered as massive particles, which leads among other things to the introduction of an analogue leptonic mixing matrix, the Pontecorvo-Maki-Nakagawa-Sakata (PMNS) matrix [48, 49]. It contains four independent parameters as well if one assumes that neutrinos are not Majorana particles.

In summary, we obtain with the Standard Model of elementary particle physics a theory that is renormalisable [50, 51], unitary and can be evaluated perturbatively at sufficiently high energies. It incorporates 25 parameters that have to be provided by measurements:

- 12 Yukawa couplings for the fermion masses
- 8 parameters for the CKM and PMNS mixing matrices
- 3 coupling constants α_s, g, g' of $SU(3)_{QCD}, SU(2)_L, U(1)_Y$ respectively
- 2 parameters from EWSB: v, m_H

At the currently accessible energy scales, the Standard Model describes successfully the interactions of the fundamental fermions and gauge bosons, with only the Higgs boson remaining to be observed. For a more detailed introduction to the Standard Model, the reader is referred to corresponding textbooks [52–54] on elementary particle physics or topical reviews like [55].

2.2 The need for the Top Quark in the Standard Model framework

The existence of the top quark was postulated well before its discovery mainly for three reasons:

The first argument comes from the necessity that the Standard Model has to be a renormalisable theory. When expressed via a perturbation series – usually depicted in Feynman diagrams with first order "tree" diagrams and

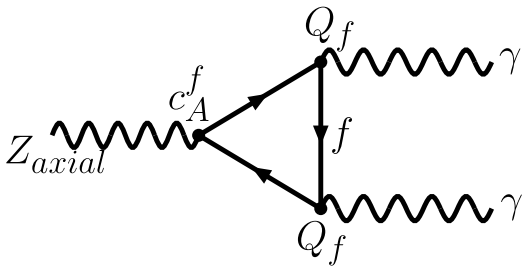

Figure 1: A "problematic" fermion triangle diagram that could introduce an anomaly.

higher order "loop" terms – certain loop diagrams cause divergences that have to cancel exactly to ensure that the theory is renormalisable. One example is the fermion triangle diagram as shown in Figure 1. The contribution for each such diagram is proportional to $c_A^f Q_f^2$ with c_A^f being the weak neutral current axial coupling strength and Q_f the electric charge for the respective fermion in the loop. Since $c_A^f = T_3$ and neutrinos obviously do not contribute, for the total strength of the anomaly to be cancelled we need to have an equal number of lepton flavours and quark doublets $N_{families}$ and quarks to occur in three colours ($N_c = 3$):

$$\sum_{i=1}^{N_{families}} \left(-\frac{1}{2}(-1)^2 + \frac{1}{2} N_c \left(+\frac{2}{3} \right)^2 - \frac{1}{2} N_c \left(-\frac{1}{3} \right)^2 \right) \stackrel{!}{=} 0.$$

Consequently, already the discovery of the τ lepton called for an additional quark doublet to be present as well to keep the Standard Model renormalisable.

The second argument results from the fact that transitions that change the flavour but not the charge of a fermion like $u \leftrightarrow c \leftrightarrow t$ or $d \leftrightarrow s \leftrightarrow b$ are experimentally observed to be strongly suppressed. The absence of these flavour-changing neutral currents (FCNC) for two quark generations could be explained with the GIM mechanism [56] by postulating the existence of the charm quark – and thus the completion of the second quark doublet – years before its discovery. This mechanism can be applied in the same way for three quark generations, and hence a sixth quark as a partner of the b quark is necessary to complete the doublet.

The third argument comes from the experimental confirmation that the b quark is not a weak isospin singlet but is part of an isospin doublet carrying the weak isospin $T_3 = -\frac{1}{2}$ and electric charge $Q_b = -\frac{1}{3}e$.

The electric charge of the b quark was measured first at the electron-positron storage ring DORIS at DESY operating on the Υ and Υ' resonances

via a measurement of the cross section for resonant hadron production σ_h [57–59]. The integral over σ_h is related with the electronic partial width Γ_{ee}, the hadronic partial width Γ_h, the total width Γ_{tot} and the resonance mass M_R via $\int \sigma_h \; dM = 6\pi^2 \Gamma_{ee} \Gamma_h / (M_R^2 \Gamma_{tot})$. Assuming that the total width is dominated by the hadronic partial width ($\Gamma_h \approx \Gamma_{tot}$), the measurement of the integrated cross section and the resonance mass allows one to extract the electronic partial width Γ_{ee} of the Υ respectively Υ'. In the framework of non-relativistic quarkonium potential models [60, 61], this partial width can then be related with the bound quark's charge.

The weak isospin of the b quark has been measured via the forward-backward asymmetry A_{FB} in the process $e^+e^- \to b\bar{b} \to \mu^{\pm}+$ hadrons with the JADE detector at PETRA [62]. The asymmetry originates from electroweak interference effects and is defined as the difference of the number of fermions produced in forward direction (with polar angle $\theta < 90°$) and the number of fermions produced in backward direction ($\theta > 90°$), normalised to the sum of both numbers. A_{FB} is proportional to the ratio of weak axial to electric charge and would vanish for a weak isospin singlet. For a $T_3 = -\frac{1}{2}, Q = -\frac{1}{3}e$ b quark the asymmetry is predicted to be -25.2%, in good agreement with the measurement of -22.8 ± 6.0 (stat.) $\pm$ 2.5 (syst.)%.

Resulting from these measurements of its weak isospin partner, the top quark's weak isospin and electric charge within the Standard Model framework could be assigned well before its actual discovery to be $T_3 = +\frac{1}{2}$, $Q_t = +\frac{2}{3}e$. The mass of the top quark however, being a free parameter in the Standard Model, is not predicted. Nevertheless, it is possible to constrain the top quark mass indirectly from electroweak precision measurements.

2.3 Top Quark mass prediction from electroweak precision measurements

As discussed above, the Standard Model comprises a set of free parameters that are a priori unknown. However, once these parameters have been measured, all physical observables can be expressed in terms of those parameters. To make optimal use of the predictive power of the theory, it is therefore crucial to measure its input parameters with the highest possible precision, allowing to experimentally probe the self-consistency of the Standard Model for possible contributions beyond its scope. Since the Standard Model is a renormalisable theory, the prediction for any observable can be calculated to any order of a perturbation series as well.

Electroweak processes mainly depend on three parameters: the coupling constants g and g' of $SU(2)_L$ and $U(1)_Y$ respectively and the Higgs vacuum

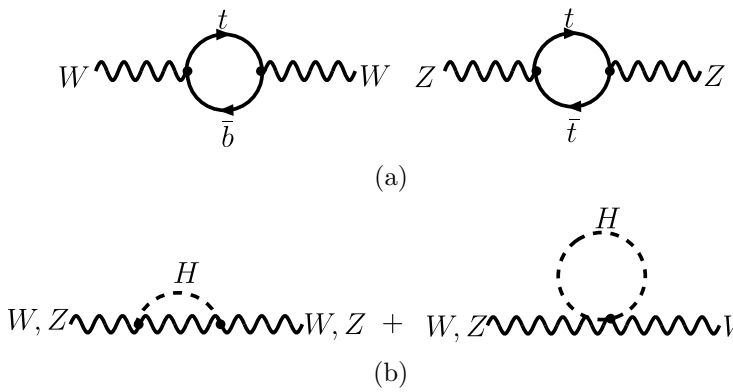

Figure 2: (a) Radiative corrections to the W and Z propagator with top quark contribution. (b) Radiative corrections to the W and Z propagator with Higgs boson contribution.

expectation value v. Since these input parameters have to be derived from experiment, it is useful to substitute them with the precisely measured quantities of the electromagnetic fine structure constant α (using electron-positron annihilations into hadrons at low centre of mass energies [63–65]), the Fermi constant G_F (using muon lifetime measurements [66, 67]) and the mass of the Z boson m_Z (using electron-positron annihilations around the Z pole [68]).

With these input values, the theoretical framework can be used to predict other quantities like the W boson mass. Given precision measurements, the W boson mass is sensitive to the mass of the top quark and the mass of the Higgs boson via higher order quantum effects leading to radiative corrections [69–71].

The most precise electroweak measurements to date have been performed at the Large Electron-Positron (LEP) Collider [72, 73] at CERN with its four experiments ALEPH [74, 75], DELPHI [76, 77], L3 [78, 79] and OPAL [80, 81] and the Stanford Linear Collider (SLC) [82, 83] with the SLD experiment [84, 85]. The LEP experiments together have analysed 17 million Z decays, being complemented by a sample of 600 thousand Z bosons produced with longitudinally polarised electron beams analysed by SLD.

Defining the electroweak mixing angle θ_W via the vector boson masses as follows:

$$\frac{m_W^2}{m_Z^2} = 1 - \sin^2\theta_W,$$

one can express the W boson mass through

$$m_W^2 = \frac{\pi\alpha}{\sqrt{2}G_F} \cdot \frac{1}{\sin^2\theta_W(1-\Delta r)}.$$

The radiative corrections Δr are a directly observable quantum correction of the electroweak theory, depending on α, m_W, m_Z, m_H and m_t. The contributions from single-loop insertions containing the top quark and the Higgs boson as depicted in Figure 2 are:

$$\begin{aligned} \Delta r^{top} &= -\frac{3\sqrt{2}G_F\cot^2\theta_W}{16\pi^2} \cdot m_t^2 \qquad (\text{for } m_t \gg m_b) \\ \Delta r^{Higgs} &= \frac{3\sqrt{2}G_F m_W^2}{16\pi^2} \cdot \left(\ln\frac{m_H^2}{m_W^2} - \frac{5}{6}\right) \quad (\text{for } m_H \gg m_W) \end{aligned}$$

A precise measurement of the W and Z boson masses thus gives access to the top quark and Higgs boson masses. The top quark contribution to the radiative corrections is sizeable especially due to the large mass difference with respect to its weak isospin partner, the b quark. While the leading top quark contribution to Δr is quadratic, it is only logarithmic for the Higgs boson contribution. Consequently, the constraints that can be derived on the top quark mass are much stronger than for the Higgs boson mass.

In 1994, the most stringent constraints on the top quark mass were derived based on preliminary LEP and SLD data, combined with W boson mass measurements from proton-antiproton experiments and neutral to charged current ratios obtained from neutrino experiments, yielding $178 \pm 11\ ^{+18}_{-19}$ GeV/c^2 [3]. As illustrated in Figure 3(a), the central value and the first set of errors are derived from the χ^2 distribution of the Standard Model fit to the electroweak precision data for a Higgs boson mass of 300 GeV/c^2, while the second set of errors stems from a variation of the Higgs boson mass between 60 and 1000 GeV/c^2.

The good agreement between the prediction and the actual observation is one of the great successes of the Standard Model, illustrated in Figure 3(b) versus time. Also the latest mass prediction from electroweak precision data, yielding $179\ ^{+12}_{-9}$ GeV/c^2 without using constraints on the Higgs boson mass [86], is in good agreement with the current world average mass of 172.4 $\pm$ 1.2 GeV/c^2 [12].

This success gives also more weight to the predictions of the mass of the Higgs boson in the Standard Model framework. Since the precision of the prediction crucially depends on the accuracy of the mass measurements of the W boson and the top quark used as input, this gives a strong motivation for improving the corresponding measurements. The currently resulting constraints on the mass of the Higgs boson will be discussed in Section 7.3.4.

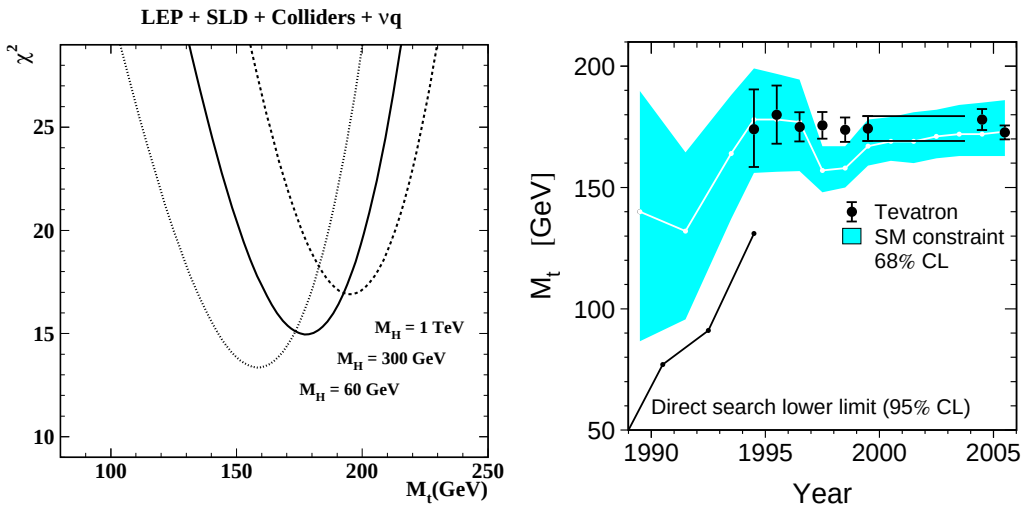

(a) (b)

Figure 3: (a) χ^2 distributions of the Standard Model fit to electroweak precision data versus top quark mass for various Higgs boson masses [3]. (b) Comparison of the indirect top quark mass measurements via radiative corrections (shaded area) with the direct measurements from the Tevatron (points) versus time [68].

More details on electroweak precision measurements can be found in corresponding topical reviews such as [87, 88].

3 Production and Decay of Top Quarks

The production of top quarks is only possible at highest centre of mass energies $\sqrt{s}$, set by the scale of the top quark mass. The necessary energies for Standard Model production of top quarks are currently (and will be at least for the next decade) only accessible at hadron colliders. The Tevatron proton-antiproton collider started operation at $\sqrt{s} = 1.8$ TeV in 1987 for a first period of data taking ("Run 0") until 1989 with the CDF experiment which recorded about 4 pb^{-1} of integrated luminosity. The next data taking period from 1992 until 1996 at $\sqrt{s} = 1.8$ TeV (the so-called Run I) was utilised by the CDF and D0 experiments and facilitated the discovery of the top quark. For the currently ongoing data taking that started in 2001 (Run II), the centre of mass energy has been increased to $\sqrt{s} = 1.96$ TeV. The Tevatron will lose its pure monopoly for top quark production only with the turning-on of the Large Hadron Collider (LHC) that will provide proton-proton collisions at $\sqrt{s} = 14$ TeV.

In the framework of the Standard Model, top quarks can be produced in pairs ($t\bar{t}$) predominantly via the strong interaction and singly via the electroweak interaction.

3.1 Top Quark Pair Production

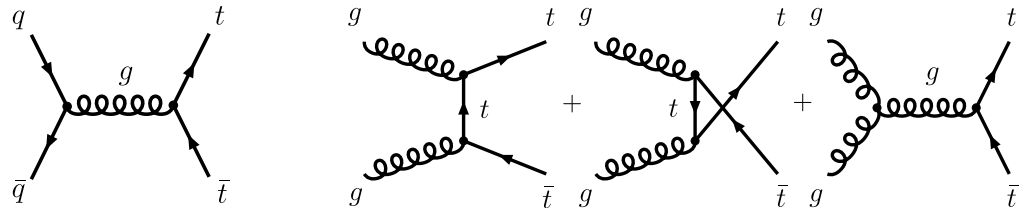

Figure 4: Leading order Feynman diagrams for top quark pair production: (a) quark-antiquark annihilation and (b) gluon-gluon fusion.

While hadron colliders give access to the highest centre of mass energies, the collision of hadrons complicates the theoretical description and prediction of physics processes like $t\bar{t}$ production since one has to consider the collision of composite particles.

The solution of this problem is provided by the QCD factorisation theorem [89, 90], separating hadron collisions into universal long distance (small momentum transfer) phenomena and perturbatively calculable short distance phenomena, involving large momentum transfers Q^2 and consequently the production of particles exhibiting large transverse momenta or large masses. These two are set apart by introducing a factorisation scale μ_F^2.

Using this approach, the (anti-) proton itself can be described by a collection of partons (quarks, antiquarks, gluons) interacting on a soft binding energy scale $\Lambda_{QCD} < 1$ GeV, whereas the collisions considered occur between the partons of the (anti-) proton on a "hard" energy scale with large transverse momenta $\geq \mathcal{O}(100$ GeV).

Consequently, the partons participating in the hard process (a, b) can be considered quasi-free and the partonic cross section $\hat{\sigma}_{a+b\to X}(\hat{s}, \alpha_s(\mu_R^2), \mu_R^2)$ of interest can be calculated using perturbative QCD independent of the type of hadrons containing the partons; the hatted variables here denote quantities on the parton rather than the hadron level. To be able to regularise the divergences occurring in higher order calculations (like ultraviolet divergences from loop insertions where the infinite range of four-momentum in the loop causes infinities in the integration from high momentum contributions), the renormalisation scale μ_R^2 needs to be introduced along with the corresponding

running coupling constant $\alpha_s(\mu_R^2)$. The leading order Feynman diagrams for $t\bar{t}$ production are shown in Figure 4.

The partons inside the incoming (anti-) proton cannot be described with perturbative QCD as the soft energy scale corresponding to small inherent momentum transfers imply large $\alpha_s(Q^2)$ couplings. The distribution of the longitudinal (anti-) proton momentum amongst the partons is described by Parton Distribution Functions (PDFs): $f_{a/A}(x, \mu_F^2)$ yields the probability to find a given parton a inside hadron A with momentum fraction x when probed at an energy scale μ_F^2. Collinear and soft (infrared) singularities that arise in the perturbative calculation of the partonic cross section discussed above are absorbed in these PDFs.

The factorisation theorem then allows one to calculate the $t\bar{t}$ production cross section via the integral over the corresponding hard scattering parton cross section folded with the parton distribution functions of the (anti-) proton as follows:

$$\sigma_{A+B\to t\bar{t}}(\sqrt{s}, m_t) = \sum_{a,b=g,q,\bar{q}} \int \hat{\sigma}_{a+b\to t\bar{t}}(\hat{s}, \alpha_s(\mu_R^2), \mu_R^2, \mu_F^2, m_t) \times f_{a/A}(x_a, \mu_F^2) f_{b/B}(x_b, \mu_F^2) dx_a dx_b.$$

The hadrons A and B correspond to proton and antiproton in case of the Tevatron and to protons in case of the LHC.

The physical cross section $\sigma_{A+B\to t\bar{t}}(\sqrt{s}, m_t)$ that would be the result of the evaluation of the full perturbation series does not depend on either of the two arbitrary scales for factorisation and renormalisation μ_F^2, μ_R^2 that had to be introduced for the above calculation. However, the parton distribution functions and the partonic cross section do depend on these scales, and hence the result of any finite order calculation will as well. This dependence gets weaker with the inclusion of higher order terms in the calculation. In practical application, both scales are usually set to the typical momentum scale of the hard scattering process Q such as the transverse momenta of the produced particles or the mass of the produced particle so that for the case of $t\bar{t}$ production one typically uses $\mu_F = \mu_R = \mu = m_t$. The scale dependence of the result is then usually tested by varying the central scale by a factor of two; the resulting variations are interpreted as systematic uncertainties which should not be mistaken as Gaussian.

The PDFs have to be determined experimentally, for example via deeply inelastic lepton scattering on nucleons, so that they can be extracted from the measured cross sections using perturbative calculations of the (hard) partonic cross sections. Once the parton densities $f_{a/A}(x_a, Q^2)$ have been measured for a certain momentum fraction x_a at a scale Q^2, their value at a different

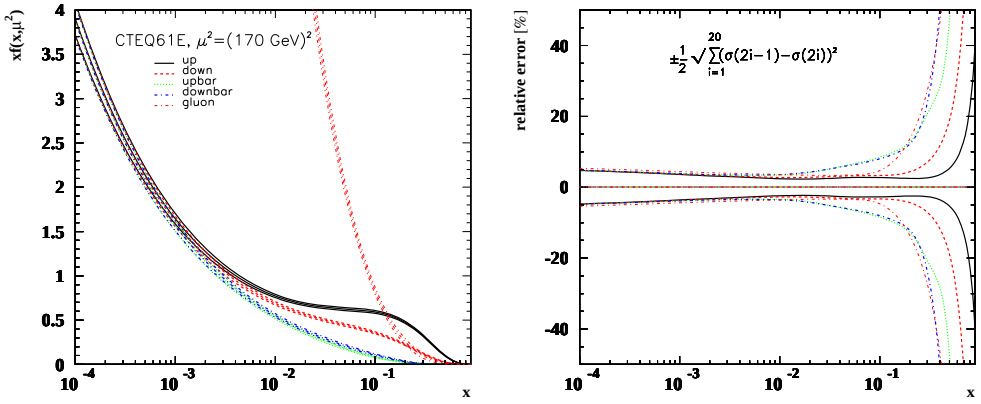

Figure 5: Left: CTEQ61 [94] parton distribution functions with uncertainty bands at the top quark mass scale ($Q^2 = (170\ \text{GeV})^2$) for (anti-) up quarks, (anti-) down quarks and gluons in the proton. Right: relative uncertainties on the PDFs shown on the left.

scale can be perturbatively predicted using the DGLAP evolution equation [91–93]. Since PDFs are universal and do not depend on the process they were derived from, they can then be used to predict the cross sections in other hard scattering processes. For consistent application, it is desirable to ensure the PDFs utilised are derived with same order perturbative calculations and renormalisation scheme as the calculation they are used for in the prediction.

The determination of PDFs proceeds via global fits to the available data and is for example pursued by the CTEQ [95], MRST [96], GRV [97], Alekhin [98], H1 [99] and ZEUS [100] groups. Different PDFs are provided based on various datasets, for different orders of perturbation theory, renormalisation schemes and fitting techniques – see for example the overview given in [101]. One commonly used set of PDFs derived at NLO and using the $\overline{MS}$ renormalisation scheme [102] is CTEQ61 [94], which incorporates especially the effects of Tevatron Run I jet production data on the gluon distribution. It also includes an error analysis based on a suit of eigenvector PDF sets that describe the behaviour of the global χ^2 function from the fit around its minimum. The resulting error on the PDF Δf can then be obtained by summing over the variations $f_i^{\pm}$ along/against each eigenvector for every free parameter in the global fit: $\Delta f = \pm\frac{1}{2}(\Sigma_{i=1}^{N_{par}}(f_i^+ - f_i^-)^2)^{\frac{1}{2}}$.

Figure 5 shows the corresponding most important parton distributions inside protons for $t\bar{t}$ production at the Tevatron or LHC and their uncer-

tainties. For antiprotons, quarks and antiquarks have to be exchanged in Figure 5. All PDFs vanish at large momentum fractions x, and the gluon density starts to dominate over the valence quark densities around $x = 0.13$. There is no flavour symmetry between the up and down quark distributions, neither on the valence nor the sea quark level (the latter is better visible at lower Q^2). At x-values below 0.1, typical relative uncertainties on the PDFs of valence quarks and gluons are around 5%. At larger x-values however, these uncertainties increase drastically, especially for gluons.

To produce a top quark pair, the squared centre of mass energy at parton level $\hat{s} = x_a x_b s$ must at least be equal to $(2m_t)^2$. Assuming $x_a \approx x_b =: x$ yields as threshold for $t\bar{t}$ production:

$$\langle x \rangle = \sqrt{\frac{\hat{s}}{s}} = \frac{2m_t}{\sqrt{s}} \approx \begin{cases} 0.192 & \text{@ Tevatron Run I, } \sqrt{s} = 1.8 \text{ TeV} \\ 0.176 & \text{@ Tevatron Run II, } \sqrt{s} = 1.96 \text{ TeV} \\ 0.025 & \text{@ LHC, } \sqrt{s} = 14 \text{ TeV} \end{cases}$$

Since large momentum fractions are necessary for $t\bar{t}$ production close to the kinematic threshold at the Tevatron, the production is dominated by quark-antiquark annihilation (Figure 4 (a)) of the valence (anti-) quarks. For Run I energies, quark-antiquark annihilation contributes roughly 90% of the total $t\bar{t}$ production rate, while for Run II energies this fraction is still 85% [18].

At the LHC, gluon-gluon fusion production dominates (Figure 4 (b)) with a contribution of about 90% [103] due to the small momentum fraction sufficient for $t\bar{t}$ production. This also allows one to use proton-proton instead of proton-antiproton collisions at the LHC without suffering major losses in the production cross section, hence avoiding the major technical challenge of producing an intense antiproton beam.

The increase in the centre of mass energy by ≈10% between Run I and Run II at the Tevatron and the correspondingly smaller minimum momentum fraction results in an increase in the $t\bar{t}$ production rate by 30%. At the LHC, it increases further by roughly a factor of 100 compared to that of the Tevatron.

The highest order complete perturbative calculations for heavy quark pair production available were performed at next-to-leading order (NLO) – to order α_s^3 – already in the late 1980s by Nason et al. [104] and Beenakker et al. [105, 106]. These calculations can be further refined by the inclusion of large logarithmic corrections [107–109] due to soft gluon emission that are particularly important for the production of heavy quarks close to the kinematic threshold ($\hat{s} \approx 4m^2, x \to 1$). The contributions of these logarithms are positive at all orders when evaluated at the heavy quark mass scale and hence their inclusion increases the production cross section above the NLO level.

Hadron Collider	Processes	$\sigma_{t\bar{t}}$ [pb]	Group
Tevatron Run I	90% $q\bar{q} \to t\bar{t}$	$5.19^{+0.52}_{-0.68}$	Cacciari et al. [117]
($p\bar{p}$, $\sqrt{s} = 1.8$ TeV)	10% $gg \to t\bar{t}$	5.24 ± 0.31	Kidonakis et al. [119]
Tevatron Run II	85% $q\bar{q} \to t\bar{t}$	$6.70^{+0.71}_{-0.88}$	Cacciari et al. [117]
($p\bar{p}$, $\sqrt{s} = 1.96$ TeV)	15% $gg \to t\bar{t}$	6.77 ± 0.42	Kidonakis et al. [119]
LHC	10% $q\bar{q} \to t\bar{t}$	833^{+52}_{-39}	Bonciani et al. [118]
(pp, $\sqrt{s} = 14$ TeV)	90% $gg \to t\bar{t}$	873^{+2}_{-28}	Kidonakis et al. [120]

Table 3: NLO cross section predictions including soft gluon resummations beyond LL for $t\bar{t}$ production at the Tevatron and the LHC for a top quark mass of 175 GeV/c^2. For the different sources of the quoted uncertainties please refer to the text.

The impact of soft gluon resummation on the $t\bar{t}$ production cross section has been studied by Berger and Contopanagos [110–112], Laenen, Smith and van Neerven [113, 114] and Catani, Mangano, Nason and Trentadue [115, 116] at the leading logarithmic (LL) level. Studies including even higher level corrections as carried out by Cacciari et al. [117], based on work by Bonciani et al. (BCMN) [118], and Kidonakis and Vogt [119, 120] are summarised in Table 3.

In the case of $t\bar{t}$ production at the Tevatron, the inclusion of leading and next-to-leading logarithmic (NLL) soft gluon resummation affects the cross section value only mildly by $\mathcal{O}(5\%)$ (indicating production occurs not too close to the threshold) while significantly reducing the scale dependence of the predictions by roughly a factor of two to a level of $\approx 5\%$ [118]. At the LHC $t\bar{t}$ production takes place even further away from the kinematic threshold, but since gluon fusion production dominates there, the enhancement of the total production rate due to soft gluon resummation and the reduction of scale dependence stay at the same level as at the Tevatron.

The results of Cacciari et al. [117] for the Tevatron use the NLO calculation with LL and NLL resummation at all orders of perturbation theory as carried out by Bonciani et al. (BCMN) [118] but are based on the more recent PDF sets with error analysis CTEQ6 [95] and MRST2001E [96] and also MRST2001 [121] which includes varied α_s values in the PDF fit. The updated PDFs cause an increase in the central values of about 3% w.r.t. [118]. While the central values are very similar for the MRST2001E and CTEQ6 PDFs, the uncertainties for CTEQ6 are almost twice as large as the MRST2001E ones unless the variations of α_s in MRST2001 are taken into

account as well. For the determination of the uncertainty on the cross section Cacciari et al. combine linearly the uncertainty due to scale variation by a factor of two with the PDF uncertainty evaluated at that scale. As central values, the CTEQ6M results are chosen, and the maximum uncertainties given in their study stem from the CTEQ6 PDF variation for the lower respectively the α_s variation in MRST2001 for the upper error bound. The PDF uncertainties and α_s variation contribute about 45% and 80% respectively to the total quoted uncertainty including the scale variations, which emphasises the importance of considering α_s uncertainties in PDF fits. The PDF uncertainties are in turn dominated by the uncertainty of the gluon PDF at large x values, for example causing the gluon fusion contribution to the total production rate to fluctuate between 11% and 21% for $\sqrt{s} = 1.96$ TeV. Despite the large uncertainties on the $t\bar{t}$ production rate given in this study, the ratio of production cross sections for the two different centre of mass energies at the Tevatron is very stable and predicted with high precision: $\sigma(1.96 \text{ TeV})/\sigma(1.8 \text{ TeV}) = 1.295 \pm 0.015$ for top quark masses between 170 and 180 GeV/c^2 [117].

A prediction for the $t\bar{t}$ production rate at the LHC applying the same level of soft gluon resummation is given by Bonciani et al. [118] using the PDF set MRS(R_2) [122]. Since no PDF uncertainties were available for this study, the quoted uncertainty in Table 3 comes from scale variation by a factor of two alone. Since gluon fusion here is the dominant contribution to the total rate, uncertainties on the gluon PDFs alone lead to an uncertainty of $\approx 10\%$ on the total production cross section [123].

The studies performed by Kidonakis and Vogt [119, 120] consider soft gluon corrections up to next-to-next-to-next-to leading logarithmic (NNNLL) terms at NNLO in a truncated resummation, resulting in a reduced sensitivity of their result w.r.t. scale variations of $\approx 3\%$. For the Tevatron, the $t\bar{t}$ production cross section is evaluated using MRST2002 NNLO [96] and CTEQ6M NLO [95] parton densities. Two different parton level kinematics are considered for the scattering process: one-particle inclusive (1PI) and pair-invariant mass (PIM) kinematics [103]. While both sets of PDFs give very similar results, the variations due to the kinematics are significant. Consequently, the average of 1PI and PIM kinematics for both PDFs is used as the central value in Table 3, while the separate averages over the PDF sets for 1PI and PIM respectively are quoted as uncertainty. For the LHC rate prediction which is dominated by the gluon fusion process, the 1PI kinematics is considered more appropriate, and the value in Table 3 gives the corresponding result using MRST2002 NNLO PDFs, using scale variation by a factor of two for the given uncertainties.

All results in Table 3 are evaluated for a top quark mass of 175 GeV/c^2,

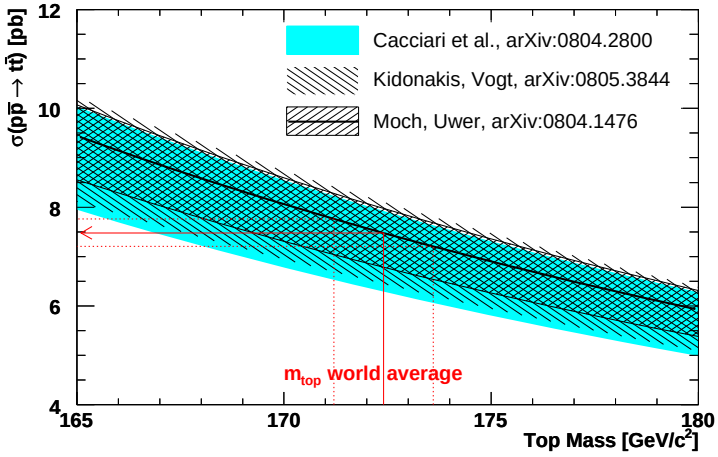

Figure 6: Dependence of the $t\bar{t}$ production cross section at the Run II Tevatron on the top quark mass. The current world average top mass and the resulting $t\bar{t}$ production cross section are indicated. The predictions are based on the CTEQ6.6M [124] PDF set.

and the given Run II predictions have been the main references used so far by CDF and D0. To be able to better compare the uncertainties of the predictions, for the Kidonakis and Vogt result an additional uncertainty obtained from the maximum simultaneous scale and PDF variation[1] was added in quadrature with the uncertainty due to the considered kinematics [125].

In spring 2008, Cacciari et al. [126] and Kidonakis et al. [127] updated their predictions using more recent PDF sets like CTEQ6.6M [124], which had only little impact on the results. In addition, Moch and Uwer [128] have now performed a complete NNLL soft gluon resummation and provide an approximation of the NNLO cross section also based on CTEQ6.6M. To illustrate the dependence of the predictions on the top quark mass, Figure 6 shows the central values and uncertainties of references [126–128] for the Run II Tevatron versus the top quark mass. The functional form of an exponential as suggested in [116] is applied in a fit to the central values and uncertainties for Kidonakis et al., while third order polynomials as provided by the authors are used for the other references. The total uncertainties are obtained by combining the provided uncertainties linearly.

For the current world average top quark mass of 172.4 ± 1.2 GeV/c^2 [12], the predicted $t\bar{t}$ production cross section is $7.2^{+0.8}_{-0.9}$ pb for Cacciari et al.,

[1]The PDF uncertainties in this case stem from CTEQ6 sets 129 and 130 alone.

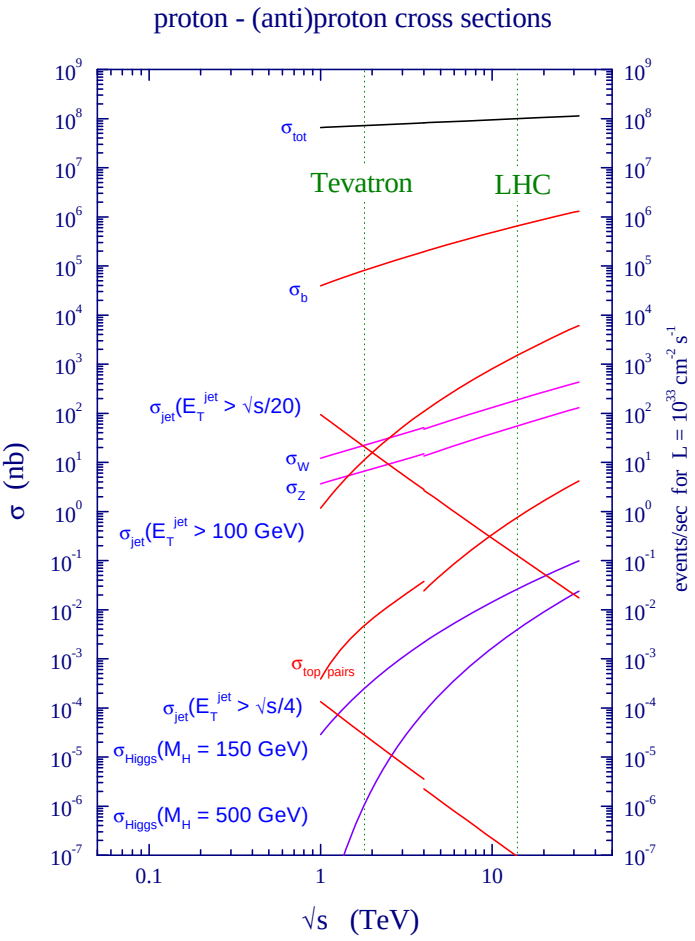

Figure 7: Cross sections for various processes at hadron colliders versus centre of mass energy [123]. σ_t denotes the $t\bar{t}$ production cross section.

$7.3^{+0.8}_{-0.9}$ pb for Kidonakis et al. and $7.5^{+0.5}_{-0.7}$ pb for Moch et al.. An additional uncertainty on these values due to the top quark mass uncertainty is ± 0.3 pb for all three predictions. It should be noted that these predictions based on MRST 2006 NNLO PDF sets [129] yield about 6% higher central values and exhibit smaller PDF uncertainties.

A precise measurement of the $t\bar{t}$ production cross section allows one to test the Standard Model predictions for physics beyond its scope. Together with a precise mass measurement, the self-consistency of the predictions can be tested as well. Since $t\bar{t}$ production is a major source of background for single top production discussed in the next section, Standard Model Higgs boson production and also many phenomena beyond the Standard Model,

its accurate understanding is crucial for these studies.

Figure 7 illustrates the production rates of various processes versus centre of mass energy for proton-antiproton collisions below $\sqrt{s} = 4$ TeV and for proton-proton collisions above $\sqrt{s} = 4$ TeV. As can be appreciated from the plot, $t\bar{t}$ production is suppressed by ten orders of magnitude w.r.t. the total interaction rate at the Tevatron and eight orders of magnitude at the LHC. While the LHC is often referred to as a "top-factory" due to the increased production cross section by two orders of magnitude, the signal extraction from the large background is still a challenge at both hadron colliders, requiring efficient triggers and selection methods. The $t\bar{t}$ cross section measurements performed at the Run II Tevatron will be described in Section 5.1.

3.2 Single Top Quark Production

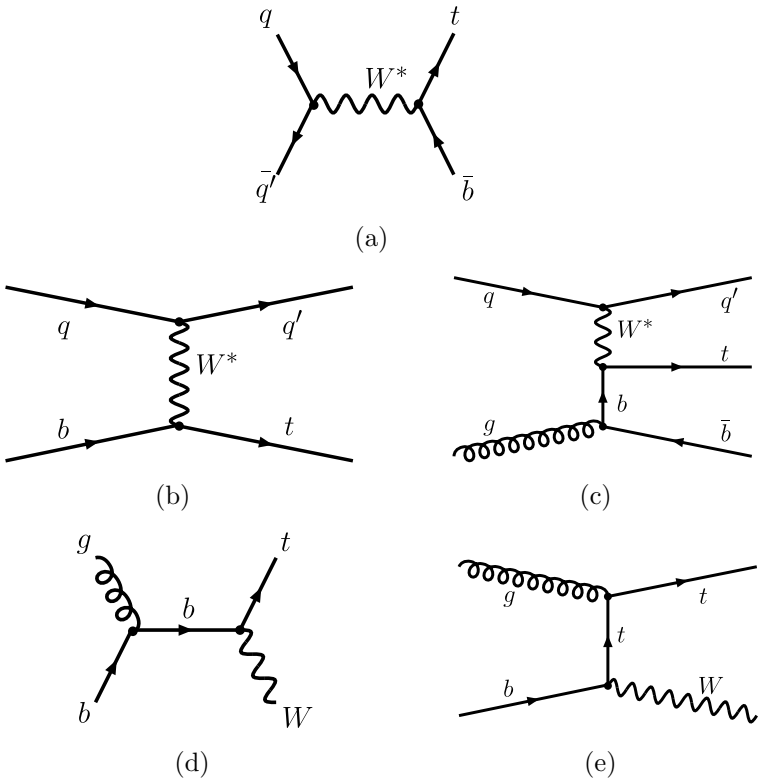

Figure 8: Representative Feynman diagrams for electroweak single top quark production: (a) s-channel, (b,c) t-channel and (d,e) associated production.

In addition to the strong pair production discussed in the previous section, top quarks can also be produced singly via the electroweak interaction

through a Wtb vertex (see Figure 8); Wts and Wtd vertices are strongly CKM suppressed (see Section 3.3.1). There are three different production modes, classified via the virtuality (negative squared four-momentum q) of the participating W boson $Q_W^2 = -q^2$:

- The Drell-Yan-like *s-channel* production proceeds via quark-antiquark annihilation into a time-like virtual W boson ($q^2 \geq (m_t + m_b)^2 > 0$) as illustrated in Figure 8(a): $q\bar{q}' \rightarrow t\bar{b}$ [130, 131].

- In the "flavour excitation" *t-channel* process a space-like virtual W boson ($q^2 < 0$) couples to a b quark from the sea to produce a top quark as shown in Figure 8(b): $qb \rightarrow q't$. A higher order contribution of $\mathcal{O}(\alpha_s)$ comes from gluon splitting as depicted in Figure 8(c) which is also referred to as W-gluon fusion: $qg \rightarrow tq'\bar{b}$ [132–135].

- In the *associated production*, an on-shell W boson ($q^2 = m_W^2$) is produced together with a top quark from a b quark and a gluon as illustrated in Figure 8(d,e): $gb \rightarrow tW$ [136–141].

In the above list, the charge conjugate processes are implied for each production mode and in the reactions q indicates a light-flavour quark. It should be noted that all three modes differ in both initial and final states. Consequently, the final states are used as well to denote s-channel (tb), t-channel (tq, tqb) and associated (tW) production. The corresponding signatures can be used to discriminate between the production modes: The s-channel is characterised by the additional b quark produced with the top quark, the t-channel by a forward light quark and associated production by the decay products of the W boson to be detected in addition to those of the top quark. Due to the incoming b quark and gluon, t-channel and tW-channel rates especially depend on the corresponding PDFs which are known with less precision than the PDFs of the proton valence quarks; the cross section measurements in return will allow one to further constrain the b quark and gluon PDFs.

The cross sections of all three modes have been evaluated at NLO, including radiative corrections of $\mathcal{O}(\alpha_s)$ (s-channel: [142–144], t-channel: [142, 145, 146], tW-channel: [147, 148]); the most recent references given here being fully differential. Later calculations also include the top quark decay at NLO (s-channel: [149–151], t-channel: [149, 151, 152], tW-channel: [153]) and recently NLO calculations with higher-order soft gluon corrections up to NNNLO at NLL accuracy have become available as well [154–156].

Table 4 summarises the expected single top production cross sections at the Tevatron and the LHC for the NLO calculations by Sullivan [157] (based

Hadron Collider	$t/\bar{t}$	σ_{tb} [pb]	σ_{tq} [pb]	σ_{tW} [pb]	Group
Tevatron Run I ($p\bar{p}$, $\sqrt{s} = 1.8$ TeV)	$t, \bar{t}$	$0.75^{+0.10}_{-0.09}$	$1.46^{+0.20}_{-0.16}$	—	Sullivan [157]
Tevatron Run II ($p\bar{p}$, $\sqrt{s} = 1.96$ TeV)	$t, \bar{t}$	$0.88^{+0.12}_{-0.11}$	$1.98^{+0.28}_{-0.22}$	—	Sullivan [157]
		0.98 ± 0.04	2.16 ± 0.12	0.26 ± 0.06	Kidonakis [156]
LHC (pp, $\sqrt{s} = 14$ TeV)	t	$6.56^{+0.69}_{-0.63}$	$155.9^{+7.5}_{-7.7}$	—	Sullivan [157]
	$\bar{t}$	$4.09^{+0.43}_{-0.39}$	$90.7^{+4.3}_{-4.5}$	—	
	t	$7.2^{+0.6}_{-0.5}$	146 ± 5	41 ± 4	Kidonakis [156]
	$\bar{t}$	4.0 ± 0.2	89 ± 4	41 ± 4	

Table 4: Cross section predictions for s-channel (tb), t-channel (tq) and associated (tW) single top production at NLO (Sullivan) and NLO including soft gluon resummations (Kidonakis) at the Tevatron and the LHC for a top quark mass of 175 GeV/c^2. For the different sources of the quoted uncertainties please refer to the text.

on the work of Harris et al. in [142]) and the NLO results including soft gluon resummations by Kidonakis [156] (based on his work in [154, 155] and matching to the exact NLO results of Harris et al. [142] and Zhu [147, 148]). Both results use current PDFs and include corresponding uncertainties.

While at the Tevatron top and antitop production are identical for all production modes, at the LHC this is only the case for associated production. Consequently, the results given for the Tevatron include both top and antitop production but are given separately for the LHC.

The NLO results by Sullivan are based on CTEQ5M1 PDFs [158] for the central values. The given uncertainties are due to PDFs, derived using CTEQ6M [95], added in quadrature with uncertainties due to scale variations by a factor of two, top quark mass variations by 4.3 GeV/c^2 (from a previous top mass world average $m_t = 178 \pm 4.3$ GeV/c^2 [159]), b quark mass and α_s uncertainties, the latter two being negligible compared to the others. The rate dependence on the top quark mass is approximated to be linear and is especially noticeable in the s-channel since a change from 175 GeV/c^2 to the current world average top quark mass of 172.4 GeV/c^2 raises the rates at the Tevatron by 7% for the s-channel and 5% for the t-channel. The observed scale uncertainties are reduced w.r.t. LO results and amount to 4-6% at the Tevatron and 2-3% at the LHC.

The NLO calculations by Kidonakis including higher order soft gluon

corrections yield single top production cross sections based on MRST2004 NNLO PDFs [160]. The quoted values are obtained by matching the NLO cross section to the results of Harris et al. [142] and Zhu [147, 148], including the additional soft gluon corrections up to NNNLO. Exceptions are the tW rate at the Tevatron where no corresponding NLO result is available and hence the value given is not matched and the t-channel rate at the LHC where no soft gluon corrections are considered and an updated NLO result with the quoted PDFs is given instead. The uncertainties given are derived from scale variations by a factor of two added in quadrature with PDF uncertainties derived using the MRST2001E NLO set [96]. No mass uncertainty is included. At the Tevatron, the t-channel uncertainty is dominated by the PDF uncertainty and corrections due to soft gluon resummations w.r.t. LO are small ($\approx$5%). In contrast to this, the soft gluon corrections have a large effect (>60%) for the s-channel at the Tevatron and scale uncertainties dominate over those from PDFs.

At the Tevatron, t-channel production dominates the total rate of single top quark production with $\approx$65% contribution, followed by s-channel production with $\approx$30%. Associated (tW) production at the Tevatron contributes only $\approx$5% to the total rate, and is usually neglected there. At the LHC, t-channel production again dominates with $\approx$74%, followed now by associated production with $\approx$23%. s-channel production only contributes $\approx$3% at the LHC due to the missing valence antiquarks in the collisions and will be difficult to discriminate from the background. Despite being a weak process, single top production occurs with a cross section of the same order of magnitude as $t\bar{t}$ production, with $\mathcal{O}(40\%)$ of the $t\bar{t}$ rate at both the Tevatron and the LHC, since only one heavy top quark is produced. Thus it is accessible with smaller and hence better populated momentum fractions of the partons. Furthermore, no colour matching is necessary for the production.

The measurement of the single top production allows one to study the top quark's weak interaction, giving direct access to the CKM matrix element $|V_{tb}|$ since the cross sections in all three production modes are proportional to $|V_{tb}|^2$. The polarisation of the top quark at production is preserved due to its short lifetime and allows one to test the $V-A$ structure of the weak interaction via angular correlations amongst the decay products [161–164]. All three production modes are differently sensitive to various types of physics beyond the Standard Model (BSM) [165] which makes their independent reconstruction desirable. The s-channel is sensitive to the existence of exotic charged bosons (like a W' or charged Higgs) coupling to the top-bottom weak isospin doublet which could be detectable through an enhancement of the observed cross section. Such effects would not be visible in the tW mode where the W boson is on-shell or in the t-channel where the virtual

W boson is space-like and cannot go on-shell like in the s-channel. The t-channel production rate could be enhanced via FCNC processes involving new couplings between the up-type quarks and a boson (Higgs, gluon, photon, Z) which would be hardly experimentally observable in the s-channel since they would remove the final state b quark which is essential for the signal discrimination in that production mode. The tW channel finally is the only mode allowing a more direct test of the Standard Model Wtb vertex since the W boson involved is not virtual.

A thorough understanding of single top quark production will also facilitate the study of processes exhibiting a similar signature like for example Standard Model W-Higgs production or BSM signals to which single top production is a background process. Despite a production rate similar to that of $t\bar{t}$, the signature for single top quark production is much harder to separate from its background processes, which delayed first measurements until very recently. The current analyses at the Tevatron give first evidence for the production of single top quarks and will be described in Section 5.8.

3.3 Top Quark Decay

3.3.1 Top Quark CKM Matrix Elements

Since the mass of the top quark is above the threshold for Wq decays with q being one of the down-type quarks d, s, b, its decay is dominated by the two-body decay $t \to Wq$. The contribution of each quark flavour to the total decay width is proportional to the square of the respective CKM matrix element V_{tq}. Utilising the unitarity of the CKM matrix and assuming three quark generations, the corresponding matrix elements can be indirectly constrained at 90% confidence level to be [166]:

$$\begin{aligned} |V_{td}| &= 0.0048 - 0.014 \\ |V_{ts}| &= 0.037 - 0.043 \\ |V_{tb}| &= 0.9990 - 0.9992 \end{aligned}$$

Consequently, the decay $t \to Wb$ is absolutely dominant and will be considered exclusively throughout this article unless explicitly noted. Potential deviations from the Standard Model decay will be discussed in Section 6.

It should be noted that the above constraints on the top quark CKM matrix elements would change dramatically (especially for V_{tb}) if more than three quark generations would exist (unitarity of the expanded matrix is

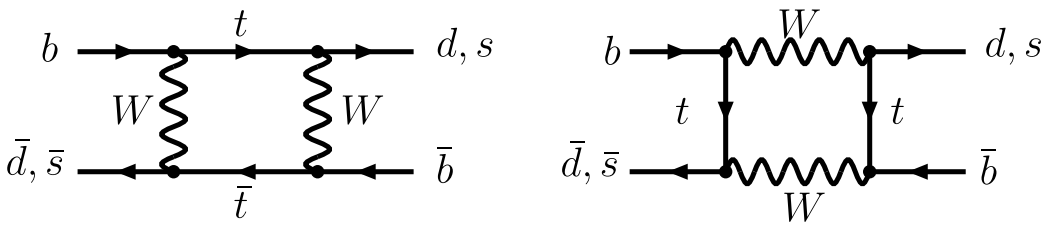

Figure 9: Feynman "box" diagrams for $B_d^0 - \overline{B_d^0}$ and $B_s^0 - \overline{B_s^0}$ mixing.

assumed) [166]:

$$\begin{aligned} |V_{td}| &= 0 - 0.08 \\ |V_{ts}| &= 0 - 0.11 \\ |V_{tb}| &= 0.07 - 0.9993 \end{aligned}$$

It is thus important to constrain these matrix elements as well by measurements, as outlined below.

The V_{td} and V_{ts} matrix elements are not measurable via tree level top decays, but in the framework of the Standard Model they can be inferred from B-meson mixing shown in Figure 9. While in the depicted box diagrams all up-type quarks can contribute, the top quark contribution is dominant [167]. The oscillation frequency given by the mass difference Δm between heavy and light mass eigenstates – Δm_d for $B_d^0 - \overline{B_d^0}$ and Δm_s for $B_s^0 - \overline{B_s^0}$ oscillations – is proportional to the combination of CKM matrix elements $|V_{tb}^* V_{td}|^2$ respectively $|V_{tb}^* V_{ts}|^2$. The mass difference for the $B_d^0 - \overline{B_d^0}$ system has been precisely measured: $\Delta m_d = 0.507 \pm 0.004$ ps^{-1} [168]. Using CKM unitarity and assuming three generations, resulting in $|V_{tb}| \approx 1$, this translates into $V_{td} = (7.4 \pm 0.8) \cdot 10^{-3}$ [169], where the uncertainty arises primarily from the theoretical uncertainty on the involved hadronic matrix element obtained from lattice QCD calculations. In order to reduce these theoretical uncertainties, the measurement of the ratio in which some uncertainties cancel is desirable: $\Delta m_d / \Delta m_s \propto |V_{td}|^2 / |V_{ts}|^2$. With the recent first measurements of B_s^0-oscillations by D0 and CDF at the Tevatron [170, 171], yielding 17 ps^{-1} $< \Delta m_s <$ 21 ps^{-1} at 90% C.L. and $\Delta m_s = (17.31^{+0.33}_{-0.18}(\text{stat.}) \pm 0.07(\text{syst.}))\text{ps}^{-1}$, this ratio could be measured for the first time: $|V_{td}/V_{ts}| = 0.208^{+0.001}_{-0.002}(\text{expt.})^{+0.008}_{-0.006}(\text{theor.})$. The obtained results are in good agreement with the Standard Model expectations.

The direct measurement of the V_{tb} matrix element without assuming three quark generations and unitarity of the CKM matrix is only possible via single top quark production described in Section 3.2, since the production rate in each channel is proportional to $|V_{tb}|^2$. One way to assess the relative size of

$|V_{tb}|$ compared to $|V_{td}|$ and $|V_{ts}|$ is to measure the ratio R of the top quark branching fractions which can be expressed via CKM matrix elements as

$$R = \frac{\mathcal{B}(t \to Wb)}{\mathcal{B}(t \to Wq)} = \frac{|\, V_{tb}\,|^2}{|\, V_{tb}\,|^2 + |\, V_{ts}\,|^2 + |\, V_{td}\,|^2}\,.$$

Assuming three generation unitarity, the denominator in the above expression is one, and constraints on $|V_{tb}|$ can be inferred. The current status of these R measurements is discussed in Section 6.2.

The most precise determination of the top quark CKM matrix elements to date proceeds via global fits to all available corresponding measurements, imposing the Standard Model constraints of three generation unitarity as done by the CKMfitter [172] or UTfit [173] groups. The CKMfitter update for summer 2007 yields [172]:

$$\begin{aligned} |V_{td}| &= 0.00868^{+0.00025}_{-0.00033} \\ |V_{ts}| &= 0.0407^{+0.0009}_{-0.0008} \\ |V_{tb}| &= 0.999135^{+0.000036}_{-0.000037}. \end{aligned}$$

3.3.2 Top Quark Decay Width

The Standard Model top quark decay width including first order QCD corrections can be expressed as follows [174, 175]:

$$\Gamma_t = |V_{tb}|^2\, \frac{G_F\, m_t^3}{8\pi\sqrt{2}} \left(1 - \frac{m_W^2}{m_t^2}\right)^2 \left(1 + 2\frac{m_W^2}{m_t^2}\right) \left[1 - \frac{2\alpha_s}{3\pi}\left(\frac{2\pi^2}{3} - \frac{5}{2}\right)\right].$$

In the above formula, we assume $m_b^2/m_t^2 \to 0$, $m_t^2 \gg m_W^2$ and ignore corrections of $\mathcal{O}(\frac{\alpha_s}{\pi}\frac{m_W^2}{m_t^2})$ and $\mathcal{O}(\alpha_s^2)$. While the above QCD corrections lower the width by ≈10%, first order electroweak corrections increase the width by 1.7% [176, 177]. However, the electroweak correction is almost cancelled when taking the non-vanishing finite width of the W boson into account, decreasing the width again by 1.5% [178, 179]. Corrections to the top quark width of $\mathcal{O}(\alpha_s^2)$ have been evaluated as well [180, 181] and lower the width by 2%. Including these effects as well, the top quark decay width is predicted in the Standard Model framework with a precision of ≈1%. The other Standard Model decays $t \to Wd, t \to Ws$ give only a negligible contribution to the total decay width $\Gamma_t = \Sigma_q \Gamma_{tq}$ proportional to $|V_{td}|^2$ and $|V_{ts}|^2$.

The above expression yields the top width with better than 2% accuracy. The width increases with the top quark mass: Using $\alpha_s(m_Z) = 0.1176$ and $G_F = 1.16637{\cdot}10^{-5}(\mathrm{GeV/c^2})^{-2}$ [41] one obtains Γ_t to be 1.02/1.26/1.54 GeV/c^2 for top quark masses of 160/170/180 GeV/c^2.

The resulting lifetime of the top quark $\tau_t = \Gamma_t^{-1} \approx (1.3\ \mathrm{GeV/c^2})^{-1}$ of approximately $5 \cdot 10^{-25}$ s is significantly shorter than the hadronisation time $\tau_{\mathrm{had}} = \Lambda_{\mathrm{QCD}}^{-1} \approx (0.2\ \mathrm{GeV})^{-1} \approx 3 \cdot 10^{-24}$ s. As a consequence, the top quark decays before it can form hadrons, and in particular there are no $t\bar{t}$ bound states (toponium), as was pointed out for a heavy top quark already in the 1980s [182–184].

It should be noted that while the top quark is generally considered as a free quark due to above feature, residual non-perturbative effects associated with hadronisation may still be present in top quark events. The fragmentation and hadronisation processes will be influenced by the colour structure of the hard interaction process. In electron-positron annihilation, top quark pairs are produced in a colour singlet state so that the occurrence of hadronisation before decay mainly depends on the top quark mass and collision energy. In hadronic top quark pair production, t and $\bar{t}$ are usually in a colour octet state, forming a colour singlet state with the proton or antiproton remnant respectively. The energy in the colour field (or in the string when using the picture of string fragmentation) is proportional to the distance between top quark and the remnant. If a characteristic length of about 1 fm is reached before the top quark decays, light hadrons can materialise out of the string's energy. The possibility for this string fragmentation to occur will depend strongly on the centre of mass energy in the hadron collisions. For Tevatron energies it can be neglected [185], while it may be more important at LHC energies where top quarks are produced with a sizeable Lorentz-boost. Since heavy quarks have hard fragmentation functions and hence the fractional energy loss of the top quarks is expected to be small, it will be difficult to experimentally establish these effects directly even at the LHC. In case no string fragmentation occurs before the top quark decays, long-distance QCD effects will still connect the decay products of the top quark.

With top quark mass measurements aiming at uncertainties of one $\mathrm{GeV/c^2}$ and below, it becomes more and more important to assess the impact of such non-perturbative effects on the measurements. One example that may play an important role in this context is the possibility of colour reconnections before hadronisation and the corresponding modelling of the underlying event (beam remnant interactions) [186, 187].

3.3.3 W boson helicity

The top quark decay in the framework of the Standard Model proceeds via the left-handed charged current weak interaction, exhibiting a vector minus axial vector ($V-A$) structure. This is reflected in the observed helicity states of the W boson which can be exploited to test the coupling at the Wtb vertex

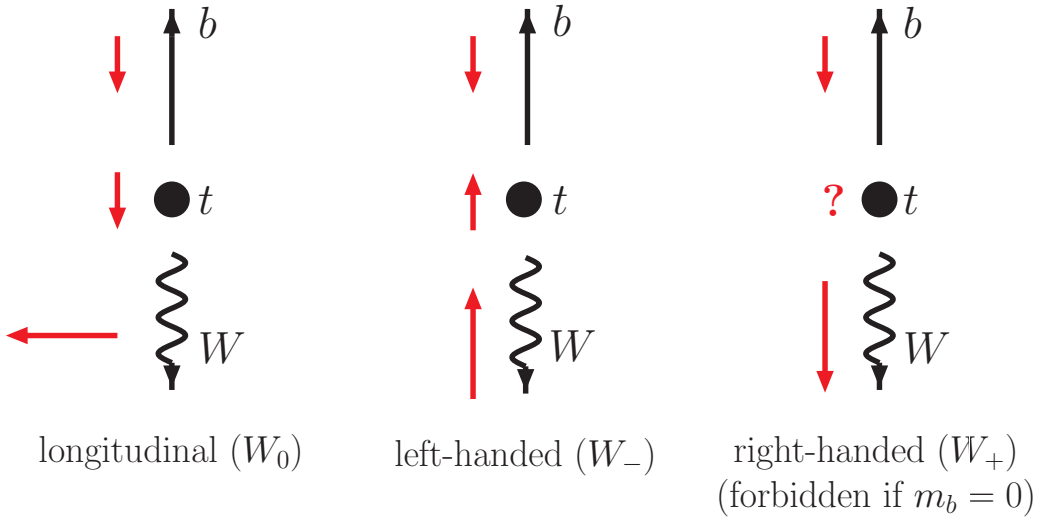

Figure 10: Angular momentum conservation in the top quark decay prevents the occurrence of right-handed W bosons in the limit of a massless b quark.

[188–190].

The emitted b quark can be regarded as massless compared to the top quark and hence is predominantly of negative helicity/left-handed, meaning its spin points opposite to its line of flight in the top quark rest frame. The emitted W boson as a massive spin 1 particle can assume any of the three helicity states: longitudinal (W_0), transverse-minus (W_-, left-handed) and transverse-plus (W_+, right-handed). To conserve angular momentum in the decay, the spin projection of the W boson onto its momentum must vanish if the b quark's spin points along the spin of the top quark, while a left-handed W boson is needed if the b quark's spin points opposite to the spin of the top quark. In the limit of a massless b quark, a right-handed W boson cannot occur in the decay, as illustrated in Figure 10. In case of the decay of an antitop quark, the left-handed W boson is forbidden.

At Born-level, the expected fractions of decays with the different W boson helicities, taking the finite b quark mass into account, are given by [191]:

$$
\begin{aligned}
f_0 &= \Gamma_0/\Gamma_t = \frac{(1-y^2)^2 - x^2(1+y^2)}{(1-y^2)^2 + x^2(1-2x^2+y^2)} \approx \frac{1}{1+2x^2} \\
f_- &= \Gamma_-/\Gamma_t = \frac{x^2(1-x^2+y^2+\sqrt{\lambda})}{(1-y^2)^2 + x^2(1-2x^2+y^2)} \approx \frac{2x^2}{1+2x^2} \\
f_+ &= \Gamma_+/\Gamma_t = \frac{x^2(1-x^2+y^2-\sqrt{\lambda})}{(1-y^2)^2 + x^2(1-2x^2+y^2)} \approx y^2\frac{2x^2}{(1-x^2)^2(1+2x^2)}
\end{aligned}
$$

where the scaled masses $x = m_W/m_t$, $y = m_b/m_t$ and the Källén-type func-

tion $\lambda = 1+x^4+y^4-2x^2y^2-2x^2-2y^2$ were used. Inserting $m_t = 175$ GeV/c^2, $m_W = 80.419$ GeV/c^2, and a pole mass of $m_b = 4.8$ GeV/c^2, the partial helicity rates are found to be [191]:

$$f_0 = 0.703,\ f_- = 0.297,\ f_+ = 0.00036.$$

The $m_b \neq 0$ effects result in a reduction of f_0 and f_- at the per mill level. Including one-loop QCD corrections [191], electroweak one-loop corrections and finite width corrections [192], one observes that the last two corrections basically cancel each other as was already mentioned in Section 3.3.2 and that the partial helicity rates f_0 and f_- only change at the 1-2% level. The right-handed helicity fraction f_+ remains at the per mill level with these corrections included. Consequently, any observation of f_+ at the percent level would signal physics beyond the Standard Model.

Using a more general extension with respect to the Standard Model Wtb interaction Lagrangian, assuming both W boson and b quark to be on-shell, one obtains [190]:

$$\mathcal{L} = \frac{g}{\sqrt{2}}\left[W_\mu^- \bar{b}\gamma^\mu \left(f_1^L P_L + f_1^R P_R\right) t - \frac{1}{m_W}\partial_\nu W_\mu^- \bar{b}\sigma^{\mu\nu}\left(f_2^L P_L + f_2^R P_R\right) t\right] + h.c.$$

where $P_{R(L)}$ are the right- and left-handed chiral projectors $P_{R(L)} = \frac{1}{2}(1 \pm \gamma^5)$ and $i\sigma^{\mu\nu} = -\frac{1}{2}[\gamma^\mu, \gamma^\nu]$.

In this model-independent extension, one obtains four form factors $f_{1,2}^{R,L}$ that enclose the Standard Model as the special case where $f_1^L = 1$ (left-handed vector coupling) and the other form factors (right-handed vector and left- respectively right-handed tensor couplings) are zero. These four couplings of the general Wtb vertex can be determined via the measurement of four different observables sensitive to this interaction: the W helicity fractions f_0 and f_+ and the single top production cross sections in the s- and t-channel. This model-independent determination of the general effective Wtb vertex in turn will allow to distinguish between different models of EWSB [193].

4 Experimental Setup

This section describes the experimental ingredients that are necessary to study top quarks. Since this review focusses mainly on results obtained at the Run II Tevatron, the corresponding accelerator and detector setups are discussed. The Run I experimental setup can be found for example in [194].

The Tevatron collider is discussed in the first part of this chapter, followed by a description of the two general purpose detectors CDF and D0 surrounding the two interaction points where protons and antiprotons are being brought to collision. Subsequently, the reconstruction and identification of the particles produced in the collisions is briefly discussed before the resulting experimental signatures of top quark events are described. Finally, the Monte Carlo (MC) simulation tools needed to model interactions in the detectors are considered.

4.1 The Tevatron Collider

The Tevatron collider is part of the Fermi National Accelerator Laboratory (Fermilab, FNAL) in Batavia, Illinois, close to Chicago. Until the Large Hadron Collider at CERN starts operation, the Tevatron remains the particle accelerator with the highest centre of mass energy worldwide. 36 bunches of protons and antiprotons with a spacing of 396 ns are being brought to collision with $\sqrt{s} = 1.96$ TeV at the two interaction points where the multipurpose detectors CDF and D0 reside. As illustrated in Figure 11, the Tevatron is the last stage in a chain of a total of eight accelerators and storage rings [195–198].

The proton beam generation starts with a magnetron surface plasma source creating H^- ions from hydrogen gas [199]. The H^- ions are then accelerated to 750 keV in a Cockcroft-Walton electrostatic accelerator, followed by a linear accelerator bringing the ions to 400 MeV. Using a carbon stripping foil, both electrons are removed from the H^- ions, and the resulting protons are then accelerated to 8 GeV within 33 ms in the first out of five synchrotrons at Fermilab called "Booster" with a ring circumference of 475 m. The components up to this point are also referred to as the Proton Source.

Acceleration continues in the oval Main Injector synchrotron with a circumference of 3.3 km. Depending on their further use, protons are brought from 8 GeV to 120 GeV within 2 s for fixed-target operation (including the production of antiprotons) or to 150 GeV within 3 s for injection into the Tevatron. With a ring radius of 1 km, the Tevatron finally is the largest synchrotron at Fermilab. It accelerates protons and antiprotons in a single

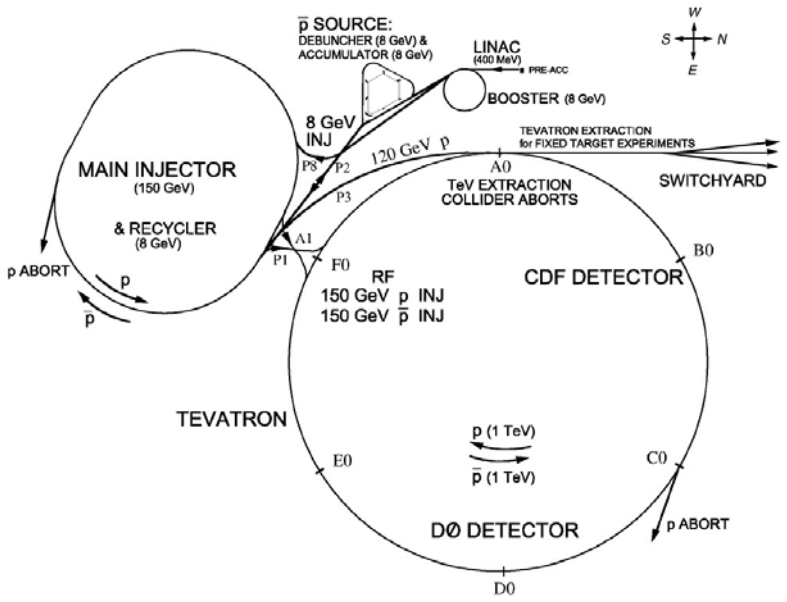

Figure 11: The Fermilab Run II accelerator complex with the Tevatron $p\bar{p}$ collider and its pre-accelerators [195, 198].

beam pipe from 150 GeV to 980 GeV in about 85 s.

For the production of antiprotons, 120 GeV protons from the Main Injector are directed at a Nickel target every two seconds, producing an 8 GeV antiproton for every $\mathcal{O}(50000)$ incident protons, in total $\mathcal{O}(10^8)$ per pulse. These antiprotons are focussed into the beamline with a Lithium lens and are separated from the other produced particles with a pulsed dipole magnet used as charge-mass spectrometer. Transferred to the Debuncher ring, the large momentum spread of the antiprotons is reduced using radio-frequency bunch rotation [200] and stochastic cooling [201] before the beam is passed on to the Accumulator ring where the antiprotons are collected ("stacked") and cooled further. For Tevatron collider operation approximately 30000 such cycles are needed. The Debuncher and Accumulator are both 8 GeV rounded triangle shaped concentric synchrotrons with circumferences of 505 m and 474 m respectively and are also referred to as the Antiproton Source together with the target station.

To operate at optimal stacking rates, every few hours antiprotons are transferred from the Accumulator to the Recycler, an 8 GeV storage ring housed in the Main Injector tunnel, providing both stochastic and electron cooling [202] and thus improved beam quality. As the name implies, the Recycler was originally planned to allow the reuse of remaining antiprotons

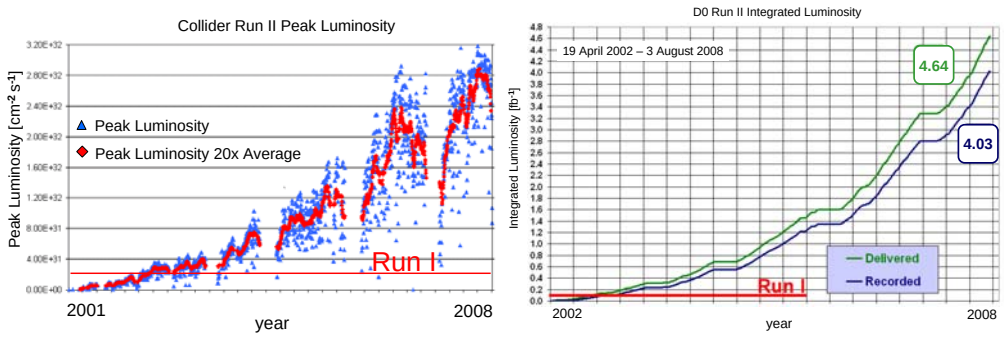

Figure 12: Left: Peak luminosities achieved at the Run II Tevatron versus time [204]. Right: Run II integrated luminosity delivered by the Tevatron and recorded by the D0 experiment versus time [205].

from the Tevatron, but this is no longer pursued in favour of large stashes ($6 \cdot 10^{12}$) of antiprotons with high beam quality [203]. The 8 GeV antiprotons from either Accumulator or Recycler are accelerated in the Main Injector to 150 GeV for injection into the Tevatron, where they are ramped up to 980 GeV together with the protons for collisions. The bunch spacing of 396 ns corresponds to a collision rate of 2.5 MHz. With 36 bunches being filled out of 53 available, the average rate is reduced to 1.7 MHz.

In such a high energy physics store at the Tevatron, about $9 \cdot 10^{10}$ antiprotons and $26 \cdot 10^{10}$ protons per bunch are used. Characteristic bunch dimensions (r.m.s.) are 45 cm (50 cm) longitudinal and 16 μm (28 μm) transverse to the beam direction for antiprotons (protons) [23]. A store enables typically 16 to 24 hours of data taking (governed by the instantaneous luminosity still available versus achievable with a new store) before the beam is dumped and the Tevatron gets refilled within two to three hours. The increased antiproton stacking rates achieved recently allow for shorter overall turnaround times and store durations while raising initial luminosities, thus allowing one to maximise the delivered luminosity per time period.

The Tevatron is performing well and keeps setting new world records on the peak luminosity at a hadron collider. As of July 2008, the record is $3.2 \cdot 10^{32}$ cm^{-2}s^{-1} [195]. For comparison, during the Run I data taking period from 1992 to 1996 at a centre of mass energy of 1.8 TeV, the record peak luminosity was $0.2 \cdot 10^{32}$ cm^{-2}s^{-1} and both experiments recorded an integrated luminosity of 0.1 fb^{-1} respectively. As illustrated in Figure 12, since the beginning of Run II in 2001, both experiments have recorded datasets in excess of 4 fb^{-1} each, and up to half of the total Run I luminosity is now collected by the experiments in one single week. The analyses discussed in this review utilise datasets up to an integrated luminosity of 2.8 fb^{-1}.

Until the scheduled end of Run II in October 2009, the Tevatron is expected to have delivered more than 6 fb^{-1} to both experiments, with possible improvements on that value crucially depending on the achievable antiproton stacking rates [196]. An extension of the Tevatron running into 2010 is currently being discussed and could increase the datasets by additional 2 fb^{-1}.

4.2 The Collider Experiments

Both general purpose detectors CDF and D0 follow the generic layout of a collider detector in having their various subdetectors arranged symmetrically around the interaction point and beam pipe (see Figure 13). The inner detectors are arranged in concentric cylindrical layers, with charged-particle tracking systems of low mass surrounded by solenoidal magnets building the core. They are enclosed by electromagnetic and hadronic calorimeters providing energy measurements and identification of electrons, photons and hadrons. The outer detectors are dedicated to muon detection, utilising the penetration capabilities of muons.

Both detectors use a right-handed coordinate system with the origin at the designated interaction point in the centre of the detector and the z-axis pointing along the direction of the proton beam. The transverse plane is spanned by the y-axis which points vertically upwards and the x-axis pointing away from the centre of the Tevatron. Positions in the transverse plane are frequently described using the azimuthal angle ϕ with respect to the x-axis, $\phi = \arctan\frac{y}{x}$ and radius $r = \sqrt{x^2 + y^2}$. Based on the polar angle θ with respect to the z-axis, the pseudo-rapidity η is defined as $\eta = -\ln(\tan\frac{\theta}{2})$. For massless particles (or in the ultra-relativistic case where masses can be neglected), the pseudo-rapidity is equivalent to the rapidity $y = \frac{1}{2}\ln((E + p_z)/(E - p_z))$ which is simply additive under parallel Lorentz transformations, resulting in Lorentz-invariant rapidity differences Δy. The distance of two objects in the $\eta - \phi$ plane is usually denoted with $\Delta R = \sqrt{\Delta\eta^2 + \Delta\phi^2}$. If it is necessary to differentiate between variables that were calculated with respect to different origins of the coordinate system – using the centre of the detector or for example the reconstructed primary vertex – the former case is usually denoted with a subscript "det" to signal detector coordinates being used.

Enclosing the luminous region that exhibits a Gaussian width of approximately 25 cm, the innermost detectors for both CDF and D0 are silicon microstrip trackers providing vertexing and tracking capabilities, extending out to pseudo-rapidities of $|\eta| \leq 2$ respectively $|\eta| \leq 3$. CDF complements its tracking system with a cylindrical open cell drift chamber performing

96 track measurements within $|\eta| \leq 1$ while D0 utilises a scintillating fibre tracker of eight cylindrical layers with two overlapping 835 μm diameter fibre doublets each, providing coverage out to $|\eta| \lesssim 1.7$. Both tracking systems are enclosed by superconducting solenoidal magnets, providing magnetic fields of 1.4 T (CDF) respectively 1.9 T (D0) along the beamline for measurements of charged-particle transverse momenta p_T.

Supplemental particle identification systems are placed inside and also outside of the magnet for the CDF and D0 detectors. Inside the magnet, CDF employs a Time-of-Flight detector based on plastic scintillator panels covering $|\eta| \lesssim 1$, mainly for discrimination of low-energetic ($p < 1.6$ GeV/c) charged pions and kaons needed for heavy-flavour physics. Outside of the magnet, CDF uses scintillator tiles for early sampling of electromagnetic showers to improve electron and photon identification in the central detector. D0 uses central ($|\eta| \leq 1.3$) and forward ($1.5 \leq |\eta| \leq 2.5$) preshower detectors with several layers of plastic scintillator strips for enhanced electron and photon identification.

Sampling calorimeters with an inner electromagnetic and an outer hadronic section enclose all subdetectors described so far, providing energy measurement and identification capabilities for photons, charged leptons and hadrons. CDF uses lead/iron-scintillator sampling devices covering pseudo-rapidities $|\eta| \lesssim 3.6$, while D0 uses mainly depleted uranium as absorber material and liquid argon as active medium for nearly compensating calorimetry within $|\eta| \lesssim 4.2$. Between the central and endcap calorimeter cryostats ($1.1 \leq |\eta| \leq 1.4$), layers of scintillating tiles provide shower sampling for D0.

The outermost subdetector serves the identification of muons, based on their ability to traverse the calorimeter as minimum ionising particles without generating electromagnetic or hadronic showers. Both CDF and D0 employ scintillators and drift tubes for muon detection within $|\eta| \leq 1.5$ respectively $|\eta| \leq 2$. Unlike CDF, D0 uses 1.8 T solid-iron toroidal magnets between the detection layers, allowing for additional stand-alone muon momentum measurements independent of the central tracking system.

The luminosity for CDF and D0 is measured using Cherenkov respectively plastic scintillation counters covering $3.6 \leq |\eta| \leq 4.6$ respectively $2.7 \leq |\eta| \leq 4.4$. To select the events of interest from the effective bunch crossing rate of 1.7 MHz, both experiments employ three-level trigger systems of dedicated hardware at the lower and commercial processor farms at the higher levels. Based on information from tracking, calorimetry and muon systems, events are recorded at a rate of approximately 100 Hz for storage and further processing.

More detailed descriptions of the CDF and D0 detectors can be found in [206, 208, 209] respectively [207].

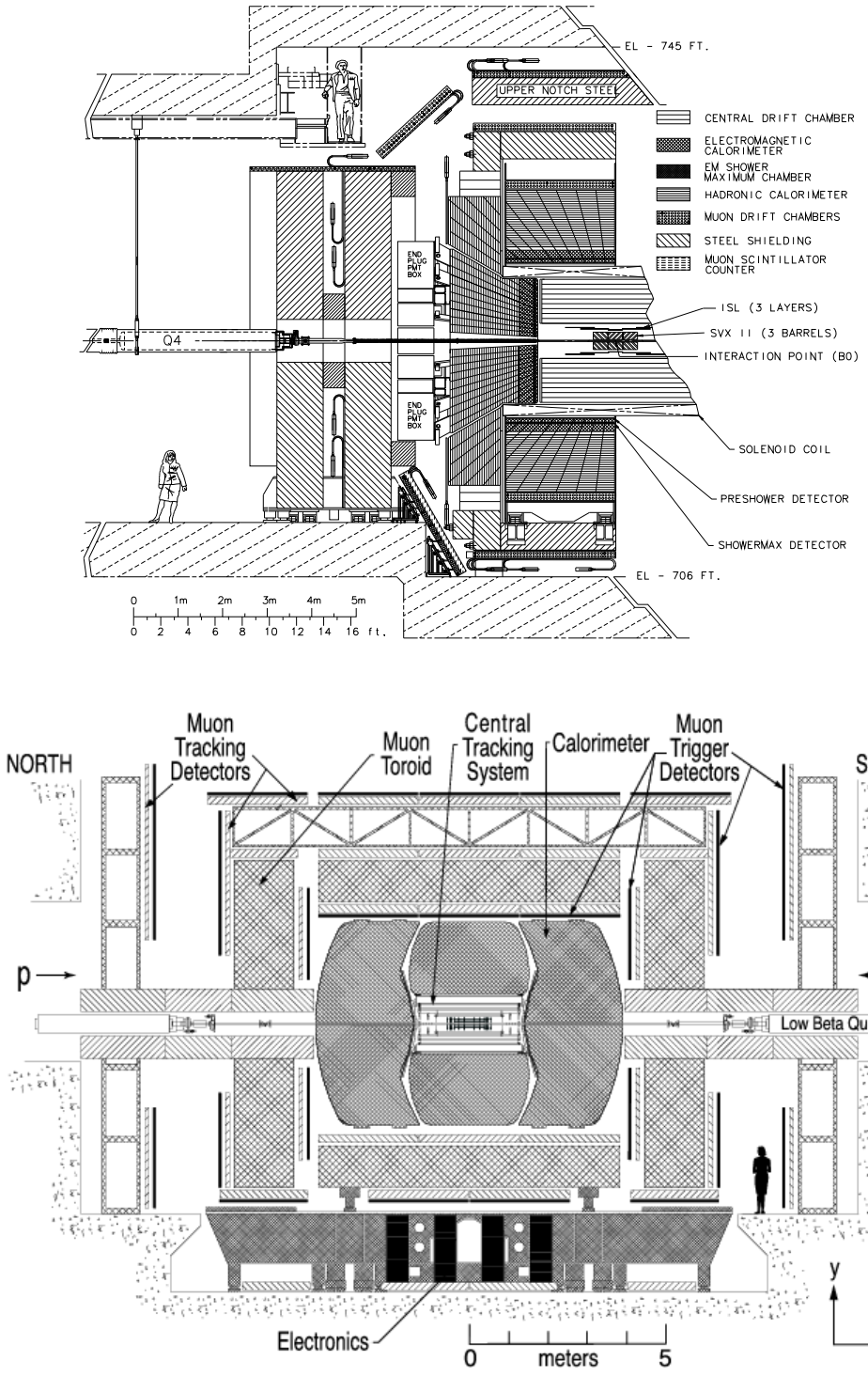

Figure 13: Cross section views of the CDF detector (top, [206]) and the D0 detector (bottom, [207]).

4.3 Object Reconstruction

To analyse top quark events and study the properties of the top quark, one first needs to reconstruct the fundamental objects resulting from the partons occurring in top quark decays. This section gives a brief overview of the objects to consider, how they can be reconstructed in the detectors described in the last section and some further issues to take into account. More information on object reconstruction specific to the CDF and D0 experiments can be found for example in [13, 210]. As will become obvious, top quark physics analyses utilise all detector components and thus need a thorough understanding of their performance and calibration.

4.3.1 Primary Vertices

The point of the primary hard scatter is referred to as the primary vertex and is determined by a fit of the common origin of well measured tracks and beamline constraints. With increasing luminosity the average number of interactions per bunch crossing increases as well, leading to the reconstruction of multiple primary vertex candidates, only one of which will be compatible with the hard interaction of interest. The selection of the primary vertex can be based for example on vicinity to a selected energetic lepton, maximal scalar sum of associated track transverse momenta or lowest compatibility with a minimum bias interaction based on track p_T templates [13, 208].

The primary vertex gives the origin of all prompt tracks including those from top quark and subsequent W boson decays which cannot be separated from the primary vertex within the detector resolution due to the extremely short top quark and W boson lifetimes (see also Section 7.2). The primary vertex is also used as an origin of the coordinate system in which kinematic variables are evaluated.

4.3.2 Charged Leptons

Leptonically decaying W bosons are a source of isolated energetic charged leptons that can be measured well with the tracking, calorimeter and muon systems described in the last section. They are part of the event signature of numerous top quark decay modes (see Section 4.4) and key in the trigger selection of such events. However, τ leptons play a special role due to their decay characteristics. τs decay leptonically in 35% of the cases, yielding electrons or muons that on average are softer compared to those from direct W boson decays but otherwise hard to distinguish due to the relatively short τ lifetime. Consequently, such decays are usually included in the event selections involving electrons and muons which are then referred

to as "leptonic" final states. Hadronic τ decays are treated separately and are discussed further below.

In the context of this review, the term "leptons" refers to electrons and muons alone unless stated otherwise. Their reconstruction proceeds as follows:

- **Electrons** leave a track in the tracking system and form showers mainly in the electromagnetic part of the calorimeter. They are reconstructed as clusters of energy depositions in the electromagnetic calorimeter matched to a reconstructed track. Further requirements include selections based on the fraction of energy deposited in electromagnetic calorimeter, isolation from further energy depositions in a cone surrounding the electron candidate, the shower shape and the ratio E/p of cluster energy and the track momentum.

- **Muons** are identified via their penetration capabilities, leaving only a "track" of energy depositions in the calorimeter as minimum ionising particles and reaching the outermost detection layers of the muon system. They are reconstructed by matching central tracks to track segments in the muon system. The track must be consistent with originating from the primary vertex and cosmic rays are suppressed via timing cuts. Isolation of the muon can be required both on the track and calorimeter levels.

The misidentification of isolated leptons has different origins for electrons and muons. Assuming contributions from hadrons punching through the calorimeter are negligible, fakely isolated muons mainly are real muons, for example from heavy flavour production with semileptonic decays where the jet (see below) is not reconstructed or the muon travels outside of the jet. While such semileptonic heavy flavour decays also contribute to fakely isolated electrons, significant contributions arise here as well for example from jets with large electromagnetic fractions faking electrons, photon conversions or photons with a random track. Such instrumental background processes are usually directly estimated from data as realistic simulation of these effects is difficult.

The lepton energy scale and resolution can be directly assessed by studying the reconstructed Z boson mass in $Z \to \ell\ell$ events. Z boson decays are useful as well for studying the lepton identification efficiencies with the "tag and probe" method: One lepton is required to be well identified (the "tag"), allowing one to obtain a reasonably pure Z boson sample, while the second lepton serves as a probe for the efficiency being studied.

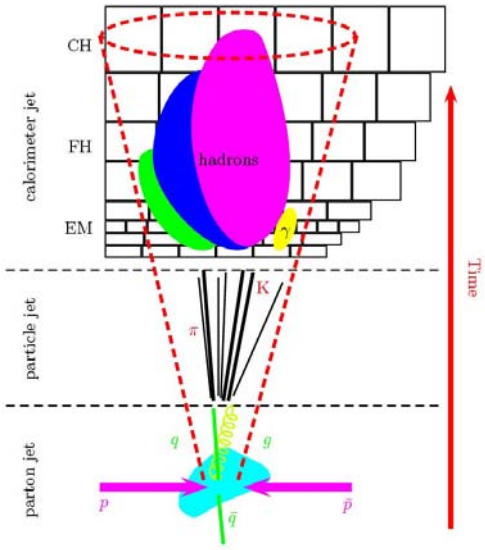

Figure 14: Illustration of the evolution of a calorimeter jet from an initial parton [211]. The dashed red line represents the jet cone.

4.3.3 Quark and Gluon Jets

The hadronisation of quarks and gluons leads to collimated showers of hadrons in a narrow cone, referred to as "jets". The jet axis is highly correlated with the original parton's direction. While it is not possible to differentiate between quark and gluon jets on a per-object basis, it is statistically possible via small differences in shower shape (gluon jets tend to be wider and contain more soft particles).

Jets are reconstructed from their energy depositions in the calorimeter using cone algorithms [212, 213] that combine calorimeter cell energies lying within a cone of fixed radius ΔR (see Figure 14). The cone radius is a compromise between collecting a high fraction of the original parton's energy and being able to still resolve the energy depositions of different initial partons, especially in busy $t\bar{t}$ events. D0 uses a cone size of $\Delta R = 0.5$ while CDF uses $\Delta R = 0.4$.

The measured jet energies are converted into particle-level energies by the application of jet energy scale (JES) corrections [214, 215]. They take into account effects like the presence of energy depositions not originating from the initial hard scattering process (noise in the calorimeter, multiple interactions,...), particles inside the jet depositing energy outside of the jet cone or vice versa due to bent trajectories in the magnetic field and showering

effects and the calorimeter response accounting for example for nonlinearities or energy losses in uninstrumented detector regions.

With the electromagnetic calorimeter scale determined from resonances like $Z \to ee$ as described above, it can be transferred to the full calorimeter by requiring E_T balance in photon plus jet events. The intercalibration of the calorimeter is then complemented with dijet events. A precise JES calibration is a challenging task with highly complex procedures to ensure proper understanding of all contributions and systematic uncertainties. D0 has achieved a JES precision at the 1-2% level over a wide kinematic range [214]. At this level of precision however the JES is only applicable directly to photon plus jet samples, and additional uncertainties need to be taken into account when transferring the JES for example to top quark samples [216]. A first direct measurement of the b quark JES at the Tevatron based on $Z \to bb$ events has been recently performed by CDF, reaching a precision of better than 2% [217].

4.3.4 Tau Jets

Tau leptons decay hadronically in 65% of the cases, with 77.5% of these decays yielding a single charged particle ("1 prong decays") and 22.5% three charged particles ("3 prong decays") [23]. Hadronic τ decays are reconstructed as jets and can be discriminated from quark and gluon jets for example via their narrow shower shape and track multiplicity in the jet cone [218, 219].

4.3.5 b Jets

The identification ("tagging") of b jets is a very powerful tool to separate the top quark signal from its background processes which typically exhibit little heavy flavour content. Also the combinatorics for reconstructing top quark events from the final state objects can be reduced with this additional information available. There are in general two different approaches to identifying the B hadrons formed from b quarks:

- **Lifetime Tagging:** Due to their lifetime of about 1.5 ps and the boost from the top quark decay, B hadrons can travel several millimetres before they decay. The resulting charged particle tracks will then originate from a vertex different from the primary one. This can be exploited by searching for significantly displaced secondary vertices with respect to the primary event vertex (*secondary vertex tagging*) or by requiring a large significant impact parameter for a certain number of

the corresponding tracks without explicit secondary vertex reconstruction (*impact parameter tagging*). One can also calculate the probability for a jet to come from the primary vertex based on the impact parameters of all its associated tracks (*jet probability tagging*) or combine all relevant information of the above tagging algorithms into a neural network (*NN tagging*). The latter two methods yield continuous variables as output that can easily be used as input for further multivariate analysis steps or allow to choose a cut value with an analysis-specific appropriate compromise between b tagging efficiency and the fraction of light quark jets that are misidentified as b jets.

- **Soft Lepton Tagging:** This tagging method is based on the frequent semileptonic decays of b and c hadrons with branching fractions of approximately 11% and 10% respectively. Taking into account two b quarks and W bosons per $t\bar{t}$ decay and the fact that about one third of the W boson decays yield charm quarks, the fraction of events containing a soft lepton in a jet is about 40% per lepton flavour (e, μ). The isolation criteria appropriate for leptonic W boson decays as discussed above cannot be applied here, and the reconstruction of these leptons embedded in a jet with comparatively low transverse momentum is challenging, especially for electrons.

It should be noted that while the mistag rate for lifetime taggers is usually very small for light quark (u, d, s) and gluon jets, this is not the case for charm jets. For example, a typical operating point for D0's NN tagger yields a b tag efficiency of $\approx 50\%$ and a mistag rate for light quark or gluon jets of $\approx 0.5\%$, while it is $\approx 10\%$ for c jets [216]. More information on b tagging algorithms and their application in top quark analyses including the performance for b jets, c jets and light quark or gluon jets can be found in [208, 210, 220] for CDF and [13, 216, 221] for D0 and references therein.

4.3.6 Neutrinos

Neutrinos are not directly detected due to their negligible weak interaction cross section. Since the energy component along the beam axis is unknown at a hadron collider, only the transverse component of the energy carried away by neutrinos (or any other "invisible" particles) can be inferred from energy conservation in the transverse plane. This missing transverse energy $\not\!\!E_T$ is calculated as the inverse (negative) of the vector sum of transverse energy depositions in the calorimeter, corrected for the energy scale corrections of reconstructed electrons and jets and for the momenta of reconstructed muons which are corrected for their energy loss in the calorimeter. The $\not\!\!E_T$ resolution

hence strongly depends on the other objects present in the event. Taking this into account, for example by using cuts on the $\not\!\!E_T$ significance rather than on plain $\not\!\!E_T$, will result in improved performance.

4.4 Standard Model Top Event Signatures

Now that the fundamental objects that can be reconstructed from the initially occurring particles have been discussed, the experimental signatures of top quark events can be examined. As explained in Section 3.3.1, the top quark decays predominantly into a W boson and a b quark in the framework of the Standard Model. Consequently, the observed final state is determined by the decay mode of the W boson.

W bosons decay into two fermions, either leptonically into a charged lepton-neutrino pair $\ell\bar{\nu}_\ell, \ell = e, \mu, \tau$ with equal probability per lepton flavour at lowest order perturbation theory or hadronically into quark-antiquark pairs $q\bar{q}'$ with $q = u, c$ and $\bar{q}' = \bar{d}, \bar{s}, \bar{b}$. At Born level, the hadronic decay widths are enhanced over the leptonic modes by a colour factor 3 (taking the three possible quark colours into account) and scaled by the squared involved CKM matrix element $|V_{qq'}|^2$. Similar to the case of the top quark decay, the off-diagonal CKM matrix elements are suppressed compared to the diagonal ones, and for simplicity only the decay modes $u\bar{d}$ and $c\bar{s}$ will be considered in the following, contributing approximately 95% of the hadronic decay width.

In summary, W bosons decay leptonically with a branching fraction of 1/9 per lepton flavour and 1/3 for each of the hadronic decays $u\bar{d}$ and $c\bar{s}$ respectively. The resulting possibilities for $t\bar{t}$ decays are illustrated in Figure 15, where also the nomenclature for the different decay modes is introduced. It should be noted that these branching fractions do not yet take into account the leptonic decays of τ leptons and their incorporation in the reconstructed final states involving leptons (electrons and muons) as discussed in Section 4.3. This is considered in the following description of the four basic $t\bar{t}$ event classes:

(i) Dilepton channels: Both W bosons decay leptonically ($\ell\bar{\nu}_\ell, \ell = e, \mu$), resulting in a final state comprising two isolated high-p_T leptons, missing transverse energy $\not\!\!E_T$ corresponding to the two neutrinos and two jets. Including leptonic τ decays, this channel has a branching fraction of approximately 6.5%, shared ≈1:1:2 by the ee, $\mu\mu$ and $e\mu$ final states. While these channels give samples with the highest $t\bar{t}$ signal purity, they suffer from limited statistics due to the small branching fraction.

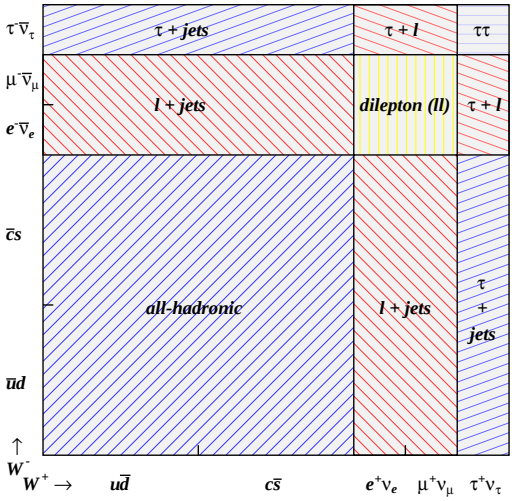

Figure 15: Illustration of the various Standard Model $t\bar{t}$ decay modes and their branching fractions via the possible W boson decays. In each decay mode, a $b\bar{b}$ quark pair from the $t\bar{t}$ decay is present as well.

(ii) Lepton plus jets channels: One W boson decays leptonically, the other one hadronically, yielding a final state containing one isolated high-p_T lepton, $\not\!\!E_T$ and four jets. Including leptonic τ decays, these channels exhibit a branching fraction of approximately 34.3%, shared about equally by the e plus jets and μ plus jets final states. These channels represent the best compromise between purity of the sample and available statistics.

(iii) All-hadronic channel: Both W bosons decay hadronically to $q\overline{q}'$ pairs, resulting in a six-jet final state. With a branching fraction of approximately 45.7%, this channel yields the highest statistics of $t\bar{t}$ events but also suffers from the large multijet production background.

(iv) Hadronic τ channels: Final states where at least one W boson yields a charged τ lepton that in turn decays hadronically are subsumed as hadronic τ channels, comprising together a branching fraction of approximately 13.5%. Depending on a hadronic, leptonic or hadronically decaying tauonic decay of the second W boson one differentiates between the τ plus jets, τ plus lepton and $\tau\tau$ final states, contributing 9.5%, 3.6% and 0.5% to the branching fraction respectively. The corresponding experimental signature is four/two/two jets, $\not\!\!E_T$, one/one/two hadronic τs and no/one/no isolated high-p_T lepton. The identification of the hadronic τs makes these final states especially

challenging to reconstruct. More inclusive sample selections requiring for example leptons and isolated tracks or $\not\!\!E_T$ and (b tagged) jets allow to include significant fractions of hadronically decaying tau leptons without explicitly reconstructing them.

In all of the above final states, two of the jets are b jets from the $t\bar{t}$ decay. The $\tau\tau$ final state remains the only channel that has not yet been investigated explicitly for $t\bar{t}$ production; all others are discussed in Section 5.1. For measurements of top quark properties, mainly the first three channels listed above are used – especially the lepton plus jets channel.

A full kinematic reconstruction of $t\bar{t}$ events is possible in the all-hadronic final state since there are no neutrinos present. In the lepton plus jets channel, a twofold ambiguity arises from the determination of the neutrino p_z when constraining the invariant mass of lepton and neutrino to m_W, while the dilepton channel is kinematically underconstrained due to the two neutrinos contributing to $\not\!\!E_T$. The unknown assignment between partons and reconstructed objects in $t\bar{t}$ events leads to various possible combinations. The combinatorics can be reduced by b jet identification. If both b jets are identified, four combinations remain to be considered in the lepton plus jets channel (including the neutrino p_z ambiguity) and six in the all-hadronic channel.

The experimental signature for single top quark production is determined by the top quark decay mode and the production channel: in the s- (tb-) channel the top quark is produced with one additional b jet while in the t- (tqb-) channel, a forward light-quark jet arises from the top quark production, sometimes accompanied by another b jet from the gluon splitting into $b\bar{b}$ (see Figure 8). The W boson from the top quark decay is usually required to decay leptonically ($\ell\bar{\nu}_\ell, \ell = e, \mu$) to suppress multijet background. Consequently, the final state signature of single top quark production contains an energetic isolated electron or muon, $\not\!\!E_T$ and at least two jets with at least one of them being a b jet.

The large mass of the top quark prevents it from being produced with large boosts at the Tevatron. Its decay products hence tend to be emitted at central rapidities, non-planar with good angular separation and exhibit a large scalar sum of transverse energy H_T. Event selections usually require the channel-characteristic objects (leptons, $\not\!\!E_T$, (b tagged) jets) to be present with energies exceeding typically 15 to 20 GeV, apart from data quality selections to ensure a well-performing detector, trigger selections and requirements on a well-reconstructed primary vertex in the central detector region. Variations in the observed jet multiplicities are possible for example due to jet reconstruction thresholds, jet splitting and merging during reconstruction

and gluon radiation (initial- and final-state radiation).

More details on the event selections used in the various analyses (including those searching for non-Standard Model signatures), background contributions and sample compositions are given in the following chapters and references therein.

4.5 Monte Carlo Generation

A reliable and well-understood Monte Carlo (MC) simulation of signal and background processes is a crucial ingredient for any top quark analysis – for example to understand detector acceptances, derive selection efficiencies and model expected kinematic distributions and their normalisation. It requires both good modelling of the physics process of interest from the parton to the hadron level and an accurate simulation of the actual detector's response when exposed to such a signature.

MC simulations of hadron interactions are based on the factorisation theorem discussed in Section 3.1, splitting up hadron collisions into universal long distance (small momentum transfer Q^2) phenomena and perturbatively calculable short distance phenomena. A generic example for the involved simulation steps of a hadron collision is illustrated in Figure 16 and described below.

The non-perturbative Parton Distribution Functions (PDFs) describe the distribution of the longitudinal (anti-) proton momentum amongst the incoming partons. The interaction of the incoming partons in the hard process of interest is then evaluated based on fixed-order (usually LO) matrix elements, yielding the outgoing partons and their characteristics like momenta and colours. The following parton shower adds higher-order effects by allowing partons to split into pairs of partons (gluon radiation, gluon-splitting, photon radiation,...) until at a sufficiently low Q^2 scale non-perturbative hadronisation sets in, forming colour-neutral hadrons from the coloured partons based on phenomenological models. Unstable particles and resonances then need to be decayed appropriately.

The coloured beam-remnants of the proton and antiproton involved in the hard scatter, possible further soft multi-parton interactions from their other partons and the colour connections with the hard process are accounted for as well and form the underlying event. Additional soft proton-antiproton collisions from the same colliding bunch (minimum bias events) have to be added depending on the instantaneous luminosity as well as possibly overlapping interactions from consecutive bunch crossings "leaking" into the current event (pile up).

In principle, for every stage in the above process different programs and

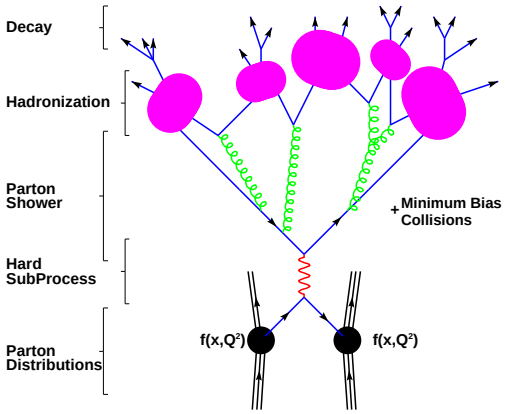

Figure 16: Illustration of a hadron collision [222] with the several steps involved for its simulation.

models can be used, and the best choice may depend on the process to be studied which illustrates the complexity of the MC simulations needed. Also, the parameters involved in some of the models need to be carefully tuned to data distributions before they provide an adequate description [223]. General purpose complete event generators like HERWIG [224] and PYTHIA [225] include LO matrix elements for a variety of processes as well as showering and hadronisation models. They are widely used either standalone or in combination with other generators that simulate the hard process and pass their information on for showering and hadronisation. A nice introduction and overview of available MC generators can be found in [226] and specific simulation tools for top quark production and decay are reviewed in [227].

CDF and D0 have implemented different simulation chains for their top quark analyses, and furthermore some specific analyses use yet additional variants compared to what is described here. CDF uses CTEQ5L [158] PDFs for its generators while D0 employs CTEQ6L1 [95] PDFs. The $t\bar{t}$ signal is either generated with PYTHIA v6.2 [228] (CDF) or ALPGEN v2.1 [229] interfaced with PYTHIA v6.3 [230] for parton showering and employing a jet-parton matching algorithm to avoid overlapping final states [231, 232] (D0). CDF uses also HERWIG v6.4 [233] for systematic cross checks of the signal modelling. For single top signal MC, D0 uses SINGLETOP [234] based on COMPHEP [235], interfaced with PYTHIA while CDF utilises MADEVENT [236] and MADGRAPH [237] interfaced with PYTHIA. Both experiments thus approximate the t channel production at NLO by a combination of the contributing $2 \to 2$ and $2 \to 3$ processes. The other obtained LO signal cross sections are scaled up to higher order theoretical predictions (see Sections 3.1

and 3.2). Most analyses use a top quark mass of 175 GeV/c^2.

For the simulation of W+jets and Z+jets background processes both collaborations utilise ALPGEN, interfaced with HERWIG (CDF) respectively PYTHIA (D0) for parton showering, and both apply the above mentioned matching technique. ALPGEN allows especially for the generation of higher final state parton multiplicities from $2 \to n$ processes and hence large jet multiplicities based on exact LO matrix elements, including the production of heavy flavours which is especially important for analyses using b tagging. For the decays of τ leptons both collaborations use TAUOLA [238, 239]; for b and c hadron decays EvtGen [240] and QQ [241] are used, the latter only by CDF. Effects of additional minimum bias events and pile up are modelled by CDF based on PYTHIA simulation and by D0 using zero bias collider data taken by randomly sampling filled bunch crossings, overlaid to the simulated event.

The simulated events are propagated through detector simulations based on GEANT [242] which contain an exhaustive description of positions, geometrical shapes and type and amount of material of the detectors. The generated particles are tracked through the detector volume, encountering energy loss and multiple scattering according to the traversed material and particles' momenta and decaying corresponding to their respective lifetimes. The response of the detector's readout electronics to these interactions including noise and inefficiencies is then obtained in a digitisation step, yielding raw simulated event data that are processed with the same reconstruction chain as real collider data.

To obtain good agreement between any physics process simulation and real experimental data is not trivial. For example, object reconstruction, identification and selection efficiencies tend to be higher in MC compared to data, and need to be corrected via scalefactors. These scalefactors are usually derived from efficiency measurements in control samples like $Z \to \ell\ell$ for leptons and γ+jets for jets in simulation and data and may be parametrised in variables to which these corrections are sensitive. Also object energy scales and resolutions generally need to be adjusted. Certain effects are hard to simulate correctly so that a derivation purely from data is necessary like for lepton fake rates.

Before any signal can be searched for, the background model needs to be verified first with data in control samples sufficiently depleted from signal, for example by requiring a reduced jet multiplicity or no b jets to be present. Sometimes the shape and/or normalisation of differential distributions need to be corrected, indicative of suboptimally tuned MC and/or insufficient precision in the used theoretical model.

With the increasing datasets at the Tevatron, data-based constraints al-

low more and more to improve upon the understanding of the dominant background processes like vector boson plus (heavy flavour) jets production both in terms of shapes and normalisation. This benefits both the precision of the measurements and the improvement of MC simulations. For example, the production of W bosons has been investigated in terms of associated jet production [243] and compared with LO and NLO predictions, or associated heavy flavour production was compared with Standard Model expectations and found to be in agreement [244, 245]. Dedicated studies of W boson plus charm [246, 247] or b jets [248, 249] production have been performed as well, with the most recent results indicating that the production rates of these processes are currently underestimated by ALPGEN.

A more detailed overview of the MC simulations used in top quark analyses at the Tevatron both for signal and background processes and the involved challenges can be found in [250, 251].

5 Measurements of Top Quark Production

In this chapter, measurements of top quark production both via the strong and electroweak interactions are described. Observed rates and mechanisms of production are compared with the Standard Model expectations and are used to derive constraints on specific extensions of the Standard Model impacting the properties under consideration.

5.1 Top Quark Pair Production Cross Section

Measurements of the $t\bar{t}$ production cross section are important for several reasons. They provide a powerful test of the predictions from perturbative QCD calculations at high transverse momenta. As shown in Section 3.1, the uncertainties on the $t\bar{t}$ rate predictions have reached the level of $\approx$10%, a precision which has already been matched by the measurements performed at the Tevatron.

Deviations from the Standard Model prediction could arise for example from novel production mechanisms like from a resonant production mode in addition to the Standard Model one as discussed in Section 5.7. New physics contributing to the electroweak symmetry breaking will probably couple to particles proportional to their mass, making the top quark and its strong coupling reflected in its production rate a highly interesting probe for such effects. Different top quark decay modes like the decay via a charged Higgs boson competing with the Standard Model decay as examined in Section 6.5 could cause apparent different production rates amongst the various decay

channels via modified branching fractions. Contributions of new physics to the background samples in the various channels could have a similar effect. Analysing different decay channels thus not only helps to improve statistics of top events and studies of properties, but is also a sensitive probe for physics beyond the Standard Model.

To extract the cross section requires good understanding of the reconstruction and identification of the involved objects and of the modelling of the contributing background processes. By providing selections for samples enriched in top quark signal and of well characterised composition, cross section analyses form the foundation of all further top quark property analyses.

Top quark pair production has been studied by now in all possible decay modes – the dilepton, lepton plus jets, all-hadronic and hadronic τ channels as defined in Section 4.4, with the $\tau\tau$ decay mode being the only exception due to marginal branching fraction and challenging separation from background processes. As mentioned before, in the context of this review the term leptons refers to electrons and muons alone unless stated otherwise.

The event selections usually require the characteristic objects from the top quark decay – leptons, $\not\!\!E_T$, (heavy flavour) jets, hadronically decaying τs – to be present with energies exceeding typically 15 to 20 GeV. Further kinematic characteristics can be exploited to separate the top quark signal from the various background processes. Due to the large mass of the top quark, its decay products tend to be very energetic, emitted at central rapidities and non-planar with good angular separation. In contrast to this, the jet energy spectrum for background processes with jets from gluon radiation is steeply falling. The observed objects are emitted less isotropically but more back to back, and mismeasured objects giving rise to $\not\!\!E_T$ tend to exhibit characteristic angular correlations with the reconstructed $\not\!\!E_T$.

Consequently, additional variables available for top quark signal selection are based on the energy present in the event like the scalar sum of transverse energy H_T or the invariant mass of a combination of reconstructed objects. Event shape variables like sphericity and aplanarity derived from the eigenvalues of the normalised momentum tensor of the objects considered [252], or centrality defined as the ratio of H_T and scalar sum of the objects' energies provide extra discrimination. Furthermore, angular relations between reconstructed objects (for example $\Delta\phi(\not\!\!E_T, \ell)$) and single object kinematics (like leading jet transverse momentum) are frequently used as well.

Depending on the $t\bar{t}$ decay mode considered, the use of b tagging in its different varieties (see Section 4.3) is optional for the event selection. In the dilepton and lepton plus jets channels selections purely based on topological and kinematic characteristics suffice for a good signal to background ratio (S/B). Adding b tagging improves sample purities but also implies a

stronger model dependence by relying on b quarks to be present in the final state. The actual extraction of the signal fraction proceeds either in a counting experiment or via template fits using the full shape information of the sensitive variable under consideration. While the latter is usually more sensitive, it also exhibits a stronger dependence on the MC modelling. Using different approaches with different systematic uncertainties to measure the same quantity allows one to assess the model assumptions made from different perspectives, provides an important way to check self-consistency and is beneficial for combinations of increased precision. Non-overlapping (orthogonal) sample selections facilitate later combinations of results as independent measurements by removing the need to evaluate the correlation amongst the measurements from ensemble tests.

Once the sample composition has been measured, the $t\bar{t}$ production cross section is calculated as follows:

$$\sigma_{t\bar{t}} = \frac{N_{\text{observed}} - N_{\text{background}}}{\varepsilon \, \mathcal{B} \, \int \mathcal{L} dt},$$

where N_{observed} and $N_{\text{background}}$ are the observed total and contributing background event yields respectively, ε is the selection efficiency including the detector acceptance, $\mathcal{B}$ is the branching fraction for the studied $t\bar{t}$ decay mode and $\int \mathcal{L} dt$ the integrated luminosity of the used dataset.

As illustrated in Section 3.1, the $t\bar{t}$ cross section depends on the top quark mass, decreasing by about 0.2 pb per additional GeV/c^2 in the mass range from 170 GeV/c^2 to 180 GeV/c^2. The $t\bar{t}$ cross section results given in the following sections generally refer to a top quark mass of 175 GeV/c^2; the few cases where a top quark mass of 178 GeV/c^2 was assumed will be pointed out explicitly. Especially for the recent measurements, a parametrisation of the obtained result versus top quark mass is provided to allow easy projection to the respectively current world average top quark mass. The cross section dependence on the mass can also be turned around to provide a measurement of the top quark mass from the cross section, which will be further discussed in Section 7.3.4.

In the following subsections the published and latest preliminary Run II results will be referenced for the various $t\bar{t}$ decay modes. Some analyses will be highlighted in a bit more detail. The agreement with the theoretical predictions is illustrated in the summary section, where also results of combinations across channels are given.

5.1.1 Dilepton Final State

A typical $t\bar{t}$ dilepton event selection requires two isolated high p_T leptons of opposite charge, $\not\!\!E_T$ and at least two central energetic jets. The domi-

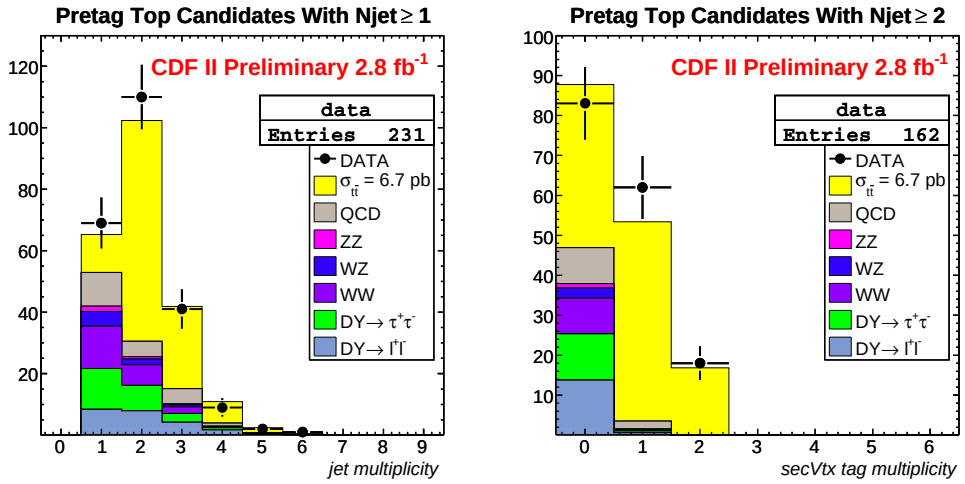

Figure 17: Jet multiplicity (left) and b tag multiplicity (right) distributions in $t\bar{t}$ dilepton candidate events with at least one respectively two jets in a 2.8 fb^{-1} dataset analysed by CDF [253].

Process	pre-tagging				b tagged
	e^+e^-	$\mu^+\mu^-$	$e^\pm\mu^\mp$	$\ell^+\ell^-$	$\ell^+\ell^-$
$t\bar{t}$, $\sigma = 6.7$ pb	29.2	21.5	59.9	110.6	65.2
$Z/\gamma^* \to \ell^+\ell^-$	9.25	4.79	0.52	14.6	0.78
$Z/\gamma^* \to \tau^+\tau^-$	2.84	2.55	6.62	12.0	0.60
$WW \to \ell^+\ell^-$	3.05	2.03	5.07	10.2	0.44
$WZ \to \ell^+\ell^-$	1.52	0.72	0.67	2.91	0.09
$ZZ \to \ell^+\ell^-$	0.80	0.40	0.26	1.46	0.10
Monte Carlo	46.7	32.0	73.0	151.7	67.2
Data SS	3.81	0.00	6.96	10.8	2.00
Sum	50.5 ± 1.7	32.0 ± 1.3	80.0 ± 2.5	162.5 ± 4.5	69.2 ±1.7
Data OS	54	33	75	162	80

Table 5: Event yields and sample composition after preselection in CDF's 2.8 fb^{-1} dilepton dataset before and after requiring at least one b tagged jet [253].

nant physics background processes exhibiting both real leptons and $\not\!\!E_T$ arise from diboson (WW, ZZ, WZ) production and from Z/γ^*+jets processes with $Z/\gamma^* \to \tau^+\tau^-, \tau \to e, \mu$. Misreconstructed $\not\!\!E_T$ due to resolution effects in Z/γ^*+jets events with $Z/\gamma^* \to e^+e^-/\mu^+\mu^-$ contributes to the instrumental background as well as W+jets and QCD multijet production where one or more jets fake the isolated lepton signature. The physics background processes are usually modelled with Monte Carlo while instrumental background processes (especially those involving fake isolated lepton signatures) typically are estimated from data. The purities in the resulting samples are usually quite good with a signal to background ratio (S/B) typically better than two.

The sample purity can be further enhanced by means of additional kinematic requirements like the scalar sum of the jet transverse momenta H_T to be above a certain threshold or by selecting events with at least one identified b jet. However, this reduces the already limited statistics in this channel even further. To increase the signal acceptance, the reconstruction and isolation requirements on the second lepton can be relaxed. If the second lepton is only required to be reconstructed as isolated track – termed lepton plus track selection – especially 1 prong hadronic τ decays can contribute as well.

In a recent preliminary analysis, CDF determines the $t\bar{t}$ cross section from a 2.8 fb^{-1} dataset by requiring two oppositely charged reconstructed isolated leptons with $E_T \geq 20$ GeV, $\not\!\!E_T \geq 25$ GeV and at least two jets within $|\eta| < 2.5$ and $E_T \geq 15$ GeV, with the leading jet fulfilling $E_T \geq 30$ GeV. The $t\bar{t}$ cross section is extracted from the resulting sample once without any additional cuts and once after increasing the purity by requiring at least one of the jets to be b tagged. The background from Z/γ^* and diboson WW, ZZ, WZ events is derived from MC, while fake isolated lepton signatures are estimated from a dilepton dataset where both leptons have the same charge (same sign, "SS"), assuming their contribution is identical in the opposite sign ("OS") signal selection [253].

The untagged sample yields 162 events with a total background contribution of 51.9 ± 4.5, where the dominant uncertainty contributions arise from the fake lepton estimate and the uncertainty on the jet multiplicity correction factors applied to the MC. Requiring at least one b tagged jet, 80 events remain with an expected total background of 4.0 ± 1.7, with the dominant uncertainty contributions arising again from the fake lepton estimate and also from uncertainties on the b tag modelling. The sample composition is illustrated in Figure 17 and detailed in Table 5. The resulting cross sections are given in Table 6 together with the other dilepton channel results obtained so far in Run II.

$\int \mathcal{L}dt$ [fb^{-1}]	Sel.	b tag	$\sigma_{t\bar{t}}\pm$(stat.)$\pm$(syst.)$\pm$(lumi.) [pb]	Ref.
0.2	$\ell\ell$,ℓ+trk	no	$7.0^{+2.4\,+1.6}_{-2.1\,-1.1} \pm 0.4$	[254]
0.2	$\ell\ell$	no	$8.6^{+3.2}_{-2.7} \pm 1.1 \pm 0.6$	[255]
0.4	$\ell\ell$,ℓ+trk	no,yes	$7.4 \pm 1.4 \pm 0.9 \pm 0.5$	[256]
0.4	$\ell\ell$	no	$8.5^{+2.6\,+0.7}_{-2.2\,-0.3}$ $(*)$	[257]
1.0	$\ell\ell$	no	$6.8^{+1.2\,+0.9}_{-1.1\,-0.8} \pm 0.4$	[258]
1.0	$\ell\ell$	no	$7.0^{+1.1\,+0.8}_{-1.0\,-0.6} \pm 0.4$	[259]
1.0	ℓ+trk	yes	$5.0^{+1.6\,+0.9}_{-1.4\,-0.8} \pm 0.3$	[260]
1.0	$\ell\ell$,ℓ+trk	no,yes	$6.2 \pm 0.9^{+0.8}_{-0.7} \pm 0.4$	[261]
1.0	ℓ+trk	yes	$10.1 \pm 1.8 \pm 1.1 \pm 0.6$	[262]
1.1	ℓ+trk	no	$8.3 \pm 1.3 \pm 0.7 \pm 0.5$	[263]
2.8	$\ell\ell$	yes	$7.8 \pm 0.9 \pm 0.7 \pm 0.4$	[253]
2.8	$\ell\ell$	no	$6.7 \pm 0.8 \pm 0.4 \pm 0.4$	[253]

Table 6: $t\bar{t}$ dilepton cross section measurements performed so far at the Run II Tevatron with their integrated luminosities, dataset selections applied ($\ell\ell$ = dilepton, ℓ+trk = lepton plus track) and analysis methods used. The first three results have been published; the others are preliminary. The measurement marked with $(*)$ refers to a top quark mass of 178 GeV/c^2 rather than 175 GeV/c^2 like the rest and incorporates the luminosity uncertainty in the first uncertainty given.

5.1.2 Lepton plus Jets Final State

A typical $t\bar{t}$ lepton plus jets event selection requires exactly one isolated high p_T lepton, $\not\!\!E_T$ and at least three central energetic jets, allowing both lepton plus jets and lepton plus hadronic τ signatures to contribute. The dominant physics background in this final state arises from W boson plus jets production, and the main instrumental background comes from QCD multijet production with a jet faking the isolated lepton signature. Additional smaller background contributions arise from Z/γ^* plus jets, diboson and single top production. While for these smaller background processes shape and normalisation commonly are determined from simulation and NLO cross sections, W plus jets events are usually normalised to data and the shape is derived from Monte Carlo. The QCD multijet background's shape and normalisation are typically derived from data, using for example datasets fulfilling the

complete event selection except the tight lepton isolation for the background shape and the fake rate derived from data for the normalisation.

Samples selected with such a basic preselection exhibit an S/B below unity, around 1/4. The sample purity can be significantly improved via further topological selections to reject more background or by using b tagging in the selected sample. If no b tagging is used, usually multiple topological and kinematic event properties are combined in a multivariate discriminant yielding good signal to background separation without relying on the presence of b jets in the events, hence being less model dependent. The sample composition can then be determined from a template fit in that sensitive variable, providing a higher sensitivity than a plain cut.

Requiring identified b jets to be present in the event is a very powerful tool to reject the background processes which exhibit little heavy flavour content. b tagging algorithms based on the long lifetime of B hadrons or reconstructing soft leptons inside a jet originating from semileptonic B decays as discussed in Section 4.3 have been deployed for that purpose. Using b tagging, very pure $t\bar{t}$ samples can be selected, exceeding easily an S/B > 10 if at least four jets and at least two identified b jets are required.

The most precise $t\bar{t}$ cross section measurement published so far has been performed by D0 on a 0.9 fb^{-1} lepton plus jets dataset [264]. Events are selected by requiring exactly one isolated electron or muon with $E_T > 20$ GeV, $\not\!\!E_T > 20$ GeV for e plus jets respectively > 25 GeV for μ plus jets and at least three jets within $|\eta| < 2.5$ and $E_T > 20$ GeV, with the leading jet $E_T > 40$ GeV. Cuts on the azimuthal separation between lepton and $\not\!\!E_T$ are applied to suppress background due to misreconstructed objects. After these cuts the $t\bar{t}$ signal contributes only about 20% of the total sample. The $t\bar{t}$ cross section is measured using two complementary analyses.

One approach is based on lifetime b tagging, requiring at least one jet in the event to be tagged and determining the $t\bar{t}$ production rate in a maximum likelihood fit to the observed event yields in the various subchannels based on lepton flavour, jet multiplicity and b tag multiplicity. The dominant systematic uncertainties arise here from uncertainties on the tagging efficiencies for b, c, q and gluon jets and the jet energy calibration. The second analysis utilises topological likelihood discriminants for the various subchannels based on lepton flavour and jet multiplicity. After applying an additional cut on the jets' $H_T > 120$ GeV for three-jet events, five or six different variables like angular object separation, sphericity and aplanarity that provide good discrimination power and are well modelled in MC are combined into discriminants for each subchannel. The sample composition is then determined in a maximum likelihood fit of templates of the signal and background contributions to the observed discriminant distributions. The dominant sys-

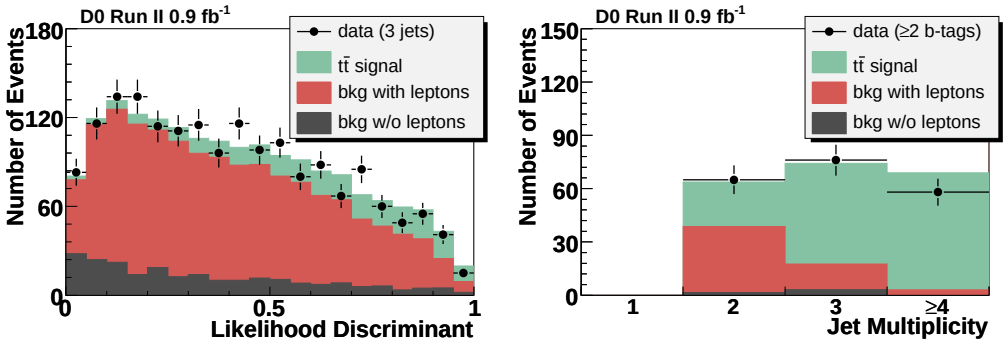

Figure 18: Topological likelihood distribution when requiring three jets (left) and jet multiplicity distribution when requiring at least two b tagged jets (right) in D0's 0.9 fb^{-1} lepton plus jets dataset [264].

	3 jets, 1 tag	3 jets, $\geq$2 tags	$\geq$4 jets, 1 tag	$\geq$4 jets, $\geq$2 tags	3 jets, topo	$\geq$4 jets, topo
$N_{t\bar{t}}$	147 $\pm$12	57 $\pm$6	130 $\pm$10	66 $\pm$7	245 $\pm$20	233 $\pm$19
$N_{W+\text{jets}}$	105 $\pm$5	10 $\pm$1	16 $\pm$2	2 $\pm$1	1294 $\pm$48	321 $\pm$30
N_{other}	27 $\pm$2	5 $\pm$1	8 $\pm$1	2 $\pm$1		
N_{multijet}	27 $\pm$6	3 $\pm$2	6 $\pm$3	0 $\pm$2	227 $\pm$28	70 $\pm$12
total	306 $\pm$14	74 $\pm$6	159 $\pm$11	69 $\pm$7	1766 $\pm$59	624 $\pm$37
N_{data}	294	76	179	58	1760	626

Table 7: Event yields and sample composition in D0's 0.9 fb^{-1} lepton plus jets dataset for both the topological and the b tagging analysis. The $t\bar{t}$ contribution is based on the measured cross section in the respective analysis [264].

tematic uncertainties arise here from uncertainties on the selection efficiencies and the likelihood fit uncertainty derived using statistical fluctuations in the likelihood discriminant template shapes. The sample compositions for both analyses are illustrated in Figure 18 and detailed in Table 7.

Both analyses exhibit a statistical correlation of 0.31 as determined by ensemble tests and are combined using the best linear unbiased estimate (BLUE) approach [278, 279]. The resulting cross section is given in Table 8 together with the other lepton plus jets channel results obtained so far in Run II.

$\int \mathcal{L}dt$ [fb^{-1}]	Sel.	b tag	$\sigma_{t\bar{t}}\pm$(stat.)$\pm$(syst.)$\pm$(lumi.) [pb]	Ref.
0.2	ℓ+jets	yes	$5.6^{+1.2\ +0.9}_{-1.1\ -0.6}$ (‡)	[208]
0.2	ℓ+jets	yes	$6.0^{+1.5\ +1.2}_{-1.6\ -1.3}$ (‡)	[265]
0.2	ℓ+jets	yes, soft-μ	$5.3 \pm 3.3^{+1.3}_{-1.0}$ (‡)	[266]
0.2	ℓ+jets	no	$6.6 \pm 1.1 \pm 1.5$ (‡)	[267]
0.2	ℓ+jets	no	$6.7^{+1.4\ +1.6}_{-1.3\ -1.1} \pm 0.4$	[268]
0.2	ℓ+jets	yes	$8.6^{+1.6}_{-1.5} \pm 0.6$ (†)	[269]
0.3	ℓ+jets	yes	$8.7 \pm 0.9^{+1.1}_{-0.9}$ ($*$, ‡)	[270]
0.3	ℓ+jets	yes	$8.9 \pm 1.0^{+1.1}_{-1.0}$ ($*$, ‡)	[210]
0.4	ℓ+jets	yes	$6.6 \pm 0.9 \pm 0.4$ (†)	[221]
0.4	ℓ+jets	no	$6.4^{+1.3}_{-1.2} \pm 0.7 \pm 0.4$	[271]
0.9	ℓ+jets	no, yes	$7.4 \pm 0.5 \pm 0.5 \pm 0.5$	[264]
0.4	ℓ+jets	yes, soft-μ	$7.3^{+2.0}_{-1.8} \pm 0.4$ (†)	[272]
0.7	ℓ+jets	yes	$8.5 \pm 0.6 \pm 1.0$ (‡)	[273]
1.0	ℓ+jets	yes	$8.2 \pm 0.5^{+0.8}_{-0.7} \pm 0.5$	[259]
1.7	ℓ+jets	yes, soft-e	$7.8 \pm 2.4 \pm 1.5 \pm 0.5$	[274]
2.0	ℓ+jets	yes, soft-μ	$8.7 \pm 1.1^{+0.9}_{-0.8} \pm 0.6$	[275]
2.7	ℓ+jets	yes	$7.2 \pm 0.4 \pm 0.5 \pm 0.4$	[276]
2.8	ℓ+jets	no	$6.8 \pm 0.4 \pm 0.6 \pm 0.4$	[277]

Table 8: $t\bar{t}$ lepton plus jets cross section measurements performed so far at the Run II Tevatron with their integrated luminosities, dataset selections applied and analysis methods used. The first eleven results have been published; the others are preliminary. The measurements marked with ($*$) refer to a top quark mass of 178 GeV/c^2 rather than 175 GeV/c^2 like the rest. Measurements marked with (‡) include the luminosity uncertainty in the systematic uncertainty given, while for measurements marked with (†) the first uncertainty given is statistical and systematic combined and the second comes from luminosity.

5.1.3 All-Hadronic Final State

To select all-hadronic $t\bar{t}$ decays, one typically requires at least six central energetic jets to be reconstructed per event, and no isolated energetic leptons or significant $\not\!\!E_T$ to be present. The overwhelming background process here is QCD multijet production, dominating over the signal by three orders of magnitude after the online selection of events with triggers on multiple jets and H_T in the event above a certain threshold. This background is usually modelled from the data themselves as the theoretical description of final states with such high jet multiplicities exhibits large uncertainties and datasets even more depleted from signal can be easily obtained for example by selecting a lower jet multiplicity.

After the preselection, signal and background are further separated by applying b jet identification and using multivariate discriminants based on topological and kinematic event properties.

CDF has published the most precise cross section analysis in the all-hadronic final state to date based on 1 fb^{-1} of data [280]. Events are required to have at least six and at most eight jets with $E_T \geq 15$ GeV, $\Delta R \geq 0.5$ from each other and $|\eta| \leq 2$, no isolated energetic electrons or muons as used in the leptonic $t\bar{t}$ analyses, and $\not\!\!E_T$ divided by $\sqrt{H_T}$ of the selected jets has to be $< 3\ \sqrt{\text{GeV}}$. This yields an S/B of about 1/370 (0.3%). The sample purity is then improved using a neural network discriminant based on variables like H_T, centrality, aplanarity and minimal/maximal invariant dijet or trijet masses of all jet permutations. The signal is modelled using MC and for the background the selected data are applied directly as the expected signal contribution is very small.

At least one of the jets in each event is required to be b tagged, and the sample composition is then determined in terms of number of tags rather than events. The average number of tags per signal event for a given neural network cut is determined from MC and is used to derive the $t\bar{t}$ cross section from the observed excess of tags above the background expectation derived from data. The tagging efficiencies of the simulation are corrected for differences w.r.t. data. The cut on the neural network discriminant N_{out} is optimised for the highest expected signal significance after b tagging, taking both statistical and systematical uncertainties of signal and background into account, yielding $N_{\text{out}} \geq 0.94$. This cut yields an S/B of approximately 1/12 before b tagging and 1/2 thereafter.

The by far dominating systematical uncertainty arises from the jet energy scale calibration, strongly impacting both the preselection of events and the input variables for the further neural network selection. The sample composition of candidate tags in data is illustrated in Figure 19 and detailed in

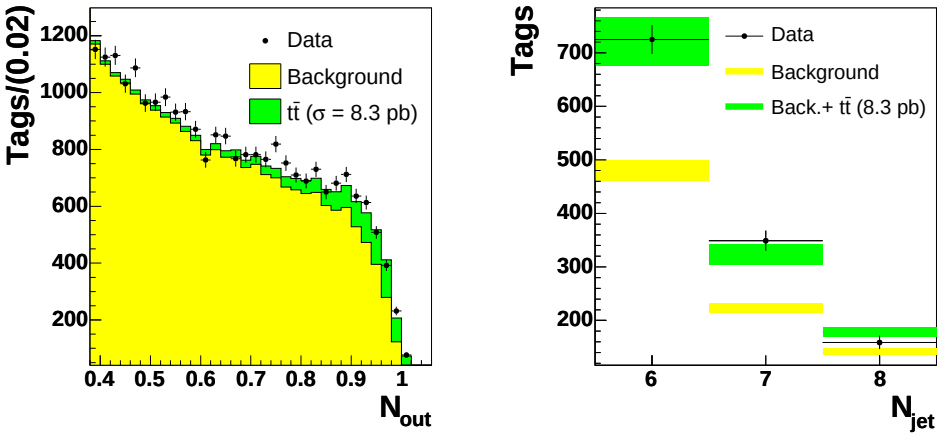

Figure 19: Left: Number of tags in 1 fb^{-1} of all-hadronic candidate events selected by CDF versus neural network discriminant $N_{\rm out}$. Right: Number of tags versus jet multiplicity after requiring $N_{\rm out} \geq 0.94$. The $t\bar{t}$ contributions are normalised to the measured cross section of 8.3 pb [280].

	4 jets	5 jets	6 jets	7 jets	8 jets
BG	16060 ± 575	2750 ± 92	536 ± 17	255 ± 8	146 ± 5
BG (corrected)	15961 ± 677	2653 ± 112	481 ± 20	223 ± 10	142 ± 7
$t\bar{t}$ ($\sigma_{t\bar{t}} = 8.3$ pb)	120 ± 20	266 ± 45	242 ± 41	101 ± 17	38 ± 7
BG + $t\bar{t}$	16081 ± 677	2919 ± 121	723 ± 46	324 ± 20	180 ± 10
Data	16555	3139	725	349	159

Table 9: Expected and observed yields of tags after requiring $N_{\rm out} \geq 0.94$ with given uncertainties corresponding to statistical and systematic contributions added in quadrature. The corrected background (BG) contribution accounts for the signal contamination in the dataset used for its estimate. After tagging, 1020 events remain in the signal sample with 1233 tags and an expected background of 846 ± 37 tags. The average number of tags for $t\bar{t}$ signal is determined to be 0.95 ± 0.07 [280].

Table 9. The resulting cross section is given in Table 10 together with the other all-hadronic channel results obtained so far in Run II.

$\int \mathcal{L}dt$ [fb^{-1}]	Sel.	b tag	$\sigma_{t\bar{t}}\pm$(stat.)$\pm$(syst.)$\pm$(lumi.) [pb]	Ref.
0.3	jets only	yes	$7.5 \pm 2.1^{+3.3\ +0.5}_{-2.2\ -0.4}$ $(*)$	[281]
0.4	jets only	yes	$4.5^{+2.0\ +1.4}_{-1.9\ -1.1} \pm 0.3$	[282]
1.0	jets only	yes	$8.3 \pm 1.0^{+2.0}_{-1.5} \pm 0.5$	[280]

Table 10: $t\bar{t}$ all-hadronic cross section measurements performed so far at the Run II Tevatron with their integrated luminosities, dataset selections applied and analysis methods used. All three results have been published. The measurement marked with $(*)$ refers to a top quark mass of 178 GeV/c^2 rather than 175 GeV/c^2 like the other two.

5.1.4 Hadronic τ channels

By choosing a more inclusive $t\bar{t}$ event selection, hadronic τ decays can easily be included as already mentioned in the lepton plus jets and dilepton channels for the τ plus lepton case. A first measurement without any explicit lepton identification has been published by CDF, selecting events with at least four jets with at least one of them being b tagged and significant $\not\!\!E_T$ not aligned with any jet. Since events with isolated energetic electrons or muons are rejected, the resulting sample is especially enriched in τ plus jets events [283].

The explicit reconstruction of hadronic τ decays is far more demanding and usually relies on multivariate discriminants. Based on the decay mode (1 prong or 3 prong, with or without associated electromagnetic subclusters from neutral pions), different discriminants may be deployed, exploiting the differences between hadronic τs and jets like isolation in tracking system and calorimetry, shower shape, track multiplicity or correlations between tracks and clusters in the calorimeter. Using such discriminants, the τ plus jets and τ plus lepton $t\bar{t}$ decay modes have been studied based on their experimental signature of $\not\!\!E_T$, at least one hadronic τ candidate, at least four respectively two jets and no respectively one isolated energetic electron or muon. b jet identification is crucial in such analyses to improve sample purity.

A first τ plus jets cross section analysis has been performed by D0 on 0.3 fb^{-1} of data, deploying a preselection and τ identification as outlined above, b jet identification and neural networks based on event topology and kinematics to further separate the $t\bar{t}$ signal and the background mainly from QCD multijet production faking τs [284]. While the measurement suffers from large statistical uncertainties, it is a proof of principle that will greatly benefit from the tenfold increased dataset already now at hand.

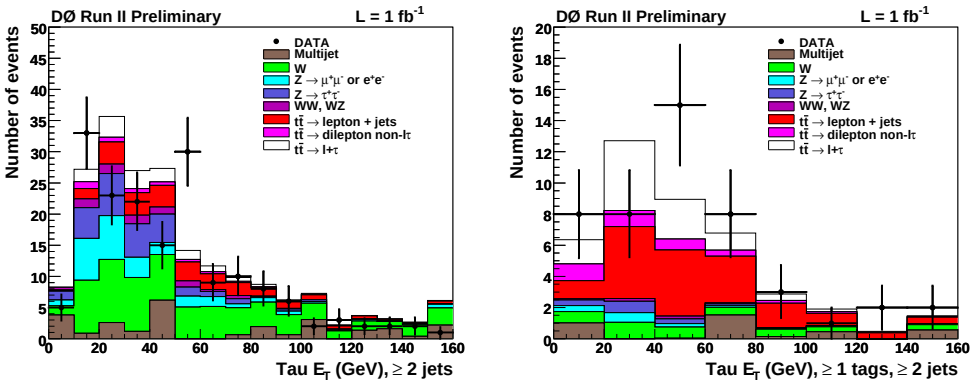

Figure 20: Hadronic τ E_T spectrum before (left) and after (right) b tagging is applied in the preselected 1 fb^{-1} $\ell + \tau$ sample analysed by D0. The $t\bar{t}$ signal is normalised to Standard Model expectation; the highest bin contains overflows [285].

D0 has performed also a first measurement of the $t\bar{t}$ production rate in the τ plus lepton final state based on 1 fb^{-1} of data [285]. Events are required to have exactly one isolated electron or muon with $E_T > 15$ GeV, $|\eta| < 1.1$ respectively $E_T > 20$ GeV, $|\eta| < 2$, at least one τ candidate of opposite charge within $|\eta| < 1$, $\not\!\!E_T$ between 15 and 200 GeV, at least two jets within $|\eta| < 2.5$ exhibiting $E_T > 20$ GeV with the leading jet above 30 GeV and at least one of them identified as b jet. Further channel specific background rejection is achieved by vetoing events in the $\mu\tau$ analysis where the invariant mass of the isolated muon with a second non-isolated muon lies between 70 and 100 GeV/c^2. In the $e\tau$ channel, events are rejected where electron and $\not\!\!E_T$ are aligned in azimuthal angle ϕ by requiring $\cos(\Delta\phi(e, \not\!\!E_T)) < 0.9$.

Background contributions arise from W boson plus jets production, Z/γ^* plus jets events with $Z/\gamma^* \to \ell^+\ell^-/\tau^+\tau^-$ and diboson production, described by MC with the W boson plus jets production normalised to data. Background from QCD multijet production is estimated based on data where lepton and τ exhibit the same charge, corrected for contributions from W boson plus jets and $t\bar{t}$ production which are most significant here. The dominant systematic uncertainties in this analysis arise from limited background/MC statistics, τ fake rate and b tagging modelling uncertainties and jet energy calibration.

The resulting sample composition is illustrated in Figure 20 and detailed in Table 11 – the significant included signal contributions from the lepton plus jets and dilepton channels should be noted. The corresponding cross

	before b tagging		after b tagging	
	$\mu\tau$	$e\tau$	$\mu\tau$	$e\tau$
W+jets	38.0 ± 1.7	34.1 ± 3.5	2.31 ± 0.22	2.13 ± 0.27
$Z/\gamma^* \to ee, \mu\mu$	20.7 ± 1.1	5.8 ± 0.6	1.09 ± 0.11	0.38 ± 0.05
$Z/\gamma^* \to \tau\tau$	19.6 ± 1.2	7.5 ± 0.6	1.02 ± 0.10	0.54 ± 0.06
Diboson	2.8 ± 0.1	5.1 ± 0.6	0.21 ± 0.01	0.34 ± 0.07
Multijet	10.6 ± 6.3	12.7 ± 6.6	4.52 ± 3.01	-1.27 ± 1.77
$t\bar{t} \to \ell + \tau$	7.8 ± 0.1	6.67 ± 0.1	5.64 ± 0.04	4.70 ± 0.05
$t\bar{t} \to \ell\ell$	4.3 ± 0.1	0.73 ± 0.1	3.14 ± 0.03	0.47 ± 0.07
$t\bar{t} \to \ell$+ jets	12.7 ± 0.1	12.41 ± 0.2	8.40 ± 0.11	7.88 ± 0.12
Total Expected	116.6 ± 6.8	85.0 ± 7.7	26.33 ± 3.02	15.17 ± 1.97
Data	104	69	29	18

Table 11: Event yields and sample composition before and after b tagging is applied in the preselected 1 fb^{-1} $\ell + \tau$ sample analysed by D0. The $t\bar{t}$ signal is normalised to Standard Model expectation; given uncertainties are statistical [285].

$\int \mathcal{L}dt$ [fb^{-1}]	Sel.	b tag	$\sigma_{t\bar{t}}\pm$(stat.)$\pm$(syst.)$\pm$(lumi.) [pb]	Ref.
0.2	$\ell + \tau$	no	$<$ 5.2·SM rate (95% C.L.)	[219]
0.3	$\not\!\!E_T$ + jets	yes	$6.0 \pm 1.2^{+0.9}_{-0.7}$ (‡)	[283]
0.3	τ+jets	yes	$5.1^{+4.3}_{-3.5} \pm 0.7 \pm 0.3$	[284]
0.4	$\ell + \tau$	no	$\approx 1\sigma$ signal evidence	[286]
1.0	$\ell + \tau$	yes	$8.3^{+2.0\ +1.4}_{-1.8\ -1.2} \pm 0.5$	[285]
1.2	$\ell + \tau$	yes	$6.4^{+1.8\ +1.4}_{-1.6\ -1.3} \pm 0.4$	[287]
2.2	$\ell + \tau$	yes	$7.3^{+1.3\ +1.2}_{-1.2\ -1.1} \pm 0.5$	[287]

Table 12: $t\bar{t}$ hadronic τ cross section measurements performed so far at the Run II Tevatron with their integrated luminosities, dataset selections applied and analysis methods used. The first two results have been published; the others are preliminary. The measurement marked with (‡) includes the luminosity uncertainty in the systematic uncertainty given.

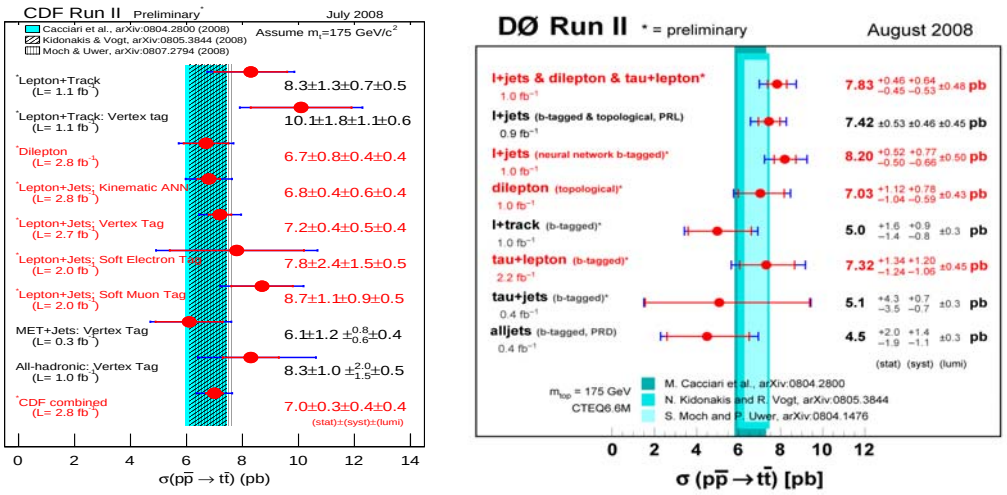

Figure 21: Current status of the $t\bar{t}$ production cross section measurements by CDF (left, [288]) and D0 (right, [289]) in comparison with theory predictions shown as coloured/hatched bands. The analysis channels entering the respective shown combination are highlighted in red [259, 290].

section is given in Table 12 together with an update obtained by adding additional 1.2 fb^{-1} of data as well as other results involving hadronic τ final states achieved so far in Run II.

5.1.5 Summary

An overview of the current status of the cross section measurements performed in the various $t\bar{t}$ decay channels is given in Figure 21 for CDF and D0, showing good agreement between the different channels, analysis methods and experiments. The theoretical predictions as discussed in Section 3.1 are also shown for comparison as coloured/hatched bands and exhibit very good agreement with the measurements as well.

CDF combines the results obtained in the lepton plus jets and dilepton channels using between 1.7 and 2.8 fb^{-1} of data, reaching a relative uncertainty on the result of 9% [290]. The most precise single measurement is obtained in the lepton plus jets channel using secondary vertex b tagging on 2.7 fb^{-1} of data yielding a relative uncertainty of about 10% [276]. D0 combines the results from lepton plus jets, dilepton and τ plus lepton channels obtained from approximately 1.0 fb^{-1} of data, yielding a relative uncertainty of about 11% [259]. The most precise single measurement here with a precision of 11% has been published in the lepton plus jets channel using both secondary vertex b tagging and kinematical information in 0.9 fb^{-1} of data

in a combined result [264]. For comparison, the final Run I combined cross section results of CDF [291, 292] and D0 [293] had a precision around 25% respectively. Unfortunately, to date no combination across the experiments exists as is the case for top quark mass measurements. However, such a combination of the $t\bar{t}$ production rate is planned for the future.

With increasing datasets, the statistical uncertainties become less important and the measurements' precision starts to be driven by systematic uncertainties which in turn can also be better constrained using additional data. One of the main challenges for future measurements will be to carefully study the contributing systematic uncertainties rather than using conservative estimates. The most precise single $t\bar{t}$ production cross section measurement at the Run II Tevatron with 8 fb^{-1} of data can be expected in the lepton plus jets channel – probably using both kinematical and b tagging information – with a relative precision of around 8%, dominated by luminosity and systematic uncertainties. For combinations, the precision may be ultimately driven by the luminosity uncertainty of currently 6% for both experiments. The luminosity uncertainty could be avoided by measuring a cross section ratio, for example w.r.t. Z boson production. With large datasets, also a ratio of the $t\bar{t}$ cross section measurements obtained in the different channels like the lepton plus jets and the dilepton channels could be measured with good statistical precision while benefiting from cancellations of common systematic uncertainties.

The precision of the $t\bar{t}$ cross section measurements matching that of the theoretical predictions allows for stringent tests of the involved perturbative QCD calculations. This furthers our understanding of the Standard Model that still provides a good description of the measurements performed so far. Based on the observed production rate alone, severe constraints on exotic models become feasible [294]. More detailed tests of the Standard Model predictions for $t\bar{t}$ production will be described in the following sections. Via its mass dependence, the $t\bar{t}$ production rate can also be used to test consistency with the top quark mass measurements performed at the Tevatron with the benefit of easier theoretical interpretation as discussed in Section 7.3.4. Investigating all available $t\bar{t}$ final states including those with hadronic τs and comparing them allows one to probe for novel physics contributions affecting the observed final states differently. For example, the searches for charged Higgs bosons in top quark decays are discussed in Section 6.5.

5.2 Top Quark Pair Production Mechanism

Top quark pair production at the Tevatron proceeds predominantly via $q\bar{q}$ annihilation as described in Section 3.1. The remaining contribution of gluon-

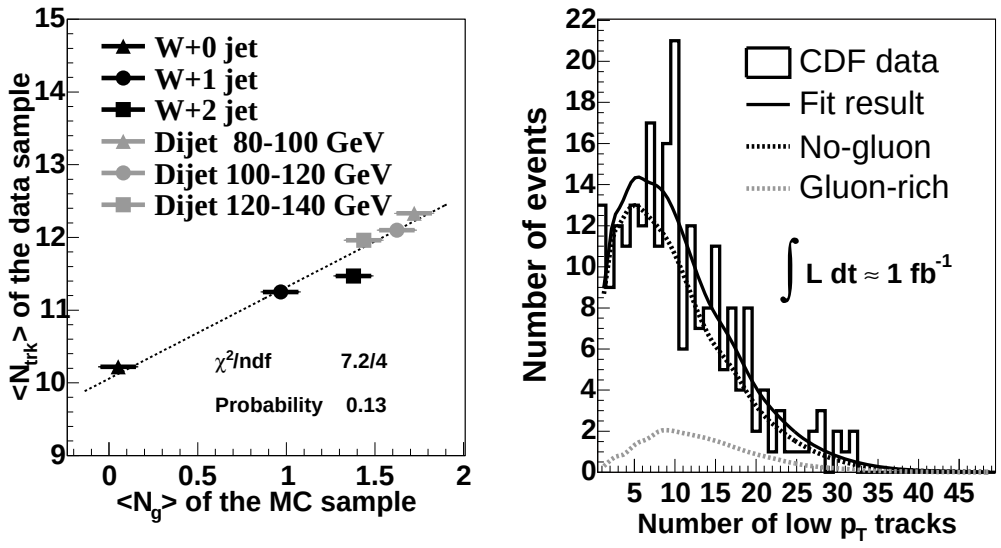

Figure 22: Left: Correlation between the soft track multiplicity observed in collider data events and the average number of gluons in the corresponding Monte Carlo samples. Right: Fit result of the soft track multiplicity distribution observed in b tagged lepton plus at least four jets $t\bar{t}$ candidate events with a no-gluon respectively a gluon-rich template [297].

gluon fusion to the total production rate is $15 \pm 5\%$, with the variation of up to a factor of two arising from the corresponding PDF uncertainties [117].

While the total $t\bar{t}$ production rate has been studied extensively (see Section 5.1) and has been found to be in agreement with the Standard Model expectation, the production mechanism itself has not yet been subject to such scrutiny. A measurement of the fraction of $t\bar{t}$ events produced via gluon-gluon fusion $f_{gg} = \sigma(gg \to t\bar{t})/\sigma(p\bar{p} \to t\bar{t})$ allows one to test the QCD prediction and can contribute to a reduction in the uncertainties of the corresponding PDFs. In addition, contributions from extensions of the Standard Model to $t\bar{t}$ production could be unveiled [295], some of which may have remained undetected so far due to compensating new decay mechanisms [296].

CDF performs a first measurement of f_{gg} in a 1 fb^{-1} b tagged lepton plus jets dataset [297]. The analysis is based on the fact that soft gluons are emitted with a higher probability from gluons than from quarks [91–93, 298], and hence the average number of charged particles (tracks) with low transverse momentum should be higher in $gg \to t\bar{t}$ events than in $q\bar{q} \to t\bar{t}$ events.

To avoid the large theoretical uncertainties on soft gluon radiation in

Monte Carlo modelling of the multiplicity of soft tracks, W plus jets and dijet collider data whose production mechanisms are well understood are used to relate the observed soft track multiplicity to the gluon content of a sample (see Figure 22). After obtaining templates for the soft track multiplicity distribution in no-gluon respectively gluon-enriched events from W plus no jets respectively dijet events with a leading jet E_T of 80-100 GeV, the observed distribution in $t\bar{t}$ candidate events is fitted with these templates. From the fit result, f_{gg} is extracted and found to be $0.07 \pm 0.14(\text{stat.}) \pm 0.07(\text{syst.})$, corresponding to a 95% C.L. upper limit of 0.33.

CDF uses a complementary second method to extract f_{gg} from the same dataset, based on templates from a neural network using kinematic event properties to separate $gg \to t\bar{t}$, $q\bar{q} \to t\bar{t}$ and the dominant W plus jets background [299], yielding a 95% C.L. upper limit of $f_{gg} < 0.61$. Combining both results yields $f_{gg} = 0.07^{+0.15}_{-0.07}(\text{stat.} + \text{syst.})$, in good agreement with the Standard Model expectation.

CDF has also performed a first measurement of f_{gg} in a 2 fb^{-1} dilepton dataset, based on the variation of the azimuthal correlation of the charged leptons caused by the different $t\bar{t}$ production modes [300]. This difference arises from the fact that close to the threshold top quark pairs are produced in a $^3S_1$ state via $q\bar{q}$ annihilation and in a $^1S_0$ state via gluon-gluon fusion (see also Section 5.5). Consequently, the top quark spins tend to be antiparallel for $t\bar{t}$ production via gluon-gluon fusion and aligned for production via $q\bar{q}$ annihilation, which is reflected in the azimuthal correlation of the charged leptons. The relative fraction of $t\bar{t}$ production via gluon fusion is determined in a fit of the observed $\Delta\phi$ distribution in data with templates for $gg \to t\bar{t}$, $q\bar{q} \to t\bar{t}$ and background arising from diboson, Z/γ^* plus jets and W boson plus jets production, yielding $f_{gg} = 0.53^{+0.35}_{-0.37}(\text{stat.})^{+0.07}_{-0.08}(\text{syst.})$ consistent with the Standard Model prediction.

5.3 Top Quark Charge Asymmetry

The strong production of top quark pairs is symmetric under charge conjugation at leading order, implying it does not discriminate between top and antitop quarks. Considering that the initial proton-antiproton state at the Tevatron is not an eigenstate of charge conjugation, this symmetry is a coincidence. At higher orders, a charge asymmetry arises from interference between amplitudes that are symmetric and antisymmetric under the exchange of top and antitop quarks [301, 302], leading to an excess of top over antitop quarks in specific kinematic areas. One resulting observable is the integrated forward-backward production asymmetry for inclusive $t\bar{t}$ production at the Tevatron. It is predicted to be $5 - 10\%$ at NLO [301–305], implying

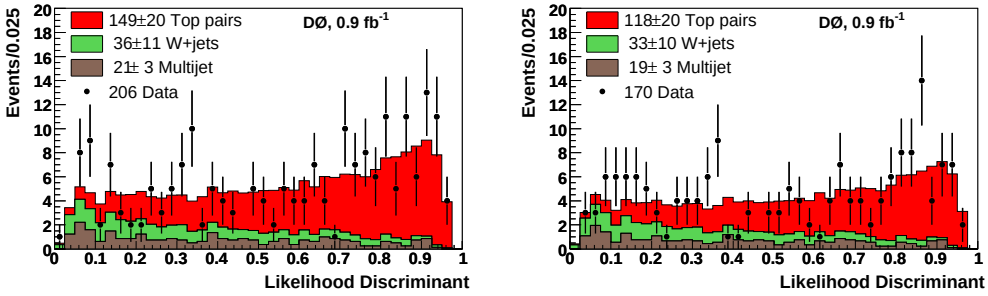

Figure 23: Likelihood discriminant distribution for the dataset with ≥ 4 jets, overlaid with the result of the template fit determining the sample composition for events with $\Delta y > 0$ (left) and $\Delta y < 0$ (right) [309].

top quarks are preferentially emitted in the direction of the incoming protons. The asymmetry depends strongly on the region of phase space being probed and particularly on the production of an additional jet: While the asymmetry for exclusive $t\bar{t}$ production without additional jets is predicted to be 6.4% [305], the inclusive $t\bar{t}$ production with one additional jet exhibits an asymmetry of about -7% at LO [305, 306] which is drastically reduced to $(-1.5 \pm 1.5)\%$ at NLO [306].

The size of higher order corrections for the $t\bar{t}$ plus jet subprocess illustrates that higher order evaluations of the whole process are still necessary for the total asymmetry prediction to converge and correctly describe the partial cancellations of the various interference contributions. It should also be noted that in the above theoretical predictions the top quark decay and possible effects on the asymmetry due to the reconstruction of the final state objects are not considered. The top quark charge asymmetry is also sensitive to possible extensions of the Standard Model in $t\bar{t}$ production like axigluons [304], technicolour [307] or an additional neutral Z' gauge boson [308]. Consequently, a measurement of the asymmetry can be used to set limits on such processes, particularly extending the sensitivity of searches for $t\bar{t}$ production via heavy resonances (see Section 5.7.1) to include not only those of narrow width but also wide resonances.

D0 has published the first measurement of the integrated forward-backward charge asymmetry in $t\bar{t}$ production, based on a 0.9 fb^{-1} b tagged lepton plus jets dataset [309]. The $t\bar{t}$ system is reconstructed using a constrained kinematic fit, where the charged lepton is used to differentiate between the top and the antitop quark. The signed rapidity difference of the top and the antitop quark $\Delta y = y_t - y_{\bar{t}}$ is used as an observable from which the charge

N_{jet}	$A_{\rm fb}^{\rm pred}$ [%]	$A_{\rm fb}^{\rm obs}$ [%]
≥ 4	$0.8 \pm 0.2(\text{stat.}) \pm 1.0(\text{acc.}) \pm 0.0(\text{dil.})$	$12 \pm 8\,(\text{stat.}) \pm 1\,(\text{syst.})$
$= 4$	$2.3 \pm 0.2(\text{stat.}) \pm 1.0(\text{acc.}) \pm 0.1(\text{dil.})$	$19 \pm 9\,(\text{stat.}) \pm 2\,(\text{syst.})$
≥ 5	$-4.9 \pm 0.4(\text{stat.}) \pm 1.0(\text{acc.}) \pm 0.2(\text{dil.})$	$-16^{+15}_{-17}\,(\text{stat.}) \pm 3\,(\text{syst.})$

Table 13: $A_{\rm fb}^{\rm pred}$: MC@NLO Standard Model prediction for the $t\bar{t}$ charge asymmetry to be observed with the D0 detector, including uncertainties from acceptance and dilution (Δy-sign misreconstruction) effects. $A_{\rm fb}^{\rm obs}$: Uncorrected $t\bar{t}$ charge asymmetry observed by D0 [309].

asymmetry is obtained as $A_{fb} = (N_f - N_b)/(N_f + N_b)$, with N_f (N_b) being the event yields with positive (negative) Δy. The sample composition is determined in a template fit based on a multivariate kinematic likelihood discriminant for both signs of the reconstructed Δy simultaneously as shown in Figure 23.

The resulting measurement is not corrected for reconstruction and acceptance effects due to the limited theoretical knowledge of the shape of the asymmetry. Instead, a prescription is provided to model the detector acceptance at particle level, allowing one to compare any model with the obtained measurement. For a comparison with the Standard Model, a slightly more precise prescription than the one provided in the paper [309] is applied to the prediction of the MC@NLO [310, 311] generator and found to be in agreement with the obtained measurement for the different jet multiplicities studied, including the change of the asymmetry sign, as shown in Table 13. The dominant systematic uncertainty of the ≥ 4 jet sample arises from the relative jet energy calibration between simulation and data respectively for its subsamples from event migration between the subsamples when splitting the sample up into one with exactly four and one with at least five jets. These uncertainties are negligible compared to the statistical ones. The measurement is also used to derive 95% C.L. limits on the fraction of $t\bar{t}$ events that are produced via a specific Z' resonance model [307, 312] with parity-violating couplings as a function of the resonance mass.

CDF has obtained two measurements of $A_{\rm fb}$ based on a 1.9 fb^{-1} b tagged lepton plus jets dataset, using different observables after reconstruction of the $t\bar{t}$ kinematics in a constrained fit [313–315]. CDF chooses a different approach for the measurements than D0 by providing results both before and after background subtraction *and* correction for acceptance and reconstruction effects.

The first analysis uses as observable the rapidity difference between hadronically and semileptonically decaying top quark multiplied by the charged

lepton charge [313, 315], equivalent to Δy used in the measurement by D0. After background subtraction, for jet multiplicities of $\geq 4, = 4$ and ≥ 5 jets asymmetries of $0.119 \pm 0.064, 0.132 \pm 0.075$ and 0.079 ± 0.123 are observed – consistent with the measurement by D0 – with corresponding MC@NLO predictions of $0.017 \pm 0.007, 0.038 \pm 0.008$ and -0.033 ± 0.012 (errors are statistical only). The result from the inclusive sample with at least four jets is then corrected for reconstruction and acceptance effects, yielding $A_{\text{fb}}^{\text{corr}} = 24 \pm 13\,(\text{stat.}) \pm 4\,(\text{syst.})\%$, with the dominant systematic uncertainty coming from the shape uncertainty of the Δy distribution. The result is higher than expected from NLO predictions, but consistent within errors.

The second analysis measures the charge asymmetry using the product of inverse lepton charge and $\cos\theta_{t_{\text{had}}}$ as observable, where $\theta_{t_{\text{had}}}$ is the angle of the top quark with the hadronic decay chain with respect to the proton beam [313, 314]. Since this measurement is performed in the laboratory frame rather than the parton rest frame, the asymmetry is reduced by about 30% [304]. For ≥ 4 jets, the corrected asymmetry is measured to be $A_{\text{fb}}^{\text{corr}} = 17 \pm 7\,(\text{stat.}) \pm 4\,(\text{syst.})\%$ with the dominant systematic uncertainty arising from background shape and normalisation. This result is consistent with the theoretical prediction at the 2σ level.

It should be noted that the forward-backward asymmetry in the laboratory frame at the LHC vanishes due to the symmetric initial state in contrast to the Tevatron $p\bar{p}$ collider. Due to the dominant $t\bar{t}$ production via charge symmetric gluon fusion at $\sqrt{s} = 14$ TeV, the observable charge asymmetry is reduced at the LHC.

5.4 Top Quark Pair Production Kinematics

Exotic contributions to $t\bar{t}$ production could alter the observed event kinematics, which is exploited in searches for such processes as described in Section 5.7. The basic kinematic properties of leptons, jets, $\not\!\!E_T$ and corresponding angular distributions are continuously compared to the Standard Model expectation both in signal-enriched datasets and signal-depleted control samples exhibiting features similar to the signal in all studies of top quark properties and especially in the cross section analyses. So far, no significant deviation from the Standard Model expectation has been found that would be indicative of new physics contamination in top quark samples.

In Run I, CDF and D0 observed a slight excess of the $t\bar{t}$ production rate over the Standard Model prediction in the dilepton channel, especially in the $e\mu$ final state [316, 317]. Since some of these events exhibit rather large $\not\!\!E_T$ and lepton p_T, their consistency with the Standard Model was questioned

and the kinematic compatibility of these events with the cascade decays of heavy supersymmetric quarks was pointed out [318].

Triggered by this, CDF has performed a search for anomalous $t\bar{t}$ kinematics in Run II, based on a 0.2 fb^{-1} dilepton dataset yielding 13 candidate events [319]. A priori four kinematic event variables including $\not\!\!E_T$ and leading lepton p_T are chosen to quantify possible deviations of the observed events from the Standard Model prediction. Using a shape comparison based on the Kolmogorov-Smirnov statistic, no significant discrepancy is found and the probability to observe a dataset less consistent with the Standard Model is determined to be 1.6%. Including systematic uncertainties, the p-value is 1.0-4.5%, where the lowest p-value is obtained from varying the background expectation down by one standard deviation. Beyond the Standard Model processes resulting in events with high $\not\!\!E_T$ and lepton p_T are not favoured by this dataset.

It is of course also of great interest to study the kinematic properties of the top quark itself and to compare this with the Standard Model expectation. In Run I, D0 performed such an analysis and found good agreement with the Standard Model [320, 321], which was then also confirmed by a dedicated study of the top quark p_T spectrum by CDF [322]. A corresponding analysis has not yet been published in Run II. However, a measurement of the differential $t\bar{t}$ production cross section $d\sigma/dM_{t\bar{t}}$ has been performed by CDF using 1.9 fb^{-1} of Run II data as described in Section 5.7.3, showing as well good agreement with the Standard Model [323].

5.5 Top Quark Pair Spin Correlations

Top quark pairs are expected to be produced essentially unpolarised in hadron collisions involving unpolarised incident particles. A small polarisation at the percent level is induced by QCD [324–326], which is perpendicular to the production plane since the strong interaction conserves parity. A measurement of this effect will be very difficult both at the Tevatron and the LHC which in return allows to use a corresponding analysis to probe for non Standard Model contributions in $t\bar{t}$ production [327]. An even smaller additional polarisation within the production plane arises from mixed strong and weak contributions to $t\bar{t}$ production at order $\alpha_s^2\alpha$ [328].

While in the framework of the Standard Model no observable spin polarisation in $t\bar{t}$ production is predicted, the spins of the top and the antitop quark are expected to be correlated [329]. This correlation depends both on the production mode of $t\bar{t}$ and the production energy. Close to the threshold, the top quark pair is produced in a $^3S_1$ state via $q\bar{q}$ annihilation and in a $^1S_0$ state via gluon-gluon fusion [330, 331]. Consequently, the top quark spins

are (anti-) parallel and the top quarks have opposite (same) helicities for $t\bar{t}$ production via $q\bar{q}$ annihilation (gluon-gluon fusion). Above the threshold, this simple picture becomes more complicated as orbital angular momentum effects then need to be taken into account. In the high energy limit where the top quark mass can be neglected finally, the conservation of chirality dictates that top and antitop quarks be produced with opposite helicities. Since at the Tevatron $t\bar{t}$ production via $q\bar{q}$ annihilation dominates as opposed to the LHC where the main contribution comes from gluon-gluon fusion, the observable correlation will have opposite signs at both colliders [332].

Due to the short lifetime of the top quark (see Section 3.3.2), its spin information is passed on to its decay products and reflected in the corresponding angular distributions. This gives experimental access to spin correlations, allowing one to test if the top quark can indeed be considered as a free quark. The resulting indirect limits on the top quark lifetime (for further measurements see Section 7.2) can provide limits for the CKM matrix element $|V_{tb}|$ free from the assumption of three quark families [333] together with the measurement of the top quark branching fractions described in Section 6.2. Furthermore, a measurement of the top quark spin correlations allows one to probe the dynamics of top quark production and decay for contributions beyond the Standard Model.

The down-type ($T_3 = -\frac{1}{2}$) decay products of the W boson from the top quark decay are most sensitive to the original top quark spin. Their angular distribution in the top quark rest frame is described by $1 + \cos\theta$, with θ being the angle between the line of flight of the down-type fermion and the top polarisation direction. The experimental difficulties of distinguishing between jets from up-type and down-type quarks (charm tagging would help only in 50% of the cases) can be avoided by focussing on the dilepton final state, where the charged leptons are clearly identified.

At the Tevatron, an optimal spin quantisation basis is given by the "off-diagonal" basis [334, 335] where the spins of top and antitop quarks produced by $q\bar{q}$ annihilation are fully aligned for all energies and only the contribution of top quark pairs produced via gluon-gluon fusion leads to a reduction of the correlation. The off-diagonal basis is defined via the top quark's velocity β^* and scattering angle θ^* with respect to the centre of mass frame of the incoming partons. The quantisation axis then forms an angle ψ with the proton-antiproton beam axis: $\tan\psi = \beta^{*2}\sin\theta^*\cos\theta^*/(1-\beta^{*2}\sin^2\theta^*)$. Consequently, in the limit of $\beta^* \to 0$ (top quark production at rest), the spins of top and antitop quarks point along the beam axis in the same direction. At very high energies, the spins are aligned with respect to the direction of the $t\bar{t}$ momenta.

Using as observables the angles θ_+ and θ_- of the down-type fermions with

respect to the quantisation axis in the rest frame of their respective parent (anti-) top quark, the spin correlation is given by [336]:

$$\frac{1}{\sigma}\frac{d^2\sigma}{d(\cos\theta_+)d(\cos\theta_-)} = \frac{1+\kappa\cdot\cos\theta_+\cdot\cos\theta_-}{4},$$

where correlation coefficient κ is predicted to be +0.88 at the Run I Tevatron when using the off-diagonal basis. Since the distribution is symmetric under exchange of the two angles, an electric charge measurement of the top decay products is not necessary.

D0 performed a first search for evidence of spin correlations in $t\bar{t}$ production in Run I, using a 0.1 fb^{-1} dilepton dataset yielding six candidate events [337]. From the dependence of a likelihood function on κ, at 68% C.L. a lower limit on κ of -0.25 is extracted. This is in agreement with the Standard Model expectation and disfavours anti-correlation of spins ($\kappa = -1$) that would arise from $t\bar{t}$ production via a scalar particle. While the obtained limit is rather weak, this is a proof of principle that the analysis can be performed. Unfortunately, there has been no result yet from Run II although it would greatly benefit from the increased datasets that are by now available.

5.6 Search for associated Higgs Boson Production

D0 performs a first search for associated $t\bar{t}$ and Standard Model Higgs boson production with a $t\bar{t}b\bar{b}$ final state in a 2.1 fb^{-1} b tagged lepton plus jet dataset [338]. While the observation of a significant signal in this channel is beyond the sensitivity available at the Tevatron, this analysis can still contribute to future combinations of the Tevatron searches for the Higgs boson at low Higgs boson masses as favoured by the Standard Model (see Section 7.3.4). The investigated events exhibit high jet and b tag multiplicity that were not studied separately before. It is thus interesting to search for deviations from the Standard Model predictions that could for example arise from anomalous top-Higgs couplings [339] or a new quark singlet of charge $\frac{2}{3}e$ [340].

The studied signal signature comprises the $t\bar{t}$ lepton plus jets characteristics with two additional b jets from the Higgs boson decay. The main background arises from $t\bar{t}$ with additional (heavy flavour) jet production, but also W boson plus jets and QCD multijet production contribute to the background. For signal discrimination, the shape of the H_T distribution of the selected jets is used in events with four or at least five jets and one, two or at least three b tags. The observed events in all these distributions are consistent with the background expectation, which is especially interesting

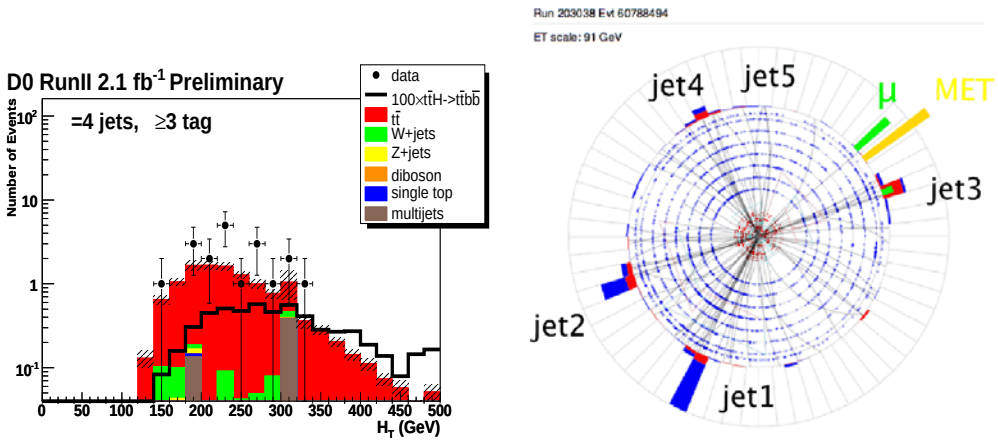

Figure 24: Left: H_T distribution observed in D0's 2.1 fb^{-1} lepton plus jets dataset with four jets and at least three b tags in comparison with expected Standard Model background processes and $t\bar{t}H$ signal scaled up by a factor of 100. Right: Event display (xy-view along the proton beam direction) for the triple b tagged event with highest H_T of 444 GeV. The first three jets are b tagged [338].

for the events with at least three b tags that were studied separately here for the first time. Figure 24 shows the observed H_T distribution for events with four jets and at least three b tags and an event display for the triple b tagged event with highest H_T.

Since no signal is observed, 95% C.L. limits on $t\bar{t}H$ production times $\mathcal{B}(H \to b\bar{b})$ in units of the Standard Model rate expectation are derived for Higgs boson masses between 105 and 155 GeV/c^2. For a Higgs boson mass of 115 GeV/c^2, the expected limit is 45 times the Standard Model production rate, with the observed limit a factor of 64 above the Standard Model expectation. Further optimisation of the preselection – currently corresponding to the standard $t\bar{t}$ selection – for the $t\bar{t}H$ signal and of the signal discrimination using more kinematic variables is under way.

5.7 Search for Top Quark Pair Production beyond the Standard Model

5.7.1 Search for a Narrow-Width Resonance decaying into $t\bar{t}$

The existence of yet undiscovered heavy resonances could be revealed through their decays into top quark pairs which would add a resonant production

mode to the Standard Model process. Various beyond the Standard Model theories predict the existence of a massive Z-like boson, for example Kaluza-Klein excitations of the gluon [341] or of the γ and Z bosons [342], extended gauge theories [343, 344], massive axigluons with axial vector couplings [345] or topcolour [346, 347].

The wealth of theoretical models demonstrates the importance of model-independent searches. One general way such an additional production mode can be observed – provided the resonance X decaying to $t\bar{t}$ is sufficiently heavy and narrow – is to analyse the $t\bar{t}$ invariant mass distribution for an excess over the Standard Model expectation. In the corresponding analyses performed at the Tevatron thus far no significant deviations from the Standard Model expectation have been observed, resulting in 95% C.L. upper limits on $\sigma_X \cdot \mathcal{B}(X \to t\bar{t})$ as a function of the resonance mass M_X.

These limits are used to set lower mass limits for a particular benchmark model, allowing easy comparison of the different results: The topcolour model [346, 347] provides a dynamic electroweak symmetry breaking mechanism via a top quark pair condensate [348] Z' formed by a new strong gauge force that couples preferentially to the third fermion generation. Particularly, a topcolour-assisted technicolour model [307, 312] predicts this Z' boson to couple strongly only to the first and third generation of quarks while exhibiting no significant coupling to leptons. This leptophobic and topophyllic Z' boson obtains a significant cross section $\sigma(p\bar{p} \to Z' \to t\bar{t})$ observable at the Tevatron for a variety of masses and widths and is used as a reference model.

CDF and D0 performed model-independent searches for narrow massive vector bosons decaying into $t\bar{t}$ already in Run I in lepton plus jets datasets of 106 pb^{-1} and 130 pb^{-1} respectively. Using the best kinematic fit to the $t\bar{t}$ hypothesis in each event, the $t\bar{t}$ invariant mass distribution is reconstructed and no excess is observed above the Standard Model expectation. The resulting upper limits on $\sigma_X \cdot \mathcal{B}(X \to t\bar{t})$ are turned into Z' 95% C.L. mass limits of $M_{Z'} > 480$ GeV/c^2 for CDF [349] and $M_{Z'} > 560$ GeV/c^2 for D0 [350]. For these results, a width of the Z' respectively X of 1.2% of its mass is assumed, well below the detector mass resolutions for $t\bar{t}$ systems. Consequently, the obtained results are dominated by the detector resolution and independent of any $\Gamma_{Z'}$ value below the mass resolution of a few percent ($\approx 0.04 M_{Z'}$ for D0 in Run I [351]). This resonance width is also used for the Run II measurements described below.

In Run II, both CDF and D0 perform the search for a generic heavy resonance X of narrow width ($\Gamma_X = 0.012 M_X$) compared to the detector mass resolution in b tagged lepton plus jets datasets. The $t\bar{t}$ invariant mass spectrum is reconstructed using either the best kinematic fit to the $t\bar{t}$ production hypothesis (CDF) or directly from the four-momenta of the up to four lead-

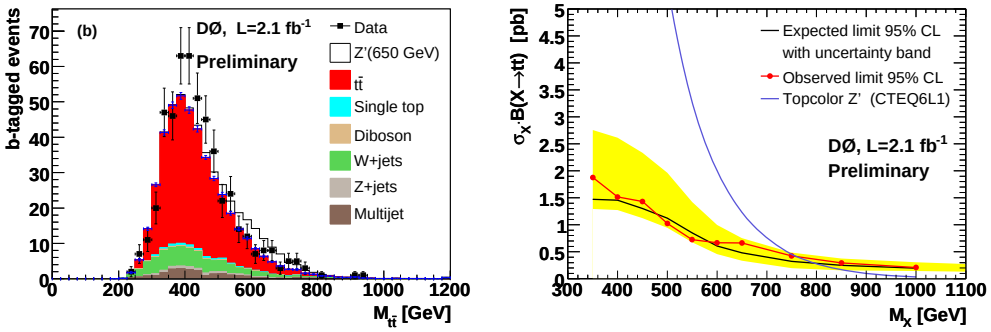

Figure 25: Left: Expected and observed $t\bar{t}$ invariant mass distribution in lepton plus jets events with four or more jets. Right: Expected and observed 95% C.L. upper limits on $\sigma_X \cdot \mathcal{B}(X \to t\bar{t})$ [352].

ing jets, the lepton and the neutrino momentum (D0). The latter approach was shown to provide better sensitivity for large resonance masses than the previously used constrained kinematic fit and also allows for the inclusion of data with fewer than four jets in case jets merged. As both experiments observe no significant deviation from the SM expectation, 95% C.L. upper limits on $\sigma_X \cdot \mathcal{B}(X \to t\bar{t})$ are given for values of M_X between 450 and 900 GeV/c^2 (CDF) respectively 350 and 1000 GeV/c^2 (D0, see Figure 25) in increments of 50 GeV/c^2.

Both experiments provide 95% C.L. mass limits for the leptophobic top-colour-assisted technicolour Z' boson as a benchmark model. With 1 fb^{-1}, CDF finds $M_{Z'} > 720$ GeV/c^2 (expected limit: 710 GeV/c^2) [353] while D0 finds $M_{Z'} > 760$ GeV/c^2 (expected limit: 795 GeV/c^2) [352] using 2.1 fb^{-1} of data, superseding a previously published result on 0.9 fb^{-1} of data [354]. CDF also obtained a result on a subset of 0.7 fb^{-1} of the data analysed above, using an untagged lepton plus jets sample where b tag information only contributes to reduce jet combinatorics in a Standard Model $t\bar{t}$ matrix element based reconstruction of $M_{t\bar{t}}$, yielding a slightly better limit than the analysis on 1 fb^{-1} of $M_{Z'} > 725$ GeV/c^2 [355].

For future studies, it would be interesting to see how sensitive the observed limits are to the assumption of Z boson-like couplings used in the analyses. The limits obtained apply to resonances of narrow width only. Wider resonances could be detected by studying the $t\bar{t}$ differential cross section (see Section 5.7.3) or the forward-backward charge asymmetry in $t\bar{t}$ production (see Section 5.3).

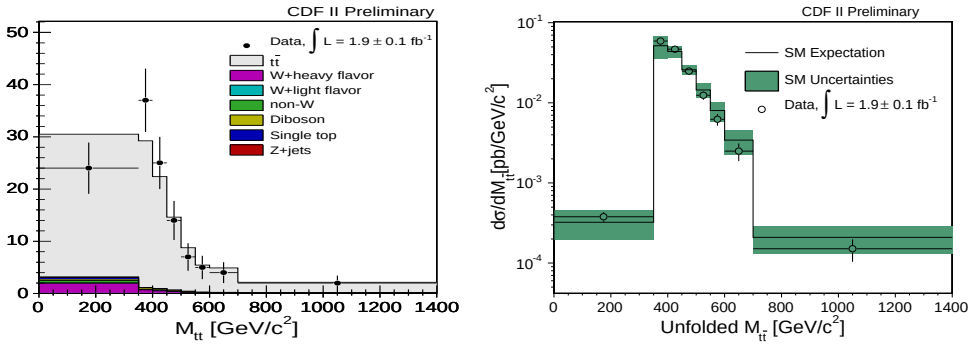

Figure 26: Left: Expected and observed reconstructed $t\bar{t}$ invariant mass distribution in lepton plus jets events with at least four jets. Right: Corresponding observed $t\bar{t}$ differential cross section, compared to the Standard Model expectation [323].

5.7.2 Search for $t\bar{t}$ Production via a Massive Gluon

Instead of a new colour singlet particle decaying into $t\bar{t}$ as described in the previous subsection, there could also be a new massive colour octet particle G contributing to $t\bar{t}$ production [346]. Such a "massive gluon" production mode would interfere with the corresponding Standard Model production process.

Assuming a Standard Model top decay, CDF has performed a search for a corresponding contribution by comparing the $t\bar{t}$ invariant mass distribution in a 1.9 fb^{-1} b tagged lepton plus jets dataset with the Standard Model expectation. As the largest discrepancy with respect to the Standard Model observed is 1.7σ for the explored mass and width range 400 GeV/c^2 $\leq M_G \leq$ 800 GeV/c^2, $0.05 \leq \Gamma_G/M_G \leq 0.5$, 95% C.L. upper and lower limits are provided on the corresponding coupling strengths of the massive gluon [356].

5.7.3 Measurement of the $t\bar{t}$ Differential Cross Section $d\sigma/dM_{t\bar{t}}$

Since new production mechanisms for top quark pairs could manifest themselves in the $t\bar{t}$ invariant mass distribution as resonances of various widths or also more general shape distortions [357], one very general approach of detecting such contributions is to compare the shape of the observed differential $t\bar{t}$ production cross section $d\sigma/dM_{t\bar{t}}$ with the Standard Model expectation.

CDF reconstructs the $t\bar{t}$ invariant mass spectrum in a 1.9 fb^{-1} b tagged lepton plus jets dataset (see Figure 26) by combining the four-vectors of the four leading jets, lepton and missing transverse energy. After subtracting the

background processes, the distortions in the reconstructed distribution due to detector effects, object resolutions and geometric respectively kinematic acceptance are corrected for by the application of a regularised unfolding technique. From the unfolded distribution, the $t\bar{t}$ differential cross section $d\sigma/dM_{t\bar{t}}$ is extracted and its shape is compared with the Standard Model expectation. The shape comparison gives good agreement with the Standard Model, yielding an Anderson-Darling p-value of 0.45 [323].

5.7.4 Search for new heavy Top-like Quark Pair Production

The number of light neutrino species ($m_\nu < m_Z/2$) has been determined to be three ($N_\nu = 2.9840 \pm 0.0082$) from the invisible Z boson decay width in electroweak precision measurements [68]. This rules out a fourth generation of fermions with a light neutrino ν_4. However, the existence of a fourth generation is consistent with electroweak precision data for a fermion mass range $m_Z/2 \lesssim m_{f4} \lesssim \mathcal{O}(\langle H \rangle)$ even without introducing new physics [358, 359]. Fourth generation quark masses up to 400 GeV/c^2 are compatible with current measurements and are constrained to exhibit a small mass splitting such that decays of an up-type fourth generation quark into Wq ($q = d, s, b$) are preferred [360]. Such an additional generation would imply drastic effects for the phenomenology of the Higgs boson, relaxing the mass bounds obtained in the Standard Model framework up to 750 GeV/c^2 at 95% C.L. and altering expected kinematics and production rates.

The existence of a fourth chiral fermion generation is predicted by various extensions of the Standard Model, for example in an SO(1,13) framework unifying charges and spins [361] or in models of flavour democracy [362, 363]. Other models adding more exotic additional heavy quarks that could decay via Wq have been brought up as well [364]. For example, the beautiful mirrors model [365] introduces mirror quark doublets with the same quantum numbers as their Standard Model counterparts but with vector couplings to the W boson. This addition helps to improve the fit of electroweak observables by removing the observed discrepancy in the forward-backward asymmetry of the b quark.

CDF performs a search for pair production of heavy top-like quarks ($t'\bar{t}'$) which don't necessarily have to exhibit Standard Model-like up-type fourth generation properties in terms of charge or spin. The analysis is based on the assumptions that the t' is pair-produced via the strong interaction, has a mass larger than that of the top quark and decays promptly into a W boson and a down-type quark d, s, b with 100% branching ratio. As a consequence, the t' decay chain is identical to that of the top quark, and $t'\bar{t}'$ production can be searched for in a lepton plus jets sample selected solely based on event

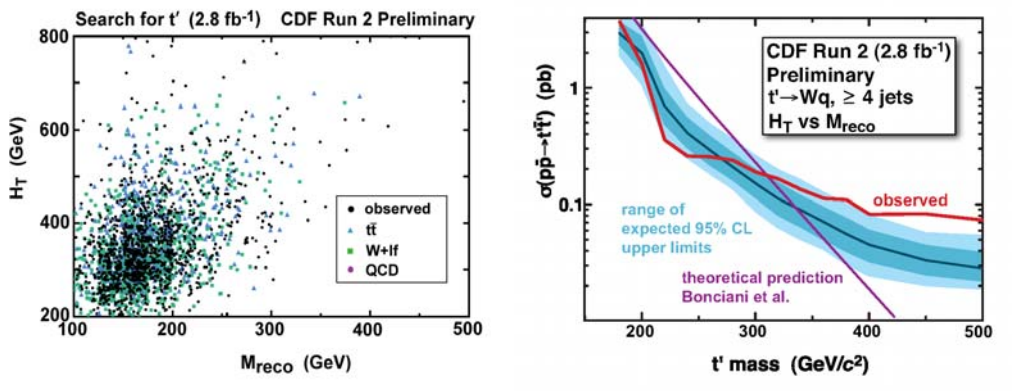

Figure 27: Left: H_T versus $M_{\rm reco}$ distribution observed in data (black points) overlaid with the fitted number of Standard Model background events from $t\bar{t}$ (blue), W+jets (green) and QCD (purple). Right: Expected and observed 95% C.L. upper limits on the $t'\bar{t}'$ production cross section, assuming 100% $\mathcal{B}(t' \to Wq)$. The dark/light blue bands represent the 1/2 σ areas around the expected limit [366].

kinematics to not restrict the search to Wb final states by using b tagging.

The t' signal can be distinguished from the Standard Model background processes using the observed distributions of total transverse energy H_T in the event based on lepton, jets and $\not\!\!E_T$ and the reconstructed t' mass $M_{\rm reco}$ based on the best kinematic fit to the $t'\bar{t}'$ hypothesis in each event (see Figure 27). Superseding a previously published result based on on 0.8 fb^{-1} [367], CDF uses a two-dimensional binned likelihood fit in H_T and $M_{\rm reco}$ to separate Standard Model background and t' signal in a 2.8 fb^{-1} dataset [366].

Since no evidence for t' production is found, 95% C.L. upper limits on the t' pair production cross section (assuming $\mathcal{B}(t' \to Wq) = 100\%$) are derived for 180 GeV/c^2 $\leq m_{t'} \leq$ 500 GeV/c^2. Assuming Standard Model couplings, a 95% C.L. lower limit on the fourth-generation t' mass of 311 GeV/c^2 based on the calculations [117, 118] is obtained, where the systematic uncertainty with the largest impact on the derived limit is the jet energy scale. The found deviation of the observed limit from the expected for t' masses above $\approx$400 GeV/c^2 is investigated. Using a priori defined groups of bins in H_T and $M_{\rm reco}$, the p-values to observe at least the number of events found in data given the Standard Model expectation are evaluated. With the smallest p-value found of 0.01, the excess in the data tails is concluded to be not statistically significant.

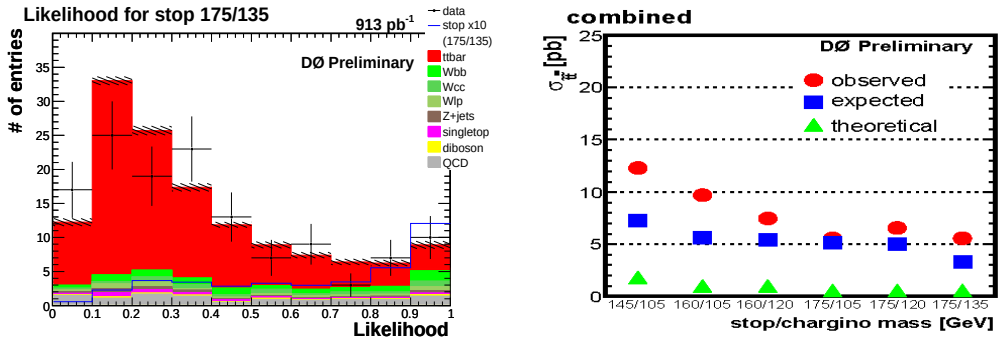

Figure 28: Left: Multivariate kinematic discriminant distribution in electron plus at least four jets events in 0.9 fb^{-1} of D0 data and simulated signal and background. The solid blue line shows the signal shape for $\tilde{t}_1/\tilde{\chi}_1^{\pm}$ masses of 175/135 GeV/c^2, enhanced by a factor of ten. Right: Expected and observed 95% C.L. limits on the $\tilde{t}_1\bar{\tilde{t}}_1$ production cross section together with the theoretical prediction for different stop and chargino mass combinations [375].

5.7.5 Search for Scalar Top Production

Many beyond the Standard Model processes exhibit a similar signature in the final state to top quark events. Consequently, the selected top quark samples could contain an admixture of such exotic processes.

For example, the Minimal Supersymmetric Standard Model (MSSM) [368] predicts the supersymmetric partners of the top quarks, scalar top or short "stop" quarks, to be predominantly produced in pairs via the strong interaction like the Standard Model top quarks. The stop quark pair production cross section has been evaluated at NLO supersymmetric QCD and depends mainly on the stop quark mass and very little on other supersymmetric parameters [369]. At a centre of mass energy of 1.96 TeV, the pair production cross section for the lightest stop quarks ($\tilde{t}_1\bar{\tilde{t}}_1$) of 175 GeV/c^2 mass is 0.58 pb [370], roughly 10% of the Standard Model top pair production rate (see Section 3.1). The observable final states from stop decays depend strongly on the chosen supersymmetric parameters, especially on the masses of the supersymmetric particles in the decay chain. In Run II, the decay mode $\tilde{t}_1 \to b\ell^+\tilde{\nu}_\ell$ has been studied by D0 [371] in 0.4 fb^{-1} of data. The decay channel $\tilde{t}_1 \to c\tilde{\chi}_1^0$ where the lightest neutralino $\tilde{\chi}_1^0$ is the lightest supersymmetric particle (LSP) was studied by CDF [372] on 0.3 fb^{-1} and by D0 [373, 374] on 0.4 respectively 1 fb^{-1} of data. 95% C.L. mass exclusion limits on the involved supersymmetric particles were provided in both decay channels.

Another possible important decay mode is $\tilde{t}_1 \to \tilde{\chi}_1^+ b$, where the lightest

chargino $\tilde{\chi}_1^+$ decays to $W^+\tilde{\chi}_1^0$, resulting in final states identical to those from $t\bar{t}$ decays with the addition of two neutralinos (LSPs) which are contributing to $\not\!\!E_T$. First limits for this channel have been provided by CDF in Run I on 0.1 fb^{-1} of lepton plus jets data [376].

D0 performs the first study of this channel in Run II on 0.9 fb^{-1} b tagged lepton plus jets data [375], setting the neutralino mass to 50 GeV/c^2 – slightly above the limit by LEP [377] – while varying the stop and chargino masses between 145 and 175 GeV/c^2 respectively 105 and 135 GeV/c^2.

A possible stop admixture in the sample is searched for by employing a multivariate discriminant based on kinematic event properties (see Figure 28), with the main challenge to separate the topologically very similar $t\bar{t}$ background and $\tilde{t}_1\bar{\tilde{t}}_1$ signal. Counterintuitively, the neutralinos do not result in large differences in $\not\!\!E_T$ that could be exploited, but the larger chargino mass compared to that of the W boson for example results in reduced phase space for the b jets in the event.

Since no significant signal admixture in the lepton plus jets dataset is found, 95% C.L. upper limits on the $\tilde{t}_1\bar{\tilde{t}}_1$ production rate are provided which are a factor of $\approx 7-12$ above the theoretical prediction as illustrated in Figure 28. Consequently, the stop quark masses considered cannot yet be excluded, and this analysis will greatly benefit from the increased datasets already at hand. The weaker observed compared to the expected limits are driven by the muon plus jets channel. The corresponding excess in data was tested with pseudo-datasets to be statistically consistent with the Standard Model expectation.

CDF searches for a stop admixture in the $t\bar{t}$ dilepton channel using a 2.7 fb^{-1} dilepton dataset of both b tagged and untagged events [378]. Assuming $\tilde{\chi}_1^0$ to be the LSP, heavy sfermions, the stop mass below the top mass and the chargino mass smaller than the mass difference of stop and b quark, the decay $\tilde{t}_1 \to \tilde{\chi}_1^+ b$ obtains a 100% branching fraction. The dilepton final state resulting from $\tilde{\chi}_1^\pm \to \tilde{\chi}_1^0 \ell^\pm \nu$ decays is then identical to the $t\bar{t}$ final state with two additional neutralinos contributing to $\not\!\!E_T$. It can be reached through a variety of chargino decay channels, resulting in variations of the branching fraction depending on SUSY parameters.

The stop quark signal is discriminated from the Standard Model background processes using a single quantity, the reconstructed stop mass, in a fit to the observed data distribution. The mass is reconstructed from this underconstrained system by treating neutralino and neutrino from each stop decay as one massive pseudo-particle and then applying a standard top mass reconstruction technique in the dilepton channel, neutrino weighting (see Section 7.3.1). Since the observed distributions are consistent with the

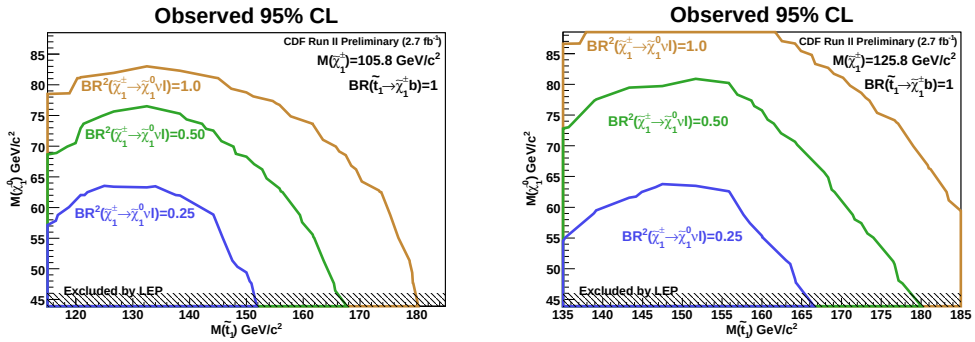

Figure 29: Excluded areas observed at 95% C.L. in the neutralino versus stop mass plane for various assumed dilepton branching fractions and two different chargino masses (left: 105.8 GeV/c^2, right: 125.8 GeV/c^2), obtained by CDF in 2.7 fb^{-1} of dilepton data. The contributions of e, μ, τ to the final state are assumed to be equal [378].

Standard Model background processes, 95% C.L. limits are derived on the dilepton branching ratio in $\tilde{t}_1\tilde{t}_1$ production for stop masses between 115 and 185 GeV/c^2, neutralino masses between 43.9 and 88.5 GeV/c^2 and chargino masses between 105.8 and 125.8 GeV/c^2, as illustrated in Figure 29. A branching fraction of 100% for $\tilde{t}_1 \to \tilde{\chi}_1^+ b$ and equal contributions from e, μ, τ to the final state are assumed throughout.

Model-independent searches for exotic admixtures in top quark samples via the search for anomalous event kinematics are discussed in Section 5.4.

5.8 Single Top Quark Production

The electroweak production of top quarks without their anti-particles allows one to directly measure the $|V_{tb}|$ CKM matrix element, to test the Wtb vertex structure and to probe for physics beyond the Standard Model like flavour changing neutral currents or new heavy gauge bosons W' (see Section 3.2). A thorough understanding of single top quark production is also instrumental for the study of processes with a similar signature, like Standard Model W-Higgs production for which this process is a background. While the single top production rate is $\mathcal{O}(40\%)$ of the strong $t\bar{t}$ production, the signal extraction from background processes is very challenging due to only one top quark signature present in the final state. Simple kinematic selections are insufficient for such an analysis, and sophisticated multivariate techniques have to be deployed.

For single top quark production at the Tevatron, only s- and t-channel

production are relevant, contributing with $0.88^{+0.12}_{-0.11}$ pb respectively $1.98^{+0.28}_{-0.22}$ pb to the total rate at NLO [157]. The experimental signature comprises a b jet and the W boson decay products from the top quark decay. In the s- (tb-) channel, one additional b jet arises from the b quark produced together with the top quark. In the t- (tqb-) channel, a forward light-quark jet arises from the top quark production, sometimes accompanied by another b jet from the gluon splitting into $b\bar{b}$ (see Figure 8). In order to suppress multijet background, the W boson is usually required to decay leptonically into an electron or muon and corresponding neutrino. Consequently, the final state signature of single top quark production contains an energetic isolated electron or muon, $\not\!\!E_T$ and two or three jets with at least one of them being a b jet. Additional jets can arise from initial- or final-state radiation.

5.8.1 Production Cross Section and V_{tb}

Searches for single top quark production were already performed in Run I using 0.1 fb^{-1} of data, first by D0 [379, 380] and then by CDF [381, 382], yielding upper limits on the production rate at least a factor of six larger than the Standard Model expectation. In Run II, first results were published using 0.2 fb^{-1} of data by CDF [383] and D0 [384, 385], where the best observed limit was less than a factor of three above the Standard Model prediction. Finally, D0 published first evidence for single top quark production using 0.9 fb^{-1} of data [13, 14], observing a signal of 3.6 standard deviations significance. Preliminary results by CDF based on 2.2 fb^{-1} then confirmed evidence for single top quark production [386–389] with an observed signal significance of 3.7 standard deviations resulting from the combination of three of these analyses [390].

The analyses yielding first evidence for electroweak top quark production apply event selections requiring one energetic isolated electron or muon and $\not\!\!E_T$. CDF uses events with two or three jets and one or two b tags, while D0 includes additionally events with four jets where the extra jet arises from initial- or final-state radiation. The signal acceptances for the s- and t-channel are 2.8% and 1.8% (CDF) respectively 3.2% and 2.1% (D0), and the expected and observed event yields are shown in Table 14. The dominant background contributions come from W+jets production, $t\bar{t}$ production in the lepton plus jets or dilepton final state where one jet or lepton is not reconstructed and from multijet production. The main sources of systematic uncertainty are background normalisation, jet energy scale and modelling of the b tagging and triggers used. As can be appreciated from the table, the uncertainty on the background is larger than the expected signal which makes advanced analysis techniques necessary.

Source	2 jets	3 jets	4 jets
tb	16±3	8±2	2±1
tqb	20±4	12±3	4±1
$t\bar{t}$	59±10	135±26	154±33
$Wb\bar{b}$	261±55	120±24	35±7
$Wc\bar{c}$,Wcj	151±31	85±17	23±5
Wjj	119±25	43±9	12±2
Multijets	95±19	77±15	29±6
BG Sum	686±41	460±39	253±38
Data	697	455	246

Source	2 jets	3 jets
tb	41.2±5.9	13.5±1.9
tqb	62.1±9.1	18.3±2.7
$t\bar{t}$	146.0±20.9	338.7±48.2
$Wb\bar{b}$	461.6±139.7	141.1±42.6
$Wc\bar{c}$,Wcj	395.0±121.8	108.8±33.5
Wjj	339.8±56.1	101.8±16.9
Multijets	59.5±23.8	21.3±8.5
Dibosons	63.2±6.3	21.5±2.2
Z+jets	26.7±3.9	11.0±1.6
BG Sum	1491.8±268.6	754.8±91.3
Data	1535	712

Table 14: Expected and observed event yields of the single top selections for e and μ, single and double b tagged channels combined – left for D0 based on 0.9 fb^{-1} [14], right for CDF based on 2.2 fb^{-1} [387]. For the D0 result, the overall W plus jets background includes Z plus jets and diboson events.

D0 applies three different multivariate analysis techniques to the preselected data sample: boosted decision trees (BDT), Bayesian neural networks (BNN) and matrix elements (ME), where the latter two were reoptimised for publication [13] compared to [14]. The ME analysis does not use four-jet events, being based on leading-order matrix elements for the description of signal and background processes. For each analysis, the combined s- and t-channel cross sections are extracted from the peak of the Bayesian posterior probability density derived from a binned likelihood of the respective discriminants. The results are then combined, yielding:

$$\begin{aligned}
\sigma^{\rm obs}(p\bar{p} \to tb + X,\ tqb + X) &= 4.9^{+1.4}_{-1.4}\ \text{pb} \quad (\text{BDT}, \quad 3.4\sigma) \\
&= 4.4^{+1.6}_{-1.4}\ \text{pb} \quad (\text{BNN}, \quad 3.1\sigma) \\
&= 4.8^{+1.6}_{-1.4}\ \text{pb} \quad (\text{ME}, \quad 3.2\sigma) \\
&= 4.7^{+1.3}_{-1.3}\ \text{pb} \quad (\text{Combined}, 3.6\sigma),
\end{aligned}$$

where the uncertainties correspond to the combination of statistical and systematic sources. The observed production rates are in agreement with the Standard Model expectation and each other. The significances are obtained from large ensembles of pseudo-experiments. The expected sensitivity of the combined result is 2.3 standard deviations, indicating that the measurement benefited from a statistical upward fluctuation. A separate measurement of the s- and t-channel cross sections is performed as well with the BDT analysis, obtaining $\sigma_s = 1.0 \pm 0.9$ pb and $\sigma_t = 4.2^{+1.8}_{-1.4}$ pb when fixing the channel not measured to its Standard Model expectation respectively. The observed

enhancement in the t-channel with respect to the Standard Model prediction is not statistically significant.

CDF uses the following multivariate analysis techniques on their preselected dataset: neural networks (NN [389]), a likelihood function (LHF [388]), a matrix element discriminant (ME [387]) and boosted decision trees (BDT [386]). The results obtained are:

$$\begin{aligned}
\sigma^{\rm obs}(p\bar{p} \to tb + X,\ tqb + X) &= 2.0^{+0.9}_{-0.8}\ \text{pb} \quad (\text{NN}, \qquad 3.2\sigma) \\
&= 1.8^{+0.9}_{-0.8}\ \text{pb} \quad (\text{LHF}, \qquad 2.0\sigma) \\
&= 2.2^{+0.8}_{-0.7}\ \text{pb} \quad (\text{ME}, \qquad 3.4\sigma) \\
&= 2.2^{+0.7}_{-0.7}\ \text{pb} \quad (\text{Combined}, 3.7\sigma) \\
&= 1.9^{+0.8}_{-0.7}\ \text{pb} \quad (\text{BDT}, \qquad 2.8\sigma),
\end{aligned}$$

where the uncertainties given are both statistical and systematic. The BDT analysis became available after the combination [390] was performed and hence is not included there. The observed results agree with each other and the Standard Model expectation. The expected sensitivity of the combination is 5.1 standard deviations, pointing to a statistical downward fluctuation of the measurement.

Figure 30 shows the discriminant outputs of the two most significant single measurements from CDF (ME) and D0 (BDT). A graphical summary of the discussed measurements in comparison to the Standard Model expectation is given in Figure 31. All analyses assume a top quark mass of 175 GeV/c^2, $\mathcal{B}(t \to Wb) = 100\%$ and the Standard Model ratio of s- and t-channel cross sections.

In a recent update, CDF has added 0.5 fb^{-1} of data to the single top analyses, resulting in an increased observed significance for all analysis techniques applied. The matrix element analysis yields again the most significant single result, exceeding four standard deviations. A combination of the measurements has not yet become available. The 2.7 fb^{-1} results with combined statistical and systematic uncertainties are:

$$\begin{aligned}
\sigma^{\rm obs}(p\bar{p} \to tb + X,\ tqb + X) &= 2.1^{+0.7}_{-0.6}\ \text{pb} \quad (\text{NN}, \ 3.7\sigma) \quad [391] \\
&= 2.0^{+0.9}_{-0.8}\ \text{pb} \quad (\text{LHF}, \ 2.6\sigma) \quad [392] \\
&= 2.7^{+0.8}_{-0.7}\ \text{pb} \quad (\text{ME}, \ 4.2\sigma) \quad [393] \\
&= 2.4^{+0.8}_{-0.7}\ \text{pb} \quad (\text{BDT}, 3.6\sigma) \quad [394].
\end{aligned}$$

Since the single top quark production rate is proportional to $|V_{tb}|^2$, the cross section measurement can be turned into a measurement of $|V_{tb}|$ under the following assumptions: There are no single top quark production modes beyond the Standard Model, single top quark production and decay are dominated by the Wtb interaction ($|V_{tb}| \gg |V_{td}|, |V_{ts}|$ as indicated by

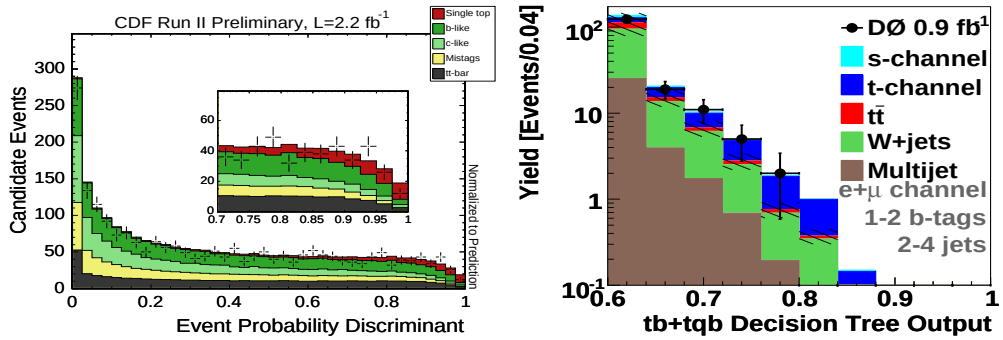

Figure 30: Multivariate discriminant outputs observed in single top candidate events compared to contributions from signal and background processes. Left: CDF matrix element discriminant with yields normalised to the Standard Model prediction [387]. Right: D0 boosted decision tree output in the signal region with the signal normalised to the measured cross section [14].

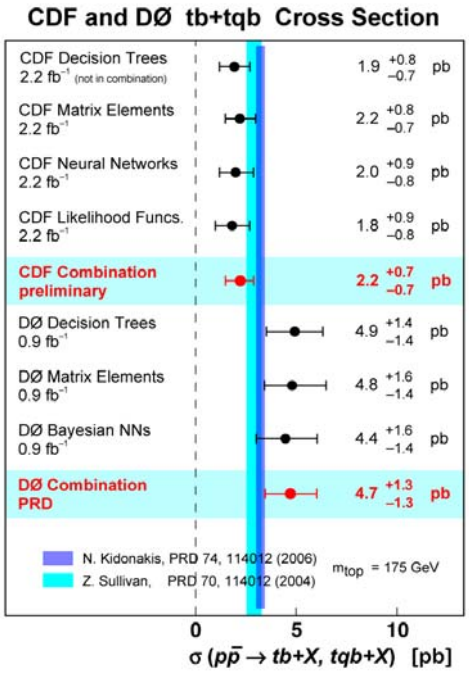

Figure 31: Cross section measurements yielding first evidence for single top production and their combinations obtained by CDF and D0 in comparison to the Standard Model prediction.

measurements of R described in Section 6.2) and the Wtb interaction exhibits a $V-A$ structure and is CP conserving. The latter premise allows for anomalous left-handed vector couplings f_1^L (see Section 3.3.3) but not for right-handed vector or tensor couplings. Anomalous f_1^L values ($\neq 1$) do not affect $t\bar{t}$ production rate and kinematics or tb respectively tqb kinematics but simply rescale the single top production rate. Consequently, $|V_{tb}f_1^L|$ extracted from the single top production cross section can be > 1, and restricting the measurement to $[0,1]$ implies $f_1^L = 1$ as predicted by the Standard Model. The measurement of $|V_{tb}f_1^L|$ respectively $|V_{tb}|$ is independent from the number of fermion generations and CKM matrix unitarity.

Using the result of the boosted decision tree analysis and a positive flat prior for $|V_{tb}|^2$, D0 obtains $|V_{tb}f_1^L| = 1.31^{+0.25}_{-0.21}$. Restricting the prior to $[0,1]$ yields $|V_{tb}| = 1.00^{+0.00}_{-0.12}$, with a corresponding 95% C.L. lower limit of $|V_{tb}| > 0.68$ [13]. CDF uses its combined measurement in the same way to obtain a 95% C.L. lower limit of $|V_{tb}| > 0.66$ [390]. The 2.7 fb^{-1} matrix element analysis yields $|V_{tb}| > 0.71$ [393].

With most of the current measurements giving evidence above three sigma for single top quark production, the observation at the five standard deviation level seems imminent at the Run II Tevatron. Extrapolating from the 2.2 fb^{-1} result as illustrated in Figure 32, CDF estimates that the five sigma significance should be reached by adding one more fb^{-1} of data to the analyses. D0 could reach the observation level already in the two fb^{-1} dataset that is currently being analysed.

As discussed in Section 3.2, s- and t-channel production exhibit different sensitivity to physics beyond the Standard Model. Measuring both rates separately then provides a valuable tool to test for various exotic model contributions in single top quark production. Figure 32 shows D0's expected sensitivity to physics beyond the Standard Model [165] with the already analysed data and with the accumulation of 6.8 fb^{-1} of Run II data. With such increased integrated luminosity, the exclusion of some exotic models at 95% C.L. should be feasible. With more than 6 fb^{-1} a measurement of $|V_{tb}|$ with an absolute uncertainty below 0.07 per experiment should be achievable as well. In addition, further refinements of the analysis techniques should facilitate improvements in precision beyond what can be expected from the accumulation of more data alone.

5.8.2 Top Quark Spin Polarisation

As opposed to top quark pair production via the strong interaction where the top quarks are produced essentially unpolarised (see Section 5.5), top quarks produced singly via the electroweak interaction are expected to be highly

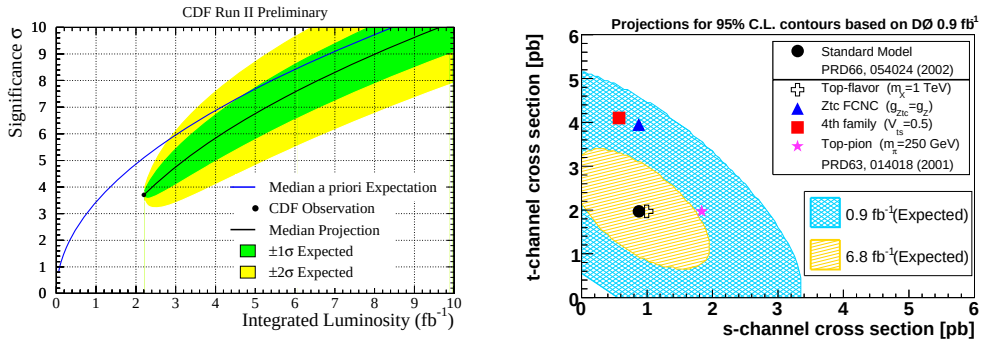

Figure 32: Left: Extrapolation of the single top signal significance versus integrated luminosity from the 2.2 fb^{-1} CDF analysis result. Right: Expected 95% C.L. contours for a simultaneous measurement of the s- and t-channel single top production rate by D0 for different integrated luminosities. The Standard Model expectation is shown together with various exotic models.

left-handedly polarised [164]. The polarisation of the top quark is reflected in the kinematic distributions of its decay products, allowing to test the $V-A$ structure of the Wtb coupling [139, 395]. An observation of this polarisation would also allow one to set limits on the top quark decay width and $|V_{tb}|$ since it would experimentally confirm that the top quark decays before it can be depolarised by QCD interactions.

Both relevant single top quark production mechanisms at the Tevatron (s- and t-channel) exhibit up-type–down-type and tb quark lines interconnected by a W boson. Since the W boson couples solely to fermions of left-handed chirality, in their rest frame single top quarks are highly polarised in the direction of the down-type quark [163, 396, 397][2]. The optimal spin basis for studying the single top spin polarisation thus will use the direction of the down-type quark.

For the s-channel production predominantly proceeding via $u\bar{d} \to t\bar{b}$ one expects the antiproton beam to provide the down-type quark most of the time. Indeed, measuring the top quark spin along the direction of the antiproton beam ("antiproton basis") results in 98% of the top quark spins aligned in that direction. For the t-channel the situation is slightly more complicated, since the down-type quark is contained in either the spectator jet or in one of the beams. With the largest contribution to the total pro-

[2] For the contributing $2 \to 2$ processes this polarisation is 100%. These diagrams are related to the top decay with hadronic W boson decay via crossing symmetry, where the down-type decay products of the W boson exhibit optimal analysing power.

duction rate coming from $ug \to t\bar{b}d$ where the down-type quark yields the (light quark) spectator jet, a reasonable choice for the spin basis is the spectator jet direction ("spectator basis"). Since the spectator jet is produced in forward direction this basis is also still compatible with the cases where the down-type quark is in the initial state, resulting in 96% of the top quarks having their spins polarised along the light quark jet direction.

With the top quark decaying before it hadronises, its spin information is passed on to its decay products. A straightforward observable is the angular distribution of the top quark decay product i in the top quark rest-frame:

$$\frac{1}{\Gamma}\,\frac{d\,\Gamma}{d\,\cos\theta_i^t} = \frac{1}{2}\Big(1 + \mathcal{A}_{\uparrow\downarrow}\alpha_i \cos\theta_i^t\Big),$$

where θ_i^t is the angle between decay product and spin quantisation axis, α_i is the analysing power describing the correlation between top quark spin and decay product and $\mathcal{A}_{\uparrow\downarrow} = N_\uparrow - N_\downarrow / N_\uparrow + N_\downarrow$ is the spin asymmetry determining the size of the observable angular correlations. The analysing power is maximal (+1) for the down-type ($T_3 = -\frac{1}{2}$) decay products of the W boson (charged lepton, d- or s-quark), making the charged lepton the most sensitive and easily accessible spin analyser. Using the spin quantisation axes described above, the spin asymmetry is 0.96 for the s-channel and 0.93 for the t-channel [163, 396, 397].

To perform a spin polarisation measurement at the Tevatron, single top quark production in the t-channel is most promising due to its higher rate compared to the s-channel. The required integrated luminosity to observe spin polarisation in the t-channel at the Tevatron was determined in a study, including effects of jet resolution and acceptance [162]. To establish the polarisation at the five standard deviations level, approximately 5 fb^{-1} of data will be needed, which should be available very soon.

At the LHC, measurements of single top spin polarisation will benefit from the high statistics single top datasets, and optimal spin bases have already been explored for the two dominant production modes (t-channel [161], associated tW production [398]). Already with the first 2 fb^{-1}, a polarisation measurement with an uncertainty of 4% should be achievable based on the t-channel production alone [399].

5.8.3 Search for W′ bosons

Electrically charged gauge bosons that are not part of the Standard Model are usually denoted as W'. Such bosons are predicted in a variety of extensions of the Standard Model incorporating larger gauge groups that can be reduced to the Standard Model group for sufficiently low energies [165, 400].

The most stringent limit to date in a direct search on the mass of such a W' boson has been set by D0 in the leptonic final state ($W' \to \ell\nu$) using 1 fb^{-1} of Run II data. Under the assumption the W' boson exhibits Standard Model W boson couplings to fermions, this search excludes the mass range below 1 TeV/c^2 at 95% C.L. by studying the tail of the transverse mass spectrum calculated from lepton transverse energy and $\not\!\!E_T$ [401]. Indirect W' mass constraints are strongly model-dependent and vary greatly between lower limits of 549 GeV/c^2 and 23 TeV/c^2, being derived from (semi-) leptonic processes as well as from astrophysical and cosmological constraints [41].

A direct search for W' bosons in the hadronic final state ($W' \to q\bar{q}'$) allows for a less model-dependent measurement since both left-handed and right-handed W' bosons can be observed in this final state, independent of any assumption on the mass of a right-handed neutrino m_{ν_R} in the latter case. In contrast to this, the leptonic final state is only accessible for a right-handed W' boson if the corresponding right-handed neutrino is not too massive ($m_{\nu_R} < m_{W'}$). Searches for W' bosons as a resonant structure in the dijet invariant mass spectrum have been carried out by UA2 [402] and at the Run I Tevatron by CDF [403] and D0 [404].

Focussing on hadronic W' searches using third generation quarks in the final state reduces the QCD background compared to the (light) dijet final state searches. Such measurements are only sensitive to W' bosons with masses above the tb threshold of $\approx$ 200 GeV/c^2, but the low mass range is excluded already by the current limits on single top quark production [405]. A W' signal would be visible as peak in the invariant mass distribution of its tb decay products (tb includes both $t\bar{b}$ and $\bar{t}b$ final states).

Since the $W' \to tb$ decay mode contributes to s-channel single top production (see Section 3.2), these searches are based on the single top production cross section analyses (see Section 5.8.1). For left-handed W' bosons interference occurs with Standard Model single top production, which is not the case for right-handed W' bosons due to the different (right-handed) final state particles. Considering a right-handed W' boson, the decay width depends on the mass of the right-handed neutrino involved in leptonic decays. If $m_{\nu_R} > m_{W'}$, only $q\bar{q}'$ final states are accessible, resulting in a width reduced by about 25%. Such a scenario generally results in a more stringent mass limit due to the enhanced tb branching fraction. A contribution of the W' boson to the top quark decay is usually not considered due to its large mass.

A first search for $W' \to tb$ was performed by CDF in Run I based on 0.1 fb^{-1} of lepton plus jets data. At 95% C.L. lower limits on the mass of a right-handed W' boson are obtained, yielding 536 GeV/c^2 for $m_{\nu_R} \ll m_{W'}$ and 566 GeV/c^2 for $m_{\nu_R} > m_{W'}$ [406].

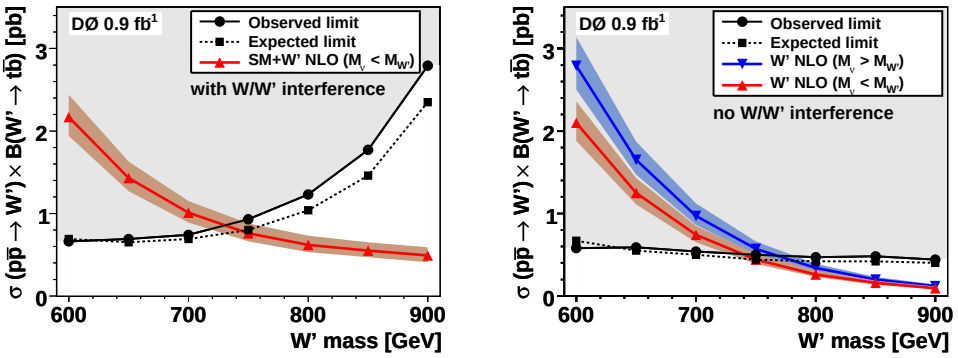

Figure 33: Theoretical prediction at NLO and 95% C.L. limits for $\sigma(p\bar{p} \to W') \times \mathcal{B}(W' \to tb)$ versus mass of the W' boson. Left: Left-handed W' boson. Right: Right-handed W' boson [407].

D0 published a first search for $W' \to tb$ in Run II based on 0.2 fb^{-1} of lepton plus jets data and the corresponding single top cross section result [385]. For a right-handed W' boson with CKM mixing equal to the Standard Model, 95% C.L. lower mass limits of 630 GeV/c^2 (670 GeV/c^2) are obtained for $m_{\nu_R} < m_{W'}$ ($m_{\nu_R} > m_{W'}$). In addition, a first corresponding lower mass limit for a left-handed W' boson is derived, taking properly the interference with the Standard Model production into account, yielding 610 GeV/c^2 [405].

Based on the 0.9 fb^{-1} lepton plus jets dataset and the analysis from which the first evidence for single top production was achieved [13, 14], D0 obtains further improved W' mass limits [407]. Using the invariant mass of charged lepton, leading two jets and neutrino as sensitive variable for separating signal and background, the 95% C.L. lower mass limit for a left-handed W' boson interfering with Standard Model single top production increases to 731 GeV/c^2. For a right-handed W' boson the 95% C.L. lower mass limits are 739 GeV/c^2 (768 GeV/c^2) for $m_{\nu_R} < m_{W'}$ ($m_{\nu_R} > m_{W'}$), as illustrated in Figure 33. The latter two cross section limits translate into upper limits on the W' gauge coupling in units of the Standard Model weak coupling of 0.72 (0.68) for a W' boson mass of 600 GeV/c^2. The dominant systematic uncertainties included in these limits are the theoretical cross sections (affecting the background normalisation) and uncertainties on the jet energy calibration and b jet simulation (affecting background normalisation and shape of the sensitive variable).

CDF has obtained a preliminary result for the $W' \to tb$ search based

on 1.9 fb^{-1} lepton plus jets Run II data using the invariant mass of the reconstructed W boson and the two leading jets as sensitive variable. 95% C.L. lower limits on the mass of a right-handed W' boson are found to be 800 GeV/c^2 for $m_{\nu_R} < m_{W'}$ and 825 GeV/c^2 for $m_{\nu_R} > m_{W'}$. Neglecting interference effects the former limit is considered to apply for a left-handed W' boson as well. The corresponding W' gauge coupling in units of the Standard Model weak coupling is found to be below 0.68 and 0.63 respectively for a W' boson mass of 600 GeV/c^2 [408].

The more general case of a W' boson with an admixture of left- and right-handed couplings to the Standard Model fermions has not been studied so far.

5.8.4 Search for Single Top Production via charged Higgs Bosons

The Standard Model Higgs sector with its single Higgs doublet of complex scalar fields to break the electroweak symmetry and generate masses for weak gauge bosons and fermions (see Section 2.1) can be easily extended to include a second Higgs doublet, resulting in "Two Higgs Doublet Models" (THDM, 2HDM) [409, 410]. In contrast to the single neutral scalar CP-even Higgs boson predicted by the Standard Model, THDMs give rise to five physical scalar Higgs bosons after electroweak symmetry breaking, two of which are charged – $H^{\pm}$ – providing a unique signature for physics beyond the Standard Model. Three different Higgs-fermion couplings are discerned in THDMs. Type-I models consider only one of the Higgs doublets to couple to fermions. In type-II models each of the doublets couples solely to up-type fermions and down-type fermions respectively, while in type-III models general couplings of both Higgs doublets to fermions are allowed. In the latter case, Higgs-mediated flavour-changing neutral currents at tree level need to be sufficiently suppressed to be compatible with experimental limits, which can be achieved by choosing the Higgs parameters correspondingly [411].

If the charged Higgs boson is heavier than the top quark ($m_{H^{\pm}} > m_t$), its production via quark fusion can contribute to single top quark production through the decay into third generation quarks: $q\bar{q}' \rightarrow H^{\pm} \rightarrow tb$. Due to the mass dependent couplings of the charged Higgs boson, such a decay is dominant in many models. The signature of this process is identical to that of s-channel single top quark production, and the search for charged Higgs bosons can be performed similar to that for W' bosons, with the simplification that interference with the Standard Model production process can be neglected.

D0 performs a first direct search for the process $q\bar{q}' \rightarrow H^{\pm} \rightarrow tb \rightarrow \ell\nu b\bar{b}$ [412], based on the analysis providing first evidence for single top pro-

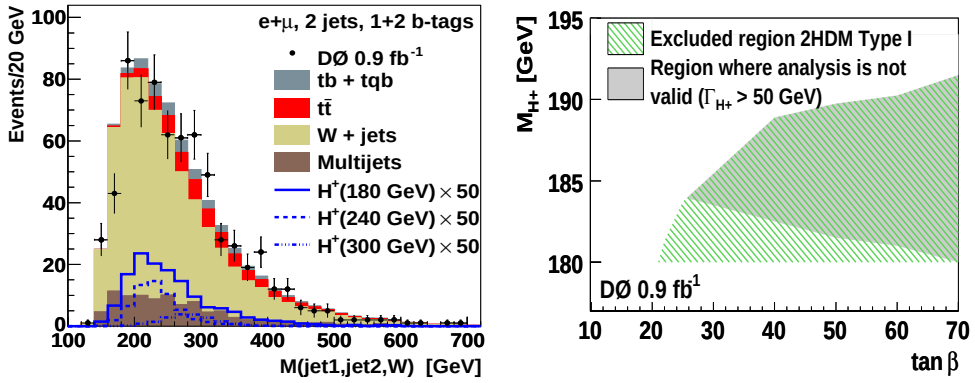

Figure 34: Left: Distribution of the invariant mass of reconstructed W boson and two jets in 0.9 fb^{-1} lepton plus jets data, Standard Model background processes and charged Higgs boson signal in a type-III THDM for various $m_{H^\pm}$, enhanced by a factor of 50. Right: 95% C.L. exclusion region in the $(m_{H^\pm}, \tan\beta)$ plane for a type-I THDM. If $\Gamma_{H^\pm}$ exceeds 50 GeV/c^2, the analysis is no longer valid, and no limits can be derived as illustrated by the darker green area [412].

duction [13, 14] in a 0.9 fb^{-1} lepton plus jets dataset. Restricting the jet multiplicity in the event selection to exactly two jets corresponding to the s-channel final state, charged Higgs bosons are searched for in the mass range 180 GeV/c^2 $\leq m_{H^\pm} \leq$ 300 GeV/c^2 for all three types of THDMs. The sensitive variable used to discriminate the charged Higgs boson signal from the Standard Model background processes is the invariant mass of the reconstructed W boson and the two jets as illustrated in Figure 34. Since no evidence for signal is observed in the data, 95% C.L. upper limits on the charged Higgs boson production cross section times branching fraction into third generation quarks are provided for all three types of THDMs, taking systematic uncertainties into account. The dominant systematic uncertainties result from the jet energy scale calibration, modelling of the b jet identification and theoretical uncertainties in modelling and normalisation of the signal. For the type-I THDM, the limits are translated into a 95% C.L. exclusion region in the $(m_{H^\pm}, \tan\beta)$ parameter space (see Figure 34), where $\tan\beta$ is the ratio of the two Higgs doublets' vacuum expectation values.

More searches for charged Higgs bosons, especially those in top quark decays (for $m_{H^\pm} < m_t$), are described in Section 6.5.

5.8.5 Search for Neutral Current Single Top Production

Single top quark production via flavour changing neutral interactions with the light quarks u, c and the Z, γ, g gauge bosons is possible in the Standard Model through higher order radiative corrections, but so strongly suppressed that it cannot be observed. Consequently, the search for these production mechanisms at tree level allows one to probe for corresponding anomalous coupling strengths κ [165, 413] that are predicted by various extensions of the Standard Model [414].

The processes involving a photon or Z boson exchange have been extensively studied at LEP and HERA. At both accelerators top quarks can only be produced singly at the available centre of mass energies due to the large top quark mass.

At LEP, single top quark production proceeds via the Standard Model process $e^+e^- \to e^-\bar{\nu}_e t\bar{b}$ which can be safely ignored in the available datasets due to its tiny production rate. All four LEP experiments searched for single top production via $e^+e^- \to t\bar{c}/t\bar{u}$ in both hadronic and semileptonic final states resulting from the different W boson decay modes from the top quark decay. While only the Standard Model decay $t \to Wb$ is considered, a possible reduction of its branching ratio due to FCNC decays is accounted for when deriving the results. Since no evidence for single top quark production is observed, 95% C.L. upper limits on the cross section are derived and corresponding model-dependent upper limits on the anomalous coupling parameters κ_γ and κ_Z are determined [415–418].

Single top quark production at HERA is possible via the charged current Standard Model process $ep \to \nu t\bar{b}X$ which exhibits a negligible production rate here as well. Both H1 and ZEUS have searched for the inclusive neutral current process $ep \to etX$. Because of the large Z boson mass, this reaction is most sensitive to couplings involving photons. Due to the large proton momentum fractions needed for single top production, the u quark contribution will dominate over that from the c quark (see Figure 5), resulting in the highest sensitivity for $tu\gamma$ couplings at HERA.

Using datasets with 0.1 fb^{-1} of integrated luminosity and assuming the Standard Model top quark decay $t \to Wb$, H1 and ZEUS search for single top production both in the leptonic and the hadronic W boson decay channel. ZEUS observes good agreement with the Standard Model prediction and sets 95% C.L. upper limits on single top production rate and the FCNC magnetic coupling $\kappa_{tu\gamma}$ and the vector coupling v_{tuZ}, neglecting charm contributions [422]. H1 observes five events in the leptonic channel with an expected Standard Model background contribution of 1.31 ± 0.22 events, while the hadronic channel exhibits no excess over the Standard Model prediction.

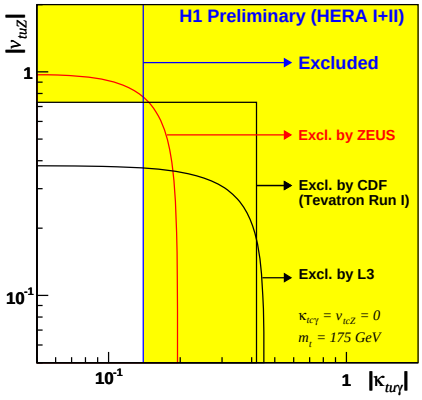

Figure 35: 95% C.L. upper limits on the top quark anomalous couplings to photon and Z boson $\kappa_{tu\gamma}$ and v_{tuZ} [419]. Depicted are the limits by CDF [420, 421], L3 [416], H1 [419] and ZEUS [422].

The two channels are compatible at the 1.1 σ level, and both a combined single top cross section with about 2 σ significance and 95% C.L. upper limits on cross section and $\kappa_{tu\gamma}$ assuming a statistical fluctuation are provided [423]. In a recent preliminary update of the measurement in the leptonic channel by H1 using an integrated luminosity of 0.5 fb^{-1} good agreement with the Standard Model expectation is observed and improved limits on single top cross section and $\kappa_{tu\gamma}$ are obtained [419].

Further limits on the anomalous couplings κ_γ and κ_Z have been measured at the Tevatron by CDF via the search for neutral current top quark decays $t \to \gamma q$ and $t \to Zq$ as discussed in detail in Section 6.3. The most stringent results on anomalous top quark couplings involving photons and Z bosons obtained at LEP, HERA and the Tevatron are summarised in Figure 35 with the exception of the latest CDF limit on $t \to Zq$ decays [424] that constrains κ_Z better than the L3 limit.

Flavour changing neutral current couplings of top quarks and gluons have not been studied as extensively. A constraint on the anomalous gluon coupling κ_{tqg}/Λ where Λ gives the scale for new physics has been derived based on the observed $t\bar{t}$ pair production cross section at the Run I Tevatron and a possible new physics contribution that could be still accommodated within two σ of combined experimental and theoretical uncertainties, yielding $\kappa_{tqg}/\Lambda < 0.52$ TeV^{-1} [425]. Another limit on the anomalous gluon coupling has been derived using the single top production cross section limit measured by ZEUS [422]. Neglecting effects that arise from the different final states

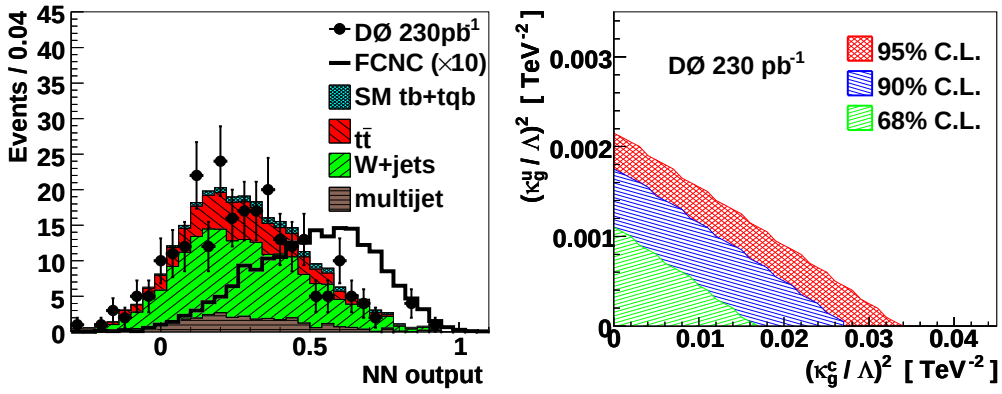

Figure 36: Left: Neural Network (NN) discriminant distribution in 0.2 fb^{-1} lepton plus jets data, simulated FCNC signal enhanced by a factor of ten and Standard Model background. The signal distribution represents the sum of tug and tcg processes, evaluated for $\kappa_{tqg}/\Lambda = 0.03$ TeV^{-1}. Right: Exclusion contours of the anomalous top-gluon couplings for different confidence levels [427].

obtained in the gluon channel compared to the original search (one additional light jet is present in the gluon case), at 95% C.L. $\kappa_{tqg}/\Lambda < 0.4$ TeV^{-1} is obtained [426].

D0 has performed a first search for single top production via flavour changing neutral current couplings to gluons at a hadron collider, using 0.2 fb^{-1} lepton plus jets data [427]. The analysis is based on the corresponding search for Standard Model single top production [384, 385] but is restricted to events with only one b tagged jet and treats s- and t-channel Standard Model single top production as background. Since the neutral current top quark decays $t \to gu/gc$ exhibit a negligible branching fraction for $\kappa_{tqg}/\Lambda \lesssim 0.2$ TeV^{-1} [428], the Standard Model top quark decay can be considered alone.

To separate the FCNC signal from the overwhelming Standard Model background processes, a neural network with ten input variables based on global event kinematics, angular correlations and kinematics of the individual reconstructed objects is deployed. The resulting data distribution is shown in Figure 36 and exhibits good agreement with the Standard Model prediction which allows one to set limits on the FCNC couplings κ_{tug}/Λ and κ_{tcg}/Λ.

Systematic uncertainties changing either the normalisation or both normalisation and shape of the distributions are taken into account when calculating the two-dimensional Bayesian posterior probability density, resulting

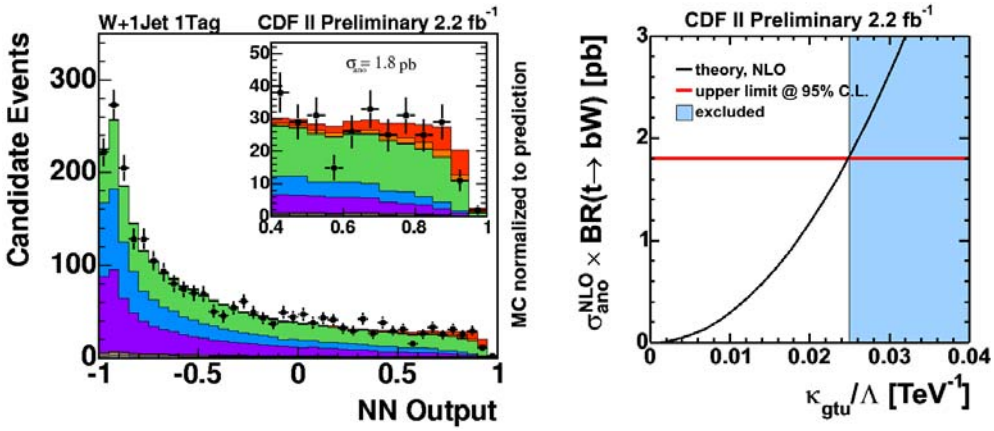

Figure 37: Left: Neural network discriminant output in W plus one b jet events observed in 2.2 fb^{-1} of CDF data (black points) and Standard Model background processes. A FCNC single top signal with the observed 95% C.L. *excluded* production rate has been added in red. Right: Derivation of the κ_{tug}/Λ limit from the intersection of observed cross section limit and theoretical rate prediction, assuming a κ_{tcg} of zero [429].

in the exclusion contours of both couplings for different confidence levels shown in Figure 36. The largest normalisation uncertainties arise from the background cross section uncertainties, including the uncertainty on the top quark mass for $t\bar{t}$ and single top samples. The largest uncertainties affecting the shape as well arise from jet energy scale calibration and b tag modeling. 95% C.L. upper limits on κ_{tug}/Λ and κ_{tcg}/Λ are obtained by integrating over the respective second dimension, yielding 0.037 TeV^{-1} and 0.15 TeV^{-1}. These limits represent a significant improvement over the previous ones by up to an order of magnitude.

In a recent preliminary result based on a 2.2 fb^{-1} dataset, CDF also searches for FCNC single top production [429]. Other than in the D0 analysis where $2 \to 2$ tcg and tug signal processes are considered, CDF investigates the $2 \to 1$ processes $u(c) + g \to t$. Since also in this analysis the Standard Model top quark decay is considered alone, events with one isolated energetic lepton, $\not\!\!E_T$ and one b tagged jet are selected.

Signal and Standard Model background processes are separated using a Bayesian neural network based on 14 input variables containing information from the reconstructed objects and event kinematics. In a template fit to the observed distribution in data good agreement with the Standard Model background is found as illustrated in Figure 37 and a 95% C.L. upper limit

on FCNC single top production via $u(c) + g \rightarrow t$ of 1.8 pb is obtained in accordance with the expected sensitivity.

Based on LO predictions of the FCNC signal process from TopReX [430] and NLO k-factors [431, 432], the obtained cross section limit can be converted into limits on the anomalous gluon couplings. No two-dimensional information is used in this analysis for contributions of tcg versus tug signal processes, and the respective other coupling is assumed to be zero when each coupling limit is derived. The resulting 95% C.L. upper limits are $\kappa_{tug}/\Lambda < 0.025$ TeV^{-1} (see Figure 37) and $\kappa_{tcg}/\Lambda < 0.105$ TeV^{-1}.

5.8.6 Anomalous Wtb couplings in Single Top Production

The couplings between quarks and electroweak gauge bosons could be directly scrutinised at LEP [86] with the exception of the top quark due to its large mass and consequent negligible production rate at LEP. At the Tevatron, the couplings of the top quark with the W boson can be studied by measurements of top quark decay properties in $t\bar{t}$ production (see for example Section 6.1) and via single top quark production. Physics beyond the Standard Model could result in the modification of the Lorentz structure of the Wtb vertex. Considering a more general extension of the Standard Model Wtb interaction Lagrangian as discussed in Section 3.3.3, such new physics could introduce non-zero contributions from right-handed vector (f_1^R) and left- respectively right-handed tensor couplings (f_2^L, f_2^R) in addition to the pure left-handed vector coupling (f_1^L) in the Standard Model framework.

D0 has published a first measurement giving direct constraints on such an extended Wtb interaction including first direct limits on the left- respectively right-handed tensor couplings [433], based on the analysis yielding first evidence for single top production in 0.9 fb^{-1} lepton plus jets data [13, 14]. In the analysis, single top quark production and decay are considered to occur via W bosons alone, with the dominant contribution arising from the Wtb interaction which is assumed to be CP conserving. Anomalous couplings in the Wtb vertex can modify both the total single top production rate and the observed kinematics in the events with respect to the Standard Model expectation [139, 434–436], the latter effect being illustrated in Figure 38 for the charged lepton transverse momentum distribution.

Since a simultaneous fit of all four couplings is not feasible with the available statistics, the Standard Model coupling is instead considered with one additional anomalous coupling contribution respectively in varying proportions, while the remaining two anomalous couplings are set to zero. The resulting scenarios are denoted as (L_1, R_1), (L_1, R_2) and (L_1, L_2). Non-negligible interference effects for the last case are taken properly into account.

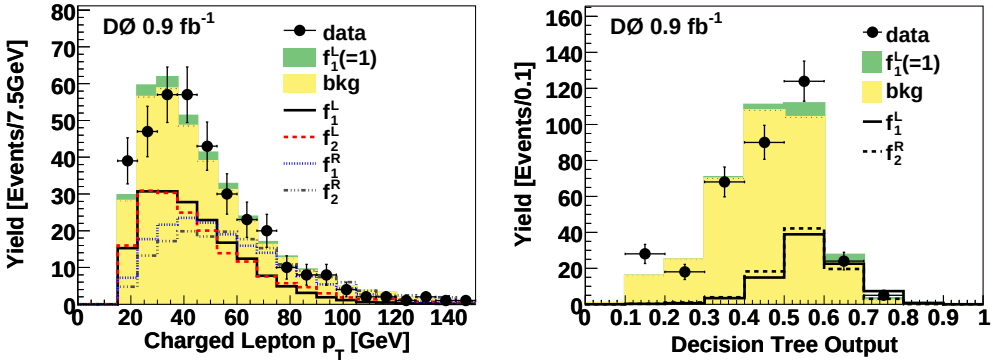

Figure 38: Left: Charged lepton transverse momentum distribution in 0.9 fb^{-1} lepton plus jets data (two jets, one b tag subsample) and corresponding Standard Model single top signal and background contributions. The effect of the four different Wtb couplings on the signal is illustrated as well (the other couplings being zero respectively) with normalisation enhanced by a factor of ten. Right: Boosted decision tree output for the same data, signal and background contributions, with the (L_1, R_2) case coupling contributions overlaid (normalisation enhanced by a factor of five) [433].

For signal discrimination from the Standard Model background, boosted decision trees are used based on the same variables as in [13, 14], with the lepton transverse momentum distribution added. One example distribution for the (L_1, R_2) case is shown in Figure 38.

The obtained decision tree output in data is compared with the various single top signal models in all twelve subchannels defined by lepton flavour (e, μ), jet multiplicity (two, three, four) and b tag multiplicity (one, two). This yields a two-dimensional Bayesian posterior probability density, depending on $|f_1^L|^2$ and the second anomalous coupling $|f_A|^2$ considered in the respective scenario. Systematic uncertainties are taken into account, with dominant contributions arising from background normalisation, modelling of b tagging and jet energy scale calibration, the latter two affecting both normalisation and shape of the simulated spectra. The maxima of the likelihoods in all three considered scenarios yield zero for $|f_A|^2$, and corresponding 95% C.L. upper limits on these couplings are provided from the one-dimensional likelihood projections. The results are summarised with the measured single top production rates and $|f_1^L|^2$ values obtained from one-dimensional likelihood projections in Table 15. The Standard Model Wtb interaction is favoured over the exotic alternatives studied. This analysis will greatly benefit from the increased datasets already at hand respectively

Scenario	Cross Section ($tb + tqb$)	Considered Couplings
(L_1, R_1)	$5.2^{+2.6}_{-3.5}$ pb	$\lvert f_1^L\rvert^2 = 1.8^{+1.0}_{-1.3}$ $\lvert f_1^R\rvert^2 < 2.5$ (95% C.L.)
(L_1, R_2)	$4.5^{+2.2}_{-2.2}$ pb	$\lvert f_1^L\rvert^2 = 1.4^{+0.9}_{-0.8}$ $\lvert f_2^R\rvert^2 < 0.3$ (95% C.L.)
(L_1, L_2)	$4.4^{+2.3}_{-2.5}$ pb	$\lvert f_1^L\rvert^2 = 1.4^{+0.6}_{-0.5}$ $\lvert f_2^L\rvert^2 < 0.5$ (95% C.L.)

Table 15: Total single top production rates obtained in the three anomalous coupling scenarios together with the corresponding one-dimensional measurements respectively limits for the involved couplings [433].

expected until the end of Run II.

6 Measurements of Top Quark Decay Properties

The previous chapter demonstrated that so far no significant deviations from the Standard Model expectations regarding top quark production both via the strong and electroweak interaction have been observed. In this chapter various decay properties of the top quark will be investigated, generally assuming top quark production according to the Standard Model. The corresponding measurements are performed in top quark pair events, where the top signal is fully established and in particular sufficient statistics are available.

6.1 Measurement of the W Boson Helicity in $t\bar{t}$ Decays

The helicity of the W boson in top quark decays can be used to test the $V-A$ Lorentz structure of the Wtb interaction (see Section 3.3.3). According to the expectation from the Standard Model, W bosons from top quark decays should be longitudinally polarised with a fraction $f_0 \approx 70\%$ and left-handed with a fraction $f_- \approx 30\%$, while the right-handed fraction f_+ is strongly suppressed and below the per mill level [191]. For the decay of antitop quarks, the CP conjugate statement is implied, resulting in either longitudinally or right-handedly polarised W^- bosons from $\bar{t}$ decays.

A pure $V + A$ structure of the Wtb interaction would result in an observation of a right-handed fraction $f_+ = 30\%$ with negligible left-handed

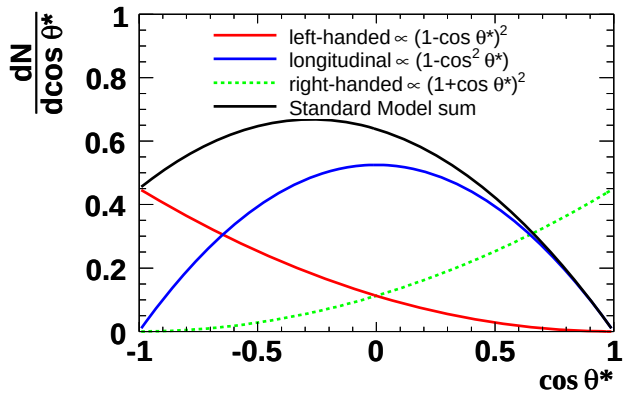

Figure 39: Helicity angle $\cos\theta^*$ distributions for left-handed (red), longitudinal (blue) and right-handed (dashed green) polarised W bosons. The superposition expected from the Standard Model is shown in black.

contribution. Small $V + A$ admixtures to the Standard Model left-handed charged current weak interaction are for instance predicted within $SU(2)_R \times SU(2)_L \times U(1)_Y$ extensions of the Standard Model [437–440]. Such contributions would result in an enhancement of f_+ while not significantly affecting f_0. Since the decay amplitude to longitudinally polarised W bosons is proportional to the top quark's Yukawa coupling [174], f_0 is sensitive to the mechanism of EWSB and would be altered for example in topcolour-assisted technicolour models [193, 441].

The radiative decay rate $b \to s\gamma$ can be used to set indirect limits on the $V + A$ admixture in top quark decays to be below a few percent [442–445], assuming there are no contributions from gluonic penguin diagrams in addition to the electroweak ones. This section will discuss the direct measurements of the W boson helicity performed at the Tevatron using lepton plus jets and dilepton datasets.

Thus far, four different analysis techniques have been deployed to extract the W boson helicity fractions, based on:

(i) *helicity angle* ($\cos\theta^*$): The helicity of the W boson is reflected in the angular distribution $\cos\theta^*$ of its decay products, with θ^* being the angle of the down-type ($T_3 = -\frac{1}{2}$) decay products of the W boson (charged lepton, d- or s-quark) in the W boson rest frame with respect to the

top quark direction [188–191]:

$$\frac{dN}{d\cos\theta^*} = f_- \cdot \frac{3}{8}(1-\cos\theta^*)^2 + f_0 \cdot \frac{3}{4}(1-\cos^2\theta^*) + f_+ \cdot \frac{3}{8}(1+\cos\theta^*)^2,$$

where f_- can be replaced by $(1 - f_+ - f_0)$. The resulting distributions for each helicity fraction and the superposition expected from the Standard Model are shown in Figure 39. A measurement of $\cos\theta^*$ provides the most direct measurement of the W boson helicity but also requires the reconstruction of the top quark and W boson momenta which is challenging and involves the use of $\not\!\!E_T$, exhibiting a rather poor resolution.

(ii) *charged lepton p_T spectrum (p_T^ℓ)*: The helicity of the W boson is correlated with the charged lepton momentum distribution: Since the ν_ℓ from W^+ decays are always left-handed while the ℓ^+ are right-handed, in case of a left-handed W^+ decay the ℓ^+ are preferentially emitted anti-parallel with respect to the momentum of the W^+. This leads to a softer p_T^ℓ spectrum in the laboratory frame. Conversely, the ℓ^+ are preferentially emitted in the direction of the W^+ momentum in case of a right-handed W^+ decay, leading to a harder p_T^ℓ spectrum. ℓ^+ from a longitudinal W^+ decay represent an intermediate case (see Figure 40).

(iii) *invariant mass of b quark and charged lepton ($M_{\ell b}^2$)*: The helicity angle distribution $\cos\theta^*$ can be approximated using the invariant mass of the system composed of the b quark and the charged lepton $M_{\ell b}^2$:

$$\cos\theta^* = \frac{p_\ell \cdot p_b - E_\ell E_b}{|\mathbf{p}_\ell||\mathbf{p}_b|} \simeq \frac{2M_{\ell b}^2}{m_t^2 - M_W^2} - 1.$$

This way one avoids the challenges involved in the kinematic reconstruction of the top quark and the application of $\not\!\!E_T$ by using only momenta in the laboratory frame.

(iv) *Matrix Element method (ME)*: The Matrix Element method was originally developed by D0 [446] yielding a very precise mass measurement given the limited Run I data sample (see also Section 7.3.2). Using the complete kinematic information available, in each event a probability for the event to correspond to a $t\bar{t}$ final state as a function of the helicity of the W boson can be calculated, based on the LO process matrix element.

The following subsections will give brief examples for each method, followed by a summary of the current status of the measurements.

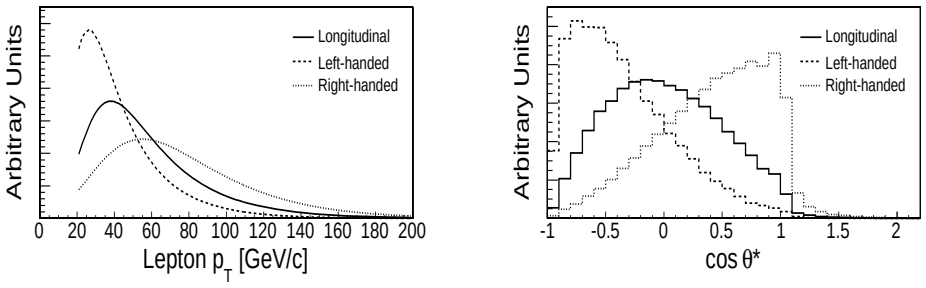

Figure 40: Distributions of reconstructed charged lepton p_T and $\cos\theta^*$ (based on the $M^2_{\ell b}$ approximation) for top quark decays involving left-handed, right-handed and longitudinally polarised W bosons [447].

6.1.1 p_T^ℓ and $M^2_{\ell b}$

CDF has measured the W boson helicity in a 0.2 fb^{-1} Run II dataset using the charged lepton p_T spectrum p_T^ℓ and the invariant mass of b quark and charged lepton $M^2_{\ell b}$ to approximate $\cos\theta^*$ [447]. The dependence of these observables on the W boson helicity for a top quark mass of 175 GeV/c^2 after event selection and reconstruction is shown in Figure 40. Since the world average top and W boson masses are used when calculating $\cos\theta^*$ instead of the corresponding event-by-event reconstructed masses that would smear out the distribution due to the larger inherent uncertainties, values outside of the physical range $-1 \leq \cos\theta^* \leq 1$ are observed.

For the p_T^ℓ analysis a b tagged lepton plus jets sample is used requiring at least three jets and yielding 57 events of which approximately 2/3 are $t\bar{t}$ signal. In addition a dilepton sample with a cut on the scalar sum of the transverse energy of jets, leptons and $\not\!\!E_T$ is analysed, yielding 13 events with a signal fraction of approximately 79%. The $M^2_{\ell b}$ analysis uses the lepton plus jets sample alone, requiring a fourth jet and a good quality kinematic fit to the $t\bar{t}$ hypothesis with a top mass of 175 GeV/c^2 which allows one to associate the lepton with the appropriate jet to form $M^2_{\ell b}$. This leaves 31 events for this analysis with a signal fraction of approximately 78%.

For both analyses, the data distributions are fitted separately to p_T^ℓ respectively $\cos\theta^*$ templates of signal with the different W boson helicities and background. Due to the limited statistics, the helicity fractions f_0 and f_+ cannot be fitted simultaneously. Consequently, f_0 respectively f_+ are constrained to their Standard Model values when fitting f_+ respectively f_0. Both analyses are finally combined taking statistical and systematic correlations into account, yielding results consistent with the Standard Model expectation as shown in Table 16. The dominant systematic uncertainties come from

Analysis	N	f_0	f_+
$M^2_{\ell b}$	31	$0.99^{+0.29}_{-0.35} \pm 0.19$	$0.23 \pm 0.16 \pm 0.08$
$p_T^\ell(\ell\ell)$	26	$-0.54^{+0.35}_{-0.25} \pm 0.16$	$-0.47 \pm 0.10 \pm 0.09$
$p_T^\ell(\ell j)$	57	$0.95^{+0.35}_{-0.42} \pm 0.17$	$0.11^{+0.21}_{-0.19} \pm 0.10$
$p_T^\ell(\ell\ell, \ell j)$	83	$0.31^{+0.37}_{-0.23} \pm 0.17$	$-0.18^{+0.14}_{-0.12} \pm 0.12$
Combined		$0.74^{+0.22}_{-0.34}$	$0.00^{+0.20}_{-0.19}$
95% C.L. limit		$< 0.95, > 0.18$	< 0.27

Table 16: Results of the single and combined measurements of f_0 and f_+ using $M^2_{\ell b}$ and p_T^ℓ. N indicates the number of events or leptons used. If two uncertainties are given, the first is statistical and the second systematic. For the combined results, the total statistical and systematic uncertainty is given. For the $p_T^\ell(\ell\ell)$ result, an observation of -0.54 or less is expected 0.5% of the time for a true Standard Model f_0 value of 0.7 [447].

uncertainties on the top quark mass, background shape and normalisation, effects of initial- and final-state radiation (ISR/FSR) and PDFs.

CDF has measured the fraction of right-handed W bosons assuming f_0 to be 0.7 using the $M^2_{\ell b}$ method alone on a 0.7 fb^{-1} Run II dataset [448]. Using a single and double b tagged lepton plus jets in addition to a dilepton dataset, f_+ is extracted via maximum likelihood fits of the $M^2_{\ell b}$ distributions obtained in data to $V + A$ and $V - A$ $t\bar{t}$ signal Monte Carlo and background processes. Including effects of the uncertainty on the $t\bar{t}$ signal and background cross sections in the uncertainties, the lepton plus jets sample yields $f_+ = 0.06 \pm 0.08$ while the dilepton sample gives $f_+ = -0.19 \pm 0.11$, corresponding to a compatibility of the measurements at the 2.3σ level. A combination of these measurements including the total systematic uncertainties yields $f_+ = -0.02 \pm 0.07(\text{stat} + \text{syst})$, corresponding to $f_+ < 0.09$ at 95% C.L.. The main contributions to the systematic uncertainty come from the jet energy scale, background shape and normalisation and limited Monte Carlo statistics.

6.1.2 Matrix Element method

D0 has used the matrix element method that was originally employed to measure the top quark mass [446] to extract the longitudinal W boson helicity fraction from 0.1 fb^{-1} of Run I data [449]. The selected lepton plus jets event sample corresponds to that of the preceding mass analysis [321] and

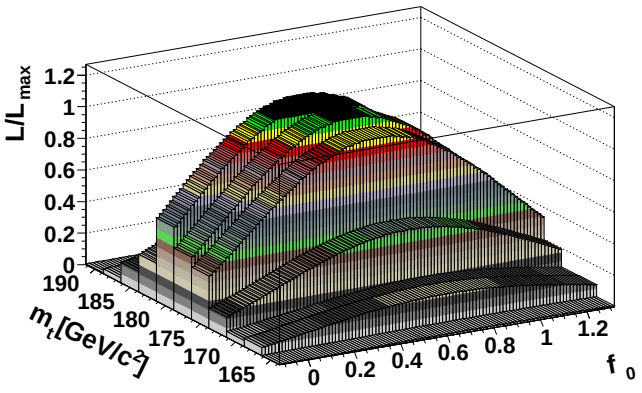

Figure 41: Two-dimensional probability density observed in 0.1 fb^{-1} lepton plus jets Run I data as a function of f_0 and top quark mass m_t [449].

comprises both soft muon b tagged events and untagged events for which additional kinematic cuts are applied, yielding 91 events.

By comparing the measured set of four-vectors in each event with the differential cross section for $t\bar{t}$ signal and the dominant $W+$jets background, f_0 can be extracted by fixing f_+ to its Standard Model value and allowing the ratio f_0/f_- to vary. The usage of both W boson decays per signal event increases the statistical sensitivity of the method. Since the calculation of signal and background probabilities is based on leading order matrix elements, only events with exactly four jets are accepted, reducing the sample to 71 events. In order to increase the sample purity, a cut on the background probability is applied, leaving 22 events to be analysed like in the corresponding matrix element mass analysis [446], with a signal to background ratio of 12/10.

To take the dependence of the f_0 measurement on the top quark mass into account, a two-dimensional likelihood depending on f_0 and m_t is calculated and corrected for response deviations from unity for different f_0 input values (see Figure 41). Since statistics is insufficient, a simultaneous optimisation for both observables is not feasible; instead f_0 is evaluated integrating over the top quark mass in a range between 165 and 190 GeV/c^2. The obtained probability maximum yields the central value of the measurement, with the 1σ uncertainty band corresponding to the convolution of statistical and top quark mass uncertainties. Other systematic uncertainties from acceptance and linearity response or jet energy scale are small compared to this, yielding

the final result:

$$f_0 = 0.56 \pm 0.31(\text{stat} \oplus \text{m}_\text{t}) \pm 0.07(\text{syst}).$$

CDF has obtained a preliminary result for f_0 using the matrix element method on 1.9 fb^{-1} Run II data for a fixed top quark mass of 175 GeV/c^2 [450]. 468 events are selected in a b tagged lepton plus jets sample with at least four jets (only the leading four are used in the analysis) and a cut applied on the scalar sum of transverse energy in the event, yielding a signal fraction of about 84%. Fixing f_+ to its Standard Model value, the longitudinal W boson helicity fraction is found to be $f_0 = 0.64 \pm 0.08(\text{stat.}) \pm 0.07(\text{syst.})$, with the dominant systematic uncertainty coming from the Monte Carlo generator used (PYTHIA versus HERWIG) for the calibration of the measurement. f_0 is found to change by ∓ 0.035 for a ± 2.5 GeV/c^2 variation in the top quark mass. So far the analysis has not yet been extended to measure f_0 and f_+ or f_0 and m_t simultaneously.

6.1.3 Helicity angle $\cos\theta^*$

D0 has published a first model-independent measurement of the W boson helicity fractions by comparing the $\cos\theta^*$ distribution in data to templates of background and purely right-handed, left-handed or longitudinal W bosons in signal, using f_+ and f_0 as freely floating parameters and $f_- = 1 - f_+ - f_0$ [451]. In a 1 fb^{-1} dataset, lepton plus at least four jets and dilepton events are selected. The signal purity is increased in each subsample by a cut on an individually optimised multivariate likelihood discriminant based on event kinematics and the output of a continuous neural network b tagging discriminant. The cut values are chosen for each subsample to yield the best expected precision of the helicity measurement.

The statistical sensitivity of the analysis is further increased by about 20% via including the hadronic W boson decays in the lepton plus jets sample in the measurement: A W boson daughter jet is picked at random for the calculation of $\cos\theta^*$, introducing a sign ambiguity. Consequently, only $|\cos\theta^*|$ can be considered which does not allow to discriminate left- from right-handed W bosons, but still adds information for the extraction of f_0.

The four-momenta of the top quarks and W bosons in the lepton plus jets sample are reconstructed based on the best kinematic fit to a top quark event hypothesis for $m_t = 172.5$ GeV/c^2, using the leading four jets to obtain $\cos\theta^*$ respectively $|\cos\theta^*|$. For the kinematically underconstrained dilepton events, a top quark mass of $m_t = 172.5$ GeV/c^2 is assumed and the kinematics is solved up to a four-fold ambiguity in addition to the two-fold ambiguity from the lepton-jet pairing (only the leading two jets are used). Jet and lepton

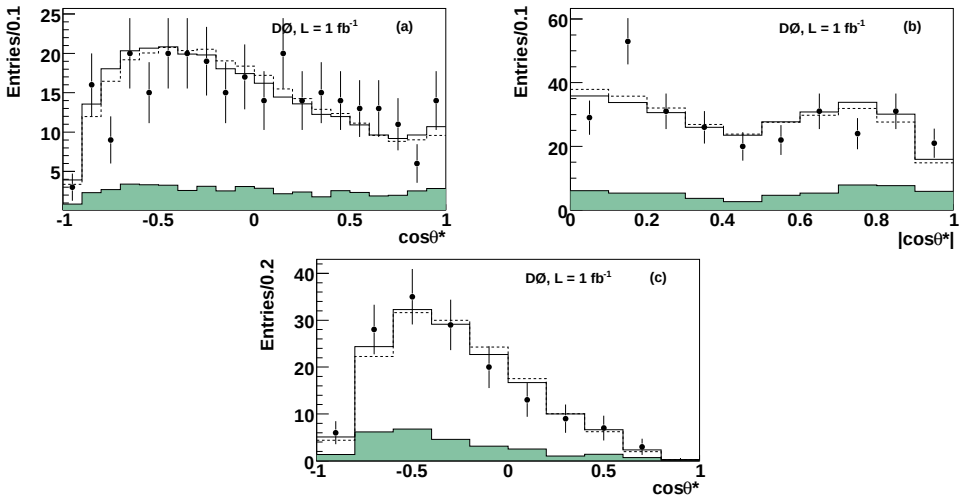

Figure 42: Helicity angle distributions in lepton plus jets (a,b) and dilepton events (c). 1 fb^{-1} of D0 data are represented by points with error bars, the solid open histogram shows the result from the model independent fit while the dashed open histogram shows the Standard Model expectation. The filled histogram represents the background contribution [451].

energies in each event are smeared within their resolutions many times to explore the phase space consistent with the observed values. The average of the obtained $\cos\theta^*$ values is then used for each charged lepton, providing two measurements per event. The resulting distributions are shown in Figure 42. Note that due to reconstruction effects the shape of the Standard Model expectation differs from the theoretical prediction in Figure 39.

A template fit of these distributions yields $f_0 = 0.425 \pm 0.166(\text{stat.}) \pm 0.102(\text{syst.})$ and $f_+ = 0.119 \pm 0.090(\text{stat.}) \pm 0.053(\text{syst.})$. The result is compatible with the Standard Model expectation at the 30% C.L.. It should be noted that the individual measurements in the lepton plus jets and dilepton channels differ by about 2.1σ [452]. The major systematic uncertainties on the measurement are summarised in Table 17, the largest uncertainty coming from $t\bar{t}$ signal modelling evaluated through varying the Monte Carlo generators used (PYTHIA versus ALPGEN) and from changing underlying event models to study the effects of gluon radiation or restricting the samples to contain only one primary vertex to study the sensitivity of the measurement to variations in instantaneous luminosity. Constraining f^0 respectively f^+ to their SM values when fitting f^+ respectively f^0, the result is $f^0 = 0.619 \pm 0.090\,(\text{stat.}) \pm 0.052\,(\text{syst.})$, $f^+ = -0.002 \pm 0.047\,(\text{stat.}) \pm 0.047\,(\text{syst.})$

Source	Uncertainty (f_0)	Uncertainty (f_+)
Top mass	0.009	0.018
Jet reconstruction eff.	0.021	0.010
Jet energy calibration	0.012	0.019
b fragmentation	0.016	0.010
$t\bar{t}$ model	0.068	0.032
Background model	0.049	0.016
Template statistics	0.049	0.025
Total	0.102	0.053

Table 17: Major systematic uncertainties on the simultaneous f_0 and f_+ measurement by D0 in a 1 fb^{-1} dataset [451].

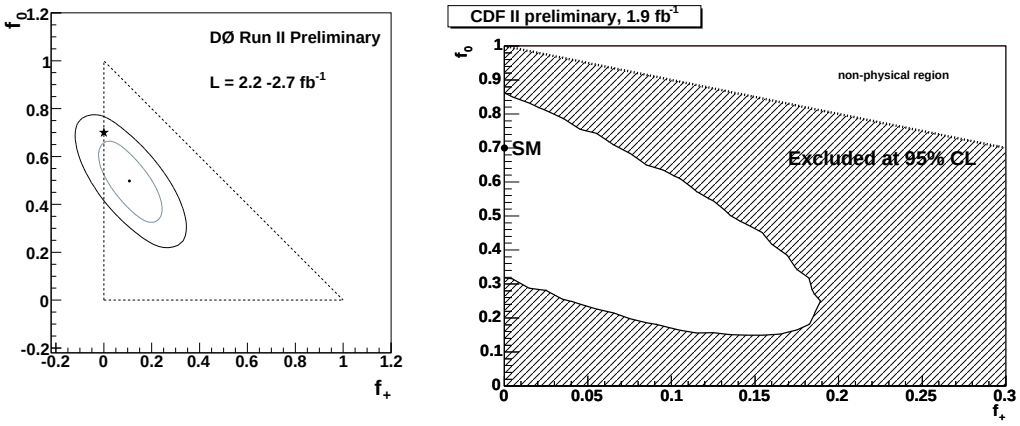

Figure 43: Left: Result of the model-independent W boson helicity fit by D0 [453]. The ellipses show the 68% and 95% C.L. contours around the measured data point. The star shows the SM expectation; the triangle denotes the physically allowed region where f_0 and f_+ sum to one or less. Right: Two-dimensional 95% C.L. exclusion area in the (f_+, f_0) plane measured by CDF [454].

in agreement with expectations from the SM.

In a recent preliminary update, D0 has added 1.2 fb^{-1} lepton plus jets and 1.7 fb^{-1} dilepton ($e\mu$ only) datasets [453] to the above analysis. The model-independent fit for the combined dataset yields $f_0 = 0.490 \pm 0.106(\text{stat.}) \pm 0.085(\text{syst.})$ and $f_+ = 0.110 \pm 0.059(\text{stat.}) \pm 0.052(\text{syst.})$, consistent at the 23% C.L. with the Standard Model (see Figure 43). The results from the

lepton plus jets and dilepton channels remain marginally consistent with a p-value of 1.6%.

CDF has obtained two preliminary results of model-independent W boson helicity fits in 1.9 fb^{-1} of data, using only the charged lepton in b tagged lepton plus at least four jets events to obtain $\cos\theta^*$ [454, 455]. A combination of both results also has become available recently [456]. The measurements are compatible with the Standard Model expectation, each other and the D0 measurements presented above and are summarised together with other results in Table 18. The two-dimensional 95% C.L. exclusion area in the (f_+, f_0) plane measured by CDF [454] is shown in Figure 43.

6.1.4 Summary

All measurements of the W boson helicity performed so far at the Tevatron are compatible with the Standard Model expectation. A summary of the measurements published thus far together with the current preliminary results is shown in Table 18.

The sensitivity of the measurements in Run I and early Run II only allowed model-dependent measurements of one of the W boson helicity fractions to be performed at a time, fixing the other fraction to its Standard Model value. With the large datasets available by now however, a simultaneous extraction of the fractions of longitudinally polarised and right-handed W bosons is possible, providing model-independent information since the third fraction is given by the constraint of their sum to unity. These measurements will clearly benefit from updates with increased datasets. A combination with the measurement of the single top production cross section in the s- and t-channel will allow one to fully specify the tWb coupling [193] (see Section 3.3.3).

The model-dependent measurements where one of the helicity fractions is fixed to its Standard Model value have reached a considerable precision with statistical uncertainties approaching the systematic ones.

It is interesting to note that discrepancies above the 2σ level between results from the dilepton and lepton plus jets samples have been observed both at CDF and D0 using different analysis techniques. This deserves further scrutiny in future analyses.

6.2 Measurement of $\mathcal{B}(t \to Wb)/\mathcal{B}(t \to Wq)$

As described in Section 3.3.1, in the Standard Model framework the top quark decays basically exclusively into a W boson and a b quark due to the dominant corresponding CKM matrix element V_{tb}. The ratio R of the top

$\int \mathcal{L}dt$ [fb^{-1}]	Sel.	f_0	f_+	2d fit	$f_+ <$ (95% C.L.)	Method	Ref.
0.1	$\ell j, \ell\ell$	$0.91 \pm 0.37 \pm 0.13$	0.11 ± 0.15	no	0.28	p_T^ℓ	[457]
0.1	$\ell j, \ell\ell$	—	-0.02 ± 0.11	no	0.18	$M_{\ell b}^2$, p_T^ℓ	[458]
0.1	ℓj	0.56 ± 0.31	—	no	—	ME	[449]
0.2	$\ell j, \ell\ell$	$0.74^{+0.22}_{-0.34}$	$0.00^{+0.20}_{-0.19}$	no	0.27	$M_{\ell b}^2$, p_T^ℓ	[447]
0.2	ℓj	—	$0.00 \pm 0.13 \pm 0.07$	no	0.25	$\cos\theta^*$	[459]
0.3	ℓj	$0.85^{+0.15}_{-0.22} \pm 0.06$	$0.05^{+0.11}_{-0.05} \pm 0.03$	no	0.26	$\cos\theta^*$	[460]
0.4	$\ell j, \ell\ell$	—	$0.06 \pm 0.08 \pm 0.06$	no	0.23	$\cos\theta^*$	[461]
0.7	$\ell j, \ell\ell$	—	-0.02 ± 0.07	no	0.09	$M_{\ell b}^2$	[448]
1.0	$\ell j, \ell\ell$	$0.62 \pm 0.09 \pm 0.05$	$0.00 \pm 0.05 \pm 0.05$	no	—	$\cos\theta^*$	[451]
		$0.43 \pm 0.17 \pm 0.10$	$0.12 \pm 0.09 \pm 0.05$	yes			
1.9	ℓj	$0.64 \pm 0.08 \pm 0.07$	—	no	—	ME	[450]
1.9	ℓj	$0.59 \pm 0.11 \pm 0.04$	$-0.04 \pm 0.04 \pm 0.03$	no	0.07	$\cos\theta^*$	[454]
		$0.65 \pm 0.19 \pm 0.03$	$-0.03 \pm 0.07 \pm 0.03$	yes	—		
1.9	ℓj	$0.66 \pm 0.10 \pm 0.06$	$0.01 \pm 0.05 \pm 0.03$	no	0.12	$\cos\theta^*$	[455]
		$0.38 \pm 0.21 \pm 0.07$	$0.15 \pm 0.10 \pm 0.05$	yes	—		
1.9	ℓj	0.62 ± 0.11	-0.04 ± 0.05	no	—	$\cos\theta^*$	[456]
		0.66 ± 0.16	-0.03 ± 0.07	yes			
2.7	$\ell j, \ell\ell$	$0.49 \pm 0.11 \pm 0.09$	$0.11 \pm 0.06 \pm 0.05$	yes	—	$\cos\theta^*$	[453]

Table 18: W boson helicity measurements performed so far at the Tevatron with their integrated luminosities, dataset selections applied (ℓj = lepton plus jets, $\ell\ell$ = dilepton) and analysis methods used. Model independent fit results are indicated by the 2d fit column. The three analyses using 0.1 fb^{-1} are from Run I; the analyses using more than 1 fb^{-1} are preliminary. [456] is a combination of the results in [454, 455].

quark branching fractions can be expressed via the CKM matrix elements as

$$R = \frac{\mathcal{B}(t \to Wb)}{\sum_{q=d,s,b} \mathcal{B}(t \to Wq)} = \frac{| V_{tb} |^2}{| V_{tb} |^2 + | V_{ts} |^2 + | V_{td} |^2} .$$

Measuring R allows one to assess the relative size of $|V_{tb}|$ compared to $|V_{td}|$ and $|V_{ts}|$, with the current measurements indicating $|V_{tb}| \gg |V_{td}|, |V_{ts}|$. While

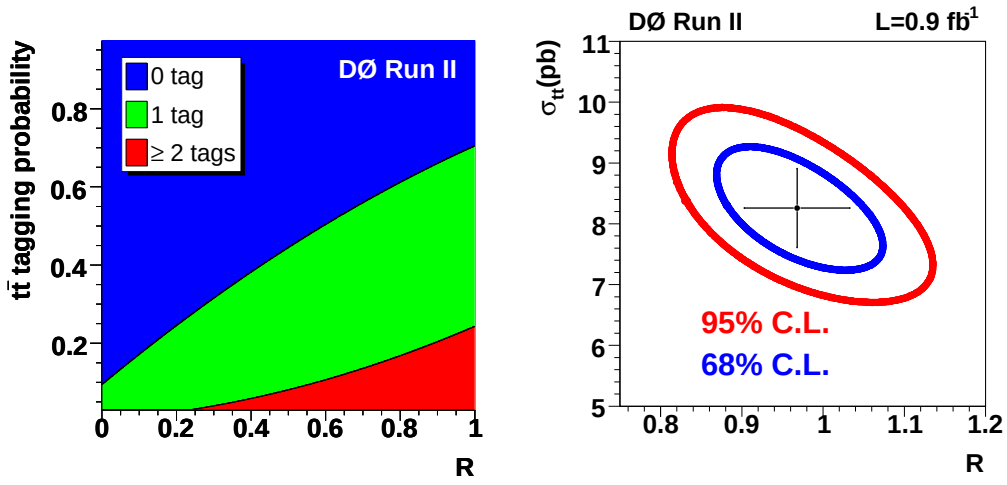

Figure 44: Left: Fractions of events with 0, 1 and ≥ 2 b tags for $t\bar{t}$ events with ≥ 4 jets as a function of R. Right: 68% and 95% C.L. statistical uncertainty contours in the R vs. $\sigma_{t\bar{t}}$ plane around the measured point in 0.9 fb^{-1} of D0 data [463].

a direct measurement of the V_{tb} matrix element is only possible via the single top quark production described in Section 3.2, model-dependent constraints on V_{tb} can also be inferred from a measurement of R: Assuming the validity of the Standard Model, specifically the existence of three fermion generations, unitarity of the CKM matrix and insignificance of non-W boson decays of the top quark (see Sections 6.3-6.5), the denominator in the above expression is one. R then simplifies to $|V_{tb}|^2$ and hence is strongly constrained: $0.9980 < R < 0.9984$ at 90% C.L. from global CKM fits [166].

Deviations of R from unity could for example be caused by the existence of a fourth heavy quark generation, non Standard Model top quark decays or non Standard Model background processes. Consequently, precise measurements of R allow to probe for physics beyond the Standard Model and provide a required ingredient for the model-independent direct determination of the $|V_{tq}|$ CKM matrix elements from electroweak single top production [462].

The most precise measurement of R thus far has been performed by D0 in the lepton plus jets channel using data corresponding to an integrated luminosity of 0.9 fb^{-1} [463], superseding the previously published measurement on 0.2 fb^{-1} [464]. The $t\bar{t}$ signal sample composition depends on R in terms of the number of b jets present in the sample as illustrated in Figure 44. By comparing the event yields with zero, one and two or more b tagged jets and using a topological discriminant to separate the $t\bar{t}$ signal from background in

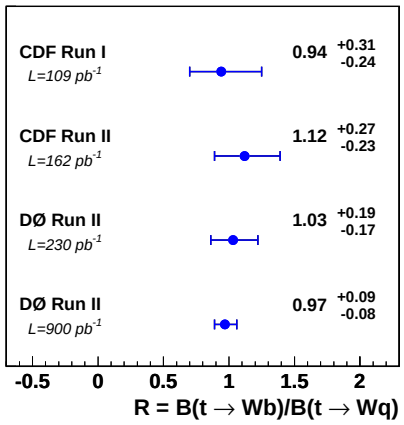

Figure 45: Summary of the branching ratio R measurements and their total uncertainties obtained at the Tevatron by CDF [465, 466] and D0 [463, 464].

events with zero b tags, R can be extracted together with the $t\bar{t}$ production cross section $\sigma_{t\bar{t}}$ simultaneously. This approach allows the measurement of $\sigma_{t\bar{t}}$ without assuming $\mathcal{B}(t \to Wb) = 100\%$ and exploits the different sensitivity of both quantities to systematic uncertainties yielding an overall improved precision.

A maximum likelihood fit to the sample composition observed in data gives

$$\begin{aligned} R &= 0.97^{+0.09}_{-0.08}\ (\text{stat.} + \text{syst.}) \text{ and} \\ \sigma_{t\bar{t}} &= 8.18^{+0.90}_{-0.84}\ (\text{stat.} + \text{syst.})\ \pm 0.50\ (\text{lumi})\ \text{pb} \end{aligned}$$

(see Figure 44) with a correlation of -58% for a top quark mass of 175 GeV/c^2 in agreement with the Standard Model prediction. From the measurement 95% C.L. limits are extracted, yielding $R > 0.79$ and $|V_{tb}| > 0.89$, the latter being model-dependent as mentioned above. R is observed to exhibit no significant dependence on the top quark mass within ± 10 GeV/c^2 while $\sigma_{t\bar{t}}$ varies by ∓ 0.09 pb per ± 1 GeV/c^2 in the same mass range. The total uncertainty on R in this measurement is 9%, dominated by the statistical uncertainty of $^{+0.067}_{-0.065}$ and the largest systematic uncertainty from the b tagging efficiency estimation of $^{+0.059}_{-0.047}$. The cross section measurement yields a result similar but not identical to the measurement on the same dataset [264] presented in Section 5.1.2 due to the assumption of $R = 1$ and a slightly different event selection in the latter analysis.

CDF performed the first measurement of R in Run I using both dilepton and lepton plus jets events on 0.1 fb^{-1} of data [466] and has repeated the analysis in Run II on 0.2 fb^{-1} of data [465], finding good agreement with the Standard Model expectation in both cases.

All measurements of R performed so far at the Tevatron are summarised in Figure 45.

6.3 Search for Neutral Current Top Decays

Flavour changing neutral interactions of the top quark with a light quark $q = u, c$ and gauge (Z, γ, g) or Higgs (H^0) bosons are not present at tree level and suppressed by the GIM mechanism [56] at the one loop level in the Standard Model framework. Consequently, the corresponding FCNC top quark decays are expected to occur with branching ratios at $\mathcal{O}(10^{-12})$ and below [414], well out of reach to be observed at the Tevatron or LHC. Any observation of such FCNC decays would signal physics beyond the Standard Model.

Many extensions of the Standard Model predict the occurrence of FCNC interactions, affecting both the electroweak single top production (see Section 5.8.5) and the top quark decay rate. The branching fractions of FCNC top decays can increase by many orders of magnitude in such models, like for example in Supersymmetry [467–469], additional broken symmetries [470], dynamical EWSB [471, 472] including topcolour-assisted technicolour [473] or extended Higgs models like Two Higgs Doublet Models [474–477]. Overviews over various exotic models and their impact on top couplings are given in [414, 478–480].

A search for the top quark FCNC decay $t \to Zq$ at the Tevatron is considered especially interesting due the large top quark mass and very distinct experimental signature (see Figure 46). It was already suggested in 1989 [481], well before the discovery of the top quark. The expected sensitivity for such a branching ratio measurement is $\mathcal{O}(10^{-2})$ at the Run II Tevatron and $\mathcal{O}(10^{-4})$ at the LHC [482], while the largest expected branching fractions from Standard Model extensions reach up to $\mathcal{O}(10^{-2})$ [471] respectively $\mathcal{O}(10^{-4})$ [414]. The best published limit before Run II on $\mathcal{B}(t \to Zq)$ was obtained at LEP by the L3 Collaboration via a search for single top quark production where no significant deviation from the Standard Model background expectation was observed, yielding $\mathcal{B}(t \to Zq) < 13.7\%$ at 95% C.L. [416].

In Run I, the CDF Collaboration performed a search for the FCNC decays $t \to Zq$ and $t \to \gamma q$ on a dataset with an integrated luminosity of 0.1 fb^{-1} [421]. In the $t \to \gamma q$ search, a photon is reconstructed as an energy cluster in the electromagnetic calorimeter with no track or with one single soft

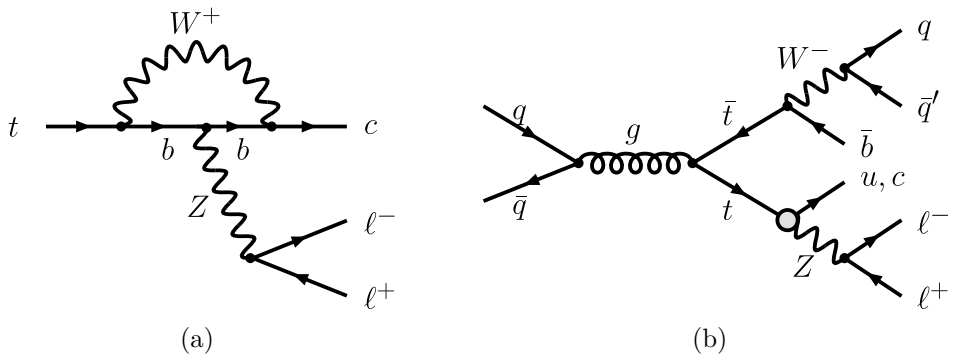

Figure 46: (a) Feynman "penguin" diagram for the FCNC decay $t \to Zc$ with $Z \to \ell^+\ell^-$. Including the corresponding diagrams with a d and s quark in the loop, the process is nearly cancelled in the Standard Model. (b) Event signature for a top quark pair containing one FCNC $t \to Zq$ decay and one hadronical W boson decay from $t \to Wb$, resulting in a final state containing a Z boson and four jets.

track (presumably a random overlap) carrying less than 10% of the photon energy pointing to the cluster. Two event signatures are considered where the W boson from the Standard Model-like second top decay decays either leptonically into $e\nu_e$ or $\mu\nu_\mu$ or hadronically into quarks $\bar{q}q'$. Consequently, these samples are selected by requiring either a charged lepton (e or μ), $\not\!\!E_T$, at least two jets and a photon or by requiring at least four jets and a photon. In both samples, a photon-jet combination must yield a mass between 140 and 210 GeV/c^2 and the Standard Model-like top decay must contain one b tag. 40% of the $t \to \gamma q$ acceptance comes from the photon plus multijet selection, while the lepton plus photon mode contributes 60%. After all selection cuts, one event remains in the leptonic channel and none in the photon plus multijet channel, with an expected background of about 0.5 events mainly from $W\gamma$ production with additional jets in each channel. This translates into a 95% C.L. upper limit on the branching fraction of $\mathcal{B}(t \to c\gamma) + \mathcal{B}(t \to u\gamma) < 3.2\%$.

In the $t \to Zq$ search, hadronic W boson decays from the Standard Model-like second top decay are considered together with a leptonically decaying Z boson into e^+e^- or $\mu^+\mu^-$. Using the leptonic W boson decay as well does not substantially increase the acceptance and consequently does not improve the limit. The resulting event signature contains four jets and two leptons with an invariant mass consistent with a Z boson, as illustrated in Figure 46. Since the branching ratio of $Z \to e^+e^-/\mu^+\mu^-$ is small, this search is less

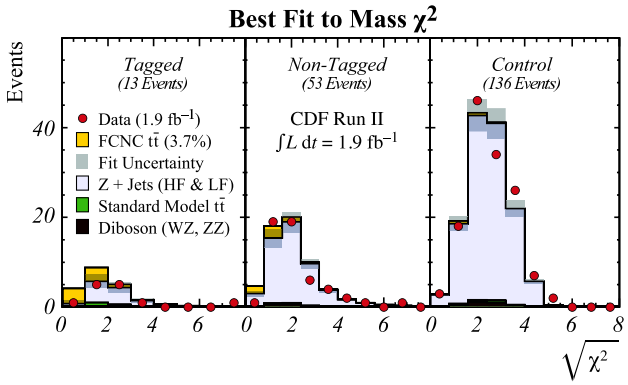

Figure 47: Expected and observed mass χ^2 distributions of $Z+ \geq 4$ jets events in signal samples with $\geq$1 and 0 b tags and a background enriched sample to control uncertainties of the background shape and normalisation in a 1.9 fb^{-1} dataset [424]. The expected FCNC $t \to Zq$ signal with the observed 95% C.L. upper limit on the branching fraction is shown as well.

sensitive than the $t \to \gamma q$ one. One $Z \to \mu^+\mu^-$ event passes the selection, with an expected background of about 0.6 events from $Z+$ multijet and $t\bar{t}$ production. This corresponds to a 95% C.L. upper limit on the branching fraction of $\mathcal{B}(t \to cZ) + \mathcal{B}(t \to uZ) < 33\%$. These measurements can be translated into limits on the FCNC couplings κ_γ and κ_Z at 95% C.L. [420]: $\kappa_\gamma^2 < 0.176$ and $\kappa_Z^2 < 0.533$ (see also Section 5.8.5 and Figure 35).

In Run II, the CDF Collaboration has performed a search for the FCNC decay $t \to Zq$ on a dataset with an integrated luminosity of 1.9 fb^{-1} [424]. Events consistent with a leptonically decaying Z boson to e^+e^- or $\mu^+\mu^-$ are selected together with at least four jets, one of which can be b tagged (see Figure 46). The event selection was optimised for a preceding version of this analysis on 1.1 fb^{-1} of data [483], a blind cut-based counting experiment. By requiring only one well-identified lepton for the Z reconstruction while the second lepton can be formed from an isolated track, the acceptance is doubled compared to using only fully identified leptons. The sensitivity of the search is further increased by dividing the data into two subsamples, one b tagged and one non-b tagged. The best discriminant found to separate signal from background processes is a mass χ^2 variable that combines the kinematic constraints present in FCNC decays: two jets in the event have to form a W boson and together with a third jet a top quark, while the Z boson has to form a top quark with the fourth jet. Because the event signature does not contain any neutrinos, the events can be fully reconstructed. The signal fraction in the selected dataset is determined via a template fit in signal

samples with 0 or ≥ 1 b tags and a background-enriched control sample to constrain uncertainties on the background shape and normalisation (see Figure 47).

Since the observed distributions are consistent with the Standard Model background processes, a 95% C.L. upper limit on the branching fraction is derived: $\mathcal{B}(t \to cZ) + \mathcal{B}(t \to uZ) < 3.7\%$. The expected limit in absence of signal is 5%. This is the best limit on $\mathcal{B}(t \to Zq)$ to date, starting to constrain the predictions made in a dynamic EWSB model [471].

6.4 Search for invisible Top Decays

Apart from the direct search for $t \to Z/\gamma\ q$ decays as described in the last section, one can also perform an indirect search for "invisible" top quark decays by comparing the predicted $t\bar{t}$ production cross section with the observed yield in data. In order to be sensitive to novel top decay modes with this method, these decays must exhibit a significantly different acceptance from the Standard Model top quark decay.

Based on a 1.9 fb^{-1} double b tagged lepton plus jets dataset, CDF searches for deviations of the observed $t\bar{t}$ production rate from the theoretical prediction [126] due to the decays $t \to Zc$, $t \to gc$, $t \to \gamma c$ and $t \to$ invisible [484]. These decays exhibit a relative acceptance $\mathcal{R}_{\mathrm{WX/WW}}$ where one novel and one Standard Model top quark decay occurs normalised to the Standard Model $t\bar{t}$ decay acceptance from 32% down to 0%.

With an observed $t\bar{t}$ production cross section of 8.8 pb and a prediction of 6.7 pb for a top quark mass of 175 GeV/c^2, the obtained limits on the novel top quark decay modes are all lower than expected, but statistically consistent with the expectation. The obtained results are summarised in Table 19 for top quark masses of 170, 172.5 and 175 GeV/c^2.

6.5 Search for Top Decays to Charged Higgs Bosons

The framework of the Standard Model incorporates one Higgs doublet of complex scalar fields to break the electroweak symmetry and generate masses for weak gauge bosons and fermions (see Section 2.1). As a consequence, one obtains one neutral scalar CP-even particle that still remains to be discovered, the Higgs boson H. A straightforward and simple extension of the Standard Model Higgs sector is possible by introducing a second Higgs doublet, referred to as Two Higgs Doublet Models (THDM, 2HDM) [409, 410]. These models yield five physical scalar Higgs bosons after electroweak symmetry breaking: two neutral CP-even Higgs bosons H^0 and h^0, one neutral pseudoscalar CP-odd Higgs particle A^0 and two charged Higgs bosons $H^{\pm}$. The

Decay	$\mathcal{R}_{\mathrm{WX/WW}}$ [%]	Limit [%] (175 GeV/c^2)	Limit [%] (172.5 GeV/c^2)	Limit [%] (170 GeV/c^2)
$\mathcal{B}(t \to Zc)$	32	13	15	18
$\mathcal{B}(t \to gc)$	27	12	14	17
$\mathcal{B}(t \to \gamma c)$	18	11	12	15
$\mathcal{B}(t \to$ invisible)	0	9	10	12

Table 19: Relative signal acceptances and observed 95% C.L. upper limits on the branching fractions for various non-Standard Model top quark decay modes and assumed top quark masses in a 1.9 fb^{-1} double b tagged lepton plus jets dataset [484].

observation of charged Higgs bosons thus would be clear evidence for physics beyond the Standard Model.

Three different choices of the Higgs-fermion couplings are differentiated in THDMs. In type-I models only one of the two Higgs doublets couples to the fermions, while in type-II models one doublet couples to the up-type fermions and the other doublet to the down-type fermions alone. Type-III models allow for general Higgs-fermion Yukawa couplings of both Higgs doublets, leading to Higgs-mediated FCNCs at tree level which requires tuning of the Higgs parameters to ensure sufficient FCNC suppression compatible with experimental limits. One example for a type-II THDM is the Minimal Supersymmetric Standard Model (MSSM) [368] which is frequently used in the analyses described below as reference. The relevant model parameters in searches for charged Higgs bosons are the ratio of the two Higgs doublets' vacuum expectation values $\tan\beta$ and the mass of the charged Higgs boson $m_{H^\pm}$.

The inclusive single charged Higgs boson production rate $\sigma(p\bar{p} \to tH^-X)$ reaches a maximum of $\mathcal{O}(1$ pb) at the Tevatron where the charged Higgs boson can be produced via the decay of a top quark. The corresponding inclusive cross section for pair production of charged Higgs bosons $\sigma(p\bar{p} \to H^+H^-X)$ is below $\mathcal{O}(0.1$ pb) [485, 486].

The decay mode $t \to Hb$ is kinematically accessible if the mass of the charged Higgs boson is smaller than the difference of top and b quark mass $m_{H^\pm} < m_t - m_b$ and will then compete with the Standard Model decay $t \to Wb$. The distinct top quark decay signature gives an additional handle for background suppression compared to direct production of charged Higgs bosons. The branching fraction of $t \to Hb$ depends on $\tan\beta$ and $m_{H^\pm}$. As illustrated in Figure 48 for the MSSM, the branching ratio of $t \to Hb$

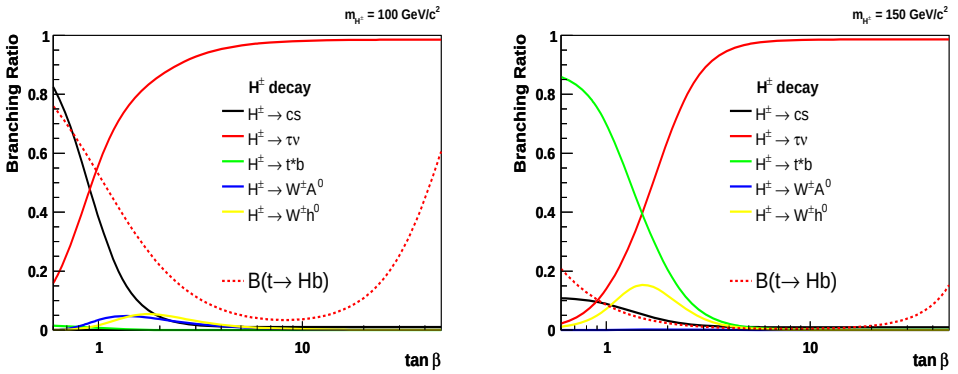

Figure 48: Branching ratios for top quark and charged Higgs boson decays versus $\tan\beta$ in the MSSM framework as simulated with CPsuperH [487] for $m_{H^\pm} = 100$ GeV/c^2 (left) and $m_{H^\pm} = 150$ GeV/c^2 (right).

increases significantly for small $\tan\beta \lesssim 1$ and large $\tan\beta \gtrsim 40$ for a given $m_{H^\pm}$; the Standard Model decay is assumed to account for the difference from unity. For a given $\tan\beta$ the branching ratio of $t \to Hb$ decreases with increasing $m_{H^\pm}$. The decay of $H^\pm$ is dominated by $H^\pm \to \tau\nu$ for large $\tan\beta$ independent of $m_{H^\pm}$ which would result in an excess of $t\bar{t}$ events in the τ decay channel compared to Standard Model expectation. At small $\tan\beta$ the decay $H^\pm \to cs$ is enhanced for low $m_{H^\pm}$ while $H^\pm \to t^*b$ dominates for $m_{H^\pm}$ approaching the top quark mass. Consequently, searches for charged Higgs bosons focus on these three fermionic decay modes.

In the early 1990s – before the discovery of the top quark – first searches for $t \to Hb$ in the $H^\pm \to \tau\nu$ decay mode for fixed assumed branching fractions were performed and limits derived in the m_t versus $m_{H^\pm}$ parameter space by the UA1 and UA2 experiments [488, 489] at the CERN $Sp\bar{p}S$ collider and also at the Run I Tevatron by CDF [490, 491]. All four LEP experiments searched for pair-production of charged Higgs bosons in $e^+e^- \to H^+H^-$, assuming only the decays $H^\pm \to \tau\nu$ and $H^\pm \to cs$ can occur [492–495] as favoured by type-II THDMs. The dominant background in the resulting three decay modes is pair production of W bosons, yielding similar final states. 95% C.L. lower mass limits independent of the $H^\pm$ decay mode are provided, yielding 78.6 GeV/c^2 in a preliminary combination of all four experiments [496], since then superseded by the more stringent limit derived by ALEPH, yielding 79.3 GeV/c^2 [495].

Indirect limits on the mass of the charged Higgs boson can be derived from measurements of the $b \to s\gamma$ FCNC process at B factories since the involved loop diagrams are sensitive to contributions from new particles like $H^\pm$. For

a type-II THDM scenario, at 95% C.L. a lower mass limit of 295 GeV/c^2 can be derived [497] if the used theoretical description is assumed to be complete. Direct searches are less model dependent and are hence an important tool to scan for new physics beyond the regions of parameter space excluded by the corresponding direct analyses described above. The searches for $t \to Hb$ performed at the Tevatron are based on type-II THDM scenarios.

After the discovery of the top quark, the first searches for $H^\pm$ in top decays $t\bar{t} \to H^\pm W^\mp b\bar{b}, H^\pm H^\mp b\bar{b}$ focussed on the decay $H^\pm \to \tau\nu$ corresponding to large $\tan\beta$. CDF published an analysis superseding and extending a previous result [498], requiring inclusive final states with $\not\!\!E_T$, a hadronically decaying tau lepton τ_h and (i) two jets and one or more additional either lepton or jet or (ii) a second energetic τ_h [499]. Another search investigated the dilepton channels $e\tau_h, \mu\tau_h$ with $\not\!\!E_T$ and at least two jets [500]. D0 performed a first $H^\pm$ analysis in Run I based on a disappearance search in the lepton plus jets channel sensitive to the $H^\pm$ fermionic decay modes, looking for a discrepancy in the event yields with respect to the Standard Model predictions [501]. This analysis was then complemented by a direct search for $H^\pm \to \tau\nu$ with a hadronically decaying τ reconstructed as narrow jet in a dataset with events containing $\not\!\!E_T$ and at least four but no more than eight jets [502]. All analyses observe good agreement with the Standard Model expectation and provide limits in the $\tan\beta, m_{H^\pm}$ plane.

It should be noted these limits are derived based on tree level MSSM calculations of the involved branching fractions depending on $\tan\beta$. By now it has become clear that higher-order radiative corrections which strongly depend on model parameters will modify these predictions significantly [503, 504]. Also, non-fermionic $H^\pm$ decay modes can have non-negligible contributions in the small $\tan\beta$ region as illustrated in Figure 48, affecting the limits derived in that area without taking this into account. Independent of these issues, one can still provide upper limits on $\mathcal{B}(t \to Hb)$ based on the observed production rate for a fixed assumed $H^\pm$ branching ratio. For example, for a purely tauonically decaying charged Higgs boson, 95% C.L. upper limits on $\mathcal{B}(t \to Hb)$ are found to be between 0.5 and 0.6 for 60 GeV/c^2 $\leq m_{H^\pm} \leq$ 160 GeV/c^2 by CDF [500]. The combined D0 result corresponds to $\mathcal{B}(t \to Hb) < 0.36$ at 95% C.L. for $m_{H^\pm} <$ 160 GeV/c^2 and $0.3 < \tan\beta < 150$ – the full range where the leading order MSSM calculation is valid [502].

CDF published a first search for $t \to Hb$ in Run II using a dataset of 0.2 fb^{-1} integrated luminosity [505]. The search is based on the corresponding $t\bar{t}$ cross section analyses [208, 219, 254] exhibiting the signature $\not\!\!E_T$ + jets + ℓ + X, where ℓ corresponds to an electron or muon and X to either ℓ (dilepton channel), τ_h (lepton plus tau channel) or one or more b tagged jets (lepton plus jets channels). Dropping the assumption of $\mathcal{B}(t \to Hb) = 0$ and ensuring

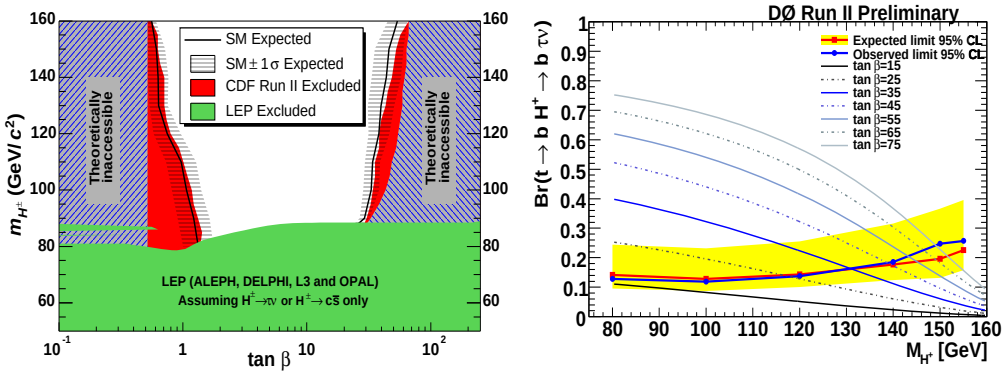

Figure 49: Left: Expected and observed 95% C.L. exclusion limits for charged Higgs bosons in the $(m_{H^\pm}, \tan\beta)$ plane derived by CDF for a MSSM benchmark scenario discussed in [505]. Right: Expected and observed 95% C.L. limits on $\mathcal{B}(t \to Hb)$ versus $m_{H^\pm}$ derived by D0 for a tauonic charged Higgs model using a simultaneous fit of $\mathcal{B}(t \to Hb)$ and $t\bar{t}$ production cross section [259]. MSSM tree-level predictions for various $\tan\beta$ values are shown as well.

no overlaps of the channel selections, the observed yields can be compared with the expected deficits or excesses in the channels with respect to the Standard Model prediction depending on the top quark and $H^\pm$ branching fractions. Apart from the Standard Model top quark decay, $t \to Hb$ is considered with $H^\pm$ decaying to $\tau\nu$, cs, t^*b or Wh^0, with $h^0 \to b\bar{b}$. The $t\bar{t}$ production rate is assumed to be not affected by the extension of the Higgs sector. Since no $H^\pm$ signal is observed, 95% C.L. upper limits on $\mathcal{B}(t \to Hb)$ are obtained for example for a tauonic Higgs model ($\mathcal{B}(H^\pm \to \tau\nu) = 1$) to be 0.4 for 80 GeV/c^2 $\leq m_{H^\pm} \leq$ 160 GeV/c^2. 95% C.L. limits are also derived in the $(m_{H^\pm}, \tan\beta)$ parameter space in the framework of the MSSM for certain benchmark scenarios of parameters, taking radiative corrections into account. While the excluded area for large $\tan\beta$ strongly depends on the different benchmarks investigated, this is not the case for small $\tan\beta$. An example result is shown in Figure 49.

D0 performs a similar analysis based on the same $t\bar{t}$ final states with 1 fb^{-1} of integrated luminosity [259]. Two different models for the decay mode of the charged Higgs boson are studied: a tauonic Higgs model ($\mathcal{B}(H^\pm \to \tau\nu) = 1$) that would result in an enhancement of the lepton plus tau channels and a deficit in the lepton plus jets and dilepton channels and a leptophobic model ($\mathcal{B}(H^\pm \to cs) = 1$) that would lead to an enhancement of the all-hadronic channel and a deficit in all channels considered in this analysis. For

both model assumptions good agreement with the Standard Model prediction is observed and 95% C.L. upper limits on $\mathcal{B}(t \to Hb)$ are provided for 80 GeV/c^2 $\leq m_{H^\pm} \leq$ 155 GeV/c^2, yielding 0.16 - 0.20 for the tauonic and 0.2 for the leptophobic model. The dominant systematic uncertainties arise here from the uncertainties on the $t\bar{t}$ cross section and the luminosity.

For the tauonic model, an improvement of the obtained limits by about 30% in the low $m_{H^\pm}$ range is possible when the $t\bar{t}$ cross section is allowed to float in the fit rather than being fixed to the Standard Model value. The resulting limits are displayed in Figure 49, ranging from 0.12 to 0.26 in the considered $m_{H^\pm}$ range. Assuming the Standard Model scenario of $\mathcal{B}(t \to Hb) = 0$, a combination of the $t\bar{t}$ cross section from the analysed final states is obtained as well and is shown in Section 5.1.5.

As illustrated in Figure 49, the results obtained in [505] leave room for improvement particularly in the area of $\tan\beta \approx 1$ and $m_{H^\pm}$ above the W boson mass. For this range of parameters, the MSSM predicts the decay $H^\pm \to cs$ to occur with a significant branching fraction. CDF has searched for $t \to Hb$ in this decay channel in 2.2 fb^{-1} double b tagged lepton plus jets data [506]. Both Standard Model and exotic decay exhibit the same final state but can be distinguished via the dijet invariant mass, where the untagged leading two jets are assigned as $W^\pm/H^\pm$ decay products. A binned likelihood fit using $W^\pm/H^\pm$ dijet mass templates yields no significant excess over the Standard Model prediction and 95% C.L. upper limits on $\mathcal{B}(t \to Hb)$ are provided for 90 GeV/c^2 $\leq m_{H^\pm} \leq$ 150 GeV/c^2, assuming a leptophobic Higgs model. The limits range from 8% for $m_{H^\pm} = 130$ GeV/c^2 to 32% for $m_{H^\pm} = 90$ GeV/c^2, complementing the analysis by D0 described above for the mass range above 100 GeV/c^2.

A first direct search for charged Higgs boson production in the mass range above the top quark mass via the process $q\bar{q}' \to H^\pm \to tb$ has been performed by D0 and is discussed in the single top production chapter, Section 5.8.4.

7 Top Quark Properties

In the last two chapters it was demonstrated that both top quark production and decay so far have been found to be consistent with the Standard Model expectations. No new particles or anomalous couplings have been observed yet. To actually confirm the top quark's Standard Model identity, its fundamental quantum numbers need to be measured and their self-consistency in the Standard Model framework needs to be confirmed as well.

In this chapter, measurements of the fundamental top quark properties performed so far at the Tevatron are described: electric charge, lifetime and

mass. Again top quark pair events are used, providing higher statistics and favourable sample purities compared to single top events. First direct measurements of the V_{tb} matrix element in electroweak single top quark production have already been discussed in Section 5.8.1.

7.1 Top Quark Electric Charge

The electric charge of quarks can for example be determined in electron-positron collisions via the ratio of the hadronic cross section to the muon cross section $R = \sigma(e^+e^- \to \text{hadrons})/\sigma(\text{e}^+\text{e}^- \to \mu^+\mu^-)$ which is proportional to the sum of the squared electric charges of the quark flavours accessible at the centre of mass energy chosen. Due to the large top quark mass however, such a direct measurement could not yet be performed at past and current electron-positron colliders. Also a direct measurement via photon radiation in $t\bar{t}$ events at hadron colliders that would give access to the top quark's charge and its electromagnetic coupling is unrealistic due to limited statistics at the Tevatron [507]. Consequently, the top quark is the only quark whose fundamental quantum numbers of weak isospin and electric charge so far could only be determined indirectly in the framework of the Standard Model from measurements of its weak isospin partner, the b quark, to be $T_3 = +\frac{1}{2}$, $Q_t = +\frac{2}{3}e$ (see Section 2.2).

Information on the electric charge of the top quark can also be inferred from the electric charges of its decay products. However, there is an inherent ambiguity in top quark pair events $p\bar{p} \to t\bar{t} \to W^+W^-b\bar{b}$ when pairing W bosons and b jets resulting in possible charges of $|Q|= 2e/3$ or $4e/3$. The existence of an exotic quark with charge $-4e/3$ being the discovered particle at the Tevatron instead of the Standard Model top quark would be compatible with electroweak precision measurements if the right-handed b quark mixes with the $-1e/3$ charged exotic doublet partner of such an exotic top quark. The Standard Model top quark with charge $2e/3$ would not have been discovered yet in this scenario due to its large mass of 271^{+33}_{-38} GeV/c^2 [365, 508, 509].

D0 has published a first measurement discriminating between the $2e/3$ and $4e/3$ top quark charge scenarios in a 0.4 fb^{-1} lepton plus jets dataset with at least two b tagged jets [510]. The obtained sample exhibits a high signal purity, with the two dominant background processes $Wb\bar{b}$ and single top production contributing 5% respectively 1% to the selected events. Each $t\bar{t}$ event provides two measurements of the absolute value of the top quark charge, one from the leptonic and one from the hadronic $t \to Wb$ decay chain. The charge of the W boson is determined from the (inverse) lepton charge for the leptonic (hadronic) W boson decay. The b jet charge discriminating between b and $\bar{b}$ jets is determined using a jet charge algorithm based on

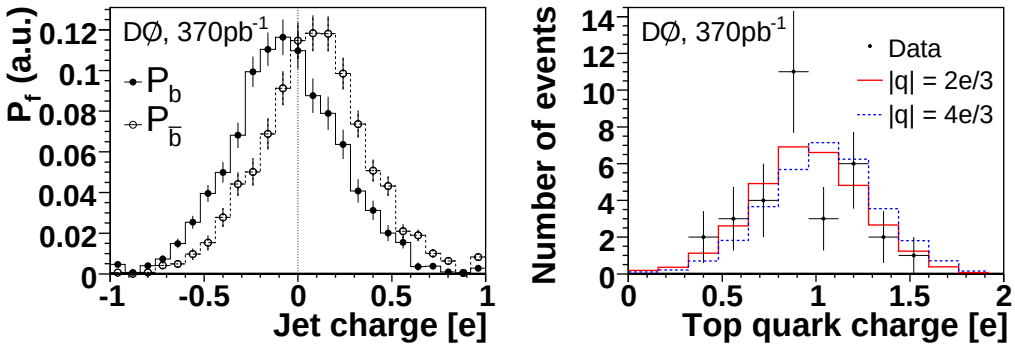

Figure 50: Left: $b/\bar{b}$ jet charge distributions obtained in dijet data. Right: Distribution of the top quark charge obtained in data, overlaid with the expectations from Standard Model and exotic model [510].

the p_T weighted average of the charges of the tracks associated with the b tagged jet. The corresponding distributions are derived from dijet collider data (see Figure 50). The top quark charge observable is then the absolute value of the sum of the W boson- and associated b jet charge, where the right pairing is determined with a constrained kinematic fit. By comparing the obtained distribution in data with the expected shape from the Standard Model respectively exotic model (see Figure 50), D0 excludes the hypothesis of only exotic quarks of charge $|Q|= 4e/3$ being produced at up to 92% C.L. and limits an exotic quark admixture in the sample to be at most 80% at the 90% C.L..

Using a similar analysis approach, CDF obtains a preliminary result on the top quark charge using double b tagged lepton plus jets and b tagged dilepton events in a 1.5 fb^{-1} dataset [511]. The observed $2\ln$(Bayes Factor) is 12, meaning that the data favour very strongly the Standard Model top quark hypothesis over the exotic model.

While the results from CDF and D0 are not directly comparable due to different statistical approaches in the interpretation of their results, both agree to favour the Standard Model top quark charge hypothesis. This is supported by the searches for new heavy top-like quark pair production (see Section 5.7.4) starting to exclude additional quark production in the mass range predicted by the exotic model. A top quark charge measurement determining the b jet charge in soft lepton tagged events from the soft lepton charge rather than the currently used track-based approach has not been performed yet.

The measurement of the top quark charge in $t\bar{t}\gamma$ events will be possible at

the LHC both due to the increased production rate and due to the reduction of irreducible background from photons radiated off the incoming quarks in $t\bar{t}$ production via $q\bar{q}$ annihilation. Consequently, top quark charge measurements via photon radiation in $t\bar{t}$ events are predicted to achieve a precision of 10% [507]. Using the top quark decay products to provide an additional charge measurement will allow one to disentangle the measurements of top quark electromagnetic coupling strength from the top quark charge in the $t\bar{t}\gamma$ events. This will help to rule out possible anomalous admixtures in the electromagnetic interaction of the top quark.

7.2 Top Quark Lifetime

The lifetime of the top quark $\tau_t = \Gamma_t^{-1} \approx (1.3\ \mathrm{GeV/c^2})^{-1}$ is approximately $5 \cdot 10^{-25}$ s in the framework of the Standard Model as discussed in Section 3.3.2. Consequently, the production and decay vertices of the top quark are separated by $\mathcal{O}(10^{-16})$m, orders of magnitude below the spatial resolution of any detector. Also the top quark width is narrower than the experimental resolution at both the Tevatron and the LHC. Consequently, a direct measurement of the top quark lifetime respectively its width will be limited by the detector resolution. A measurement of the top quark lifetime is still useful to confirm the Standard Model nature of the top quark and exclude new top quark production channels via long-lived particles. A measurable lifetime of the top quark itself would imply a correspondingly small V_{tb} matrix element and render single top quark production at the Tevatron undetectable, in contradiction with the observed first evidence described in Section 5.8.

CDF has set limits on the top quark lifetime respectively width using two different approaches. One analysis uses a b tagged lepton plus jets dataset of 0.3 fb^{-1} [512] to measure the impact parameter (smallest distance) between the top quark production vertex and the lepton track from the leptonic W boson decay in the plane orthogonal to the beam direction. Fitting the obtained distribution with signal Monte Carlo templates for $c\tau_t$ between 0 and 500 μm and a background template, the 0 μm template describes the data best which translates into a 95% C.L. limit of $c\tau_t < 52.5$ μm.

The second analysis uses a b tagged lepton plus jets dataset of 1 fb^{-1}[513] to reconstruct the top quark mass in each event using a kinematic fit. The observed distribution is compared in a fit to $t\bar{t}$ signal Monte Carlo templates of various widths for a top quark mass of 175 GeV/c^2 and background templates. From the fit result, at 95% C.L. the top quark width is found to be smaller than 12.7 GeV/c^2, corresponding to a lower limit on the top quark lifetime of $5.2 \cdot 10^{-26}$ s.

7.3 Top Quark Mass

The top quark is set apart from all other known fundamental particles by its large mass. Being the only particle with its Yukawa coupling close to unity raises the question whether it plays a special role in the process of mass generation. Since the lifetime of the top quark is so short (see Sections 3.3.2 and 7.2), it does not hadronise unlike the other quarks and hence properties like its mass can be determined directly without the complication of studying a quark embedded in a hadron. Being a sensitive probe for physics beyond the Standard Model, it is important to measure its mass also in the various decay modes that could be affected differently by novel physics contributions.

In the framework of the Standard Model, the top quark mass is a free parameter. As discussed in Section 2.3, its precise determination together with a precise W boson mass measurement allows both to test the self-consistency of the theoretical framework and to constrain the mass of the yet undiscovered Higgs boson (or also new particles [514, 515]) via electroweak radiative corrections.

Measurements of the top quark mass have been performed so far only in $t\bar{t}$ events, mainly in the dilepton, lepton plus jets and all-hadronic final states. A complete kinematic reconstruction of the top quark pair from the measured objects in the event can be performed in the all-hadronic final state where no neutrinos are present. Assuming $\not\!\!E_T$ arises solely from the neutrino in the lepton plus jets channel, a kinematic fit can be performed here constraining the invariant mass of charged lepton and neutrino to that of the W boson, yielding a twofold ambiguity for the neutrino longitudinal momentum solution. Due to the presence of two neutrinos contributing to $\not\!\!E_T$ in the dilepton final state however, a direct kinematic reconstruction is not possible here without adding more information respectively making assumptions on the kinematics of the involved objects.

Since the assignment between partons and reconstructed objects in the event is unknown, additional combinatorial ambiguities arise in all channels. Depending on the analysis technique pursued, either all combinations are used to extract the top quark mass or the best combinations – for example based on the lowest χ^2 with respect to the $t\bar{t}$ event hypothesis obtained in a kinematic fit – are selected. b jet identification can be used to reduce the number of combinations to be considered in the lepton plus jets and the all-hadronic channel. Even if both b jets from the $t\bar{t}$ decay are identified, in the lepton plus jets channel four combinations remain to be considered including the neutrino p_z ambiguity and six in the all-hadronic channel. In these channels, usually at least one b tagged jet is required to increase the sample purity, or datasets are split up with respect to b tag multiplicity and

hence different purity to optimise the overall sensitivity.

The techniques used in top quark mass analyses can be divided into three categories:

(i) Template Method (TM): Observables that are sensitive to the mass of the top quark like the reconstructed top quark mass m_{reco} or H_T are evaluated in the dataset under consideration. The resulting distribution is then compared in a fit with those for contributing background processes and top quark signal with varying top quark masses.

(ii) Matrix Element Method (ME): Using the four-vectors of the reconstructed objects, for each event a probability density is calculated as a function of the top quark mass, based on the leading order matrix elements of the contributing signal and background processes. The total likelihood of the dataset is obtained as the product of the individual event likelihoods. This method is also referred to as Dynamical Likelihood Method (DLM).

(iii) Ideogram Method (ID): An event-by-event likelihood depending on the assumed top quark mass is formed based on a constrained fit of the event kinematics, taking all object permutations and possible background contributions into account. As mentioned above, such a constrained fit is only possible in the all-hadronic and lepton plus jets channels.

Naturally, the analyses most sensitive to the top quark mass are also very sensitive to the jet energy scale (JES) calibration. The systematic uncertainty due to the external jet energy calibration (see Section 4.3.3) then is usually the by far dominating systematic uncertainty in such an analysis. It can be reduced in the decay channels where at least one W boson decays hadronically by using the well-measured W boson mass to constrain "in-situ" the jet energy calibration in top quark events [516, 517]. Deriving such an overall scale factor for jet energies absorbs a large part of this uncertainty into an uncertainty scaling with sample statistics, while residual uncertainties for example due to η and p_T dependences of JES corrections and differences between light quark and b quark JES remain. By performing an analysis simultaneously in the dilepton and all-hadronic and/or lepton plus jets channels, the in-situ JES calibration can also be transferred to the dilepton channel [518].

Another approach to reduce the dependence of top quark mass measurements on the JES is to utilise observables with minimal JES dependence that are still correlated with the top quark mass like the mean p_T of the charged

lepton from the W boson decay p_T^ℓ or the mean transverse decay length of b jets L_{xy} in $t\bar{t}$ events [519]. While such measurements are statistically limited at the Tevatron, their uncertainties are basically uncorrelated with those of other statistically more sensitive analyses. This is useful to reduce the overall uncertainty on the top quark mass when combining all measurements. To increase the overall sensitivity on the top quark mass, one can also use the observed signal event yield via the mass dependence of the $t\bar{t}$ production cross section as an additional constraint [520].

Performance, calibration and statistical uncertainty derivation of each analysis are checked using sets simulated pseudo-experiments (ensemble tests), based on mean and rms of the obtained mass and pull distributions.

Measurements of the top quark mass were pioneered in Run I based on 0.1 fb^{-1} of data by both experiments in the dilepton [317, 521–524], lepton plus jets [320, 321, 446, 525, 526] and all-hadronic [527, 528] channels. A combination of the Run I mass results yields $m_t = 178.0 \pm 2.7(\text{stat.}) \pm 3.3(\text{syst.})$ GeV/c^2 [159]. Also in Run II, results are derived mainly in the dilepton, lepton plus jets and all-hadronic channels, with the most precise results coming from lepton plus jets samples. One analysis uses an inclusive $\not\!\!E_T$ plus jets signature, vetoing energetic isolated leptons and thus enhancing the τ plus jets signal contribution to 44% [529]. This result is listed together with measurements in the all-hadronic channel in Section 7.3.3 and is consistent with the world average top quark mass. A top quark mass measurement with explicit hadronic τ reconstruction has not been performed so far, but given the recent progress in the corresponding cross section analyses discussed in Section 5.1.4, this could still be feasible at the Tevatron.

In the following sections, the most recent final Run I results are given along with the current preliminary respectively published Run II top quark mass measurements using various analysis techniques for each of the three decay channels. Some of the most precise analyses entering the world average top quark mass combination will be highlighted. A more detailed review of the top quark mass analysis techniques pursued at the Tevatron can be found in [530]. The final section presents the current world average and some of its implications.

7.3.1 Dilepton Final State

Analyses in the dilepton final state are performed either based on the matrix element or the template method. For the template approach, additional assumptions on the kinematics of the involved objects are made in order to be able to solve the otherwise underconstrained system kinematics. Assuming various top quark masses, the consistency of the observed event kinematics

can be used to obtain weights for each event versus top quark mass based on input parton distribution functions and the observed charged lepton energies ("matrix weighting" $\mathcal{M}$) or using simulated neutrino pseudo-rapidity or azimuthal angle ("neutrino weighting": ν_η, ν_ϕ) or $t\bar{t}$ longitudinal momentum ($p_z^{t\bar{t}}$) distributions [522, 531]. Top quark mass estimators are derived from the obtained weight distributions like the peak mass position or mean and rms of the distributions. These are then used in a template fit to obtain the top quark mass from the data sample.

The most precise top quark mass result in the dilepton channel entering the world average has been obtained by D0 with a precision of 2.2% [532]. It combines results from neutrino weighting (ν_η) obtained on 1 fb^{-1} in the dielectron, dimuon and lepton plus track channels [533] with a measurement in the $e\mu$ channel based on 2.8 fb^{-1} of data using the matrix element method [532].

The matrix element method evaluates the probability density for each event P_{evt} with measured object four-vectors x to arise from $t\bar{t}$ production depending on the top quark mass or from the dominant background arising from $Z \to \tau\tau$ plus jets production in the following linear combination, based on the known expected signal fraction in the sample f:

$$P_{\text{evt}}(x; m_t) = f \cdot P_{\text{sig}}(x; m_t) + (1 - f) \cdot P_{\text{bkg}}(x).$$

P_{sig} and P_{bkg} are the signal and background probability densities for $t\bar{t}$ and $Z \to \tau\tau$ plus jets production, based on the leading order matrix element for $q\bar{q} \to t\bar{t}$ respectively the VECBOS [544] parametrisation of the matrix element. The probability densities are calculated by integrating over all unknown quantities like the unmeasured neutrino energies and all parton states that can lead to x observed in the detector:

$$P_{\text{sig}}(x; m_t) = 1/\sigma_{\text{obs}}(m_t) \int_{q_1,q_2,y} \sum_{\text{flavours}} dq_1 dq_2 f(q_1) f(q_2) \frac{(2\pi)^4 |\mathcal{M}|^2}{q_1 q_2 s} d\Phi_6 W(x, y),$$

where q_1 and q_2 are the momentum fractions of the colliding partons from proton and antiproton, $f(q_i)$ the corresponding PDFs, $\mathcal{M}$ is the matrix element for the signal process yielding the partonic final state y, s is the squared centre-of-mass energy and $d\Phi_6$ a six-body phase space element. The transfer function $W(x, y)$ finally incorporates the detector resolution, describing the probability for a final state x in the detector to be reconstructed from the partonic state y. The two possible permutations from the unknown jet-parton assignment are summed over and the probability is normalised with the expected observed production rate $\sigma_{\text{obs}}(m_t)$. The calculation of $P_{\text{bkg}}(x)$ proceeds in an analogue way.

$\int \mathcal{L}dt$ [fb^{-1}]	Selection	Method	$m_t \pm$ (stat.) $\pm$ (syst.) [GeV/c^2]	Ref.
0.1	$\ell\ell$	TM:ν_η	$167.4 \pm 10.3 \pm 4.8$	[523, 524]
0.1	$\ell\ell$	TM:$\mathcal{M}, \nu_\eta$	$168.4 \pm 12.3 \pm 3.7$	[521]
0.3	$\ell\ell$	ME	$165.2 \pm 6.1 \pm 3.4$	[534, 535]
0.4	$\ell\ell$,ℓ+trk	TM:$\nu_\eta, \nu_\phi, p_z^{t\bar{t}}$	$170.1 \pm 6.0 \pm 4.1$	[531]
0.4	$\ell\ell$,ℓ+trk	TM:$\mathcal{M}, \nu_\eta$	$178.1 \pm 6.7 \pm 4.8$	[536]
1.0	$\ell\ell$	ME	$164.5 \pm 3.9 \pm 3.9$	[537]
1.0	$\ell\ell$	TM:$\mathcal{M}$	$175.2 \pm 6.1 \pm 3.4$	[538]*
1.0	$\ell\ell$,ℓ+trk	TM:ν_η	$176.0 \pm 5.3 \pm 2.0$	[533]*
1.2	$\ell\ell$	TM:$p_z^{t\bar{t}}$	$169.7^{+5.2}_{-4.9} \pm 3.1$	[520]
1.2	$\ell\ell$	TM:$p_z^{t\bar{t}} \oplus \sigma_{t\bar{t}}$	$170.7^{+4.2}_{-3.9} \pm 2.6 \pm 2.4$(th.)	[520]
1.8	$\ell\ell$	TM:p_T^{ℓ}	$156^{+22}_{-19} \pm 4.6$	[539]*
1.8	$\ell\ell$	TM:ν_η	$172.0^{+5.0}_{-4.9} \pm 3.6$	[540]*
1.8	$\ell\ell$	ME	$170.4 \pm 3.1 \pm 3.0$	[541]*
2.0	$\ell\ell \oplus$ NN	ME	$171.2 \pm 2.7 \pm 2.9$	[542]
2.8	ℓ+trk	TM:ν_ϕ	$165.1^{+3.3}_{-3.2} \pm 3.1$	[543]*
2.8	$e\mu$	ME	$172.9 \pm 3.6 \pm 2.3$	[532]*
2.8	$e\mu$/$\ell\ell$,ℓ+trk	ME/TM:ν_η	$174.4 \pm 3.2 \pm 2.1$	[532]*

Table 20: Top quark mass measurements performed so far at the Tevatron in the dilepton channel with their integrated luminosities, dataset selections applied ($\ell\ell$ = dilepton, ℓ+trk = lepton plus track, NN = neural network) and analysis methods used. The two analyses using 0.1 fb^{-1} are from Run I; the references marked with a * correspond to preliminary results.

The top quark mass of an event sample can simply be obtained by maximising the total likelihood function being the product of the individual event probabilities with respect to m_t. In this way, each event contributes according to its quality and inherent resolution. While this analysis technique exploits the full kinematic information available and usually yields the statistically most sensitive measurements, it is also very computationally intensive due to the involved complex integrations. The result of the 2.8 fb^{-1} $e\mu$ analysis is given together with other top quark mass measurements performed in the dilepton channel at the Tevatron in Table 20. The dominant systematic uncertainty in this analysis arises – as expected – from systematic uncertainties

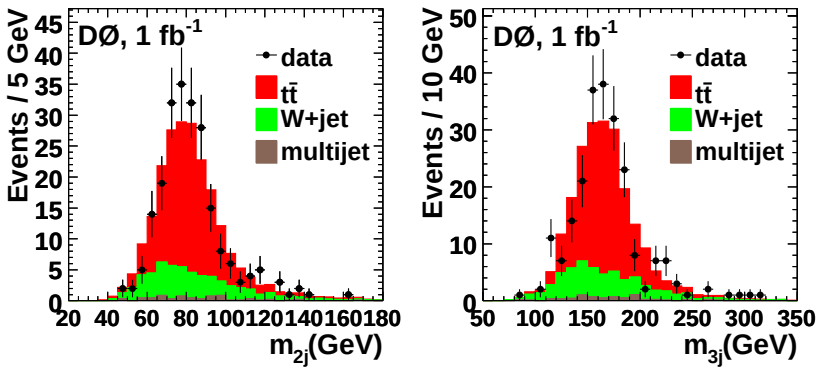

Figure 51: Dijet (left) and three-jet (right) invariant mass distributions in 1 fb^{-1} of D0 data with simulated signal and background contributions [547].

on the JES calibration and response differences between light quarks and b quarks.

7.3.2 Lepton plus Jets Final State

The precision of the top quark mass world average is driven by measurements in the lepton plus jets channel that provides the best compromise between sample purity and signal statistics. In this channel, all three analysis methods (TM, ME, ID) have been deployed, with the most precise results consistently coming from matrix element analyses, starting with the first application in Run I [446].

In the current world average, CDF and D0 both contribute measurements in the lepton plus jets channel based on the matrix element method as explained in the last section, simultaneously fitting top quark mass and an overall in-situ JES scale factor in the data. Events with one energetic isolated lepton, large $\not\!\!E_T$ and exactly four jets are selected since a leading order matrix element is used in the calculations, with at least one of the jets being b tagged. Using datasets of 2.7 respectively 2.2 fb^{-1}, CDF [545] and D0 [546] both measure the top quark mass with a precision of 1.0%, incidentally even yielding the same mass value of 172.2 GeV/c^2. A comparison of the invariant dijet and three-jet mass distributions based on the permutation with the largest weight in data and simulation is shown in Figure 51 for a 1 fb^{-1} subset [547] of D0's 2.2 fb^{-1} analysis.

The largest systematic uncertainties on the measurement by CDF arise from the MC generator used for the calibration of the result (PYTHIA versus HERWIG) and the residual JES uncertainty. For D0, the dominant uncer-

$\int \mathcal{L}dt$ [fb^{-1}]	Selection	Method	$m_t \pm$ (stat.) $\pm$ (syst.) [GeV/c^2]	Ref.
0.1	ℓ+jets	TM:$m_{\rm reco}$	$176.1 \pm 5.1 \pm 5.3$	[525]
0.1	ℓ+jets	ME	$180.1 \pm 3.6 \pm 3.9$	[446]
0.3	ℓ+jets	DLM	$173.2^{+2.6}_{-2.4} \pm 3.2$	[517, 548]
0.3	ℓ+jets	TM:$m_{\rm reco} \oplus$ JES	$173.5^{+3.7}_{-3.6} \pm 1.3^{\dagger}$	[516, 517]
0.4	ℓ+jets	ME $\oplus$ JES	$170.3^{+4.1\ +1.2}_{-4.5\ -1.8}{}^{\dagger}$	[549]
0.4	ℓ+jets	ME $\oplus$ JES	$169.2^{+5.0\ +1.5}_{-7.4\ -1.4}{}^{\dagger}$	[549]
0.4	ℓ+jets	ID $\oplus$ JES	$173.7 \pm 4.4^{+2.1}_{-2.0}{}^{\dagger}$	[550]
0.7	ℓ+jets	TM:L_{xy}	$180.7^{+15.5}_{-13.4} \pm 8.6$	[551]
1.0	ℓ+jets	ME $\oplus$ JES	$171.5 \pm 1.8 \pm 1.1^{\dagger}$	[547]
1.0	ℓ+jets	ME $\oplus$ JES	$170.8 \pm 2.2 \pm 1.4^{\dagger}$	[552]
1.0	ℓ+jets	TM:$m_{\rm reco}$	$168.9 \pm 2.2 \pm 4.2$	[553]*
1.2	ℓ+jets	ME $\oplus$ JES	$173.0 \pm 1.9 \pm 1.0^{\dagger}$	[546]*
1.7	ℓ+jets	DLM $\oplus$ JES	$171.6 \pm 2.0 \pm 1.3^{\dagger}$	[554]*
1.9	ℓ+jets	TM:L_{xy}, p_T^{ℓ}	$175.3 \pm 6.2 \pm 3.0$	[519]*
1.9	ℓ+jets $\ell\ell$	TM:$m_{\rm reco} \oplus$ JES TM:ν_η, H_T	$171.9 \pm 1.7 \pm 1.0^{\dagger}$	[518]*
2.2	ℓ+jets	ME $\oplus$ JES	$172.2 \pm 1.0 \pm 1.4$	[546]*
2.7	ℓ+jets	ME $\oplus$ JES	$172.2 \pm 1.3 \pm 1.0^{\dagger}$	[545]*

Table 21: Top quark mass measurements performed so far at the Tevatron in the lepton plus jets channel with their integrated luminosities, dataset selections applied (ℓ+jets = lepton plus jets, $\ell\ell$ = dilepton) and analysis methods used. The two analyses using 0.1 fb^{-1} are from Run I; the references marked with a * correspond to preliminary measurements. Results marked with a † contain the uncertainty from the in-situ JES calibration in the statistical uncertainty.

tainty comes from the b jet over light jet calorimeter response ratio and the signal modelling uncertainty, taking the modelling uncertainty for extra jets into account based on the observed four to at least five jet event ratio in data. Both experiments are in the process of streamlining the methods used to assess systematic uncertainties as well as exploring new sources of uncertainties that start to become important at the reached level of precision [555]. Examples for the latter are differences arising when using NLO rather than LO MC generators or non-perturbative QCD effects like colour reconnection [186, 187].

Table 21 summarises the most recent final Run I results and the current preliminary respectively published Run II top quark mass measurements in the lepton plus jets channel.

7.3.3 All-Hadronic Final State

Analyses in the all-hadronic channel have been performed so far using template and ideogram methods, with comparable sensitivity. The precision in this channel by now is similar to that in the dilepton final state, mainly due to the application of in-situ JES calibration, reducing the otherwise overwhelming systematic uncertainty from the JES.

CDF's best measurement in the all-hadronic channel entering the world average has been performed using a template method on 2.1 fb^{-1} of data, yielding a precision of 2.4% [556]. Similar to the analysis [280] described in Section 5.1.3, events are required to have between six and eight energetic central jets, no isolated energetic lepton or significant $\not\!\!E_T$ and have to pass a selection based on the output of a neural network discriminant. The dataset is split into subsamples with exactly one respectively two b tagged jets.

The leading six jets in each event are used to build $t\bar{t}$ signal and multijet background templates for the reconstructed mass of the top quark and the W boson based on a kinematic fit where the permutation with lowest χ^2 is selected respectively. While the signal templates depend on top quark mass and JES scale factor, the background templates do not depend on the top quark mass, and no JES dependence is considered either. The measurement is then performed in a two-dimensional fit of top quark mass and in-situ JES scale factor using these templates and the observed distribution in data in both subsamples, including a Gaussian constraint from the external JES calibration. The reconstructed mass distributions obtained in data with two b tags, overlaid with expected background and $t\bar{t}$ signal templates with a top quark mass of 177 GeV/c^2 and unchanged JES with respect to the external calibration as preferred by the fit are shown in Figure 52.

The result of the analysis is given together with other top quark mass

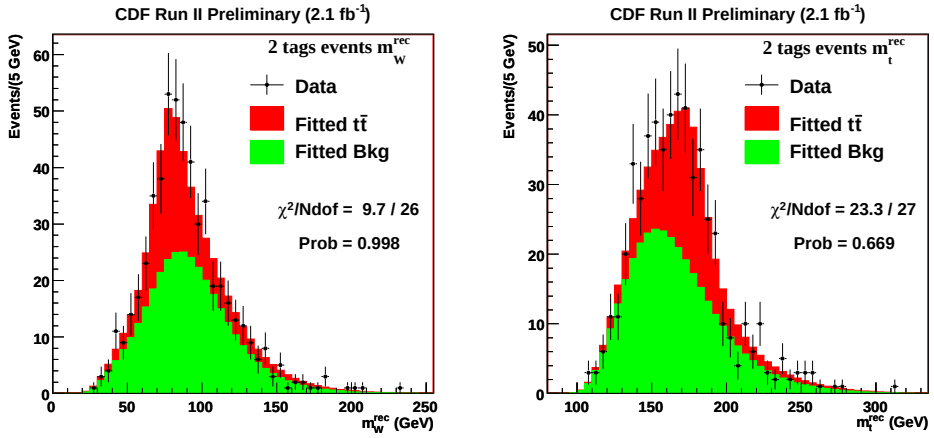

Figure 52: Reconstructed W boson (left) and top quark (right) mass distributions obtained in 2.1 fb^{-1} of double b tagged CDF data in comparison to the expected contributions from multijet background and 177 GeV/c^2 $t\bar{t}$ signal with default JES corresponding to the fit result [556].

measurements performed in the all-hadronic channel at the Tevatron in Table 22. The dominant systematic uncertainties in this analysis arise from uncertainties on shape and normalisation of the background templates and residual JES uncertainties. The compatibility of this measurement with the result from the ideogram method [557] on an overlapping dataset of almost the same size yielding a central value almost 12 GeV/c^2 lower is currently being investigated.

7.3.4 World Average Top Quark Mass

The top quark mass has been measured at the Tevatron in the three main decay channels with various methods as described in the last sections. In the lepton plus jets channel precisions of 1% are achieved in single measurements while in the dilepton and all-hadronic channels the precision is about 2%. The different methods assume Standard Model $t\bar{t}$ production and decay, but still exhibit differences in the strength of their model dependence. While ME methods provide the best sensitivity, they also are strongly model dependent via their implemented matrix elements. Template methods purely relying on the measured event kinematics are more robust with respect to possible deviations from the Standard Model, but in general exhibit lower sensitivity.

Pursuing mass measurements in all $t\bar{t}$ decay channels with different methods is a valuable test of the self-consistency of the Standard Model assump-

$\int \mathcal{L}dt$ [fb^{-1}]	Selection	Method	$m_t \pm$ (stat.) $\pm$ (syst.) [GeV/c^2]	Ref.
0.1	jets only	TM:$m_{\rm reco}$	$178.5 \pm 13.7 \pm 7.7$	[527]
0.1	jets only	TM:$m_{\rm reco}$	$186 \pm 10 \pm 5.7$	[525, 528]
0.3	$\not\!\!E_T$+jets	TM:H_T	$172.3^{+10.8}_{-9.6} \pm 10.8$	[529]
0.3	jets only	ID	$177.1 \pm 4.9 \pm 4.7$	[558]
0.9	jets only	TM:ME $\oplus$ JES	$171.1 \pm 3.7 \pm 2.1^{\dagger}$	[559]*
1.0	jets only	TM:$m_{\rm reco}$	$174.0 \pm 2.2 \pm 4.8$	[280]
1.9	jets only	ID $\oplus$ JES	$165.2 \pm 4.4 \pm 1.9^{\dagger}$	[557]*
2.1	jets only	TM:$m_{\rm reco}$ $\oplus$ JES	$176.9 \pm 3.8 \pm 1.7^{\dagger}$	[556]*

Table 22: Top quark mass measurements performed so far at the Tevatron in the all-hadronic channel with their integrated luminosities, dataset selections applied and analysis methods used. The two analyses using 0.1 fb^{-1} are from Run I; the references marked with a * correspond to preliminary measurements. Results marked with a † contain the uncertainty from the in-situ JES calibration in the statistical uncertainty.

tions and can be used to probe for new phenomena as well [296]. While so far no top quark mass measurement has been performed in $t\bar{t}$ decay modes involving hadronic τs, the progress in the corresponding cross section analyses discussed in Section 5.1.4 indicates this could still be possible at the Tevatron, completing the $t\bar{t}$ decay channels used for mass measurements.

CDF and D0 have combined their recent preliminary Run II results with their measurements obtained in Run I. Based on the results with highest sensitivity in the dilepton, lepton plus jets and all-hadronic channels (CDF) respectively in the dilepton and lepton plus jets channels (D0), both experiments yield a total precision of 0.9% on their combined measurements. Based on analyses using up to 2.7 fb^{-1}, CDF yields 172.4 ± 1.0(stat.) ± 1.3(syst.) GeV/c^2 [560], while D0 obtains 172.8 ± 0.9(stat.) ± 1.3(syst.) GeV/c^2 [561] using analyses on up to 2.8 fb^{-1} of data.

The results of both experiments are in very good agreement, and their combination yields 172.4 ± 0.7(stat.)± 1.0(syst.) GeV/c^2 [12] corresponding to an overall precision of 0.7% as illustrated in Figure 53. Combining the results from all-hadronic, lepton plus jets and dilepton channels separately yields 177.5 ± 4.0 GeV/c^2, 172.2 ± 1.2 GeV/c^2 and 171.5 ± 2.6 GeV/c^2 respectively. These results are consistent with each other exhibiting χ^2 probabilities of at least 17% between any two of the channels.

All these combinations are performed using the BLUE method [278, 279] and assume Gaussian systematic uncertainties with their correlations prop-

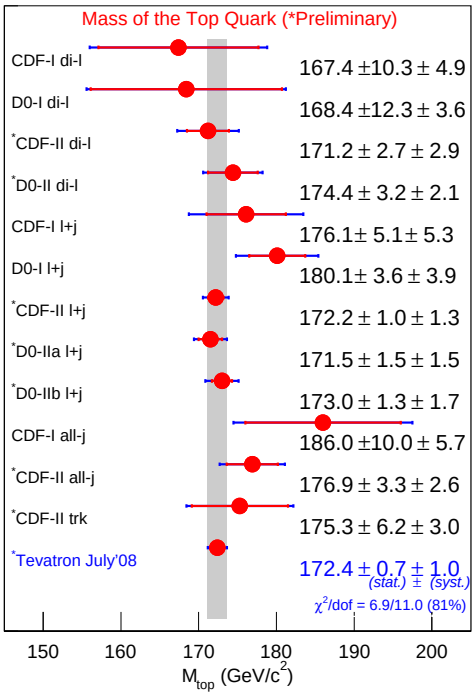

Figure 53: Top quark mass measurements used as input for the current preliminary world average [12].

erly accounted for. The different sources of systematic uncertainties are broken down into twelve orthogonal categories. Six of them deal with uncertainties related to the JES, while others address signal and background modelling, fitting procedures, specifics of MC generation and lepton energy scale. The main contributions to the 1.0 GeV/c^2 systematic error on the world average top quark mass are (in units of GeV/c^2): total JES ($\pm$0.8), signal, background and MC model ($\pm$0.3 each) and lepton scale and fitting procedure ($\pm$0.1 each).

Having reached a precision of 0.7%, the world average top quark mass is now limited by the systematic uncertainties which in turn are dominated by JES related uncertainties. Further improvements on the JES can be expected since the increasing datasets will also allow one to constrain the corresponding uncertainties better, especially the significant contribution from in-situ JES calibration. While a final absolute top quark mass uncertainty below $\Delta m_t = 1$ GeV/c^2 should be achievable by the end of the Tevatron Run II, it will still require a significant effort to carefully study the contributing systematic uncertainties consistently among the experiments and evaluate possible new contributions that should be considered with the reached precision.

This measurement marks the most precise determination of a quark mass and will certainly be a legacy well into the LHC era where it will serve as an important calibration signal until large datasets allow further refined measurements. Improvements on the top quark mass precision by another order of magnitude however can only be expected from a threshold scan of $t\bar{t}$ production at a future linear e^+e^- collider [562–564].

Before the impact of the current top quark mass measurement is discussed, it should be noted that the value of this Standard Model parameter depends on the used convention. For instance, the $\overline{MS}$ top quark mass is lower than the pole top quark mass by about 10 GeV/c^2 at $\mathcal{O}(\alpha_s^3)$. The pole mass itself exhibits an intrinsic ambiguity of $\mathcal{O}(\Lambda_{\mathrm{QCD}}) \approx 0.2$ GeV (see for example [565] and references therein).

The top quark mass measurements described here are usually interpreted as representing the pole mass. However, they are calibrated using LO MC simulations with higher orders approximated by parton showers where the top mass parameter does not follow a theoretically well-defined convention. Further calculations and predictions using the measured top quark mass as the pole mass should thus be taken with a grain of salt.

D0 has conducted valuable consistency checks of the compatibility of the direct top quark mass measurements performed so far at the Tevatron with the pole mass extracted from the $t\bar{t}$ production rate [264, 566]. By comparing the measured $t\bar{t}$ production cross section with theoretical Standard Model predictions derived at NLO including soft gluon resummations that are performed in a well-defined renormalisation scheme using the top quark pole mass, constraints on the top quark mass are derived. The cross section measurements depend less on the MC modelling of the signal kinematics than direct mass measurements. The MC is mainly needed for the signal acceptance determination which is expected to be rather insensitive to higher order corrections since a comparison of NLO and LO predictions shows that higher order corrections affect more the normalisation than the shape of the relevant kinematic distributions [567].

In a recent analysis, D0 uses two cross section measurements to extract constraints on the top quark mass by comparison with theoretical predictions [566]. One result is obtained in the lepton plus jets channel based on the combination of a counting experiment using b tagging and an analysis utilising a topological multivariate discriminant on 0.9 fb^{-1} of data [264] as discussed in Section 5.1.2. The second result combines measurements in the lepton plus jets, dilepton and τ plus lepton channels obtained from approximately 1.0 fb^{-1} of data [259] (see Section 5.1.5). Being based on different analysis techniques and final states, both results exhibit a different dependence on the top quark mass as illustrated in Figure 54.

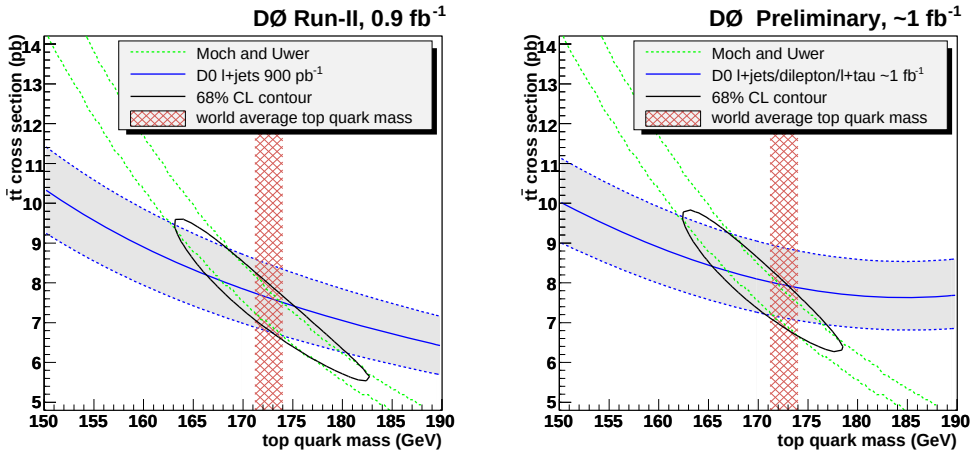

Figure 54: Mass dependence of the $t\bar{t}$ production cross section measurements by D0 in the lepton plus jets channel (left, [264]) respectively in a combination of lepton plus jets, dilepton and τ plus lepton channels (right, [259]) and the theoretical prediction by Moch and Uwer [128] based on CTEQ6.6M [124] PDFs. The previous world average top quark mass of 172.6 ± 1.4 GeV/c^2 [568] is shown as well as the joint likelihood 68% C.L. contours resulting from the convolutions of measurement and prediction [566].

One theoretical prediction used for the comparison is that of Moch and Uwer [128] based on CTEQ6.6M [124] PDFs (see Section 3.1). A joint likelihood depending on top quark mass and pair production rate is obtained as the product of the likelihood functions of the measurement including its total experimental uncertainty and the theoretical prediction including scale and PDF uncertainties. The contour of the joint likelihood's smallest region containing 68% of its integral is shown as well in Figure 54 for both measurements. By integrating over the $t\bar{t}$ production rate, the top quark mass can be extracted. For the lepton plus jets channel measurement a top quark mass of $171.2^{+6.5}_{-6.2}$ GeV/c^2 is obtained while the combined lepton plus jets, dilepton and τ plus lepton measurement yields $169.6^{+5.4}_{-5.5}$ GeV/c^2, including an additional systematic uncertainty of 1 GeV/c^2 due to a smaller mass dependence range available from this measurement. Both mass results are in good agreement with the world average top quark mass obtained from the complementary direct measurements.

The current world average top quark mass of 172.4 ± 1.2 GeV/c^2 [12] is also in good agreement with its predicted value in the framework of the Standard Model obtained from electroweak precision data, yielding $179\ ^{+12}_{-9}$

GeV/c^2 as discussed in Section 2.3. Using the top quark mass measurement as input together with that of the W boson mass – 80.398 ± 0.025 GeV/c^2 [23] – to obtain limits on the Higgs boson mass via the radiative corrections on the W boson mass in a global electroweak fit, one obtains $m_H = 84^{+34}_{-26}$ GeV/c^2 [569] as illustrated in Figure 55, where the uncertainties are experimental only. To demonstrate the impact of the recent improvements in precision for the measurements of both the top quark and W boson mass since the beginning of Run II, the corresponding fit results in spring 2004 are shown as well [570]. The current resulting 95% C.L. upper limit on the Higgs boson mass is 154 GeV/c^2, including both experimental and theoretical uncertainties.

The result of the direct searches for the Standard Model Higgs boson at LEP yielding a 95% C.L. lower bound of 114.4 GeV/c^2 [571] is illustrated in Figure 55 as well. CDF and D0 have recently excluded a Standard Model Higgs boson of 170 GeV/c^2 mass at 95% C.L. and a mass range of about 165 to 175 GeV/c^2 at 90% C.L. [572] based on three fb^{-1} datasets, which is not reflected in Figure 55.

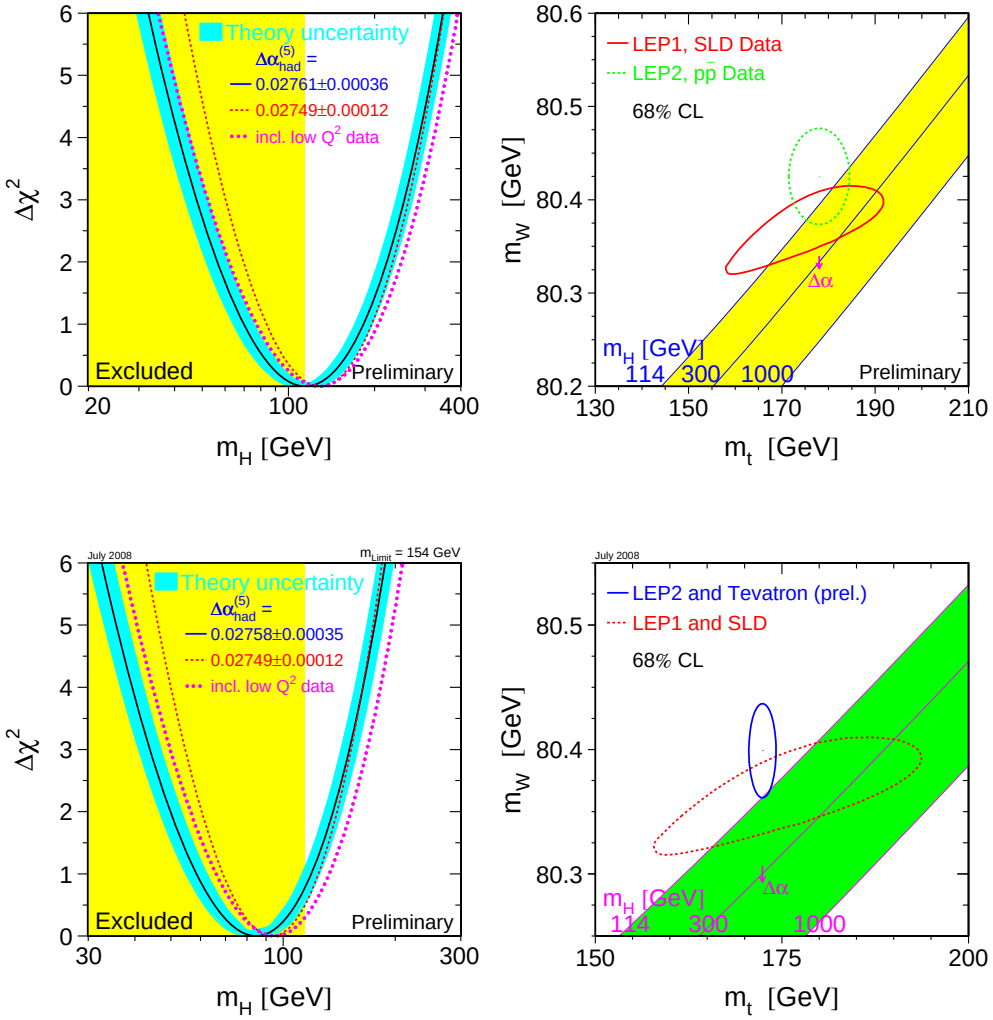

Figure 55: Higgs boson mass constraints in 2004 (top, [570]), using the Tevatron Run I mass combination result $m_t = 178.0 \pm 4.3$ GeV/c^2 [159], and now (bottom, [569]), using the current preliminary world-average result $m_t = 172.4 \pm 1.2$ GeV/c^2 [12].

8 Summary

More than thirteen years after its discovery, the properties of the top quark are being studied at the Tevatron with unprecedented precision by the CDF and D0 collaborations. The Tevatron is operating very smoothly and has already delivered more than four fb^{-1} of integrated luminosity to each experiment. Until the end of Run II in 2009 or 2010, it is expected to deliver two fb^{-1} per year. CDF and D0 have exploited these increasing datasets together with novel advanced analysis techniques to not only improve upon previous measurements but also to explore top quark properties that were not accessible before like its electroweak production which allows first direct measurements of the $|V_{tb}|$ CKM matrix element. So far all results are consistent with the Standard Model expectations and between the experiments which allows one to constrain specific extensions of the Standard Model impacting the properties under consideration.

Top quark pair production is well established in the lepton plus jets, dilepton and all-hadronic final states, and these channels are also used to study further properties of the top quark like its mass. The top quark signal is being established now in final states involving hadronically decaying τ leptons as well, in particular in the lepton plus τ channel. The observed production rates in all final states under investigation are consistent with each other and the Standard Model expectation. No novel contributions to $t\bar{t}$ production and signal samples are observed, and corresponding constraints are derived on $t\bar{t}$ production via resonances or massive gluons and possible contributions of a fourth fermion generation or scalar top quarks to the selected signal samples. The kinematics in the observed event samples also agree with the Standard Model prediction. Since contributions of physics beyond the Standard Model could affect the observed final states differently also via the top quark decay, for example due to top quark decays into charged Higgs bosons, corresponding limits are derived as well.

The $t\bar{t}$ production rate has been measured now to be about 7.3 pb for a top quark mass of 175 GeV/c^2 with a precision of 10%, matching the uncertainties of the theoretical predictions which allows stringent tests of the corresponding perturbative QCD calculations. Ultimately, the precision of the cross section measurements at the Tevatron might reach the 6% level, dominated by the uncertainty on the integrated luminosity. First measurements have been performed to determine the contributions of $q\bar{q}$ annihilation and gluon-gluon fusion to $t\bar{t}$ production and are found to be consistent with the QCD predictions. Also higher order effects like the top quark charge asymmetry could be measured for the first time and agree with the Standard Model expectation within statistical precision.

First evidence for electroweak single top quark production has been found by both experiments and observation at the five standard deviation level appears imminent. The observed production rates are consistent with the Standard Model expectation of about three pb and allow first direct measurements of the CKM matrix element $|V_{tb}|$. The most stringent 95% C.L. lower limit is found to be $|V_{tb}| > 0.71$. Searches for exotic single top production via W' or charged Higgs bosons or flavour changing neutral interactions with gluons are performed as well. Since no significant deviations from the Standard Model are observed, corresponding stringent limits are derived. With single top production being a sensitive probe of the Wtb vertex structure, also constraints on an extended Wtb interaction are derived, including first limits on the left- respectively right-handed tensor couplings.

The decay properties of top quarks are studied using $t\bar{t}$ samples providing both sufficient statistics and sample purity. The W boson helicity in $t\bar{t}$ decays can now be measured in a model independent way by extracting the fractions of left-handed and longitudinally polarised W bosons simultaneously. This provides additional information about the Wtb vertex structure that can be used together with constraints from single top quark production to fully specify the Wtb coupling. The W boson helicity measurements are consistent with the Standard Model expectation and further studies in the lepton plus jets and dilepton final states will scrutinise the observed discrepancies between both channels at the two standard deviations level. The determination of the ratio of branching fractions $R = \mathcal{B}(t \to Wb)/\mathcal{B}(t \to Wq)$ by now has reached a precision of 9%, yielding $R = 0.97^{+0.09}_{-0.08}$ and confirming the expectation of a dominant $t \to Wb$ decay mode assumed in most top quark analyses. Top quark decays beyond the Standard Model are searched for due to neutral currents, invisible decay modes or decays into charged Higgs bosons. No significant deviations from the Standard Model are observed, yielding strong limits on the considered processes.

Measurements of fundamental top quark properties – charge, lifetime, mass – are performed as well based on top quark pair samples and help to confirm the Standard Model identity of the top quark. First measurements of charge and lifetime are consistent with the expectation, helping to constrain exotic models. The top quark mass has now been measured in the lepton plus jets, dilepton and all-hadronic final states, yielding consistent results amongst the considered channels and the CDF and D0 experiments. A combination of the results yields $m_t = 172.4 \pm 1.2$ GeV/c^2, marking the most precise measurement of a quark mass with a precision of 0.7%. By the end of Run II, a measurement with an absolute precision below $\Delta m_t = 1$ GeV/c^2 should be achievable. This measurement will be a legacy beyond the Tevatron Run II and will allow the top quark to be used as a calibration object at the LHC

until large datasets there will allow further refined measurements.

While the top quark mass measurements are usually interpreted as representing the pole mass, their calibration with the currently used Monte Carlo simulations which do not reflect this theoretically well-defined concept should be kept in mind. Indirect mass measurements utilising the mass dependence of the $t\bar{t}$ production rate of measurements in comparison with theoretical predictions based on the pole mass however are consistent with the direct measurements. Utilising the radiative corrections on the W boson mass in a global electroweak fit with the measured world average top quark and W boson masses as input, the mass of the yet unobserved Standard Model Higgs boson can be constrained. This results in a 95% C.L. upper limit on the Higgs boson mass of 154 GeV/c^2.

The large mass of the top quark does not only render it an ideal window to new physics as the most massive known fundamental object but also leads to a lifetime which is short in comparison to hadronisation timescales. Consequently, observables sensitive to the top quark spin can be accessed undisturbed from hadronisation processes. Spin-related measurements have not been performed yet in Run II at the Tevatron. While it was shown in Run I that a measurement of top quark pair spin correlations is feasible, this measurement that will greatly benefit from the increased available dataset still remains to be performed. The observation of single top quark production in addition should allow one to study the polarisation of top quarks when produced singly via the electroweak interaction.

For precision measurements like those of top quark mass and pair production cross section the careful study of systematic uncertainties – consistently across experiments – and evaluation of possible new contributions not considered so far is becoming the priority. Other measurements – especially those involving single top quark production – will remain statistically limited throughout Run II. The LHC will be a "top factory", producing millions of top quarks per year thanks to increased top production cross sections by two orders of magnitude and enhanced luminosity compared to the Tevatron. A broad top quark physics program is in preparation at the LHC [399, 565] that will complement and further expand that of the Tevatron.

A wealth of analyses is being pursued at the Tevatron, characterising top quark samples both as signal and as background for other processes of similar signature that yet remain to be discovered. The top quark itself serves as a probe for new physics in both production and decay that could manifest itself via new particles being produced or modified couplings with respect to the Standard Model expectation. While so far all measurements are in agreement with the Standard Model, there is still plenty of room for new physics to be explored both at the Tevatron and the LHC.

Acknowledgements

The author would like to thank all his colleagues working on the CDF and D0 experiments and the Fermilab accelerator complex who made the reviewed results possible through their dedicated work. The author's research financial support from the Alexander von Humboldt Foundation, the University of Rochester and the University of Bonn is gratefully acknowledged.

The author is indebted to Tom Ferbel and Regina Demina at the University of Rochester for introducing him to the world of top quark physics and for their continued encouragement. Norbert Wermes and Eckhard von Törne at the University of Bonn are gratefully acknowledged for their support of the author's research and writing process. Special thanks go to all the group members at the Universities of Rochester and Bonn for their contribution to making this work such a fruitful and inspiring experience.

The author is in particular grateful to Florencia Canelli, Frédéric Déliot, Amnon Harel, Ann Heinson, Ulrich Heintz, Ulrich Husemann, Michelangelo Mangano, Heather Pleier, Iris Rottländer, Christian Schwanenberger, Lisa Shabalina, Kirsten Tollefson, Eckhard von Törne and Norbert Wermes for helpful discussions and/or comments on the manuscript. SDG.

References

[1] M. L. Perl *et al.*, "Evidence for Anomalous Lepton Production in $e^+ - e^-$ Annihilation," *Phys. Rev. Lett.* **35** (1975) 1489–1492.

[2] S. W. Herb *et al.*, "Observation of a dimuon resonance at 9.5 GeV in 400 GeV proton - nucleus collisions," *Phys. Rev. Lett.* **39** (1977) 252–255.

[3] **ALEPH, DELPHI, L3, OPAL** Collaboration, the LEP Electroweak Working Group, "Combined preliminary data on Z parameters from the LEP experiments and constraints on the Standard Model". Contributed to the 27th International Conference on High- Energy Physics - ICHEP 94, Glasgow, Scotland, UK, 20 - 27 Jul 1994, CERN/PPE/94-187.

[4] **DØ** Collaboration, S. Abachi *et al.*, "Search for the top quark in $p\bar{p}$ collisions at $\sqrt{s} = 1.8$ TeV," *Phys. Rev. Lett.* **72** (1994) 2138–2142.

[5] **CDF** Collaboration, F. Abe *et al.*, "Evidence for top quark production in $\bar{p}p$ collisions at $\sqrt{s} = 1.8$ TeV," *Phys. Rev.* **D50** (1994) 2966–3026.

[6] **CDF** Collaboration, F. Abe *et al.*, "Evidence for top quark production in $\bar{p}p$ collisions at $\sqrt{s} = 1.8$ TeV," *Phys. Rev. Lett.* **73** (1994) 225–231, hep-ex/9405005.

[7] **DØ** Collaboration, S. Abachi *et al.*, "Search for high mass top quark production in $p\bar{p}$ collisions at $\sqrt{s} = 1.8$ TeV," *Phys. Rev. Lett.* **74** (1995) 2422–2426, hep-ex/9411001.

[8] **CDF** Collaboration, F. Abe *et al.*, "Kinematic evidence for top quark pair production in W + multi - jet events in $p\bar{p}$ collisions at $\sqrt{s} = 1.8$ TeV," *Phys. Rev.* **D51** (1995) 4623–4637, hep-ex/9412009.

[9] **DØ** Collaboration, S. Abachi *et al.*, "Top quark search with the DØ 1992 - 1993 data sample," *Phys. Rev.* **D52** (1995) 4877–4919.

[10] **DØ** Collaboration, S. Abachi *et al.*, "Observation of the Top Quark," *Phys. Rev. Lett.* **74** (1995) 2632–2637, hep-ex/9503003.

[11] **CDF** Collaboration, F. Abe *et al.*, "Observation of Top Quark Production in $\bar{p}p$ Collisions," *Phys. Rev. Lett.* **74** (1995) 2626–2631, hep-ex/9503002.

[12] **CDF, DØ** Collaboration, the Tevatron Electroweak Working Group, "Combination of CDF and D0 Results on the Mass of the Top Quark," arXiv:0808.1089.

[13] **DØ** Collaboration, V. M. Abazov *et al.*, "Evidence for production of single top quarks," *Phys. Rev.* **D78** (2008) 012005, arXiv:0803.0739.

[14] **DØ** Collaboration, V. M. Abazov *et al.*, "Evidence for production of single top quarks and first direct measurement of $|V_{tb}|$," *Phys. Rev. Lett.* **98** (2007) 181802, arXiv:hep-ex/0612052.

[15] **CDF, DØ** Collaboration, M.-A. Pleier, "Top Quark Pair Production and Properties Measurements at the Tevatron," arXiv:0804.4288.

[16] **CDF, DØ** Collaboration, M.-A. Pleier, "Top Quark Physics at the Tevatron," *Acta Phys. Polon. Supp.* **1** (2008) 237–244, arXiv:0709.2665.

[17] **DØ** Collaboration, M.-A. Pleier, "DØ Top Physics," *Lake Louise 2005, Fundamental Interactions* (April, 2005) 264–268, hep-ex/0511034.

[18] M. Mangano and T. G. Trippe, "The Top Quark," *Phys. Lett.* **B592** (2004) 482–487.

[19] D. Chakraborty, J. Konigsberg, and D. L. Rainwater, "Review of top quark physics," *Ann. Rev. Nucl. Part. Sci.* **53** (2003) 301–351, `hep-ph/0303092`.

[20] R. Kehoe, M. Narain, and A. Kumar, "Review of Top Quark Physics Results," *Int. J. Mod. Phys.* **A23** (2008) 353–470, `arXiv:0712.2733`.

[21] A. Quadt, "Top quark physics at hadron colliders," *Eur. Phys. J.* **C48** (2006) 835–1000.

[22] W. Wagner, "Top quark physics in hadron collisions," *Rept. Prog. Phys.* **68** (2005) 2409–2494, `hep-ph/0507207`.

[23] **Particle Data Group** Collaboration, C. Amsler *et al.*, "Review of particle physics," *Physics Letters* **B667** (2008) 1.

[24] H. D. Politzer, "Reliable Perturbative Results for Strong Interactions?," *Phys. Rev. Lett.* **30** (1973) 1346–1349.

[25] D. J. Gross and F. Wilczek, "Ultraviolet Behavior of Nonabelian Gauge Theories," *Phys. Rev. Lett.* **30** (1973) 1343–1346.

[26] S. Weinberg, "Current algebra and gauge theories. 2. NonAbelian gluons," *Phys. Rev.* **D8** (1973) 4482–4498.

[27] S. Weinberg, "Nonabelian Gauge Theories of the Strong Interactions," *Phys. Rev. Lett.* **31** (1973) 494–497.

[28] D. J. Gross and F. Wilczek, "Asymptotically Free Gauge Theories. 1," *Phys. Rev.* **D8** (1973) 3633–3652.

[29] H. Fritzsch, M. Gell-Mann, and H. Leutwyler, "Advantages of the Color Octet Gluon Picture," *Phys. Lett.* **B47** (1973) 365–368.

[30] S. L. Glashow, "Partial Symmetries of Weak Interactions," *Nucl. Phys.* **22** (1961) 579–588.

[31] A. Salam and J. C. Ward, "Electromagnetic and weak interactions," *Phys. Lett.* **13** (1964) 168–171.

[32] S. Weinberg, "A Model of Leptons," *Phys. Rev. Lett.* **19** (1967) 1264–1266.

[33] T. W. B. Kibble, "Symmetry breaking in non-Abelian gauge theories," *Phys. Rev.* **155** (1967) 1554–1561.

[34] G. S. Guralnik, C. R. Hagen, and T. W. B. Kibble, "Global Conservation Laws and Massless Particles," *Phys. Rev. Lett.* **13** (1964) 585–587.

[35] F. Englert and R. Brout, "Broken Symmetry and the Mass of Gauge Vector Mesons," *Phys. Rev. Lett.* **13** (1964) 321–322.

[36] P. W. Higgs, "Spontaneous Symmetry Breakdown Without Massless Bosons," *Phys. Rev.* **145** (1966) 1156–1163.

[37] P. W. Higgs, "Broken Symmetries and the Masses of Gauge Bosons," *Phys. Rev. Lett.* **13** (1964) 508–509.

[38] P. W. Higgs, "Broken symmetries, massless particles and gauge fields," *Phys. Lett.* **12** (1964) 132–133.

[39] N. Cabibbo, "Unitary Symmetry and Leptonic Decays," *Phys. Rev. Lett.* **10** (1963) 531–532.

[40] M. Kobayashi and T. Maskawa, "CP Violation in the Renormalizable Theory of Weak Interaction," *Prog. Theor. Phys.* **49** (1973) 652–657.

[41] **Particle Data Group** Collaboration, W. M. Yao *et al.*, "Review of particle physics," *J. Phys.* **G33** (2006) 1–1232.

[42] **K2K** Collaboration, M. H. Ahn *et al.*, "Indications of neutrino oscillation in a 250-km long-baseline experiment," *Phys. Rev. Lett.* **90** (2003) 041801, `hep-ex/0212007`.

[43] **Super-Kamiokande** Collaboration, S. Fukuda *et al.*, "Determination of solar neutrino oscillation parameters using 1496 days of Super-Kamiokande-I data," *Phys. Lett.* **B539** (2002) 179–187, `hep-ex/0205075`.

[44] **SNO** Collaboration, Q. R. Ahmad *et al.*, "Measurement of the charged current interactions produced by B-8 solar neutrinos at the Sudbury Neutrino Observatory," *Phys. Rev. Lett.* **87** (2001) 071301, `nucl-ex/0106015`.

[45] **Super-Kamiokande** Collaboration, Y. Fukuda *et al.*, "Evidence for oscillation of atmospheric neutrinos," *Phys. Rev. Lett.* **81** (1998) 1562–1567, `hep-ex/9807003`.

[46] B. T. Cleveland *et al.*, "Measurement of the solar electron neutrino flux with the Homestake chlorine detector," *Astrophys. J.* **496** (1998) 505–526.

[47] J. Davis, Raymond, D. S. Harmer, and K. C. Hoffman, "Search for neutrinos from the sun," *Phys. Rev. Lett.* **20** (1968) 1205–1209.

[48] Z. Maki, M. Nakagawa, and S. Sakata, "Remarks on the unified model of elementary particles," *Prog. Theor. Phys.* **28** (1962) 870.

[49] B. Pontecorvo, "Neutrino experiments and the question of leptonic-charge conservation," *Sov. Phys. JETP* **26** (1968) 984–988.

[50] G. 't Hooft, "Renormalizable Lagrangians for Massive Yang-Mills Fields," *Nucl. Phys.* **B35** (1971) 167–188.

[51] G. 't Hooft, "Renormalization of Massless Yang-Mills Fields," *Nucl. Phys.* **B33** (1971) 173–199.

[52] M. Treichel, "Teilchenphysik und Kosmologie : Eine Einführung in Grundlagen und Zusammenhänge". Springer, Berlin, Germany (2000), 389p.

[53] H.-K. Quang and X. Y. Pham, "Elementary Particles and Their Interactions". Springer, Berlin, Germany (1998), 661p.

[54] F. Halzen and A. D. Martin, "QUARKS AND LEPTONS: An Introductory Course in Modern Particle Physics". John Wiley & Sons, New York, USA (1984), 396p.

[55] A. Djouadi, "The anatomy of electro-weak symmetry breaking. I: The Higgs boson in the standard model," *Phys. Rept.* **457** (2008) 1–216, `hep-ph/0503172`.

[56] S. L. Glashow, J. Iliopoulos, and L. Maiani, "Weak Interactions with Lepton-Hadron Symmetry," *Phys. Rev.* **D2** (1970) 1285–1292.

[57] J. K. Bienlein *et al.*, "Observation of a Narrow Resonance at 10.02 GeV in e^+e^- Annihilations," *Phys. Lett.* **B78** (1978) 360–363.

[58] C. W. Darden *et al.*, "Observation of a Narrow Resonance at 9.46 GeV in Electron-Positron Annihilations," *Phys. Lett.* **B76** (1978) 246.

[59] **PLUTO** Collaboration, C. Berger *et al.*, "Observation of a Narrow Resonance Formed in e^+e^- Annihilation at 9.46 GeV," *Phys. Lett.* **B76** (1978) 243–245.

[60] J. L. Rosner, C. Quigg, and H. B. Thacker, "Determining the Fifth Quark's Charge: The Role of Upsilon Leptonic Widths," *Phys. Lett.* **B74** (1978) 350.

[61] K. Gottfried, "The Spectroscopy of the New Particles". Invited paper presented at Int. Symp. on Lepton and Photon Interactions at High Energies, Hamburg, Germany, Aug 25-31, 1977.

[62] **JADE** Collaboration, W. Bartel *et al.*, "A Measurement of the Electroweak Induced Charge Asymmetry in $e^+e^- \to$ B anti-B," *Phys. Lett.* **B146** (1984) 437.

[63] **KLOE** Collaboration, A. Aloisio *et al.*, "Measurement of $\sigma(e^+e^- \to \pi^+\pi^-\gamma)$ and extraction of $\sigma(e^+e^- \to \pi^+\pi^-)$ below 1 GeV with the KLOE detector," *Phys. Lett.* **B606** (2005) 12–24, `hep-ex/0407048`.

[64] **CMD-2** Collaboration, R. R. Akhmetshin *et al.*, "Reanalysis of hadronic cross section measurements at CMD- 2," *Phys. Lett.* **B578** (2004) 285–289, `hep-ex/0308008`.

[65] **BES** Collaboration, J. Z. Bai *et al.*, "Measurements of the cross section for $e^+e^- \to$ hadrons at center-of-mass energies from 2 GeV to 5 GeV," *Phys. Rev. Lett.* **88** (2002) 101802, `hep-ex/0102003`.

[66] **FAST** Collaboration, A. Barczyk *et al.*, "Measurement of the Fermi Constant by FAST," *Phys. Lett.* **B663** (2008) 172–180, `arXiv:0707.3904`.

[67] T. van Ritbergen and R. G. Stuart, "On the precise determination of the Fermi coupling constant from the muon lifetime," *Nucl. Phys.* **B564** (2000) 343–390, `hep-ph/9904240`.

[68] The ALEPH, DELPHI, L3, OPAL, SLD Collaborations, the LEP Electroweak Working Group, the SLD Electroweak and Heavy Flavour Groups, "Precision Electroweak Measurements on the Z Resonance," *Phys. Rept.* **427** (2006) 257, `hep-ex/0509008`.

[69] P. Langacker, "Implications of Recent $M_{Z,W}$ and Neutral Current Measurements for the Top Quark Mass," *Phys. Rev. Lett.* **63** (1989) 1920.

[70] G. Burgers and F. Jegerlehner, "Δr, or The Relation Between The Electroweak Couplings And The Weak Vector Boson Masses". To appear in the Proceedings of the Workshop on Z Physics at LEP, Geneva, Switzerland, Feb 20, 1989 and edited by G. Altarelli, R. Kleiss and C. Verzegnassi.

[71] W. F. L. Hollik, "Radiative Corrections in the Standard Model and their Role for Precision Tests of the Electroweak Theory," *Fortschr. Phys.* **38** (1990) 165–260.

[72] D. Brandt, H. Burkhardt, M. Lamont, S. Myers, and J. Wenninger, "Accelerator physics at LEP," *Rept. Prog. Phys.* **63** (2000) 939–1000.

[73] S. Myers and E. Picasso, "The Design, construction and commissioning of the CERN Large Electron Positron collider," *Contemp. Phys.* **31** (1990) 387–403.

[74] **ALEPH** Collaboration, D. Buskulic *et al.*, "Performance of the ALEPH detector at LEP," *Nucl. Instrum. Meth.* **A360** (1995) 481–506.

[75] **ALEPH** Collaboration, D. Decamp *et al.*, "ALEPH: A Detector For Electron - Positron Annihilations At LEP," *Nucl. Instrum. Meth.* **A294** (1990) 121–178.

[76] **DELPHI** Collaboration, P. Abreu *et al.*, "Performance of the DELPHI detector," *Nucl. Instrum. Meth.* **A378** (1996) 57–100.

[77] **DELPHI** Collaboration, P. Aarnio *et al.*, "The DELPHI detector at LEP," *Nucl. Instrum. Meth.* **A303** (1991) 233–276.

[78] **L3 F/B Muon Group** Collaboration, A. Adam *et al.*, "The forward muon detector of L3," *Nucl. Instrum. Meth.* **A383** (1996) 342–366.

[79] **L3** Collaboration, B. Adeva *et al.*, "The Construction of the L3 Experiment," *Nucl. Instrum. Meth.* **A289** (1990) 35–102.

[80] **OPAL** Collaboration, P. P. Allport *et al.*, "The OPAL silicon strip microvertex detector with two coordinate readout," *Nucl. Instrum. Meth.* **A346** (1994) 476–495.

[81] **OPAL** Collaboration, K. Ahmet *et al.*, "The OPAL detector at LEP," *Nucl. Instrum. Meth.* **A305** (1991) 275–319.

[82] B. Richter, "SLC Status And SLAC Future Plans," *Part. Accel.* **26** (1990) 33–50.

[83] "SLAC Linear Collider Conceptual Design Report". SLAC-R-0229.

[84] K. Abe *et al.*, "Design and performance of the SLD vertex detector, a 307 Mpixel tracking system," *Nucl. Instrum. Meth.* **A400** (1997) 287–343.

[85] **SLD** Collaboration, W. W. Ash *et al.*, "SLD Design Report". SLAC-0273.

[86] **ALEPH, DELPHI, L3, OPAL** Collaboration, the LEP Electroweak Working Group, "Precision Electroweak Measurements and Constraints on the Standard Model," `arXiv:0712.0929`.

[87] M. W. Grünewald, "Experimental tests of the electroweak standard model at high energies," *Phys. Rept.* **322** (1999) 125–346.

[88] G. Quast, "Experimental results on the electroweak interaction," *Prog. Part. Nucl. Phys.* **43** (1999) 87–166.

[89] J. C. Collins, D. E. Soper, and G. Sterman, "Heavy Particle Production in High-Energy Hadron Collisions," *Nucl. Phys.* **B263** (1986) 37.

[90] J. C. Collins and D. E. Soper, "The Theorems of Perturbative QCD," *Ann. Rev. Nucl. Part. Sci.* **37** (1987) 383–409.

[91] Y. L. Dokshitzer, "Calculation of the Structure Functions for Deep Inelastic Scattering and e^+e^- Annihilation by Perturbation Theory in Quantum Chromodynamics. (In Russian)," *Sov. Phys. JETP* **46** (1977) 641–653.

[92] G. Altarelli and G. Parisi, "Asymptotic Freedom in Parton Language," *Nucl. Phys.* **B126** (1977) 298.

[93] V. N. Gribov and L. N. Lipatov, "Deep inelastic e p scattering in perturbation theory," *Sov. J. Nucl. Phys.* **15** (1972) 438–450.

[94] D. Stump *et al.*, "Inclusive jet production, parton distributions, and the search for new physics," *JHEP* **10** (2003) 046, `hep-ph/0303013`.

[95] J. Pumplin *et al.*, "New generation of parton distributions with uncertainties from global QCD analysis," *JHEP* **07** (2002) 012, `hep-ph/0201195`.

[96] A. D. Martin, R. G. Roberts, W. J. Stirling, and R. S. Thorne, "Uncertainties of predictions from parton distributions. I: Experimental errors," *Eur. Phys. J.* **C28** (2003) 455–473, hep-ph/0211080.

[97] M. Glück, E. Reya, and A. Vogt, "Dynamical parton distributions revisited," *Eur. Phys. J.* **C5** (1998) 461–470, hep-ph/9806404.

[98] S. Alekhin, "Parton distributions from deep-inelastic scattering data," *Phys. Rev.* **D68** (2003) 014002, hep-ph/0211096.

[99] **H1** Collaboration, C. Adloff *et al.*, "Deep-inelastic inclusive e p scattering at low x and a determination of alpha(s)," *Eur. Phys. J.* **C21** (2001) 33–61, hep-ex/0012053.

[100] **ZEUS** Collaboration, S. Chekanov *et al.*, "A ZEUS next-to-leading-order QCD analysis of data on deep inelastic scattering," *Phys. Rev.* **D67** (2003) 012007, hep-ex/0208023.

[101] R. S. Thorne, "Parton distributions - DIS06," hep-ph/0606307.

[102] W. A. Bardeen, A. J. Buras, D. W. Duke, and T. Muta, "Deep Inelastic Scattering Beyond the Leading Order in Asymptotically Free Gauge Theories," *Phys. Rev.* **D18** (1978) 3998.

[103] N. Kidonakis, E. Laenen, S. Moch, and R. Vogt, "Sudakov resummation and finite order expansions of heavy quark hadroproduction cross sections," *Phys. Rev.* **D64** (2001) 114001, hep-ph/0105041.

[104] P. Nason, S. Dawson, and R. K. Ellis, "The Total Cross-Section for the Production of Heavy Quarks in Hadronic Collisions," *Nucl. Phys.* **B303** (1988) 607.

[105] W. Beenakker, W. L. van Neerven, R. Meng, G. A. Schuler, and J. Smith, "QCD corrections to heavy quark production in hadron hadron collisions," *Nucl. Phys.* **B351** (1991) 507–560.

[106] W. Beenakker, H. Kuijf, W. L. van Neerven, and J. Smith, "QCD Corrections to Heavy Quark Production in p anti-p Collisions," *Phys. Rev.* **D40** (1989) 54–82.

[107] S. Catani and L. Trentadue, "Comment on QCD exponentiation at large x," *Nucl. Phys.* **B353** (1991) 183–186.

[108] S. Catani and L. Trentadue, "Resummation of the QCD Perturbative Series for Hard Processes," *Nucl. Phys.* **B327** (1989) 323.

[109] G. Sterman, "Summation of Large Corrections to Short Distance Hadronic Cross-Sections," *Nucl. Phys.* **B281** (1987) 310.

[110] E. L. Berger and H. Contopanagos, "Threshold resummation of the total cross section for heavy quark production in hadronic collisions," *Phys. Rev.* **D57** (1998) 253–264, `hep-ph/9706206`.

[111] E. L. Berger and H. Contopanagos, "The Perturbative Resummed Series for Top Quark Production in Hadron Reactions," *Phys. Rev.* **D54** (1996) 3085–3113, `hep-ph/9603326`.

[112] E. L. Berger and H. Contopanagos, "Perturbative gluon resummation of the top quark production cross-section," *Phys. Lett.* **B361** (1995) 115–120, `hep-ph/9507363`.

[113] E. Laenen, J. Smith, and W. L. van Neerven, "Top quark production cross-section," *Phys. Lett.* **B321** (1994) 254–258, `hep-ph/9310233`.

[114] E. Laenen, J. Smith, and W. L. van Neerven, "All order resummation of soft gluon contributions to heavy quark production in hadron hadron collisions," *Nucl. Phys.* **B369** (1992) 543–599.

[115] S. Catani, M. L. Mangano, P. Nason, and L. Trentadue, "The Resummation of Soft Gluon in Hadronic Collisions," *Nucl. Phys.* **B478** (1996) 273–310, `hep-ph/9604351`.

[116] S. Catani, M. L. Mangano, P. Nason, and L. Trentadue, "The Top Cross Section in Hadronic Collisions," *Phys. Lett.* **B378** (1996) 329–336, `hep-ph/9602208`.

[117] M. Cacciari, S. Frixione, M. L. Mangano, P. Nason, and G. Ridolfi, "The $t\bar{t}$ cross-section at 1.8 TeV and 1.96 TeV: A study of the systematics due to parton densities and scale dependence," *JHEP* **04** (2004) 068, `hep-ph/0303085`.

[118] R. Bonciani, S. Catani, M. L. Mangano, and P. Nason, "NLL resummation of the heavy-quark hadroproduction cross- section," *Nucl. Phys.* **B529** (1998) 424–450, `hep-ph/9801375`.

[119] N. Kidonakis and R. Vogt, "Top quark production at the Tevatron at NNLO," *Eur. Phys. J.* **C33** (2004) S466–S468, `hep-ph/0309045`.

[120] N. Kidonakis and R. Vogt, "Next-to-next-to-leading order soft-gluon corrections in top quark hadroproduction," *Phys. Rev.* **D68** (2003) 114014, hep-ph/0308222.

[121] A. D. Martin, R. G. Roberts, W. J. Stirling, and R. S. Thorne, "MRST2001: Partons and alpha(s) from precise deep inelastic scattering and Tevatron jet data," *Eur. Phys. J.* **C23** (2002) 73–87, hep-ph/0110215.

[122] A. D. Martin, R. G. Roberts, and W. J. Stirling, "Parton distributions: A study of the new HERA data, alpha(s), the gluon and p anti-p jet production," *Phys. Lett.* **B387** (1996) 419–426, hep-ph/9606345.

[123] S. Catani, "Aspects of QCD, from the Tevatron to the LHC," hep-ph/0005233.

[124] P. M. Nadolsky *et al.*, "Implications of CTEQ global analysis for collider observables," *Phys. Rev.* **D78** (2008) 013004, arXiv:0802.0007.

[125] N. Kidonakis, "Consideration of PDF uncertainties in addition to 1PI/PIM uncertainty in top pair cross section evaluations". Private communication (2006).

[126] M. Cacciari, S. Frixione, M. M. Mangano, P. Nason, and G. Ridolfi, "Updated predictions for the total production cross sections of top and of heavier quark pairs at the Tevatron and at the LHC," *JHEP* **09** (2008) 127, arXiv:0804.2800.

[127] N. Kidonakis and R. Vogt, "The theoretical top quark cross section at the Tevatron and the LHC," arXiv:0805.3844.

[128] S. Moch and P. Uwer, "Theoretical status and prospects for top-quark pair production at hadron colliders," *Phys. Rev.* **D78** (2008) 034003, arXiv:0804.1476. The CTEQ6.6 results were provided as private communication.

[129] A. D. Martin, W. J. Stirling, R. S. Thorne, and G. Watt, "Update of Parton Distributions at NNLO," *Phys. Lett.* **B652** (2007) 292–299, arXiv:0706.0459.

[130] T. Stelzer and S. Willenbrock, "Single top quark production via q anti-q → t anti-b," *Phys. Lett.* **B357** (1995) 125–130, hep-ph/9505433.

[131] S. Cortese and R. Petronzio, "The Single top production channel at Tevatron energies," *Phys. Lett.* **B253** (1991) 494–498.

[132] R. K. Ellis and S. J. Parke, "Top quark production by W gluon fusion," *Phys. Rev.* **D46** (1992) 3785–3788.

[133] C. P. Yuan, "A New Method to Detect a Heavy Top Quark at the Tevatron," *Phys. Rev.* **D41** (1990) 42.

[134] S. S. D. Willenbrock and D. A. Dicus, "Production of Heavy Quarks from W Gluon Fusion," *Phys. Rev.* **D34** (1986) 155.

[135] S. Dawson, "The Effective W Approximation," *Nucl. Phys.* **B249** (1985) 42–60.

[136] A. Belyaev and E. Boos, "Single top quark t W + X production at the LHC: A closer look," *Phys. Rev.* **D63** (2001) 034012, `hep-ph/0003260`.

[137] T. M. P. Tait, "The t W- mode of single top production," *Phys. Rev.* **D61** (2000) 034001, `hep-ph/9909352`.

[138] A. S. Belyaev, E. E. Boos, and L. V. Dudko, "Single top quark at future hadron colliders: Complete signal and background study," *Phys. Rev.* **D59** (1999) 075001, `hep-ph/9806332`.

[139] A. P. Heinson, A. S. Belyaev, and E. E. Boos, "Single top quarks at the Fermilab Tevatron," *Phys. Rev.* **D56** (1997) 3114–3128, `hep-ph/9612424`.

[140] S. Moretti, "Single-top production in the $tW^{\pm}$ channel and Higgs signals via $H \to W^{+}W^{-}$ at the Large Hadron Collider," *Phys. Rev.* **D56** (1997) 7427–7433, `hep-ph/9705388`.

[141] G. A. Ladinsky and C. P. Yuan, "The W - top background to heavy Higgs production," *Phys. Rev.* **D43** (1991) 789–793.

[142] B. W. Harris, E. Laenen, L. Phaf, Z. Sullivan, and S. Weinzierl, "The fully differential single top quark cross section in next-to-leading order QCD," *Phys. Rev.* **D66** (2002) 054024, `hep-ph/0207055`.

[143] S. Mrenna and C. P. Yuan, "Effects of QCD resummation on W+ h and t anti-b production at the Tevatron," *Phys. Lett.* **B416** (1998) 200–207, `hep-ph/9703224`.

[144] M. C. Smith and S. Willenbrock, "QCD and Yukawa Corrections to Single-Top-Quark Production via q qbar → t bbar," *Phys. Rev.* **D54** (1996) 6696–6702, hep-ph/9604223.

[145] T. Stelzer, Z. Sullivan, and S. Willenbrock, "Single-top-quark production via W-gluon fusion at next-to- leading order," *Phys. Rev.* **D56** (1997) 5919–5927, hep-ph/9705398.

[146] G. Bordes and B. van Eijk, "Calculating QCD corrections to single top production in hadronic interactions," *Nucl. Phys.* **B435** (1995) 23–58.

[147] S. Zhu, "Erratum to: Next-to-leading order QCD corrections to b g → t W- at the CERN Large Hadron Collider," *Phys. Lett.* **B537** (2002) 351–352.

[148] S. Zhu, "Next-to-leading order QCD corrections to b g → t W- at the CERN Large Hadron Collider," *Phys. Lett.* **B524** (2002) 283–288.

[149] Q.-H. Cao and C. P. Yuan, "Single top quark production and decay at next-to-leading order in hadron collision," *Phys. Rev.* **D71** (2005) 054022, hep-ph/0408180.

[150] Q.-H. Cao, R. Schwienhorst, and C. P. Yuan, "Next-to-leading order corrections to single top quark production and decay at Tevatron. I: s-channel process," *Phys. Rev.* **D71** (2005) 054023, hep-ph/0409040.

[151] J. Campbell, R. K. Ellis, and F. Tramontano, "Single top production and decay at next-to-leading order," *Phys. Rev.* **D70** (2004) 094012, hep-ph/0408158.

[152] Q.-H. Cao, R. Schwienhorst, J. A. Benitez, R. Brock, and C. P. Yuan, "Next-to-leading order corrections to single top quark production and decay at the Tevatron. II: t-channel process," *Phys. Rev.* **D72** (2005) 094027, hep-ph/0504230.

[153] J. Campbell and F. Tramontano, "Next-to-leading order corrections to W t production and decay," *Nucl. Phys.* **B726** (2005) 109–130, hep-ph/0506289.

[154] N. Kidonakis, "Single top production at the Tevatron: Threshold resummation and finite-order soft gluon corrections," *Phys. Rev.* **D74** (2006) 114012, hep-ph/0609287.

[155] N. Kidonakis, "Higher-order soft gluon corrections in single top quark production at the LHC," *Phys. Rev.* **D75** (2007) 071501, hep-ph/0701080.

[156] N. Kidonakis, "Higher-order Threshold Corrections for Single Top Quark Production," arXiv:0705.2431.

[157] Z. Sullivan, "Understanding single-top-quark production and jets at hadron colliders," *Phys. Rev.* **D70** (2004) 114012, hep-ph/0408049.

[158] **CTEQ** Collaboration, H. L. Lai *et al.*, "Global QCD analysis of parton structure of the nucleon: CTEQ5 parton distributions," *Eur. Phys. J.* **C12** (2000) 375–392, hep-ph/9903282.

[159] **CDF, DØ** Collaboration, the Tevatron Electroweak Working Group, "Combination of CDF and D0 results on the top-quark mass," hep-ex/0404010.

[160] A. D. Martin, R. G. Roberts, W. J. Stirling, and R. S. Thorne, "Physical gluons and high-E(T) jets," *Phys. Lett.* **B604** (2004) 61–68, hep-ph/0410230.

[161] G. Mahlon and S. J. Parke, "Single top quark production at the LHC: Understanding spin," *Phys. Lett.* **B476** (2000) 323–330, hep-ph/9912458.

[162] T. Stelzer, Z. Sullivan, and S. Willenbrock, "Single top quark production at hadron colliders," *Phys. Rev.* **D58** (1998) 094021, hep-ph/9807340.

[163] G. Mahlon and S. J. Parke, "Improved spin basis for angular correlation studies in single top quark production at the Tevatron," *Phys. Rev.* **D55** (1997) 7249–7254, hep-ph/9611367.

[164] D. O. Carlson and C. P. Yuan, "Studying the top quark via the W - gluon fusion process," *Phys. Lett.* **B306** (1993) 386–390.

[165] T. Tait and C. P. Yuan, "Single top quark production as a window to physics beyond the Standard Model," *Phys. Rev.* **D63** (2001) 014018, hep-ph/0007298.

[166] **Particle Data Group** Collaboration, S. Eidelman *et al.*, "Review of Particle Physics," *Phys. Lett.* **B592** (2004) 1.

[167] A. J. Buras, W. Slominski, and H. Steger, "B0 anti-B0 Mixing, CP Violation and the B Meson Decay," *Nucl. Phys.* **B245** (1984) 369.

[168] **Heavy Flavor Averaging Group (HFAG)** Collaboration, E. Barberio *et al.*, "Averages of b-hadron properties at the end of 2005," `hep-ex/0603003`.

[169] M. Okamoto, "Full determination of the CKM matrix using recent results from lattice QCD," *PoS* **LAT2005** (2006) 013, `hep-lat/0510113`.

[170] **CDF** Collaboration, A. Abulencia *et al.*, "Measurement of the $B_s^0 - \bar{B}_s^0$ Oscillation Frequency," *Phys. Rev. Lett.* **97** (2006) 062003, `hep-ex/0606027`.

[171] **DØ** Collaboration, V. M. Abazov *et al.*, "First Direct Two-Sided Bound on the B_s^0 Oscillation Frequency," *Phys. Rev. Lett.* **97** (2006) 021802, `arXiv:hep-ex/0603029`.

[172] **CKMfitter Group** Collaboration, J. Charles *et al.*, "CP violation and the CKM matrix: Assessing the impact of the asymmetric B factories," *Eur. Phys. J.* **C41** (2005) 1–131, `hep-ph/0406184`. Updated results and plots available at: http://ckmfitter.in2p3.fr.

[173] **UTfit** Collaboration, M. Bona *et al.*, "The Unitarity Triangle Fit in the Standard Model and Hadronic Parameters from Lattice QCD: A Reappraisal after the Measurements of Δm_s and $BR(B \to \tau\nu_\tau)$," *JHEP* **10** (2006) 081, `hep-ph/0606167`.

[174] J. H. Kühn, "Theory of top quark production and decay," `hep-ph/9707321`.

[175] M. Jezabek and J. H. Kühn, "QCD Corrections to Semileptonic Decays of Heavy Quarks," *Nucl. Phys.* **B314** (1989) 1.

[176] G. Eilam, R. R. Mendel, R. Migneron, and A. Soni, "Radiative corrections to top quark decay," *Phys. Rev. Lett.* **66** (1991) 3105–3108.

[177] A. Denner and T. Sack, "The Top width," *Nucl. Phys.* **B358** (1991) 46–58.

[178] M. Jezabek and J. H. Kühn, "Erratum: Top quark width: Theoretical update," *Phys. Rev.* **D49** (May, 1994) 4970.

[179] M. Jezabek and J. H. Kühn, "The Top width: Theoretical update," *Phys. Rev.* **D48** (1993) 1910–1913, hep-ph/9302295.

[180] K. G. Chetyrkin, R. Harlander, T. Seidensticker, and M. Steinhauser, "Second order QCD corrections to $\Gamma(t \to Wb)$," *Phys. Rev.* **D60** (1999) 114015, hep-ph/9906273.

[181] A. Czarnecki and K. Melnikov, "Two-loop QCD corrections to top quark width," *Nucl. Phys.* **B544** (1999) 520–531, hep-ph/9806244.

[182] I. I. Y. Bigi, Y. L. Dokshitzer, V. A. Khoze, J. H. Kühn, and P. M. Zerwas, "Production and Decay Properties of Ultraheavy Quarks," *Phys. Lett.* **B181** (1986) 157.

[183] J. H. Kühn, "Weak Decays Of Open And Hidden Top," *Acta Phys. Austriaca Suppl.* **24** (1982) 203.

[184] J. H. Kühn, "Weak Interactions Of Quarkonia," *Acta Phys. Polon.* **B12** (1981) 347.

[185] L. H. Orr, "Decay versus hadronization for top quarks produced in hadron colliders," *Phys. Rev.* **D44** (1991) 88–98.

[186] D. Wicke and P. Z. Skands, "Non-perturbative QCD Effects and the Top Mass at the Tevatron," arXiv:0807.3248.

[187] P. Skands and D. Wicke, "Non-perturbative QCD effects and the top mass at the Tevatron," *Eur. Phys. J.* **C52** (2007) 133–140, hep-ph/0703081.

[188] C. A. Nelson, B. T. Kress, M. Lopes, and T. P. McCauley, "General tests for $t \to W^+ b$ couplings at hadron colliders," *Phys. Rev.* **D56** (1997) 5928–5944, hep-ph/9707211.

[189] R. H. Dalitz and G. R. Goldstein, "The Decay and polarization properties of the top quark," *Phys. Rev.* **D45** (1992) 1531–1543.

[190] G. L. Kane, G. A. Ladinsky, and C. P. Yuan, "Using the top quark for testing standard model polarization and CP predictions," *Phys. Rev.* **D45** (1992) 124–141.

[191] M. Fischer, S. Groote, J. G. Körner, and M. C. Mauser, "Longitudinal, transverse-plus and transverse-minus W bosons in unpolarized top quark decays at O(alpha(s))," *Phys. Rev.* **D63** (2001) 031501, hep-ph/0011075.

[192] H. S. Do, S. Groote, J. G. Körner, and M. C. Mauser, "Electroweak and finite width corrections to top quark decays into transverse and longitudinal W-bosons," *Phys. Rev.* **D67** (2003) 091501, hep-ph/0209185.

[193] C.-R. Chen, F. Larios, and C. P. Yuan, "General analysis of single top production and W helicity in top decay," *Phys. Lett.* **B631** (2005) 126–132, hep-ph/0503040.

[194] P. C. Bhat, H. Prosper, and S. S. Snyder, "Top quark physics at the Tevatron," *Int. J. Mod. Phys.* **A13** (1998) 5113–5218, hep-ex/9809011.

[195] Fermilab Accelerator Division, http://www-bd.fnal.gov/.

[196] R. S. Moore, "Performance and Future of the Tevatron," *Nucl. Phys. Proc. Suppl.* **177-178** (2008) 5–7.

[197] C. Y. Tan, "Tune tracking with a PLL in the Tevatron," *Nucl. Instrum. Meth.* **A557** (2006) 615–620.

[198] D. P. McGinnis, "FNAL Tevatron operational status". Prepared for Particle Accelerator Conference (PAC 05), Knoxville, Tennessee, 16-20 May 2005.

[199] **Proton Driver** Collaboration, D. P. Moehs, J. Peters, and J. Sherman, "Negative hydrogen ion sources for accelerators," *IEEE Trans. Plasma Sci.* **33** (2005) 1786–1798.

[200] J. E. Griffin, J. Maclachlan, A. G. Ruggiero, and K. Takayama, "Time and Momentum Exchange for Production and Collection of Intense Antiproton Beams at Fermilab," *IEEE Trans. Nucl. Sci.* **30** (1983) 2630–2632.

[201] D. Mohl, G. Petrucci, L. Thorndahl, and S. Van Der Meer, "Physics and Technique of Stochastic Cooling," *Phys. Rept.* **58** (1980) 73–119.

[202] G. I. Budker, "An effective method of damping particle oscillations in proton and anti-proton storage rings," *Sov. Atom. Energ.* **22** (1967) 438–440.

[203] P. F. Derwent, "Status of the Fermilab Recycler," *Conf. Proc.* **C07091010** (2007) mom1i01. Presented at International Workshop On Beam Cooling And Related Topics (COOL07), Bad Kreuznach, Germany, 10-14 Sep 2007.

[204] Fermilab Operations Department, http://www-bdnew.fnal.gov/operations/lum/lum.html.

[205] D0 Run II Operations Group, http://d0server1.fnal.gov/Projects/Operations/D0RunII_DataTaking.htm.

[206] **CDF** Collaboration, A. Abulencia *et al.*, "Measurements of Inclusive W and Z Cross Sections in p-pbar Collisions at sqrts =1.96 TeV," *J. Phys.* **G34** (2007) 2457–2544, hep-ex/0508029.

[207] **DØ** Collaboration, V. M. Abazov *et al.*, "The Upgraded DØ Detector," *Nucl. Instrum. Meth.* **A565** (2006) 463–537, arXiv:physics/0507191.

[208] **CDF** Collaboration, D. E. Acosta *et al.*, "Measurement of the $t\bar{t}$ production cross section in $p\bar{p}$ collisions at $\sqrt{s} = 1.96$ TeV using lepton + jets events with secondary vertex $b-$tagging," *Phys. Rev.* **D71** (2005) 052003, hep-ex/0410041.

[209] **CDF** Collaboration, R. Blair *et al.*, "The CDF-II detector: Technical design report". FERMILAB-PUB-96-390-E.

[210] **CDF** Collaboration, A. Abulencia *et al.*, "Measurement of the $t\bar{t}$ Production Cross Section in $p\bar{p}$ collisions at $\sqrt{s} = 1.96$ TeV using Lepton + Jets Events with Jet Probability b-tagging," *Phys. Rev.* **D74** (2006) 072006, hep-ex/0607035.

[211] DZero Final RunIIa Jet Energy Scale, http://www-d0.fnal.gov/phys_id/jes/public_RunIIa/.

[212] G. C. Blazey *et al.*, "Run II jet physics," hep-ex/0005012.

[213] **CDF** Collaboration, F. Abe *et al.*, "The Topology of three jet events in $\bar{p}p$ collisions at $\sqrt{s} = 1.8$ TeV," *Phys. Rev.* **D45** (1992) 1448–1458.

[214] **DØ** Collaboration, J. Hegeman, "Jet energy scale calibration in the D0 experiment," *Journal of Physics: Conference Series* (2008). Proceedings of the XIII International Conference on Calorimetry in High Energy Physics (CALOR08), 26 - 30 May 2008, Pavia.

[215] A. Bhatti *et al.*, "Determination of the jet energy scale at the Collider Detector at Fermilab," *Nucl. Instrum. Meth.* **A566** (2006) 375–412, hep-ex/0510047.

[216] **DØ** Collaboration, A. Harel, "Tools for top physics at D0," arXiv:0807.3926. Presented at TOP2008: International Workshop on Top-Quark Physics, La Biodola, Isola d'Elba, Italy, 18-24 May 2008.

[217] J. Donini *et al.*, "Energy Calibration of b-Quark Jets with $Z \to b\bar{b}$ Decays at the Tevatron Collider," arXiv:0801.3906.

[218] **DØ** Collaboration, V. M. Abazov *et al.*, "Measurement of $\sigma(p\bar{p} \to Z)\cdot\mathrm{Br}(Z \to \tau^+\tau^-)$ with 1 fb^{-1} at $\sqrt{s}$ =1.96 TeV," *DØ conference note* **5484** (2007).

[219] **CDF** Collaboration, A. Abulencia *et al.*, "A search for $t \to \tau\nu q$ in $t\bar{t}$ production," *Phys. Lett.* **B639** (2006) 172, hep-ex/0510063.

[220] **CDF** Collaboration, E. Palencia, "Tools for Top Physics at CDF," *CDF conference note* **9371** (2008). Presented at TOP2008: International Workshop on Top-Quark Physics, La Biodola, Isola d'Elba, Italy, 18-24 May 2008.

[221] **DØ** Collaboration, V. M. Abazov *et al.*, "Measurement of the $t\bar{t}$ production cross section in $p\bar{p}$ collisions at $\sqrt{s} = 1.96$ TeV using secondary vertex b tagging," *Phys. Rev.* **D74** (2006) 112004, arXiv:hep-ex/0611002.

[222] M. Dobbs and J. B. Hansen, "The HepMC C++ Monte Carlo event record for High Energy Physics," *Comput. Phys. Commun.* **134** (2001) 41–46.

[223] **QCD Tools Working Group** Collaboration, R. K. Ellis *et al.*, "Report of the QCD tools working group," hep-ph/0011122.

[224] G. Marchesini *et al.*, "HERWIG: A Monte Carlo event generator for simulating hadron emission reactions with interfering gluons. Version 5.1 - April 1991," *Comput. Phys. Commun.* **67** (1992) 465–508.

[225] T. Sjöstrand *et al.*, "High-energy-physics event generation with PYTHIA 6.1," *Comput. Phys. Commun.* **135** (2001) 238–259, hep-ph/0010017.

[226] M. A. Dobbs *et al.*, "Les Houches guidebook to Monte Carlo generators for hadron collider physics," hep-ph/0403045.

[227] S. R. Slabospitsky, "Event generators for top quark production and decays," *PoS* **TOP2006** (2006) 019, hep-ph/0603124.

[228] T. Sjöstrand, L. Lonnblad, and S. Mrenna, "PYTHIA 6.2: Physics and manual," hep-ph/0108264.

[229] M. L. Mangano, M. Moretti, F. Piccinini, R. Pittau, and A. D. Polosa, "ALPGEN, a generator for hard multiparton processes in hadronic collisions," *JHEP* **07** (2003) 001, hep-ph/0206293.

[230] T. Sjöstrand, L. Lonnblad, S. Mrenna, and P. Skands, "PYTHIA 6.3: Physics and manual," hep-ph/0308153.

[231] M. L. Mangano, M. Moretti, F. Piccinini, and M. Treccani, "Matching matrix elements and shower evolution for top- quark production in hadronic collisions," *JHEP* **01** (2007) 013, hep-ph/0611129.

[232] S. Höche *et al.*, "Matching parton showers and matrix elements," hep-ph/0602031.

[233] G. Corcella *et al.*, "HERWIG 6: An event generator for hadron emission reactions with interfering gluons (including supersymmetric processes)," *JHEP* **01** (2001) 010, hep-ph/0011363.

[234] E. E. Boos, V. E. Bunichev, L. V. Dudko, V. I. Savrin, and A. V. Sherstnev, "Method for simulating electroweak top-quark production events in the NLO approximation: SingleTop event generator," *Phys. Atom. Nucl.* **69** (2006) 1317–1329.

[235] **CompHEP** Collaboration, E. Boos *et al.*, "CompHEP 4.4: Automatic computations from Lagrangians to events," *Nucl. Instrum. Meth.* **A534** (2004) 250–259, hep-ph/0403113.

[236] F. Maltoni and T. Stelzer, "MadEvent: Automatic event generation with MadGraph," *JHEP* **02** (2003) 027, hep-ph/0208156.

[237] T. Stelzer and W. F. Long, "Automatic generation of tree level helicity amplitudes," *Comput. Phys. Commun.* **81** (1994) 357–371, hep-ph/9401258.

[238] Z. Was and P. Golonka, "TAUOLA as tau Monte Carlo for future applications," *Nucl. Phys. Proc. Suppl.* **144** (2005) 88–94, hep-ph/0411377.

[239] S. Jadach, J. H. Kühn, and Z. Was, "TAUOLA: A Library of Monte Carlo programs to simulate decays of polarized tau leptons," *Comput. Phys. Commun.* **64** (1990) 275–299.

[240] D. J. Lange, "The EvtGen particle decay simulation package," *Nucl. Instrum. Meth.* **A462** (2001) 152–155.

[241] P. Avery, K. Read, and G. Trahern *CLEO Report* **CSN-212** (1985). Unpublished, see http://www.lepp.cornell.edu/public/CLEO/soft/QQ/.

[242] R. Brun *et al.*, "GEANT - Detector Description and Simulation Tool," *CERN Program Library Long Writeup* **W5013** (1994).

[243] **CDF** Collaboration, T. Aaltonen *et al.*, "Measurement of the cross section for W-boson production in association with jets in ppbar collisions at $\sqrt{s}$=1.96 TeV," *Phys. Rev.* **D77** (2008) 011108, arXiv:0711.4044.

[244] **CDF** Collaboration, A. Abulencia *et al.*, "Search for anomalous semileptonic decay of heavy flavor hadrons produced in association with a W boson at CDF II," *Phys. Rev.* **D73** (2006) 051101, hep-ex/0512065.

[245] **DØ** Collaboration, V. M. Abazov *et al.*, "A Search for Anomalous Heavy-Flavor Quark Production in Association with W Bosons," *Phys. Rev. Lett.* **94** (2005) 152002, arXiv:hep-ex/0411084.

[246] **DØ** Collaboration, V. M. Abazov *et al.*, "Measurement of the ratio of the $p\bar{p} \to W$+c-jet cross section to the inclusive $p\bar{p} \to W$+jets cross section," *Phys. Lett.* **B666** (2008) 23–30, arXiv:0803.2259.

[247] **CDF** Collaboration, T. Aaltonen *et al.*, "First Measurement of the Production of a W Boson in Association with a Single Charm Quark in Proton Anti-proton Collisions at $\sqrt{s}$=1.96 TeV," *Phys. Rev. Lett.* **100** (2008) 091803, arXiv:0711.2901.

[248] **CDF** Collaboration, T. Aaltonen *et al.*, "Measurement of the b Jet Production Cross Section in Events with a $W^{\pm}$ Boson," *CDF conference note* **9321** (2008).

[249] **DØ** Collaboration, V. M. Abazov *et al.*, "A search for $Wb\bar{b}$ and WH production in $p\bar{p}$ collisions at $\sqrt{s} = 1.96$ TeV," *Phys. Rev. Lett.* **94** (2005) 091802, hep-ex/0410062.

[250] **CDF, DØ** Collaboration, A. Harel, "Monte Carlo for top background at the Tevatron," arXiv:0807.4127. Presented at TOP2008: International Workshop on Top-Quark Physics, La Biodola, Isola d'Elba, Italy, 18-24 May 2008.

[251] **CDF, DØ** Collaboration, U. Husemann, "Monte Carlo Simulations for Top Pair and Single Top Production at the Tevatron," arXiv:0807.4589. Presented at TOP2008: International Workshop on Top-Quark Physics, La Biodola, Isola d'Elba, Italy, 18-24 May 2008.

[252] V. D. Barger, J. Ohnemus, and R. J. N. Phillips, "Event shape criteria for single lepton top signals," *Phys. Rev.* **D48** (1993) 3953–3956, hep-ph/9308216.

[253] **CDF** Collaboration, T. Aaltonen *et al.*, "Measurement of ttbar production cross section using dilepton events in 2.8 fb^{-1}," *CDF conference note* **9399** (2008).

[254] **CDF** Collaboration, D. E. Acosta *et al.*, "Measurement of the $t\bar{t}$ production cross section in $p\bar{p}$ collisions at $\sqrt{s} = 1.96$ TeV using dilepton events," *Phys. Rev. Lett.* **93** (2004) 142001, hep-ex/0404036.

[255] **DØ** Collaboration, V. M. Abazov *et al.*, "Measurement of the $t\bar{t}$ Production Cross Section in $p\bar{p}$ Collisions at $\sqrt{s} = 1.96$ TeV in Dilepton Final States," *Phys. Lett.* **B626** (2005) 55–64, arXiv:hep-ex/0505082.

[256] **DØ** Collaboration, V. M. Abazov *et al.*, "Measurement of the $t\bar{t}$ production cross section in $p\bar{p}$ collisions using dilepton events," *Phys. Rev.* **D76** (2007) 052006, arXiv:0706.0458.

[257] **CDF** Collaboration, A. Abulencia *et al.*, "Cross section measurements of high-p_T dilepton final-state processes using a global fitting method," *Phys. Rev.* **D78** (2008) 012003, hep-ex/0612058.

[258] **DØ** Collaboration, V. M. Abazov *et al.*, "Measurement of the $t\bar{t}$ Production cross section at $\sqrt{s} = 1.96$ TeV in Dilepton Final States Using 1 fb^{-1}," *DØ conference note* **5371** (2007).

[259] **DØ** Collaboration, V. M. Abazov *et al.*, "A search for charged Higgs bosons in $t\bar{t}$ events," *DØ conference note* **5715** (2008).

[260] **DØ** Collaboration, V. M. Abazov *et al.*, "Measurement of the $t\bar{t}$ Production Cross Section in the Lepton+Track Channel with 1 fb^{-1} of Run II Data," *DØ conference note* **5465** (2007).

[261] **DØ** Collaboration, V. M. Abazov *et al.*, "Combined $t\bar{t}$ Production Cross Section in the Lepton+Track and Dilepton Final States Using 1 fb^{-1} of data," *DØ conference note* **5477** (2007).

[262] **CDF** Collaboration, T. Aaltonen *et al.*, "A Measurement of the $p\bar{p} \to t\bar{t} \to b\bar{b}\ell^+\nu\ell^-\nu$ Cross-Section in 1.0 fb^{-1} Using Lepton plus Isolated Track Selection with Identified b-Jets at $\sqrt{s} = 1.96$ TeV," *CDF conference note* **8912** (2007).

[263] **CDF** Collaboration, T. Aaltonen *et al.*, "A Measurement of the $p\bar{p} \to t\bar{t} \to b\bar{b}\ell^+\nu\ell^-\nu$ Cross-Section in 1.1 fb^{-1} Using Lepton plus Isolated Track Selection at $\sqrt{s} = 1.96$ TeV," *CDF conference note* **8770** (2007).

[264] **DØ** Collaboration, V. M. Abazov *et al.*, "Measurement of the $t\bar{t}$ production cross section in $p\bar{p}$ collisions at $\sqrt{s} = 1.96$ TeV," *Phys. Rev. Lett.* **100** (2008) 192004, arXiv:0803.2779.

[265] **CDF** Collaboration, D. E. Acosta *et al.*, "Measurement of the $t\bar{t}$ production cross section in $p\bar{p}$ collisions at $\sqrt{s} = 1.96$ TeV using kinematic fitting of $b-$tagged lepton + jet events," *Phys. Rev.* **D71** (2005) 072005, hep-ex/0409029.

[266] **CDF** Collaboration, D. E. Acosta *et al.*, "Measurement of the $t\bar{t}$ production cross section in $p\bar{p}$ collisions at $\sqrt{s} = 1.96$ TeV using lepton plus jets events with semileptonic B decays to muons," *Phys. Rev.* **D72** (2005) 032002, hep-ex/0506001.

[267] **CDF** Collaboration, D. E. Acosta *et al.*, "Measurement of the cross section for $t\bar{t}$ production in $p\bar{p}$ collisions using the kinematics of lepton + jets events," *Phys. Rev.* **D72** (2005) 052003, hep-ex/0504053.

[268] **DØ** Collaboration, V. M. Abazov *et al.*, "Measurement of the $t\bar{t}$ Production Cross Section in $p\bar{p}$ Collisions at $\sqrt{s} = 1.96$ TeV using Kinematic Characteristics of Lepton + Jets Events," *Phys. Lett.* **B626** (2005) 45–54, arXiv:hep-ex/0504043.

[269] **DØ** Collaboration, V. M. Abazov *et al.*, "Measurement of the $t\bar{t}$ Production Cross Section in $p\bar{p}$ Collisions at $\sqrt{s} = 1.96$ TeV using Lepton + Jets Events with Lifetime b-tagging," *Phys. Lett.* **B626** (2005) 35–44, arXiv:hep-ex/0504058.

[270] **CDF** Collaboration, A. Abulencia *et al.*, "Measurement of the $t\bar{t}$ Production Cross Section in $p\bar{p}$ Collisions at $\sqrt{s} = 1.96$ TeV," *Phys. Rev. Lett.* **97** (2006) 082004, hep-ex/0606017.

[271] **DØ** Collaboration, V. M. Abazov *et al.*, "Measurement of the $t\bar{t}$ production cross section in $p\bar{p}$ collisions at $\sqrt{s} = 1.96$ TeV using

kinematic characteristics of lepton + jets events," *Phys. Rev.* **D76** (2007) 092007, arXiv:0705.2788.

[272] **DØ** Collaboration, V. M. Abazov *et al.*, "Measurement of the $t\bar{t}$ Production Cross Section in $p\bar{p}$ Collisions at $\sqrt{s} = 1.96$ TeV Using Soft Muon b-tagged Lepton+Jets Events," *DØ conference note* **5257** (2006).

[273] **CDF** Collaboration, T. Aaltonen *et al.*, "Measurement of the $t\bar{t}$ Production Cross Section in SecVtx- and Neural Network-Tagged Lepton+Jets Events," *CDF conference note* **8272** (2006).

[274] **CDF** Collaboration, T. Aaltonen *et al.*, "Measurement of the $t\bar{t}$ Production Cross Section in $p\bar{p}$ collisions at $\sqrt{s} = 1.96$ TeV using Lepton + Jets Events with Soft Electron b-Tagging," *CDF conference note* **9348** (2008).

[275] **CDF** Collaboration, T. Aaltonen *et al.*, "Measurement of the $t\bar{t}$ Production Cross Section in $p\bar{p}$ Collisions at $\sqrt{s} = 1.96$ TeV Using Lepton Plus Jets Events with Soft Muon b-Tagging," *CDF conference note* **9304** (2008).

[276] **CDF** Collaboration, T. Aaltonen *et al.*, "Measurement of the Top Pair Cross Section in the Lepton Plus Jets Decay Channel with 2.7 fb^{-1}," *CDF conference note* **9462** (2008).

[277] **CDF** Collaboration, T. Aaltonen *et al.*, "Measurement of the $t\bar{t}$ Cross Section in the Lepton Plus Jets Channel Using Neural Networks in 2.8 fb^{-1} of CDF data," *CDF conference note* **9474** (2008).

[278] A. Valassi, "Combining correlated measurements of several different physical quantities," *Nucl. Instrum. Meth.* **A500** (2003) 391–405.

[279] L. Lyons, D. Gibaut, and P. Clifford, "How To Combine Correlated Estimates Of A Single Physical Quantity," *Nucl. Instrum. Meth.* **A270** (1988) 110.

[280] **CDF** Collaboration, T. Aaltonen *et al.*, "Measurement of the $p\bar{p} \to t\bar{t}$ production cross- section and the top quark mass at $\sqrt{s} = 1.96$- TeV in the all-hadronic decay mode," *Phys. Rev.* **D76** (2007) 072009, arXiv:0706.3790.

[281] **CDF** Collaboration, A. Abulencia *et al.*, "Measurement of the $t\bar{t}$ Production Cross Section in $p\bar{p}$ collisions at $\sqrt{s} = 1.96$ TeV in the All

Hadronic Decay Mode," *Phys. Rev.* **D74** (2006) 072005, hep-ex/0607095.

[282] **DØ** Collaboration, V. M. Abazov *et al.*, "Measurement of the $p\bar{p} \to t\bar{t}$ production cross section at $\sqrt{s} = 1.96$ TeV in the fully hadronic decay channel," *Phys. Rev.* **D76** (2007) 072007, arXiv:hep-ex/0612040.

[283] **CDF** Collaboration, A. Abulencia *et al.*, "Measurement of the t anti-t production cross section in p anti-p collisions at $\sqrt{s} = 1.96$ TeV using missing E(t) + jets events with secondary vertex b-tagging," *Phys. Rev. Lett.* **96** (2006) 202002, hep-ex/0603043.

[284] **DØ** Collaboration, V. M. Abazov *et al.*, "Measurement of $\sigma(p\bar{p} \to t\bar{t})$ in τ + jets channel," *DØ conference note* **5234** (2006).

[285] **DØ** Collaboration, V. M. Abazov *et al.*, "Measurement of $t\bar{t}$ Production Cross Section in the Lepton + Tau + b-jet(s) + Missing Transverse Energy Channel Using 1 fb^{-1} of Run II Data," *DØ conference note* **5451** (2007).

[286] **CDF** Collaboration, T. Aaltonen *et al.*, "Search for $t\bar{t}$ in the τ dilepton channels based on 350 pb^{-1} of CDF data," *CDF conference note* **8376** (2008).

[287] **DØ** Collaboration, V. M. Abazov *et al.*, "Measurement of $t\bar{t}$ Production Cross Section in the Lepton + Tau + b-jet(s) + Missing Transverse Energy Channel Using 1.2 fb^{-1} of Run IIb Data," *DØ conference note* **5607** (2008).

[288] http://www-cdf.fnal.gov/physics/new/top/top.html.

[289] http://www-d0.fnal.gov/Run2Physics/top/index.html.

[290] **CDF** Collaboration, T. Aaltonen *et al.*, "Combination of CDF top quark pair production cross section measurements with 2.8 fb^{-1}," *CDF conference note* **9448** (2008).

[291] **CDF** Collaboration, A. A. Affolder *et al.*, "Erratum: Measurement of the $t\bar{t}$ production cross section in $p\bar{p}$ collisions at $\sqrt{s} = 1.8$ tev [phys. rev. d 64, 032002 (2001)]," *Phys. Rev.* **D67** (Jun, 2003) 119901.

[292] **CDF** Collaboration, A. A. Affolder *et al.*, "Measurement of the $t\bar{t}$ production cross section in $p\bar{p}$ collisions at $\sqrt{s} = 1.8$ TeV," *Phys. Rev.* **D64** (2001) 032002, hep-ex/0101036.

[293] **DØ** Collaboration, V. M. Abazov *et al.*, "$t\bar{t}$ production cross section in $p\bar{p}$ collisions at $\sqrt{s} = 1.8$ TeV," *Phys. Rev.* **D67** (2003) 012004, hep-ex/0205019.

[294] M. Guchait, F. Mahmoudi, and K. Sridhar, "Tevatron constraint on the Kaluza-Klein gluon of the bulk Randall-Sundrum model," *JHEP* **05** (2007) 103, hep-ph/0703060.

[295] L. Zhang, X.-L. Wang, Y.-P. Kuang, and H.-Y. Zhou, "Pseudo-Goldstone boson effects in t anti-t productions at high energy hadron colliders and testing technicolor models," *Phys. Rev.* **D61** (2000) 115007, hep-ph/9910265.

[296] G. L. Kane and S. Mrenna, "Do About Half the Top Quarks at FNAL Come From Gluino Decays?," *Phys. Rev. Lett.* **77** (1996) 3502–3505, hep-ph/9605351.

[297] **CDF** Collaboration, T. Aaltonen *et al.*, "First Measurement of the Fraction of Top Quark Pair Production Through Gluon-Gluon Fusion," arXiv:0712.3273.

[298] L. N. Lipatov, "The parton model and perturbation theory," *Sov. J. Nucl. Phys.* **20** (1975) 94–102.

[299] **CDF** Collaboration, T. Aaltonen *et al.*, "Measurement of the fraction of t-tbar production via gluon-gluon fusion in p-pbar collisions at $\sqrt{s}$=1.96 TeV," arXiv:0807.4262.

[300] **CDF** Collaboration, T. Aaltonen *et al.*, "Measurement of the Gluon Fusion Fraction in $t\bar{t}$ Production using Azimuthal Correlation of Charged Leptons," *CDF conference note* **9432** (2008).

[301] J. H. Kühn and G. Rodrigo, "Charge asymmetry of heavy quarks at hadron colliders," *Phys. Rev.* **D59** (1999) 054017, hep-ph/9807420.

[302] J. H. Kühn and G. Rodrigo, "Charge asymmetry in hadroproduction of heavy quarks," *Phys. Rev. Lett.* **81** (1998) 49–52, hep-ph/9802268.

[303] L. G. Almeida, G. Sterman, and W. Vogelsang, "Threshold Resummation for the Top Quark Charge Asymmetry," *Phys. Rev.* **D78** (2008) 014008, arXiv:0805.1885.

[304] O. Antunano, J. H. Kühn, and G. Rodrigo, "Top Quarks, Axigluons and Charge Asymmetries at Hadron Colliders," *Phys. Rev.* **D77** (2008) 014003, arXiv:0709.1652.

[305] M. T. Bowen, S. D. Ellis, and D. Rainwater, "Standard model top quark asymmetry at the Fermilab Tevatron," *Phys. Rev.* **D73** (2006) 014008, hep-ph/0509267.

[306] S. Dittmaier, P. Uwer, and S. Weinzierl, "NLO QCD corrections to t anti-t + jet production at hadron colliders," *Phys. Rev. Lett.* **98** (2007) 262002, hep-ph/0703120.

[307] C. T. Hill, "Topcolor assisted technicolor," *Phys. Lett.* **B345** (1995) 483–489, hep-ph/9411426.

[308] M. S. Carena, A. Daleo, B. A. Dobrescu, and T. M. P. Tait, "Z' gauge bosons at the Tevatron," *Phys. Rev.* **D70** (2004) 093009, hep-ph/0408098.

[309] **DØ** Collaboration, V. M. Abazov *et al.*, "First measurement of the forward-backward charge asymmetry in top quark pair production," *Phys. Rev. Lett.* **100** (2008) 142002, arXiv:0712.0851.

[310] S. Frixione, P. Nason, and B. R. Webber, "Matching NLO QCD and parton showers in heavy flavour production," *JHEP* **08** (2003) 007, hep-ph/0305252.

[311] S. Frixione and B. R. Webber, "Matching NLO QCD computations and parton shower simulations," *JHEP* **06** (2002) 029, hep-ph/0204244.

[312] R. M. Harris, C. T. Hill, and S. J. Parke, "Cross section for topcolor Z'(t) decaying to t anti-t," hep-ph/9911288.

[313] **CDF** Collaboration, T. Aaltonen *et al.*, "Forward-Backward Asymmetry in Top Quark Production in ppbar Collisions at sqrts=1.96 TeV," arXiv:0806.2472.

[314] **CDF** Collaboration, T. Aaltonen *et al.*, "Measurement Of The Front Back Asymmetry In Top-Antitop Quark Pairs In 1.9 fb^{-1}," *CDF conference note* **9169** (2008).

[315] **CDF** Collaboration, T. Aaltonen *et al.*, "Measurement of the Charge Asymmetry in Top Pair Production using 1.9 fb^{-1}," *CDF conference note* **9156** (2008).

[316] **DØ** Collaboration, S. Abachi *et al.*, "Measurement of the top quark pair production cross section in $p\bar{p}$ collisions," *Phys. Rev. Lett.* **79** (1997) 1203–1208, hep-ex/9704015.

[317] **CDF** Collaboration, F. Abe *et al.*, "Measurement of the top quark mass and $t\bar{t}$ production cross section from dilepton events at the Collider Detector at Fermilab," *Phys. Rev. Lett.* **80** (1998) 2779–2784, hep-ex/9802017.

[318] R. M. Barnett and L. J. Hall, "A multilepton signal for supersymmetric particles in Tevatron data?," *Phys. Rev. Lett.* **77** (1996) 3506–3509, hep-ph/9607342.

[319] **CDF** Collaboration, D. E. Acosta *et al.*, "Search for anomalous kinematics in $t\bar{t}$ dilepton events at CDF II," *Phys. Rev. Lett.* **95** (2005) 022001, hep-ex/0412042.

[320] **DØ** Collaboration, S. Abachi *et al.*, "Direct measurement of the top quark mass," *Phys. Rev. Lett.* **79** (1997) 1197–1202, hep-ex/9703008.

[321] **DØ** Collaboration, B. Abbott *et al.*, "Direct measurement of the top quark mass at DØ," *Phys. Rev.* **D58** (1998) 052001, hep-ex/9801025.

[322] **CDF** Collaboration, A. A. Affolder *et al.*, "Measurement of the top quark p_T distribution," *Phys. Rev. Lett.* **87** (2001) 102001.

[323] **CDF** Collaboration, T. Aaltonen *et al.*, "Measurement of the $t\bar{t}$ differential cross section, $d\sigma/dM_{t\bar{t}}$," *CDF conference note* **9157** (2008).

[324] W. G. D. Dharmaratna and G. R. Goldstein, "Single quark polarization in quantum chromodynamics subprocesses," *Phys. Rev.* **D53** (1996) 1073–1086.

[325] W. Bernreuther, A. Brandenburg, and P. Uwer, "Transverse Polarization of Top Quark Pairs at the Tevatron and the Large Hadron Collider," *Phys. Lett.* **B368** (1996) 153–162, hep-ph/9510300.

[326] W. G. D. Dharmaratna and G. R. Goldstein, "Gluon Fusion As A Source For Massive Quark Polarization," *Phys. Rev.* **D41** (1990) 1731.

[327] W. Bernreuther, A. Brandenburg, Z. G. Si, and P. Uwer, "Spin properties of top quark pairs produced at hadron colliders," *Acta Phys. Polon.* **B34** (2003) 4477–4490, hep-ph/0304244.

[328] W. Bernreuther, M. Fuecker, and Z. G. Si, "Mixed QCD and weak corrections to top quark pair production at hadron colliders," *Phys. Lett.* **B633** (2006) 54–60, hep-ph/0508091.

[329] J. H. Kühn, "How to Measure the Polarization of Top Quarks," *Nucl. Phys.* **B237** (1984) 77.

[330] T. Arens and L. M. Sehgal, "Azimuthal Correlation of Charged Leptons Produced in $p\bar{p} \to t\bar{t} + ...$," *Phys. Lett.* **B302** (1993) 501–506.

[331] Y. Hara, "Angular Correlation Of Charged Leptons From $t\bar{t}$ Produced In The Gluon Fusion," *Prog. Theor. Phys.* **86** (1991) 779–781.

[332] W. Bernreuther, A. Brandenburg, Z. G. Si, and P. Uwer, "Top quark pair production and decay at hadron colliders," *Nucl. Phys.* **B690** (2004) 81–137, `hep-ph/0403035`.

[333] T. Stelzer and S. Willenbrock, "Spin Correlation in Top-Quark Production at Hadron Colliders," *Phys. Lett.* **B374** (1996) 169–172, `hep-ph/9512292`.

[334] G. Mahlon and S. J. Parke, "Maximizing spin correlations in top quark pair production at the Tevatron," *Phys. Lett.* **B411** (1997) 173–179, `hep-ph/9706304`.

[335] S. J. Parke and Y. Shadmi, "Spin correlations in top quark pair production at e^+e^- colliders," *Phys. Lett.* **B387** (1996) 199–206, `hep-ph/9606419`.

[336] G. Mahlon and S. J. Parke, "Angular Correlations in Top Quark Pair Production and Decay at Hadron Colliders," *Phys. Rev.* **D53** (1996) 4886–4896, `hep-ph/9512264`.

[337] **DØ** Collaboration, B. Abbott *et al.*, "Spin correlation in $t\bar{t}$ production from $p\bar{p}$ collisions at $\sqrt{s} = 1.8$ TeV," *Phys. Rev. Lett.* **85** (2000) 256–261, `hep-ex/0002058`.

[338] **DØ** Collaboration, V. M. Abazov *et al.*, "Search for the Standard Model Higgs boson in the $t\bar{t}H \to t\bar{t}b\bar{b}$ channel," *DØ conference note* **5739** (2008).

[339] T.-F. Feng, X.-Q. Li, and J. Maalampi, "The anomalous Higgs - top couplings in the MSSM," *Phys. Rev.* **D69** (2004) 115007, `hep-ph/0310247`.

[340] J. A. Aguilar-Saavedra, "Light Higgs boson discovery in the standard model and beyond," *JHEP* **12** (2006) 033, `hep-ph/0603200`.

[341] B. Lillie, L. Randall, and L.-T. Wang, "The Bulk RS KK-gluon at the LHC," *JHEP* **09** (2007) 074, hep-ph/0701166.

[342] T. G. Rizzo, "Testing the nature of Kaluza-Klein excitations at future lepton colliders," *Phys. Rev.* **D61** (2000) 055005, hep-ph/9909232.

[343] A. Leike, "The phenomenology of extra neutral gauge bosons," *Phys. Rept.* **317** (1999) 143–250, hep-ph/9805494.

[344] J. L. Rosner, "Prominent decay modes of a leptophobic Z'," *Phys. Lett.* **B387** (1996) 113–117, hep-ph/9607207.

[345] L. M. Sehgal and M. Wanninger, "Forward - backward asymmetry in two jet events: Signature of axigluons in proton - anti-proton collisions," *Phys. Lett.* **B200** (1988) 211.

[346] C. T. Hill and S. J. Parke, "Top production: Sensitivity to new physics," *Phys. Rev.* **D49** (1994) 4454–4462, hep-ph/9312324.

[347] C. T. Hill, "Topcolor: Top quark condensation in a gauge extension of the standard model," *Phys. Lett.* **B266** (1991) 419–424.

[348] G. Cvetic, "Top quark condensation: A review," *Rev. Mod. Phys.* **71** (1999) 513–574, hep-ph/9702381.

[349] **CDF** Collaboration, A. A. Affolder *et al.*, "Search for new particles decaying to $t\bar{t}$ in $p\bar{p}$ collisions at $\sqrt{s} = 1.8$ TeV," *Phys. Rev. Lett.* **85** (2000) 2062–2067, hep-ex/0003005.

[350] **DØ** Collaboration, V. M. Abazov *et al.*, "Search for narrow $t\bar{t}$ resonances in $p\bar{p}$ collisions at $\sqrt{s} = 1.8$ TeV," *Phys. Rev. Lett.* **92** (2004) 221801, hep-ex/0307079.

[351] S. Jain, "Search for t anti-t resonances in p anti-p collisions at $\sqrt{s} =$ 1.8 TeV". FERMILAB-THESIS-2003-03.

[352] **DØ** Collaboration, V. M. Abazov *et al.*, "Search for $t\bar{t}$ Resonances in the Lepton+Jets Final State in $p\bar{p}$ Collisions at $\sqrt{s} = 1.96$ TeV," *DØ conference note* **5600** (2008).

[353] **CDF** Collaboration, T. Aaltonen *et al.*, "Limits on the Production of Narrow t-tbar Resonances in p- pbar Collisions at $\sqrt{s}$=1.96 TeV," *Phys. Rev.* **D77** (2008) 051102, arXiv:0710.5335.

[354] **DØ** Collaboration, V. M. Abazov *et al.*, "Search for $t\bar{t}$ resonances in the lepton plus jets final state in $p\bar{p}$ collisions at $\sqrt{s} = 1.96$ TeV," *Phys. Lett.* **B668** (2008) 98–104, arXiv:0804.3664.

[355] **CDF** Collaboration, T. Aaltonen *et al.*, "Search for resonant $t\bar{t}$ production in $p\bar{p}$ collisions at $\sqrt{s} = 1.96$ TeV," *Phys. Rev. Lett.* **100** (2008) 231801, arXiv:0709.0705.

[356] **CDF** Collaboration, T. Aaltonen *et al.*, "A Search for Massive Gluon decaying to Top Pair in Lepton+Jet channel," *CDF conference note* **9164** (2008).

[357] R. Frederix and F. Maltoni, "Top pair invariant mass distribution: a window on new physics," arXiv:0712.2355.

[358] V. A. Novikov, L. B. Okun, A. N. Rozanov, and M. I. Vysotsky, "Extra generations and discrepancies of electroweak precision data," *Phys. Lett.* **B529** (2002) 111–116, hep-ph/0111028.

[359] H.-J. He, N. Polonsky, and S.-f. Su, "Extra families, Higgs spectrum and oblique corrections," *Phys. Rev.* **D64** (2001) 053004, hep-ph/0102144.

[360] G. D. Kribs, T. Plehn, M. Spannowsky, and T. M. P. Tait, "Four Generations and Higgs Physics," *Phys. Rev.* **D76** (2007) 075016, arXiv:0706.3718.

[361] N. Borstnik *et al.*, "What comes beyond the standard models. Proceedings, 9th Workshop, Bled, Slovenia, September 16-26, 2006," hep-ph/0612250.

[362] E. Arik, O. Cakir, S. A. Cetin, and S. Sultansoy, "Observability of the Higgs boson and extra SM families at the Tevatron," *Acta Phys. Polon.* **B37** (2006) 2839–2850, hep-ph/0502050.

[363] J. I. Silva-Marcos, "Symmetries, large leptonic mixing and a fourth generation," *JHEP* **12** (2002) 036, hep-ph/0204217.

[364] P. H. Frampton, P. Q. Hung, and M. Sher, "Quarks and leptons beyond the third generation," *Phys. Rept.* **330** (2000) 263, hep-ph/9903387.

[365] D. Choudhury, T. M. P. Tait, and C. E. M. Wagner, "Beautiful mirrors and precision electroweak data," *Phys. Rev.* **D65** (2002) 053002, hep-ph/0109097.

[366] **CDF** Collaboration, T. Aaltonen *et al.*, "Search for Heavy Top $t' \to Wq$ In Lepton Plus Jets Events," *CDF conference note* **9446** (2008).

[367] **CDF** Collaboration, T. Aaltonen *et al.*, "Search for Heavy Top-like Quarks $t' \to Wq$ Using Lepton Plus Jets Events in 1.96 TeV Proton-Antiproton Collisions," *Phys. Rev. Lett.* **100** (2008) 161803, arXiv:0801.3877.

[368] S. P. Martin, "A supersymmetry primer," hep-ph/9709356.

[369] W. Beenakker, M. Kramer, T. Plehn, M. Spira, and P. M. Zerwas, "Stop production at hadron colliders," *Nucl. Phys.* **B515** (1998) 3–14, hep-ph/9710451.

[370] W. Beenakker, R. Hopker, and M. Spira, "PROSPINO: A program for the PROduction of Supersymmetric Particles In Next-to-leading Order QCD," hep-ph/9611232. http://www.ph.ed.ac.uk/~tplehn/prospino/.

[371] **DØ** Collaboration, V. M. Abazov *et al.*, "Search for the lightest scalar top quark in events with two leptons in $p\overline{p}$ collisions at $\sqrt{\mathrm{s}} =$ 1.96 TeV," *Phys. Lett.* **B659** (2008) 500–508, arXiv:0707.2864.

[372] **CDF** Collaboration, T. Aaltonen *et al.*, "Search for Direct Pair Production of Supersymmetric Top and Supersymmetric Bottom Quarks in $p\bar{p}$ Collisions at $\sqrt{s} = 1.96$ TeV," *Phys. Rev.* **D76** (2007) 072010, arXiv:0707.2567.

[373] **DØ** Collaboration, V. M. Abazov *et al.*, "Search for scalar top quarks in the acoplanar charm jets and missing transverse energy final state in $p\bar{p}$ collisions at $\sqrt{s} = 1.96$ TeV," *Phys. Lett.* **B665** (2008) 1–8, arXiv:0803.2263.

[374] **DØ** Collaboration, V. M. Abazov *et al.*, "Search for the pair production of scalar top quarks in the acoplanar charm jet final state in $p\bar{p}$ collisions at $\sqrt{s} = 1.96\,\mathrm{TeV}$," *Phys. Lett.* **B645** (2007) 119–127, arXiv:hep-ex/0611003.

[375] **DØ** Collaboration, V. M. Abazov *et al.*, "Search for Scalar Top Admixture in the $t\bar{t}$ Lepton+Jets Final State at $\sqrt{s} = 1.96$ TeV in 1 fb^{-1} of DØ data," *DØ conference note* **5438** (2007).

[376] **CDF** Collaboration, A. A. Affolder *et al.*, "Search for scalar top quark production in $p\bar{p}$ collisions at $\sqrt{s} = 1.8$ TeV," *Phys. Rev. Lett.* **84** (2000) 5273–5278, hep-ex/9912018.

[377] **ALEPH, DELPHI, L3 and OPAL** Collaboration, the LEPSUSY working group, "Combined Lower Bound of the Neutralino Mass in a Constrained MSSM model," *Note LEPSUSYWG/04-07.1* (2004). http://lepsusy.web.cern.ch/lepsusy/Welcome.html.

[378] **CDF** Collaboration, T. Aaltonen *et al.*, "Search for Pair Production of Stop Quarks Mimicking Top Event Signatures," *CDF conference note* **9439** (2008).

[379] **DØ** Collaboration, V. M. Abazov *et al.*, "Search for single top quark production at DØ using neural networks," *Phys. Lett.* **B517** (2001) 282–294, hep-ex/0106059.

[380] **DØ** Collaboration, B. Abbott *et al.*, "Search for electroweak production of single top quarks in $p\bar{p}$ collisions," *Phys. Rev.* **D63** (2000) 031101, hep-ex/0008024.

[381] **CDF** Collaboration, D. E. Acosta *et al.*, "Optimized search for single top quark production at the Fermilab Tevatron," *Phys. Rev.* **D69** (2004) 052003.

[382] **CDF** Collaboration, D. E. Acosta *et al.*, "Search for single top quark production in $p\bar{p}$ collisions at $\sqrt{s} = 1.8$ TeV," *Phys. Rev.* **D65** (2002) 091102, hep-ex/0110067.

[383] **CDF** Collaboration, D. E. Acosta *et al.*, "Search for electroweak single top quark production in $p\bar{p}$ collisions at $\sqrt{s} = 1.96$ TeV," *Phys. Rev.* **D71** (2005) 012005, hep-ex/0410058.

[384] **DØ** Collaboration, V. M. Abazov *et al.*, "Multivariate searches for single top quark production with the DØ detector," *Phys. Rev.* **D75** (2007) 092007, arXiv:hep-ex/0604020.

[385] **DØ** Collaboration, V. M. Abazov *et al.*, "Search for single top quark production in $p\bar{p}$ collisions at $\sqrt{s}$ =1.96 TeV," *Phys. Lett.* **B622** (2005) 265–276, arXiv:hep-ex/0505063.

[386] **CDF** Collaboration, T. Aaltonen *et al.*, "Search for Single Top Quark Production using Boosted Decision Trees in 2.2 fb^{-1} of CDF Data," *CDF conference note* **9313** (2008).

[387] **CDF** Collaboration, T. Aaltonen *et al.*, "Measurement of Single Top Quark Production in 2.2 fb^{-1} of CDF II Data using the Matrix Element Technique," *CDF conference note* **9223** (2008).

[388] **CDF** Collaboration, T. Aaltonen *et al.*, "Multivariate Likelihood Search for Single-Top-Quark Production with 2.2 fb^{-1}," *CDF conference note* **9221** (2008).

[389] **CDF** Collaboration, T. Aaltonen *et al.*, "Search for Electroweak Single Top-Quark Production using Neural Networks with 2.2 fb^{-1} of CDF II data," *CDF conference note* **9217** (2008).

[390] **CDF** Collaboration, T. Aaltonen *et al.*, "Combination of CDF Single Top Quark Searches with 2.2 fb^{-1} of Data," *CDF conference note* **9251** (2008).

[391] **CDF** Collaboration, T. Aaltonen *et al.*, "Search for Electroweak Single Top-Quark Production using Neural Networks with 2.7 fb^{-1} of CDF II data," *CDF conference note* **9479** (2008).

[392] **CDF** Collaboration, T. Aaltonen *et al.*, "Multivariate Likelihood Function Measurement of Single-Top-Quark Production with 2.7 fb^{-1}," *CDF conference note* **9451** (2008).

[393] **CDF** Collaboration, T. Aaltonen *et al.*, "Measurement of Single Top Quark Production in 2.7 fb^{-1} of CDF II Data Using a Matrix Element Technique," *CDF conference note* **9464** (2008).

[394] **CDF** Collaboration, T. Aaltonen *et al.*, "Search for Single Top Quark Production using Boosted Decision Trees in 2.7 fb^{-1} of CDF Data," *CDF conference note* **9445** (2008).

[395] M. Jezabek and J. H. Kühn, "V-A tests through leptons from polarized top quarks," *Phys. Lett.* **B329** (1994) 317–324, `hep-ph/9403366`.

[396] G. Mahlon, "Observing spin correlations in single top production and decay," `hep-ph/0011349`.

[397] G. Mahlon, "Spin polarization in single top events," `hep-ph/9811219`.

[398] E. E. Boos and A. V. Sherstnev, "Spin effects in processes of single top quark production at hadron colliders," *Phys. Lett.* **B534** (2002) 97–105, `hep-ph/0201271`.

[399] M. Beneke *et al.*, "Top quark physics," `hep-ph/0003033`.

[400] E. Boos, V. Bunichev, L. Dudko, and M. Perfilov, "Interference between W' and W in single-top quark production processes," *Phys. Lett.* **B655** (2007) 245–250, `hep-ph/0610080`.

[401] **DØ** Collaboration, V. M. Abazov *et al.*, "Search for W' bosons decaying to an electron and a neutrino with the D0 detector," *Phys. Rev. Lett.* **100** (2008) 031804, `arXiv:0710.2966`.

[402] **UA2** Collaboration, J. Alitti *et al.*, "A Search for new intermediate vector mesons and excited quarks decaying to two jets at the CERN anti-p p collider," *Nucl. Phys.* **B400** (1993) 3–24.

[403] **CDF** Collaboration, F. Abe *et al.*, "Search for new particles decaying to dijets at CDF," *Phys. Rev.* **D55** (1997) 5263–5268, `hep-ex/9702004`.

[404] **DØ** Collaboration, V. M. Abazov *et al.*, "Search for new particles in the two-jet decay channel with the DØ detector," *Phys. Rev.* **D69** (2004) 111101, `hep-ex/0308033`.

[405] **DØ** Collaboration, V. M. Abazov *et al.*, "Search for W' boson production in the top quark decay channel," *Phys. Lett.* **B641** (2006) 423–431, `arXiv:hep-ex/0607102`.

[406] **CDF** Collaboration, D. E. Acosta *et al.*, "Search for a W' boson decaying to a top and bottom quark pair in 1.8 TeV $p\bar{p}$ collisions," *Phys. Rev. Lett.* **90** (2003) 081802, `hep-ex/0209030`.

[407] **DØ** Collaboration, V. M. Abazov *et al.*, "Search for W' boson resonances decaying to a top quark and a bottom quark," *Phys. Rev. Lett.* **100** (2008) 211803, `arXiv:0803.3256`.

[408] **CDF** Collaboration, T. Aaltonen *et al.*, "W'-like Resonances in the $t\bar{b}$ Decay Channel with 1.9 fb^{-1}," *CDF conference note* **9150** (2008).

[409] J. F. Gunion, H. E. Haber, G. L. Kane, and S. Dawson, "Errata for the Higgs Hunter's Guide," `hep-ph/9302272`.

[410] J. F. Gunion, H. E. Haber, G. L. Kane, and S. Dawson, "The Higgs Hunter's Guide". Addison-Wesley, Reading, MA, USA (1990), 425p.

[411] H.-J. He and C. P. Yuan, "New method for detecting charged (pseudo-)scalars at colliders," *Phys. Rev. Lett.* **83** (1999) 28–31, hep-ph/9810367.

[412] **DØ** Collaboration, V. M. Abazov *et al.*, "Search for charged Higgs bosons decaying to top and bottom quarks in $p\bar{p}$ collisions," arXiv:0807.0859.

[413] T. Han, M. Hosch, K. Whisnant, B.-L. Young, and X. Zhang, "Single top quark production via FCNC couplings at hadron colliders," *Phys. Rev.* **D58** (1998) 073008, hep-ph/9806486.

[414] J. A. Aguilar-Saavedra, "Top flavour-changing neutral interactions: Theoretical expectations and experimental detection," *Acta Phys. Polon.* **B35** (2004) 2695–2710, hep-ph/0409342.

[415] **OPAL** Collaboration, G. Abbiendi *et al.*, "Search for single top quark production at LEP2," *Phys. Lett.* **B521** (2001) 181–194, hep-ex/0110009.

[416] **L3** Collaboration, P. Achard *et al.*, "Search for single top production at LEP," *Phys. Lett.* **B549** (2002) 290–300, hep-ex/0210041.

[417] **DELPHI** Collaboration, J. Abdallah *et al.*, "Search for single top production via FCNC at LEP at $\sqrt{s} = 189$ GeV - 208 GeV," *Phys. Lett.* **B590** (2004) 21–34, hep-ex/0404014.

[418] **ALEPH** Collaboration, A. Heister *et al.*, "Search for single top production in e^+e^- collisions at $\sqrt{s}$ up to 209 GeV," *Phys. Lett.* **B543** (2002) 173–182, hep-ex/0206070.

[419] **H1** Collaboration, D. M. South, "Single W and Anomalous Single Top Production at HERA," arXiv:0806.0069.

[420] V. F. Obraztsov, S. R. Slabospitsky, and O. P. Yushchenko, "Search for anomalous top-quark interaction at LEP-2 collider," *Phys. Lett.* **B426** (1998) 393–402, hep-ph/9712394.

[421] **CDF** Collaboration, F. Abe *et al.*, "Search for flavor-changing neutral current decays of the top quark in $p\bar{p}$ collisions at $\sqrt{s} = 1.8$ TeV," *Phys. Rev. Lett.* **80** (1998) 2525–2530.

[422] **ZEUS** Collaboration, S. Chekanov *et al.*, "Search for single-top production in e p collisions at HERA," *Phys. Lett.* **B559** (2003) 153–170, hep-ex/0302010.

[423] **H1** Collaboration, A. Aktas *et al.*, "Search for single top quark production in e p collisions at HERA," *Eur. Phys. J.* **C33** (2004) 9–22, hep-ex/0310032.

[424] **CDF** Collaboration, T. Aaltonen *et al.*, "Search for the Flavor Changing Neutral Current Decay t $\to Zq$ in $p\bar{p}$ Collisions at $\sqrt{s} = 1.96$," arXiv:0805.2109.

[425] Y. P. Gouz and S. R. Slabospitsky, "Double top production at hadronic colliders," *Phys. Lett.* **B457** (1999) 177–185, hep-ph/9811330.

[426] A. A. Ashimova and S. R. Slabospitsky, "The constraint on FCNC coupling of the top quark with a gluon from e p collisions," hep-ph/0604119.

[427] **DØ** Collaboration, V. M. Abazov *et al.*, "Search for production of single top quarks via flavor-changing neutral currents at the Tevatron," *Phys. Rev. Lett.* **99** (2007) 191802, arXiv:hep-ex/0702005.

[428] M. Hosch, K. Whisnant, and B. L. Young, "Direct top quark production at hadron colliders as a probe of new physics," *Phys. Rev.* **D56** (1997) 5725–5730, hep-ph/9703450.

[429] **CDF** Collaboration, T. Aaltonen *et al.*, "Search for top quark production via flavor-changing neutral currents at CDF," *CDF conference note* **9440** (2008).

[430] S. R. Slabospitsky and L. Sonnenschein, "TopReX generator (version 3.25): Short manual," *Comput. Phys. Commun.* **148** (2002) 87–102, hep-ph/0201292.

[431] L. L. Yang, C. S. Li, Y. Gao, and J. J. Liu, "Threshold resummation effects in direct top quark production at hadron colliders," *Phys. Rev.* **D73** (2006) 074017, hep-ph/0601180.

[432] J. J. Liu, C. S. Li, L. L. Yang, and L. G. Jin, "Next-to-leading order QCD corrections to the direct top quark production via model-independent FCNC couplings at hadron colliders," *Phys. Rev.* **D72** (2005) 074018, hep-ph/0508016.

[433] **DØ** Collaboration, V. M. Abazov *et al.*, "Search for anomalous Wtb couplings in single top quark production," arXiv:0807.1692.

[434] E. Boos, L. Dudko, and T. Ohl, "Complete calculations of W b anti-b and W b anti-b + jet production at Tevatron and LHC: Probing anomalous W t b couplings in single top production," *Eur. Phys. J.* **C11** (1999) 473–484, hep-ph/9903215.

[435] E. Malkawi and C. P. Yuan, "A Global analysis of the top quark couplings to gauge bosons," *Phys. Rev.* **D50** (1994) 4462–4477, hep-ph/9405322.

[436] D. O. Carlson, E. Malkawi, and C. P. Yuan, "Probing the couplings of the top quark to gauge bosons," *Phys. Lett.* **B337** (1994) 145–151, hep-ph/9405277.

[437] S.-h. Nam, "B anti-B mixing and CP violation in SU(2)L x SU(2)R x U(1) models," *Phys. Rev.* **D66** (2002) 055008, hep-ph/0206037.

[438] M. A. B. Bég, R. V. Budny, R. Mohapatra, and A. Sirlin, "Manifest left-right symmetry and its experimental consequences," *Phys. Rev. Lett.* **39** (Jul, 1977) 54.

[439] M. A. B. Bég, R. V. Budny, R. N. Mohapatra, and A. Sirlin, "Manifest Left-Right Symmetry and Its Experimental Consequences," *Phys. Rev. Lett.* **38** (1977) 1252.

[440] W. Bernreuther, M. Fücker, and Y. Umeda, "Semileptonic decays of polarised top quarks: V + A admixture and QCD corrections," *Phys. Lett.* **B582** (2004) 32–38, hep-ph/0308296.

[441] X.-l. Wang, Q.-l. Zhang, and Q.-p. Qiao, "Studying top quark decay into the polarized W-boson in the TC2 model," *Phys. Rev.* **D71** (2005) 014035, hep-ph/0501145.

[442] C. Jessop, "A world average for $B \to X_s\gamma$". SLAC-PUB-9610.

[443] M. Hosch, K. Whisnant, and B.-L. Young, "Unitarity constraints on anomalous top quark couplings to weak gauge bosons," *Phys. Rev.* **D55** (1997) 3137–3142, hep-ph/9607413.

[444] P. L. Cho and M. Misiak, "b → s gamma decay in SU(2)-L x SU(2)-r x U(1) extensions of the Standard Model," *Phys. Rev.* **D49** (1994) 5894–5903, hep-ph/9310332.

[445] K. Fujikawa and A. Yamada, "Test of the chiral structure of the top - bottom charged current by the process b → s γ," *Phys. Rev.* **D49** (1994) 5890–5893.

[446] **DØ** Collaboration, V. M. Abazov *et al.*, "A precision measurement of the mass of the top quark," *Nature* **429** (2004) 638–642, hep-ex/0406031.

[447] **CDF** Collaboration, A. Abulencia *et al.*, "Measurement of the helicity of W bosons in top-quark decays," *Phys. Rev.* **D73** (2006) 111103, hep-ex/0511023.

[448] **CDF** Collaboration, A. Abulencia *et al.*, "Search for V + A current in top quark decay in p anti-p collisions at $\sqrt{s} = 1.96$ TeV," *Phys. Rev. Lett.* **98** (2007) 072001, hep-ex/0608062.

[449] **DØ** Collaboration, V. M. Abazov *et al.*, "Helicity of the W boson in lepton + jets $t\bar{t}$ events," *Phys. Lett.* **B617** (2005) 1–10, hep-ex/0404040.

[450] **CDF** Collaboration, T. Aaltonen *et al.*, "Measurement of W Boson Helicity Fractions in Top Quark Decay to Lepton+Jets Events using a Matrix Element Analysis Technique with 1.9 fb^{-1} of Data," *CDF conference note* **9144** (2007).

[451] **DØ** Collaboration, V. M. Abazov *et al.*, "Model-independent measurement of the W boson helicity in top quark decays at D0," *Phys. Rev. Lett.* **100** (2008) 062004, arXiv:0711.0032.

[452] E. W. Varnes. Private communication, 2008.

[453] **DØ** Collaboration, V. M. Abazov *et al.*, "Model-independent measurement of the W boson helicity in top quark decays at D0," *DØ conference note* **5722** (2008).

[454] **CDF** Collaboration, T. Aaltonen *et al.*, "Measurement of W-Boson Helicity Fractions in Top-Quark Decays Using $\cos\theta^*$," *CDF conference note* **9215** (2009).

[455] **CDF** Collaboration, T. Aaltonen *et al.*, "Measurement of the W Helicity in Fully Reconstructed Top Anti-Top Events using 1.9 fb^{-1}," *CDF conference note* **9114** (2008).

[456] **CDF** Collaboration, T. Aaltonen *et al.*, "Measurement of W-Boson Helicity Fractions in Top-Quark Decays Using $\cos\theta^*$," *CDF conference note* **9431** (2008).

[457] **CDF** Collaboration, A. A. Affolder *et al.*, "Measurement of the helicity of W bosons in top quark decays," *Phys. Rev. Lett.* **84** (2000) 216–221, hep-ex/9909042.

[458] **CDF** Collaboration, D. E. Acosta *et al.*, "Measurement of the W boson polarization in top decay at CDF at $\sqrt{s} = 1.8$ TeV," *Phys. Rev.* **D71** (2005) 031101, hep-ex/0411070.

[459] **DØ** Collaboration, V. M. Abazov *et al.*, "Measurement of the W Boson Helicity in Top Quark Decays," *Phys. Rev.* **D72** (2005) 011104, arXiv:hep-ex/0505031.

[460] **CDF** Collaboration, A. Abulencia *et al.*, "Measurement of the Helicity Fractions of W Bosons from Top Quark Decays using Fully Reconstructed $t\bar{t}$ Events with CDF II," *Phys. Rev.* **D75** (2007) 052001, hep-ex/0612011.

[461] **DØ** Collaboration, V. M. Abazov *et al.*, "Measurement of the W boson helicity in top quark decay at DØ," *Phys. Rev.* **D75** (2007) 031102, arXiv:hep-ex/0609045.

[462] J. Alwall *et al.*, "Is V(tb) = 1?," *Eur. Phys. J.* **C49** (2007) 791–801, hep-ph/0607115.

[463] **DØ** Collaboration, V. M. Abazov *et al.*, "Simultaneous measurement of the ratio $\mathcal{B}(t \to Wb)/\mathcal{B}(t \to Wq)$ and the top quark pair production cross section with the D0 detector at $\sqrt{s} = 1.96$ TeV," *Phys. Rev. Lett.* **100** (2008) 192003, arXiv:0801.1326.

[464] **DØ** Collaboration, V. M. Abazov *et al.*, "Measurement of $\mathcal{B}(t \to Wb)/\mathcal{B}(t \to Wq)$ at $\sqrt{s} = 1.96$ TeV," *Phys. Lett.* **B639** (2006) 616–622, arXiv:hep-ex/0603002.

[465] **CDF** Collaboration, D. E. Acosta *et al.*, "Measurement of $B(t \to Wb)/B(t \to Wq)$ at the Collider Detector at Fermilab," *Phys. Rev. Lett.* **95** (2005) 102002, hep-ex/0505091.

[466] **CDF** Collaboration, A. A. Affolder *et al.*, "First measurement of the ratio $B(t \to Wb)/B(t \to Wq)$ and associated limit on the CKM element $|V_{tb}|$," *Phys. Rev. Lett.* **86** (2001) 3233–3238, hep-ex/0012029.

[467] G. Eilam, A. Gemintern, T. Han, J. M. Yang, and X. Zhang, "Top quark rare decay $t \to ch$ in R-parity-violating SUSY," *Phys. Lett.* **B510** (2001) 227–235, hep-ph/0102037.

[468] J. L. Lopez, D. V. Nanopoulos, and R. Rangarajan, "New supersymmetric contributions to $t \to cV$," *Phys. Rev.* **D56** (1997) 3100–3106, hep-ph/9702350.

[469] G. M. de Divitiis, R. Petronzio, and L. Silvestrini, "Flavour changing top decays in supersymmetric extensions of the standard model," *Nucl. Phys.* **B504** (1997) 45–60, hep-ph/9704244.

[470] H. Fritzsch and D. Holtmannspotter, "The production of single t-quarks at LEP and HERA," *Phys. Lett.* **B457** (1999) 186–192, hep-ph/9901411.

[471] B. A. Arbuzov and M. Y. Osipov, "Enhancement of the neutral t c transition in the model of dynamical electroweak-symmetry breaking," *Phys. Atom. Nucl.* **62** (1999) 485–490, hep-ph/9802392.

[472] R. D. Peccei and X. Zhang, "Dynamical Symmetry Breaking and Universality Breakdown," *Nucl. Phys.* **B337** (1990) 269–283.

[473] C.-X. Yue, G.-R. Lu, Q.-J. Xu, G.-L. Liu, and G.-P. Gao, "The flavor-changing rare top decays $t \to cVV$ in topcolor assisted technicolor theory," *Phys. Lett.* **B508** (2001) 290–294, hep-ph/0103081.

[474] D. Atwood, L. Reina, and A. Soni, "Probing flavor changing top - charm - scalar interactions in e^+e^- collisions," *Phys. Rev.* **D53** (1996) 1199–1201, hep-ph/9506243.

[475] W.-S. Hou, "Tree level t → c h or h → t anti-c decays," *Phys. Lett.* **B296** (1992) 179–184.

[476] G. Eilam, J. L. Hewett, and A. Soni, "Erratum: Rare decays of the top quark in the standard and two-Higgs-doublet models," *Phys. Rev.* **D59** (1998) 039901.

[477] G. Eilam, J. L. Hewett, and A. Soni, "Rare decays of the top quark in the standard and two-Higgs-doublet models," *Phys. Rev.* **D44** (1991) 1473–1484.

[478] F. del Aguila, J. A. Aguilar-Saavedra, and R. Miquel, "Constraints on top couplings in models with exotic quarks," *Phys. Rev. Lett.* **82** (1999) 1628–1631, hep-ph/9808400.

[479] T. Han and J. L. Hewett, "Top charm associated production in high energy e^+e^- collisions," *Phys. Rev.* **D60** (1999) 074015, hep-ph/9811237.

[480] T. Han, K. Whisnant, B. L. Young, and X. Zhang, "Searching for $t \to cg$ at the Fermilab Tevatron," *Phys. Lett.* **B385** (1996) 311–316, hep-ph/9606231.

[481] H. Fritzsch, "t Quarks May Decay Into Z Bosons And Charm," *Phys. Lett.* **B224** (1989) 423.

[482] T. Han, R. D. Peccei, and X. Zhang, "Top quark decay via flavor changing neutral currents at hadron colliders," *Nucl. Phys.* **B454** (1995) 527–540, hep-ph/9506461.

[483] **CDF** Collaboration, T. Aaltonen *et al.*, "Search for the Flavor Changing Neutral Current Decay $t \to Zq$ in $p\bar{p}$ Collisions at $\sqrt{s} = 1.96$ TeV," *CDF conference note* **8888** (2007).

[484] **CDF** Collaboration, T. Aaltonen *et al.*, "Search for Invisible Top Decays with 1.9 fb^{-1} of CDF-II Data," *CDF conference note* **9496** (2008).

[485] M. S. Carena and H. E. Haber, "Higgs boson theory and phenomenology. ((V))," *Prog. Part. Nucl. Phys.* **50** (2003) 63–152, hep-ph/0208209.

[486] F. Borzumati, J.-L. Kneur, and N. Polonsky, "Higgs-strahlung and R-parity violating slepton-strahlung at hadron colliders," *Phys. Rev.* **D60** (1999) 115011, hep-ph/9905443.

[487] J. S. Lee *et al.*, "CPsuperH: A computational tool for Higgs phenomenology in the minimal supersymmetric standard model with explicit CP violation," *Comput. Phys. Commun.* **156** (2004) 283–317, hep-ph/0307377.

[488] **UA2** Collaboration, J. Alitti *et al.*, "A Search for charged Higgs from top quark decay at the CERN anti-p p collider," *Phys. Lett.* **B280** (1992) 137–145.

[489] **UA1** Collaboration, C. Albajar *et al.*, "Limits on t quark decay into charged Higgs from a direct search at the CERN p anti-p collider," *Phys. Lett.* **B257** (1991) 459–468.

[490] **CDF** Collaboration, F. Abe *et al.*, "Search for the top quark decaying to a charged Higgs boson in $\bar{p}p$ collisions at $\sqrt{s} = 1.8$ TeV," *Phys. Rev. Lett.* **73** (1994) 2667–2671.

[491] **CDF** Collaboration, F. Abe *et al.*, "A Search for the top quark decaying to charged Higgs in $p\bar{p}$ collisions at $\sqrt{s} = 1.8$ TeV," *Phys. Rev. Lett.* **72** (1994) 1977–1981.

[492] **OPAL** Collaboration, G. Abbiendi *et al.*, "Search for Higgs bosons in e^+e^- collisions at 183 GeV," *Eur. Phys. J.* **C7** (1999) 407–435, `hep-ex/9811025`.

[493] **L3** Collaboration, P. Achard *et al.*, "Search for charged Higgs bosons at LEP," *Phys. Lett.* **B575** (2003) 208–220, `hep-ex/0309056`.

[494] **DELPHI** Collaboration, J. Abdallah *et al.*, "Search for charged Higgs bosons at LEP in general two Higgs doublet models," *Eur. Phys. J.* **C34** (2004) 399–418, `hep-ex/0404012`.

[495] **ALEPH** Collaboration, A. Heister *et al.*, "Search for charged Higgs bosons in e^+e^- collisions at energies up to $\sqrt{s} = 209$ GeV," *Phys. Lett.* **B543** (2002) 1–13, `hep-ex/0207054`.

[496] **LEP Higgs Working Group for Higgs boson searches** Collaboration, G. Abbiendi *et al.*, "Search for charged Higgs bosons: Preliminary combined results using LEP data collected at energies up to 209 GeV," `hep-ex/0107031`.

[497] M. Misiak *et al.*, "The first estimate of $\mathcal{B}(\bar{B} \to X_s\gamma)$ at $\mathcal{O}(\alpha_s^2)$," *Phys. Rev. Lett.* **98** (2007) 022002, `hep-ph/0609232`.

[498] **CDF** Collaboration, F. Abe *et al.*, "Search for charged Higgs decays of the top quark using hadronic tau decays," *Phys. Rev.* **D54** (1996) 735–742, `hep-ex/9601003`.

[499] **CDF** Collaboration, F. Abe *et al.*, "Search for charged Higgs decays of the top quark using hadronic decays of the tau lepton," *Phys. Rev. Lett.* **79** (1997) 357–362, `hep-ex/9704003`.

[500] **CDF** Collaboration, A. A. Affolder *et al.*, "Search for the charged Higgs boson in the decays of top quark pairs in the $e\tau$ and $\mu\tau$ channels at $\sqrt{s} = 1.8$ TeV," *Phys. Rev.* **D62** (2000) 012004, `hep-ex/9912013`.

[501] **DØ** Collaboration, B. Abbott *et al.*, "Search for charged Higgs bosons in decays of top quark pairs," *Phys. Rev. Lett.* **82** (1999) 4975–4980, hep-ex/9902028.

[502] **DØ** Collaboration, V. M. Abazov *et al.*, "Direct search for charged Higgs bosons in decays of top quarks," *Phys. Rev. Lett.* **88** (2002) 151803, hep-ex/0102039.

[503] M. S. Carena, D. Garcia, U. Nierste, and C. E. M. Wagner, "Effective Lagrangian for the anti-t b H+ interaction in the MSSM and charged Higgs phenomenology," *Nucl. Phys.* **B577** (2000) 88–120, hep-ph/9912516.

[504] J. A. Coarasa, J. Guasch, and J. Sola, "Radiative corrections to top quark decay into charged Higgs at the Tevatron," hep-ph/9903212.

[505] **CDF** Collaboration, A. Abulencia *et al.*, "Search for charged Higgs bosons from top quark decays in $p\bar{p}$ collisions at $\sqrt{s} = 1.96$ TeV," *Phys. Rev. Lett.* **96** (2006) 042003, hep-ex/0510065.

[506] **CDF** Collaboration, T. Aaltonen *et al.*, "A search for charged Higgs in lepton + jets $t\bar{t}$ events using 2.2 fb^{-1} of CDF data," *CDF conference note* **9322** (2008).

[507] U. Baur, M. Buice, and L. H. Orr, "Direct measurement of the top quark charge at hadron colliders," *Phys. Rev.* **D64** (2001) 094019, hep-ph/0106341.

[508] D. Chang, W.-F. Chang, and E. Ma, "Fitting precision electroweak data with exotic heavy quarks," *Phys. Rev.* **D61** (2000) 037301, hep-ph/9909537.

[509] D. Chang, W.-F. Chang, and E. Ma, "Alternative interpretation of the Tevatron top events," *Phys. Rev.* **D59** (1999) 091503, hep-ph/9810531.

[510] **DØ** Collaboration, V. M. Abazov *et al.*, "Experimental discrimination between charge $2e/3$ top quark and charge $4e/3$ exotic quark production scenarios," *Phys. Rev. Lett.* **98** (2007) 041801, arXiv:hep-ex/0608044.

[511] **CDF** Collaboration, T. Aaltonen *et al.*, "First CDF Measurement of the Top Quark Charge using the Top Decay Products," *CDF conference note* **8967** (2007).

[512] **CDF** Collaboration, T. Aaltonen *et al.*, "First direct limit on the top quark lifetime," *CDF conference note* **8104** (2006).

[513] **CDF** Collaboration, T. Aaltonen *et al.*, "A Limit on the Top Quark Width and the Lifetime using the Template Method in the Lepton plus Jets Channel at CDF II," *CDF conference note* **8953** (2007).

[514] S. Heinemeyer, W. Hollik, A. M. Weber, and G. Weiglein, "Z Pole Observables in the MSSM," *JHEP* **04** (2008) 039, arXiv:0710.2972.

[515] S. Heinemeyer, S. Kraml, W. Porod, and G. Weiglein, "Physics impact of a precise determination of the top quark mass at an e^+e^- linear collider," *JHEP* **09** (2003) 075, hep-ph/0306181.

[516] **CDF** Collaboration, A. Abulencia *et al.*, "Top quark mass measurement using the template method in the lepton + jets channel at CDF II," *Phys. Rev.* **D73** (2006) 032003, hep-ex/0510048.

[517] **CDF** Collaboration, A. Abulencia *et al.*, "Precision top quark mass measurement in the lepton + jets topology in p anti-p collisions at $\sqrt{s} = 1.96$ TeV," *Phys. Rev. Lett.* **96** (2006) 022004, hep-ex/0510049.

[518] **CDF** Collaboration, T. Aaltonen *et al.*, "Combined template-based Top Quark Mass Measurement in the Lepton+jets and Dilepton channels Using 1.9 fb^{-1} of data," *CDF conference note* **9206** (2008).

[519] **CDF** Collaboration, T. Aaltonen *et al.*, "Measurement of the Top Quark Mass using Quantities with Minimal Dependence on the Jet Energy Scale," *CDF conference note* **9414** (2008).

[520] **CDF** Collaboration, T. Aaltonen *et al.*, "Cross Section Constrained Top Quark Mass Measurement from Dilepton Events at the Tevatron," *Phys. Rev. Lett.* **100** (2008) 062005, arXiv:0710.4037.

[521] **DØ** Collaboration, B. Abbott *et al.*, "Measurement of the top quark mass in the dilepton channel," *Phys. Rev.* **D60** (1999) 052001, hep-ex/9808029.

[522] **DØ** Collaboration, B. Abbott *et al.*, "Measurement of the top quark mass using dilepton events. DØ Collaboration," *Phys. Rev. Lett.* **80** (1998) 2063–2068, hep-ex/9706014.

[523] **CDF** Collaboration, F. Abe *et al.*, "Erratum: Measurement of the top quark mass with the collider detector at fermilab [phys. rev. lett. 82, 271 (1999)]," *Phys. Rev. Lett.* **82** (Mar, 1999) 2808–2809.

[524] **CDF** Collaboration, F. Abe *et al.*, "Measurement of the top quark mass with the Collider Detector at Fermilab," *Phys. Rev. Lett.* **82** (1999) 271–276, hep-ex/9810029.

[525] **CDF** Collaboration, A. A. Affolder *et al.*, "Measurement of the top quark mass with the Collider Detector at Fermilab," *Phys. Rev.* **D63** (2001) 032003, hep-ex/0006028.

[526] **CDF** Collaboration, F. Abe *et al.*, "Measurement of the top quark mass," *Phys. Rev. Lett.* **80** (1998) 2767–2772, hep-ex/9801014.

[527] **DØ** Collaboration, V. M. Abazov *et al.*, "Measurement of the top quark mass in all-jet events," *Phys. Lett.* **B606** (2005) 25–33, hep-ex/0410086.

[528] **CDF** Collaboration, F. Abe *et al.*, "First observation of the all hadronic decay of $t\bar{t}$ pairs," *Phys. Rev. Lett.* **79** (1997) 1992–1997.

[529] **CDF** Collaboration, T. Aaltonen *et al.*, "Measurement of the top-quark mass using missing E_T + jets events with secondary vertex $b-$tagging at CDF II," *Phys. Rev.* **D75** (2007) 111103, arXiv:0705.1594.

[530] F. Fiedler, "Precision Measurements of the Top Quark Mass". Habilitation thesis (2007), http://www.etp.physik.uni-muenchen.de/dokumente/thesis/habil_ffiedler.pdf.

[531] **CDF** Collaboration, A. Abulencia *et al.*, "Measurement of the top quark mass using template methods on dilepton events in proton antiproton collisions at $\sqrt{s} = 1.96$ TeV," *Phys. Rev.* **D73** (2006) 112006, hep-ex/0602008.

[532] **DØ** Collaboration, V. M. Abazov *et al.*, "Measurement of the Top Quark Mass in the Electron-Muon Channel using the Matrix Element Method with 2.8 fb^{-1}," *DØ conference note* **5743** (2008).

[533] **DØ** Collaboration, V. M. Abazov *et al.*, "Measurement of Top Quark Mass in Dilepton Final States via Neutrino Weighting," *DØ conference note* **5746** (2008).

[534] **CDF** Collaboration, A. Abulencia *et al.*, "Top quark mass measurement from dilepton events at CDF II," *Phys. Rev. Lett.* **96** (2006) 152002, hep-ex/0512070.

[535] **CDF** Collaboration, A. Abulencia *et al.*, "Top quark mass measurement from dilepton events at CDF II with the matrix-element method," *Phys. Rev.* **D74** (2006) 032009, hep-ex/0605118.

[536] **DØ** Collaboration, V. M. Abazov *et al.*, "Measurement of the top quark mass in the dilepton channel," *Phys. Lett.* **B655** (2007) 7, arXiv:hep-ex/0609056.

[537] **CDF** Collaboration, A. Abulencia *et al.*, "Precision measurement of the top quark mass from dilepton events at CDF II," *Phys. Rev.* **D75** (2007) 031105, hep-ex/0612060.

[538] **DØ** Collaboration, V. M. Abazov *et al.*, "Measurement of the Top Quark Mass in the Dilepton Channel Using the Matrix Weighting Method at DØ," *DØ conference note* **5463** (2007).

[539] **CDF** Collaboration, T. Aaltonen *et al.*, "Measurement of the top quark mass from the lepton transverse momentum in the $t\bar{t} \to$ dilepton channel at the Tevatron," *CDF conference note* **8959** (2007).

[540] **CDF** Collaboration, T. Aaltonen *et al.*, "Measurement of the top quark mass in the dilepton channel using the Neutrino Weighting Algorithm at the CDF-II detector with 1.8 fb^{-1} of data," *CDF conference note* **8955** (2007).

[541] **CDF** Collaboration, T. Aaltonen *et al.*, "Measurement of the Top Quark Mass in the Dilepton Channel using a Matrix Element Method with 1.8 fb^{-1}," *CDF conference note* **8951** (2008).

[542] **CDF** Collaboration, T. Aaltonen *et al.*, "Measurement of the top quark mass with dilepton events selected using neuroevolution at CDF," arXiv:0807.4652.

[543] **CDF** Collaboration, T. Aaltonen *et al.*, "Top Quark Mass Measurement in the 2.8 fb^{-1} Tight Lepton and Isolated Track Sample using Neutrino ϕ Weighting Method," *CDF conference note* **9456** (2008).

[544] F. A. Berends, H. Kuijf, B. Tausk, and W. T. Giele, "On the production of a W and jets at hadron colliders," *Nucl. Phys.* **B357** (1991) 32–64.

[545] **CDF** Collaboration, T. Aaltonen *et al.*, "Top Mass Measurement in the Lepton + Jets Channel Using a Matrix Element Method with

Quasi-Monte Carlo Integration and in situ Jet Calibration with 2.7 fb^{-1}," *CDF conference note* **9427** (2008).

[546] **DØ** Collaboration, V. M. Abazov *et al.*, "Measurement of the Top Quark Mass in the Lepton+Jets Channel Using the Matrix Element Method on 2.2 fb^{-1} of DØ Run II Data," *DØ conference note* **5750** (2008).

[547] **DØ** Collaboration, V. M. Abazov *et al.*, "Precise measurement of the top quark mass from lepton+jets events," `arXiv:0807.2141`.

[548] **CDF** Collaboration, A. Abulencia *et al.*, "Measurement of the top quark mass with the dynamical likelihood method using lepton plus jets events with b-tags in $p\bar{p}$ collisions at $\sqrt{s} = 1.96$ TeV," *Phys. Rev.* **D73** (2006) 092002, `hep-ex/0512009`.

[549] **DØ** Collaboration, V. M. Abazov *et al.*, "Measurement of the top quark mass in the lepton+jets final state with the matrix element method," *Phys. Rev.* **D74** (2006) 092005, `arXiv:hep-ex/0609053`.

[550] **DØ** Collaboration, V. M. Abazov *et al.*, "Measurement of the top quark mass in the lepton+jets channel using the Ideogram Method," *Phys. Rev.* **D75** (2007) 092001, `arXiv:hep-ex/0702018`.

[551] **CDF** Collaboration, A. Abulencia *et al.*, "Measurement of the Top Quark Mass in $p\bar{p}$ Collisions at $\sqrt{s} = 1.96$ TeV using the Decay Length Technique," *Phys. Rev.* **D75** (2007) 071102, `hep-ex/0612061`.

[552] **CDF** Collaboration, A. Abulencia *et al.*, "Precise measurement of the top quark mass in the lepton+jets topology at CDF II," *Phys. Rev. Lett.* **99** (2007) 182002, `hep-ex/0703045`.

[553] **CDF** Collaboration, T. Aaltonen *et al.*, "Top Mass Measurement on 1 fb^{-1} using the 3 Best Combinations Method," *CDF conference note* **8669** (2007).

[554] **CDF** Collaboration, T. Aaltonen *et al.*, "Top Quark Mass Measurement using the Dynamical Likelihood Method in the lepton plus jets channel at CDF Run II," *CDF conference note* **9135** (2007).

[555] http://www-cdf.fnal.gov/physics/new/top/systematics/.

[556] **CDF** Collaboration, T. Aaltonen *et al.*, "Measurement of the top mass with in situ jet energy scale calibration in the all-hadronic

channel using the Template Method with 2.1 fb^{-1}," *CDF conference note* **9165** (2008).

[557] **CDF** Collaboration, T. Aaltonen *et al.*, "Measurement of the top quark mass with in situ jet energy scale calibration in the all-hadronic channel using the Ideogram method with 1.9 fb^{-1}," *CDF conference note* **9265** (2008).

[558] **CDF** Collaboration, T. Aaltonen *et al.*, "Measurement of the top-quark mass in all-hadronic decays in p anti-p collisions at CDF II," *Phys. Rev. Lett.* **98** (2007) 142001, `hep-ex/0612026`.

[559] **CDF** Collaboration, T. Aaltonen *et al.*, "Measurement of the top quark mass in the all hadronic channel using an in-situ calibration of the dijet invariant mass with 943 pb^{-1}," *CDF conference note* **8709** (2007).

[560] **CDF** Collaboration, T. Aaltonen *et al.*, "Combination of CDF Top Mass Results for July 2008," *CDF conference note* **9450** (2008).

[561] **DØ** Collaboration, V. M. Abazov *et al.*, "Combination of the DØ top quark mass measurements," *DØ conference note* **5747** (2008).

[562] **ILC** Collaboration, T. Behnke *et al.*, "ILC Reference Design Report: ILC Global Design Effort and World Wide Study, Volume 4 - Detectors," `arXiv:0712.2356`.

[563] **ILC** Collaboration, J. Brau *et al.*, "ILC Reference Design Report: ILC Global Design Effort and World Wide Study, Volume 1 - Executive Summary," `arXiv:0712.1950`.

[564] **ILC** Collaboration, J. Brau *et al.*, "ILC Reference Design Report: ILC Global Design Effort and World Wide Study, Volume 2 - Physics at the ILC," `arXiv:0709.1893`. ILC-REPORT-2007-001.

[565] W. Bernreuther, "Top quark physics at the LHC," *J. Phys.* **G35** (2008) 083001, `arXiv:0805.1333`.

[566] **DØ** Collaboration, V. M. Abazov *et al.*, "Top Quark Mass Extraction from $t\bar{t}$ Cross Section Measurements," *DØ conference note* **5742** (2008).

[567] S. Frixione, M. L. Mangano, P. Nason, and G. Ridolfi, "Top quark distributions in hadronic collisions," *Phys. Lett.* **B351** (1995) 555–561, `hep-ph/9503213`.

[568] **CDF, DØ** Collaboration, the Tevatron Electroweak Working Group, "A Combination of CDF and D0 Results on the Mass of the Top Quark," arXiv:0803.1683.

[569] **ALEPH, DELPHI, L3, OPAL** Collaboration, the LEP Electroweak Working Group, "Precision Electroweak Measurements and Constraints on the Standard Model," arXiv:0712.0929. Updated for 2008 summer conferences, 28 July 2008, http://www.cern.ch/LEPEWWG.

[570] **ALEPH, DELPHI, L3, OPAL, SLD** Collaboration, the LEP Electroweak Working Group, the SLD Electroweak and Heavy Flavour Groups, "A Combination of preliminary electroweak measurements and constraints on the standard model," hep-ex/0412015.

[571] **LEP Working Group for Higgs boson searches** Collaboration, R. Barate *et al.*, "Search for the standard model Higgs boson at LEP," *Phys. Lett.* **B565** (2003) 61–75, hep-ex/0306033.

[572] **CDF, DØ** Collaboration, the Tevatron New-Phenomena and Higgs working group, "Combined CDF and DØ Upper Limits on Standard Model Higgs Boson Production at High Mass ($155 - 200$ GeV) with 3 fb^{-1} of data," *DØ conference note* **5754** (2008).